Uncovering Plant Tolerance to Cyst Nematode Infections - Jaap-Jan Willig 2024

Uncovering Plant Tolerance to Cyst Nematode Infections

Jaap-Jan Willig

Propositions

1. Root architecture plasticity modulates tolerance to cyst nematodes. (this thesis)

2. Modulating reactive oxygen species is a common mechanism in biotic and abiotic stress tolerance. (this thesis)

3. Climate change challenges ecosystem restoration.

4. Social-economic status drives the evolution of *Homo sapiens.*

5. Short news videos stimulate polarisation in society.

6. Plants are more tolerant than human beings.

Propositions belonging to the thesis, entitled

Uncovering Plant Tolerance to Cyst Nematode Infections

Jaap-Jan Willig

Wageningen, 25 September 2024

Uncovering Plant Tolerance to Cyst Nematode Infections

Jaap-Jan Willig

Thesis committee

Promotor

Prof. Dr G. Smant
Professor of Nematology
Wageningen University & Research

Co-promotors
Dr M. G. Sterken
Assistant professor at the Laboratory of Nematology
Wageningen University & Research

Dr J. L. Lozano Torres
Assistant professor at the Laboratory of Nematology
Wageningen University & Research

Other members
Prof. Dr G. H. J. Kema, Wageningen University & Research
Prof. Dr G. A. F. J. M. Ackerveken, University of Utrecht, Utrecht
Dr S. Eves-van den Akker, University of Cambridge UK
Dr R. Heidstra, Wageningen University & Research

This research was conducted under the auspices of the Graduate School Experimental Plant Sciences

Uncovering Plant Tolerance to Cyst Nematode Infections

Jaap-Jan Willig

Thesis
submitted in fulfilment of the requirements for the degree of doctor
at Wageningen University
by the authnority of the Rector Magnificus,
Prof. Dr C. Kroeze,
in the presence of the
Thesis Committee by the Academic Board
to be defended in public
on Wednesday 25 September 2025
at 10:30 a.m. in the Omnia Auditorium.

Jaap-Jan Willig

Uncovering Plant Tolerance to Cyst Nematode Infections, 220 pages.

PhD thesis, Wageningen University, Wageningen, the Netherlands (2024)
With references, with summary in English and Dutch

DOI: https://doi.org/10.18174/662138

Table of Contents

Chapter 1

General introduction

Plant-parasitic nematodes

Nematodes are the most abundant animals on Earth (van den Hoogen et al., 2019). They are characterised by their unsegmented vermiform body surrounded by a cuticle. Up to now, over 27,000 species from the phylum *Nematoda* have been taxonomically described, which are classified into 12 clades based on their feeding behaviour and molecular characteristics (Van Megen et al., 2009; Quist et al., 2015). Some of them, approximately 4000, parasitize plants. Plant parasitism has independently evolved in at least four nematode clades (Quist et al., 2015; Smant et al., 2018). Despite having different evolutionary origins, all plant-parasitic nematodes can be recognised by a protrusible oral stylet, which they use for feeding on plant cells, and by their large oesophageal gland cells, which they use for effector protein production.

Plant-parasitic nematodes cause non-specific disease symptoms, which can easily be confused with symptoms of abiotic stresses (e.g., drought and nutrient deficiency). These symptoms include wilting, stunted growth of aboveground plant parts, and altered root development. Many plant-parasitic nematodes are obligate biotrophs; therefore, infected host plants rarely die even at high nematode population densities. Nonetheless, nematode infections can inflict substantial damage to crops, resulting in significant yield losses. Globally, plant-parasitic nematodes cause more than 10% yearly yield losses (Jones et al., 2013; Bebber et al., 2014; Savary et al., 2019; Sikora et al., 2023). With the increasing world population, which will consist of around 9.7 billion people by 2050 (United Nations, 2022), it is important to minimize crop losses due to pest and disease.

Different nematodes, different types of stress(es)

The biotic stress on host plants can differ depending on nematode species. This can nicely be illustrated by the three economically most damaging families of plant parasitic nematodes: the root-knot nematodes, the cyst nematodes, and the root lesion nematodes (Jones et al., 2013). Members of these three families have distinct host invasion, migration, and feeding behaviours (Fig. 1). Initially, they all start as infective second-stage juveniles that hatch from eggs in the soil upon perceiving specific host cues. Following gradients of these cues, they migrate through the soil to the surface of a nearby root of a host plant (Perry and Moens, 2011). There, they penetrate the root using fierce thrusts of the oral stylet and by releasing plant cell wall-degrading enzymes (Rehman et al., 2009; Goverse and Smant, 2014). Hereafter, the behaviours of root-knot nematodes, cyst nematodes, and root lesion nematodes start to differentiate. Root lesion nematodes remain mobile throughout their entire life cycle. Along their way, root lesion nematodes feed on plant cells at different locations in the root and may even move between hosts. By contrast, cyst nematodes and root-knot nematodes engage in a more sophisticated and intimate interaction with their host plants. They become sedentary after initiating a permanent feeding structure within the root vasculature in the early stages of parasitism (Sijmons et al., 1994). This permanent feeding structure is the sole source of nutrients for sedentary nematodes on which they depend throughout the remainder of their life cycle. In the following three paragraphs, I will describe in more detail how root lesion nematodes, cyst nematodes, and root-knot nematodes interact with their host plants and how this interaction leads to different types of biotic stress on host plants.

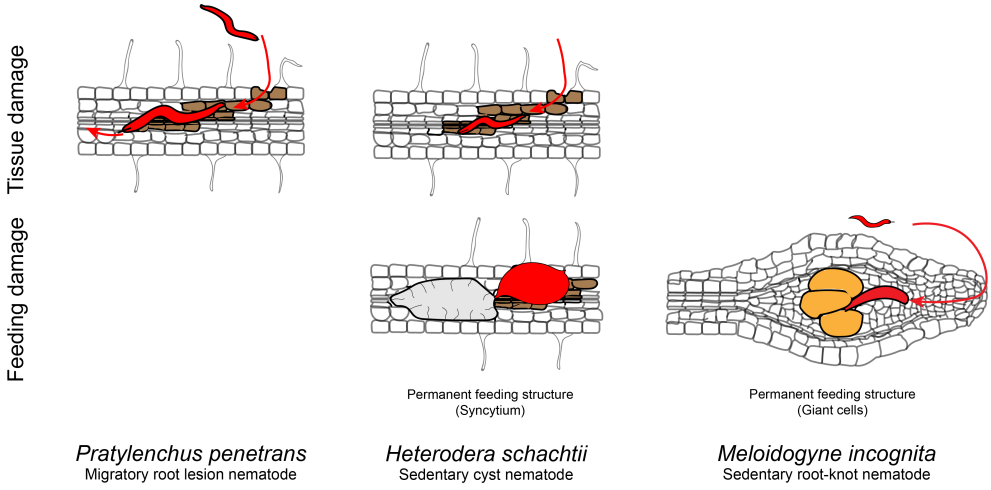

Figure 1: Schematic overview of types of infection of endo-parasitic nematodes. Brown areas indicate tissue damage. Red arrows indicate migration route. Grey cell indicates the syncytium formed by cyst nematodes. Orange cells indicate giant cells formed by root-knot nematodes.

Root lesion nematodes can move about within and between host roots while intermittently feeding on host cells (Zunke, 1990a). Root lesion nematodes typically invade the host root cortex at the elongation zone, where they migrate intracellularly causing the formation of extensive lesions. These lesions consist of dark brown plant tissue mainly harbouring necrotic cells (Fig. 1) (Zunke, 1990b; Zunke, 1990a). It is thought that cortical cells are the primary food source for root lesion nematodes (Duncan and Moens, 2013). Root lesion nematodes show two types of feeding behaviours, i.e., brief feeding and extended feeding. Brief feeding on cortical cells is mainly done by younger stages of juveniles and can last from 5 to 10 minutes (Zunke, 1990a). Host cells rarely die during this type of feeding. Extended feeding is mainly done by older staged nematodes, and it can take several hours. In contrast to brief feeding, extended feeding involves evident cellular changes to cortical cells. The tonoplast shrinks, occasionally affecting the tonoplast of adjacent cells, secondary vacuole-like structures form, and the nucleus gradually becomes hypertrophic. Extended feeding always ends in the death of the host cell. Adult root lesion nematodes deposit eggs inside the cortex and on the root surface (Zunke, 1990a; Castillo and Vovlas, 2007). During oviposition, females move far less than other life stages. Feeding by multiple root lesion nematodes at the same place can lead to the coalescence of large lesions and further root decay. Juvenile root lesion nematodes migrate from decaying roots to healthy parts of the root system or a new host, creating new infection sites.

Cyst nematodes also cause extensive damage to host tissue during host invasion, albeit at different places in the root (Fig. 1) (Wyss and Zunke, 1986; Wyss, 1992). These nematodes migrate intracellularly through the root cortex using brute force with fierce stylet thrusts and secretion of plant cell wall-degrading enzymes (Rehman et al., 2009). Several hours after penetrating the root epidermis, cyst nematodes change their behaviour. They subtly select a host cell to initiate the

formation of a permanent feeding structure, hereafter called a syncytium, and stop moving. Hereto, cyst nematodes inject stylet-secreted effectors into the apoplast and cytoplasm of this host cell, which initiate partial plant cell wall degradation and fusion with neighbouring cells (Bohlmann and Sobczak, 2014). More host cells fuse into the syncytium during subsequent cyst nematode feeding. The syncytium forms the sole source of plant nutrients for cyst nematodes. It provides feeding nematodes efficient access to the flow of assimilates, minerals, and water in the surrounding xylem and phloem. Depending on the nutrient supply by syncytia (Anwer et al., 2018), sedentary cyst nematodes can either develop into males or females. Adult males become mobile again, allowing them to inseminate adult females. By contrast, females remain sedentary and thus firmly attached to the syncytium throughout their lifecycle. Meanwhile, female cyst nematodes increase in size as their bodies swell by feeding and become filled with fertilized eggs after insemination by males. The end of parasitism for cyst nematodes is marked by the death of the females, which still carry the eggs inside their bodies as a protective capsule. The remnants of the dead female harbouring the eggs is referred to as a cyst.

In contrast to root lesion nematodes and cyst nematodes, **root-knot nematodes** cause little damage to host cells during invasion (Fig. 1). These nematodes primarily invade the root elongation zone close the meristematic zone, after which the infective juveniles migrate intercellularly through the cortex and root meristem to enter the vascular cylinder by gently pushing cells aside (Wyss and Grundler, 1992; Caillaud et al., 2008). Once inside the vascular cylinder, the J2s establish permanent feeding structures, which are referred to as giant cells. Hereto, the infective J2s carefully penetrate the cell walls of a small number of vascular parenchyma cells with their stylet and inject effectors into the apoplast and cytoplasm of these cells. The effectors are thought to bring about significant cellular changes, including acytokinetic mitosis and endoreduplication, leading to hypertrophic cells with multinucleate cytoplasm and polytene chromosomes (Kyndt et al., 2013). Like cyst nematodes, sedentary root-knot nematodes extract large amounts of plant assimilates from their feeding structures to support their growth and development into the reproductive adult stage.

In conclusion, root lesion nematodes predominantly induce stress in host plants by killing host cells during migration and feeding. Cyst nematodes cause stress by killing host cells during intracellular migration and by loss of assimilates during prolonged feeding. Root-knot nematodes primarily cause stress on host plants by loss of assimilates during prolonged feeding.

Damage control

Farmers manage nematode outbreaks, and subsequently crop damage, by combining five different strategies (i.e., crop rotation, cultivar choice, soil management, targeted control, and monitoring and evaluating infestations) (Reviewed in Sikora et al., 2023). Nevertheless, implementing these strategies by farmers remains challenging (Bridge, 1996; Coyne et al., 2018), particularly in developing countries (Onyango et al., 2021). However, new plant health policies and regulations (Molendijk and de Jongh, 2018) reduce the options for targeted control of nematode outbreaks. For instance,

chemical control with non-selective nematicides can effectively reduce nematode populations, but many of these pesticides currently face a global ban due to their detrimental environmental impact (Fuller et al., 2007; The European Commission, 2023). The phasing out of non-selective nematicides increases nematode diversity in the soil, which benefits soil health. However, it can also increase the overall infection pressure imposed by plant-parasitic nematodes on crops.

Using nematode-resistant crop cultivars, heralded as the most cost-effective means of nematode control, relies on the availability of major *resistance* (*R*-)genes. Resistance is based on direct and indirect molecular interactions between plant R-proteins and nematode elicitors (Jones and Dangl, 2006; Sacco et al., 2009; Lozano-Torres et al., 2012), followed by a programmed cell death response that stops further nematode development. Major nematode resistance genes work well, but their use has limitations. For instance, nematode resistances are often highly specific, limiting their use with increasing nematode diversity in arable farming. Secondly, many nematode resistances follow the gene-for-gene principle and rely on a match with a single avirulence locus in nematodes, which increases the risk of resistance breakthrough through mutations or recombination (Pink, 2002). Thirdly, only a few *R*-genes against plant-parasitic nematodes are available for commercial use in crops. Therefore, stacking multiple *R*-genes to different nematode species (or even pathotypes) is rare. Finally, another important limitation is that nematode-resistant cultivars may still display significant yield loss when exposed to low levels of nematode infection (Trudgill and Cotes, 1983). This is because these plants are intolerant to nematode damage. By contrast, heavily infected susceptible varieties may still produce acceptable yields because they tolerate biotic stress by feeding nematodes.

Defining tolerance of plants to nematodes

Despite its alluring potential for higher crop yield in the presence of nematode infection, tolerance remains a poorly understood trait (Peterson et al., 2017). Tolerance of plants to nematode infections has been defined as the ability to withstand or recover from the damaging effects of nematodes (Painter, 1951; Evans and Haydock, 1990; Trudgill, 1991). Tolerance and resistance are genetically and physiologically distinct (Fox and Spasoff, 1976; Fisher et al., 1981). Tolerance does not affect nematode parasitism directly but focuses on plant fitness. Resistance, on the other hand, reduces nematode infectivity, development, and/or reproduction, and thereby focuses on nematode fitness. In this thesis, I specify tolerance as the ability of the plant to mitigate the impact of biotic stress by disease-causing agents without affecting their fitness.

Tolerance levels of plant genotypes to plant parasitic nematodes are determined by exposing them to a range of nematode densities (Trudgill, 1986). Early observations suggested a strong relationship between the number of pre-planting nematodes (initial density) and plant yield (Oostenbrink, 1966). The yield remains unaffected until a certain initial nematode density is reached, beyond which yield declines until a minimum yield level is reached (Brown, 1969). These findings led to the development of the Seinhorst Yield Loss Model (SYLM), which expresses

the mathematical relationship between yield and initial nematode density (Seinhorst, 1986). Using the SYLM, differences in cultivar performance to nematode attack can be assessed. The SYLM typically follows an inverted sigmoid shape, with yield remaining stable up to a certain nematode density (tolerance limit), followed by an exponential decline leading to a minimum yield level (Fig. 2).

The tolerance of plants can be deduced from different components of the SYLM. The tolerance limit is the most important parameter to determine whether a plant is more tolerant (Fig. 2a). The tolerance limit is defined as the initial density of nematodes (*Pi*) that causes the first observable decline in yield. Some plants display an increase in yield at low initial nematode densities, while others do not (Fig. 2b). This is also known as overcompensation or hormesis (Agathokleous et al., 2019). The level of overcompensation in the SYLM can also be used to compare tolerance levels of plants. The steepness in yield decline (i.e., linearity) also allows to differentiate tolerance levels of plants (Fig. 2c) e.g., a steeper decline reflects less tolerance. Finally, plants may differ in the length of their linear decline, leading to desensitization and inherent impunity at different yields (minimum yield) (Fig. 2d). These differential mathematical expressions may reflect different mechanisms underlying tolerance plants for mitigating the effects of nematode damage (Pedigo et al., 1986; Peterson et al., 2017).

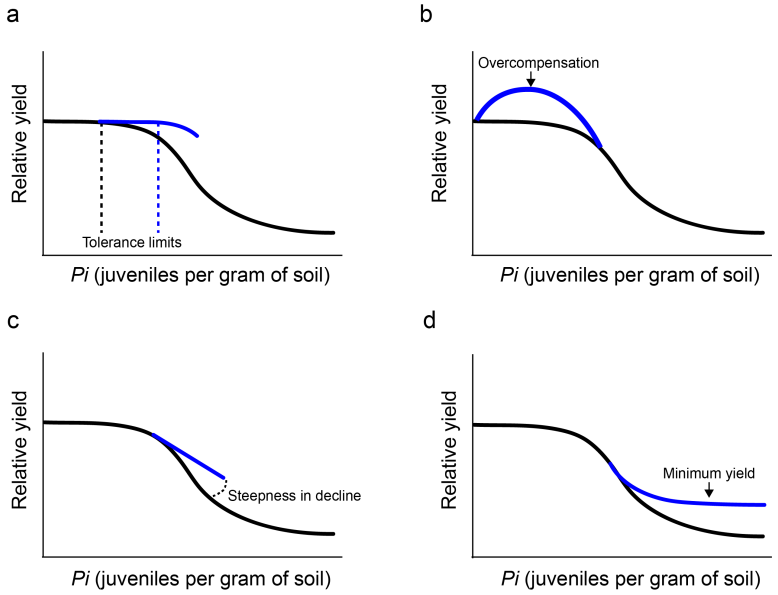

Figure 2: Key aspects of the damage curve and tolerance expressions. a) Tolerant plants may exhibit an initial zero slope extension, implying that higher levels of injury do not result in damage per unit Pi (initial density of nematodes) to the same extent as observed in nontolerant plants. **b)** Tolerant plants may express overcompensation. **c)** The slope of a tolerant plant could be less negative compared to that of a nontolerant plant. **d)** Desensitization and inherent impunity (minimum yield) may occur at a higher yield level. The black line represents the reference line, while the blue line represents an alternative response contributing to tolerance. Figure adapted from (Seinhorst, 1985; adopted from Peterson et al., 2017).

Challenges in quantifying yield in response to nematode infection

There are multiple reasons why disease tolerance remains a poorly understood concept in plant sciences. Tolerance experiments are often performed in field or glasshouses where plants are exposed to changing environmental conditions (e.g., temperature, humidity, drought, excessive radiation, and nutrient deficiency). Evidence based on field experiments suggests that disease tolerance strongly interacts with abiotic stress responses. For instance, nutrient deficiency affects the tolerance of barley to nematodes by increasing the damage resulting from infection (Wilhelm et al., 1985). Similarly, potato tuber yield was also more affected by cyst nematode infection in combination with drought (Fatemy and Evans, 1986). This may not be surprising as the symptoms of nematode infections are similar to those associated with abiotic stress. For example, the destruction of potato roots by cyst nematodes leads to a decrease in plant water uptake (Evans et al., 1975). Also, disruption of the vascular system by *Meloidogyne javanica* in tomato induces wilting (Meon et al., 1978). Therefore, it is necessary to use a fully controlled experimental design to unravel the genetic and molecular mechanisms underlying tolerance to nematodes.

Another important bottleneck towards better understanding the mechanisms underlying nematode tolerance has been the sole focus of most studies on destructive end-point measurements (Been *et al.*, 2015; Sasanelli *et al.*, 2013). For instance, many studies on tolerance to root-parasitic nematodes have focused on yield loss, such as tuber weight or haulm height (Seinhorst, 1986; Norshie et al., 2011; Sasanelli et al., 2013; Been et al., 2015; Moosavi, 2015). Indeed, for farmers, having acceptable yields while growing crops on nematode-infested fields is most important. However, tolerance is a complex plant trait and acceptable yields are most likely a culmination of different physiological processes, each of which can contribute to tolerance differently depending on circumstances such as infection pressure, plant age, and environmental conditions. For example, delayed senescence, shoot root ratio efficiency in K and Ca uptake, stomatal resistance, enhanced water and nutrient uptake abilities, increased photosynthesis capacity and enhanced root growth can all contribute to tolerance (Reviewed in Wallace, 1987). Likewise, plant parasitic nematodes can also cause different types of stress depending on their life stage and time in the growing season. By only focussing on end-point measurements, important phenotypic variation related to different physiological processes underlying tolerance will be missed.

Monitoring how root-feeding nematodes affect plant growth over time is not straightforward. While *in vitro* bioassays permit continuous recording of root system architecture changes of plants inoculated with plant parasitic nematodes, they only remotely simulate natural conditions in soil. High throughput monitoring of the impact of plant parasitic nematodes on root systems below-ground is still a major technical challenge (Miltner et al., 1991; Kerstens et al., 2021). Compared to below-ground plant parameters, high throughput measuring above-ground plant features is easier. In studies focusing on tolerance to abiotic stresses (i.e., salt and drought stress), it is common to measure aboveground plant parts, such as the green canopy area (Julkowska et al., 2016; Wang et al., 2021; Zhang et al., 2023). Still, very few studies report on the effect of nematodes on aboveground plant parts (Norshie et al., 2011; Joalland et al., 2016; Joalland et al., 2017; Ravelombola et al., 2019; Ravelombola et al., 2020). Therefore, more research is needed to assess if above-ground plant features are a good proxy for the impact of below-ground stress by root-feeding

nematodes.

Do plants harbour significant variation in tolerance to nematodes?

Quantitative variation in aboveground plant parts associated with tolerance to plant parasitic nematodes may provide leads to resolving the genetic architecture of tolerance. However, it is unclear whether natural plant populations harbour significant variation in nematode tolerance and whether this variation can be genetically mapped at high resolution. Two recent studies used a breeding panel of soybean accessions to identify quantitative trait loci associated with tolerance to the soybean cyst nematode *Heterodera glycines* at relatively low resolution (Ravelombola et al., 2019; Ravelombola et al., 2020). Accessions in this breeding panel also segregated in resistance to *H. glycines,* which made it more difficult to differentiate between plant susceptibility and tolerance to cyst nematode infections. Furthermore, breeding panels often harbour less genetic variation than populations of natural plant isotypes specifically assembled for genome-wide association studies (GWAS). GWAS panels of Arabidopsis isotypes would offer clear benefits for resolving the genetic architecture underlying tolerance to plant parasitic nematodes. GWAS has been used to identify quantitative trait loci (QTLs) in Arabidopsis associated with susceptibility to *M. incognita* (Warmerdam et al., 2018) and with sex-determination of *H. schachtii* (Anwer et al., 2018). However, Arabidopsis has yet to be used as a model to study tolerance to plant parasitic nematodes. Thus, whether Arabidopsis harbours significant variation in tolerance to plant parasitic nematodes and if this can be mapped on the Arabidopsis genome is still a knowledge gap.

Phenotypic plasticity in root architecture as a disease tolerance mechanism

Root-parasitic nematodes have a significant impact on root growth. Root systems of nematode-intolerant plants remain smaller and become denser upon nematode infection (Evans and Haydock, 1990). However, some plants, like the tolerant soybean cultivar Wright, show enhanced rooting in response to the cyst nematode infection. Based on the limited literature, the capacity for enhanced root growth seems to be one of the physiological processes conferring tolerance to nematode infection (Wallace, 1987; Miltner et al., 1991).

In *Arabidopsis thaliana*, the beet cyst nematode *Heterodera schachtii* triggers secondary root formation near the infection site (Grymaszewska and Golinowski, 1991; Goverse et al., 2000; Lee et al., 2011). Syncytium site formation is accompanied by local auxin accumulation (Karczmarek et al., 2004; Grunewald et al., 2009), a key hormone regulating *de novo* secondary root formation (Cai et al., 2014; Sheng et al., 2017). Depending on where and how secondary roots are formed, they are classified as lateral or adventitious (Sheng et al., 2017). In unstressed conditions, periodic oscillations of auxin maxima at the root tip prime cells to form **lateral roots** that emerge in a regular acropetal pattern from the growing primary root (Fukaki and Tasaka, 2009; van den Berg et al., 2016). This involves the transcription factors auxin-responsive factor (ARF)7 and ARF19, which directly regulate *LATERAL ORGAN BOUNDARIES DOMAIN* (*LBD*) genes, including *LBD16* (Okushima et al., 2007). By contrast, in response to stress, **adventitious lateral roots** emerge in between and opposite of existing lateral roots, creating an

irregular rooting pattern. In response to tissue damage, the jasmonic acid-dependent transcription factor ETHYLENE RESPONSIVE FACTOR (ERF)109 activates local auxin biosynthesis and subsequently triggers *de novo* secondary root formation via (Cai et al., 2014; Liu et al., 2014; Hu and Xu, 2016; Zhang et al., 2019). Similarly, damage-dependent local accumulation of auxin triggers the expression of the auxin-sensitive transcription factor WUSCHEL-RELATED HOMEOBOX (WOX)11 (Liu et al., 2014; Hu and Xu, 2016; Sheng et al., 2017). Local stress in roots caused by the damaging migratory behaviour of *H. schachtii* may also trigger *ERF109* and *WOX11* expression and, subsequently, *de novo* secondary root formation. However, whether cyst nematodes trigger secondary root formation via JA-dependent activation of ERF109 and WOX11, and whether this secondary root formation benefits the plant remains to be tested.

Members of the *TEOSINTE BRANCHED1/CYCLOIDEA/ PROLIFERATING CELL FACTOR1* (TCP) transcription factor family convert environmental signals into adaptive growth responses in plants (Danisman, 2016). Some of them modulate adaptations in root system architecture in response to abiotic stress. For instance, TCP20 regulates preferential lateral root growth in response to nitrates in a process called root foraging (Guan et al., 2014). Likewise, TCP13 regulates leaf and root growth in Arabidopsis in response to conditions simulating drought (Urano et al., 2022). Another member of the TCP family, TCP9 in soybean, enhances salt tolerance (Zhang et al., 2023). Heterologous expression of *PeTCP10* of bamboo (*Phyllostachys edulis*) in transgenic Arabidopsis induces secondary root growth under treatments simulating drought conditions (Liu et al., 2020) and salt stress (Xu et al., 2021). As members of the TCP family in Arabidopsis regulate root system architectural changes in response to abiotic stresses, we asked ourselves whether they might also be involved in root plasticity under biotic stress by cyst nematode infection.

Scope of the thesis

This thesis aims to identify molecular and genetic mechanisms underlying tolerance to plant-parasitic nematodes in plants. I used two complementary approaches to address these objectives. First, I used an exploratory strategy where I focused on identifying the genetic mechanism underlying cyst nematode tolerance using a genome-wide association mapping. My second strategy was more hypothesis-driven, wherein I investigated whether phenotypic plasticity in root architecture, modulated by specific transcription factors, contribute to plant tolerance to cyst nematode infections. For both approaches, we selected *A. thaliana* and the beet cyst nematode *H. schachtii* as our model pathosystem for several reasons. First, cyst nematodes have commonalities in their way of infecting with *M. incognita* (i.e., stress by loss of assimilates) and *P. penetrans* (migratory damage). Using *H. schachtii* in our experiments might reveal tolerance mechanisms that can also effectively mitigate biotic stress by root-knot nematodes and/or root lesion nematodes, for which *A. thaliana* is also a good host (Sijmons et al., 1991). Second, *A. thaliana* is a rich resource for studying the role of natural genetic variation, molecular, and cellular mechanisms underlying nematode-plant interactions (Grunewald et al., 2009; Absmanner et al., 2013; Lozano-Torres et al., 2014; Siddique et al., 2014; Anwer et al., 2018; Warmerdam et al., 2018; Olmo et al., 2020). Third, multiple studies showed that *A. thaliana* is highly suitable for high-throughput phenotyping (Julkowska et al., 2016; Awlia et al., 2021; Busoms et al., 2021; Meng et al., 2022).

Disease tolerance in plants is a complex trait that can be multi-factorial. In other words, tolerance can reveal itself through different plant features or proxies at different moments during disease development and, therefore, likely does not rely on a single gene. Before starting the multiyear GWAS phenotyping program, I first tested which plant features robustly measure the impact of biotic stress by *H. schachtii* on *A. thaliana*. In **Chapter 2**, we quantified multiple development and growth characteristics of nematode-infected *A. thaliana* (i.e., root architecture components, flowers, siliques, and green canopy area) at different inoculation densities. We discovered that the green canopy area accurately reflects the impact of biotic stress and can be easily monitored aboveground. Subsequently, we used the green canopy area to develop a high-throughput phenotyping platform for tolerance of Arabidopsis to *H. schachtii* and *M. incognita*.

In **Chapter 3**, we used our high-throughput phenotyping platform to resolve the genetic architecture of tolerance of *A. thaliana* to the beet cyst nematode *H. schachtii*. To this end, we inoculated 154 *A. thaliana* isotypes with six densities of *H. schachtii* and monitored growth responses over time to capture as many tolerance traits as possible. Additionally, we measured the susceptibility of the GWAS panel by counting the cysts from all nematode-inoculated plants. This allowed us to separate tolerance-specific QTLs from susceptibility QTLs.

The work described in Chapter 3 took almost three years of experimentation. Meanwhile, I also focused on a hypothesis-driven approach. Enhanced root growth contributes to better maintenance of plant growth. In response to damage by mechanical injury, plants form additional secondary roots to minimize growth reduction. One symptom of cyst nematode infection is the outgrowth of extra secondary roots. In **Chapter 4**, I hypothesized that damage caused by cyst nematode migration triggers *de novo* secondary root formation in a jasmonic acid-dependent manner. In response to mechanical damage, the transcription factor ERF109 initiates *de novo* secondary root emergence upon perception of jasmonic acid. In this chapter, we challenged *erf109* knockout mutants with *H. schachtii* to test whether the jasmonic acid-dependent activation of ERF109 modulates nematode-triggered *de novo* secondary root formation.

The classification of secondary roots as either lateral roots or adventitious lateral roots depends upon their location and manner of initiation. Lateral root formation follows a highly regulating pattern and is mediated by the transcription factors ARF7 and ARF19. The transcription factor WOX11 mediates the formation of adventitious lateral roots, which does not follow a specific root patterning. The secondary roots formed in response to *H. schachtii* emerge adjacent and opposite of each other near nematode infection sites. In **Chapter 5**, I hypothesized that nematode-triggered secondary roots are adventitious lateral roots. To test this hypothesis, I challenged the transcriptional repressor mutant *35S:WOX11-SRDX* with cyst nematodes to determine whether WOX11 modulates nematode-triggered secondary root formation. Moreover, I tested whether secondary root formation benefits the maintenance of plant growth during nematode infection and thus contribute to plant tolerance to biotic stress caused by cyst nematodes.

In **Chapter 6**, I tested whether TCP transcription factor family members modulate tolerance to cyst nematode infection. In several plant species (i.e., bamboo, rice, *A.*

thaliana), TCP proteins modulate tolerance to abiotic stresses (i.e., drought, salt, nutrient deficiency). The symptoms of stress caused by cyst nematode infection resemble symptoms of abiotic stress (i.e., nutrient deficiency, reduced water uptake). We, therefore, reasoned that members of the TCP transcription factor family also modulate tolerance to cyst nematode infection. To test this hypothesis, we first performed an RNA-seq experiment to identify which *TCP* genes in *A. thaliana* might modulate tolerance to *H. schachtii*. Subsequently, we used functional TCP knockout mutants to test whether they differ in tolerance to nematode infection compared to wildtype Arabidopsis plants.

In **Chapter 7**, I summarise all main findings of this thesis and discuss them in the broader context of our field of science.

Acknowledgements

I thank José L. Lozano-Torres, Mark G. Sterken, and Geert Smant for providing helpful comments on earlier version of this chapter.

References

Absmanner B, Stadler R, Hammes UZ (2013) Phloem development in nematode-induced feeding sites: The implications of auxin and cytokinin. Front Plant Sci **4**: 1–14

Agathokleous E, Kitao M, Calabrese EJ (2019) Hormesis: A Compelling Platform for Sophisticated Plant Science. Trends Plant Sci **24**: 318–327

Anwer MA, Anjam MS, Shah SJ, Hasan MS, Naz AA, Grundler FMW, Siddique S (2018) Genome-wide association study uncovers a novel QTL allele of AtS40-3 that affects the sex ratio of cyst nematodes in Arabidopsis. J Exp Bot **69**: 1805–1814

Awlia M, Alshareef N, Saber N, Korte A, Oakey H, Panzarová K, Trtílek M, Negrão S, Tester M, Julkowska MM (2021) Genetic mapping of the early responses to salt stress in Arabidopsis thaliana. Plant Journal **107**: 544–563

Bebber DP, Holmes T, Gurr SJ (2014) The global spread of crop pests and pathogens. Global Ecology and Biogeography **23**: 1398–1407

Been TH, Teklu MG, Heve WK, Schomaker CH (2015) Damage thresholds and population dynamics of Meloidogyne chitwoodi on carrot (Daucus carota) at different seed densities. Nematology **17**: 501–514

van den Berg T, Korver RA, Testerink C, ten Tusscher KHWJ (2016) Modeling halotropism: A key role for root tip architecture and reflux loop remodeling in redistributing auxin. Development (Cambridge) **143**: 3350–3362

Bohlmann H, Sobczak M (2014) The plant cell wall in the feeding sites of cyst nematodes. Front Plant Sci **5**: 1–10

Bridge J (1996) Nematode Management in Sustainable and Subsistence Agriculture. Annu Rev Phytopathol **34**: 201–225

Brown EB (1969) Assessment of the damage caused to potatoes by potato cyst eelworm, Heterodera rostochiensis Woll. Annals of Applied Biology **63**: 493–502

Busoms S, Pérez-Martín L, Llimós M, Poschenrieder C, Martos S (2021) Genome-Wide Association Study Reveals Key Genes for Differential Lead Accumulation and Tolerance in Natural Arabidopsis thaliana Accessions. Front Plant Sci. doi: 10.3389/fpls.2021.689316

Cai XT, Xu P, Zhao PX, Liu R, Yu LH, Xiang C Bin (2014) Arabidopsis ERF109 mediates cross-talk between jasmonic acid and auxin biosynthesis during

lateral root formation. Nat Commun. doi: 10.1038/ncomms6833
Caillaud MC, Dubreuil G, Quentin M, Perfus-Barbeoch L, Lecomte P, de Almeida Engler J, Abad P, Rosso MN, Favery B (2008) Root-knot nematodes manipulate plant cell functions during a compatible interaction. J Plant Physiol **165**: 104–113
Castillo P, Vovlas N (2007) Pratylenchus (Nematoda: Pratylenchidae): Diagnosis, Biology, Pathogenicity and Management. doi: 10.1163/ej.9789004155640.i-523
Coyne DL, Cortada L, Dalzell JJ, Claudius-Cole AO, Haukeland S, Luambano N, Talwana H (2018) Plant-Parasitic Nematodes and Food Security in Sub-Saharan Africa. doi: 10.1146/annurev-phyto-080417
Danisman S (2016) TCP Transcription Factors at the Interface between Environmental Challenges and the Plant's Growth Responses. Front Plant Sci **7**: 1–13
Duncan LW, Moens M (2013) Migratory endoparasitic nematodes. Plant nematology. CABI, UK, pp 144–178
Evans K, Haydock PPJ (1990) A review of tolerance by potato plants of cyst nematode attack, with consideration of what factors may confer tolerance and methods of assaying and improving it in crops. Annual applied Biology **117**: 703–740
Evans K, Trudgill DL, Parrott DM (1975) Effects of Potato Cyst-Nematodes On Potato Plants. Nematologica **21**: 169–182
Fatemy F, Evans K (1986) Effects of Globodera rostochiensis and water stress on Shoot and Root Growth and Nutrient Uptake of Potatoes. Revue Nématologie **9**: 181–184
Fisher J, Rathjen A, Dube A (1981) Tolerance of commercial cultivars and breeders' lines of wheat to Heterodera avenae Woll. Aust J Agric Res **32**: 545
Fox JA, Spasoff L (1976) Resistance and tolerance of tobacco to Heterodera solanacearum. J Nematol 8:
Fukaki H, Tasaka M (2009) Hormone interactions during lateral root formation. Plant Mol Biol **69**: 437–449
Fuller VL, Lilley CJ, Urwin PE (2007) Nematode resistance. New Phytologist 243–255
Goverse A, Overmars H, Engelbertink J, Schots A, Bakker J, Helder J (2000) Both Induction and Morphogenesis of Cyst Nematode Feeding Cells Are Mediated by Auxin. Molecular Plant-Microbe Interactions® **13**: 1121–1129
Goverse A, Smant G (2014) The Activation and Suppression of Plant Innate Immunity by Parasitic Nematodes. Annu Rev Phytopathol **52**: 243–265
Grunewald W, Cannoot B, Friml J, Gheysen G (2009) Parasitic nematodes modulate PIN-mediated auxin transport to facilitate infection. PLoS Pathog. doi: 10.1371/journal.ppat.1000266
Grymaszewska G, Golinowski W (1991) Structure of Syncytia Induced by Heterodera avenae Woll. in Roots of Susceptible and Resistant Wheat (Triticum aestivum L.). Journal of Phytopathology **133**: 307–319
Guan P, Wang R, Nacry P, Breton G, Kay SA, Pruneda-Paz JL, Davani A, Crawford NM (2014) Nitrate foraging by Arabidopsis roots is mediated by the transcription factor TCP20 through the systemic signaling pathway. Proceedings of the National Academy of Sciences **111**: 15267–15272
van den Hoogen J, Geisen S, Routh D, Ferris H, Traunspurger W, Wardle DA, de Goede RGM, Adams BJ, Ahmad W, Andriuzzi WS, et al (2019) Soil nematode abundance and functional group composition at a global scale. Nature **572**: 194–198
Hu X, Xu L (2016) Transcription Factors WOX11/12 Directly Activate *WOX5/7* to Promote Root Primordia Initiation and Organogenesis. Plant Physiol **172**: 2363–2373
Joalland S, Screpanti C, Gaume A, Walter A (2016) Belowground biomass

accumulation assessed by digital image based leaf area detection. Plant Soil **398**: 257–266

Joalland S, Screpanti C, Liebisch F, Varella HV, Gaume A, Walter A (2017) Comparison of visible imaging, thermography and spectrometry methods to evaluate the effect of Heterodera schachtii inoculation on sugar beets. Plant Methods **13**: 1–14

Jones JDG, Dangl JL (2006) The plant immune system. Nature **444**: 323–329

Jones JT, Haegeman A, Danchin EGJ, Gaur HS, Helder J, Jones MGK, Kikuchi T, Manzanilla-López R, Palomares-Rius JE, Wesemael WML, et al (2013) Top 10 plant-parasitic nematodes in molecular plant pathology. Mol Plant Pathol **14**: 946–961

Julkowska MM, Klei K, Fokkens L, Haring MA, Schranz ME, Testerink C (2016) Natural variation in rosette size under salt stress conditions corresponds to developmental differences between Arabidopsis accessions and allelic variation in the LRR-KISS gene. J Exp Bot **67**: 2127–2138

Karczmarek A, Overmars H, Helder J, Goverse A (2004) Feeding cell development by cyst and root-knot nematodes involves a similar early, local and transient activation of a specific auxin-inducible promoter element. Mol Plant Pathol **5**: 343–346

Kerstens M, Hesen V, Yalamanchili K, Bimbo A, Grigg S, Opdenacker D, Beeckman T, Heidstra R, Willemsen V (2021) Nature and Nurture: Genotype-Dependent Differential Responses of Root Architecture to Agar and Soil Environments. Genes (Basel) **12**: 1028

Kyndt T, Vieira P, Gheysen G, de Almeida-Engler J (2013) Nematode feeding sites: Unique organs in plant roots. Planta **238**: 807–818

Lee C, Chronis D, Kenning C, Peret B, Hewezi T, Davis EL, Baum TJ, Hussey R, Bennett M, Mitchum MG (2011) The Novel Cyst Nematode Effector Protein 19C07 Interacts with the Arabidopsis Auxin Influx Transporter LAX3 to Control Feeding Site Development. Plant Physiol **155**: 866–880

Liu H, Gao Y, Wu M, Shi Y, Wang H, Wu L, Xiang Y (2020) TCP10, a TCP transcription factor in moso bamboo (Phyllostachys edulis), confers drought tolerance to transgenic plants. Environ Exp Bot 104002

Liu J, Sheng L, Xu Y, Li J, Yang Z, Huang H, Xu L (2014) *WOX11* and *12* Are Involved in the First-Step Cell Fate Transition during de Novo Root Organogenesis in *Arabidopsis*. Plant Cell **26**: 1081–1093

Lozano-Torres JL, Wilbers RHP, Gawronski P, Boshoven JC, Finkers-Tomczak A, Cordewener JHG, America AHP, Overmars HA, Van 't Klooster JW, Baranowski L, et al (2012) Dual disease resistance mediated by the immune receptor Cf-2 in tomato requires a common virulence target of a fungus and a nematode. Proceedings of the National Academy of Sciences **109**: 10119–10124

Lozano-Torres JL, Wilbers RHP, Warmerdam S, Finkers-Tomczak A, Diaz-Granados A, van Schaik CC, Helder J, Bakker J, Goverse A, Schots A, et al (2014) Apoplastic Venom Allergen-like Proteins of Cyst Nematodes Modulate the Activation of Basal Plant Innate Immunity by Cell Surface Receptors. PLoS Pathog. doi: 10.1371/journal.ppat.1004569

Van Megen H, Van Den Elsen S, Holterman M, Karssen G, Mooyman P, Bongers T, Holovachov O, Bakker J, Helder J (2009) A phylogenetic tree of nematodes based on about 1200 full-length small subunit ribosomal DNA sequences. Nematology **11**: 927–950

Meng X, Li L, Pascual J, Rahikainen M, Yi C, Jost R, He C, Fournier-Level A, Borevitz J, Kangasjärvi S, et al (2022) GWAS on multiple traits identifies mitochondrial ACONITASE3 as important for acclimation to submergence stress. Plant Physiol **188**: 2039–2058

Meon S, Wallace HR, Fisher JM (1978) Water relations of tomato (Lycopersicon

esculentum Mill. cv. Early Dwarf Red) infected with Meloidogyne javanica (Treub), Chitwood. Physiol Plant Pathol **13**: 275–281

Miltner ED, Karnok KJ, Hussey RS (1991) Root Response of Tolerant and Intolerant Soybean Cultivars to Soybean Cyst Nematode. Agron J **83**: 571–576

Molendijk L, de Jongh E (2018) Beheersing van aardappelmoehied in de akkerbouw. 3–21

Moosavi MR (2015) Damage of the root-knot nematode Meloidogyne javanica to bell pepper, Capsicum annuum. Journal of Plant Diseases and Protection **122**: 244–249

Norshie PM, Been TH, Schomaker CH (2011) Estimation of partial resistance in potato genotypes against Meloidogyne chitwoodi. Nematology **13**: 477–489

Okushima Y, Fukaki H, Onoda M, Theologis A, Tasaka M (2007) ARF7 and ARF19 regulate lateral root formation via direct activation of LBD/ASL genes in Arabidopsis. Plant Cell **19**: 118–130

Olmo R, Cabrera J, Díaz-Manzano FE, Ruiz-Ferrer V, Barcala M, Ishida T, García A, Andrés MF, Ruiz-Lara S, Verdugo I, et al (2020) Root-knot nematodes induce gall formation by recruiting developmental pathways of post-embryonic organogenesis and regeneration to promote transient pluripotency. New Phytologist **227**: 200–215

Onyango CM, Nyaga JM, Wetterlind J, Söderström M, Piikki K (2021) Precision agriculture for resource use efficiency in smallholder farming systems in sub-saharan africa: A systematic review. Sustainability (Switzerland) **13**: 1–18

Oostenbrink M (1966) Major characteristics of the relation between nematodes and plants. Mededelingen Landbouwhogeschool Wageningen **66**: 46

Painter RH (1951) Insect resistance in crop plants.

Pedigo LP, Hutchins SH, Higley LG (1986) Economic Injury Levels in Theory and Practice. Annu Rev Entomol **31**: 341–368

Perry RN, Moens M (2011) Genomics and Molecular Genetics of Plant-Nematode Interactions. Genomics and Molecular Genetics of Plant-Nematode Interactions. doi: 10.1007/978-94-007-0434-3

Peterson RKD, Varella AC, Higley LG (2017) Tolerance: the forgotten child of plant resistance. PeerJ **5**: e3934

Pink DAC (2002) Strategies using genes for non-durable disease resistance. Euphytica **124**: 227–236

Quist CW, Smant G, Helder J (2015) Evolution of Plant Parasitism in the Phylum Nematoda. Annu Rev Phytopathol **53**: 289–310

Ravelombola WS, Qin J, Shi A, Nice L, Bao Y, Lorenz A, Orf JH, Young ND, Chen S (2019) Genome-wide association study and genomic selection for soybean chlorophyll content associated with soybean cyst nematode tolerance. BMC Genomics **20**: 1–18

Ravelombola WS, Qin J, Shi A, Nice L, Bao Y, Lorenz A, Orf JH, Young ND, Chen S (2020) Genome-wide association study and genomic selection for tolerance of soybean biomass to soybean cyst nematode infestation. PLoS One **15**: 1–20

Rehman S, Butterbach P, Popeijus H, Overmars H, Davis EL, Jones JT, Goverse A, Bakker J, Smant G (2009) Identification and Characterization of the Most Abundant Cellulases in Stylet Secretions from Globodera rostochiensis. Phytopathology **99**: 194–202

Sacco MA, Koropacka K, Grenier E, Jaubert MJ, Blanchard A, Goverse A, Smant G, Moffett P (2009) The cyst nematode SPRYSEC protein RBP-1 elicits Gpa2- and RanGAP2-dependent plant cell death. PLoS Pathog. doi: 10.1371/journal.ppat.1000564

Sasanelli N, Vovlas N, Trisciuzzi N, Cantalapiedra-Navarrete C, Palomares-Rius JE, Castillo P (2013) Pathogenicity and host-parasite relationships of Heterodera cruciferae in cabbage. Plant Dis **97**: 333–338

Savary S, Willocquet L, Pethybridge SJ, Esker P, McRoberts N, Nelson A (2019) The global burden of pathogens and pests on major food crops. Nat Ecol Evol **3**: 430–439

Seinhorst JW (1986) Effects of nematode attack on the growth and yield of crop plants. *In* F Lamberti, CE Taylor, eds, Cyst Nematodes. Plenum Press, New York and London, pp 191–209

Sheng L, Hu X, Du Y, Zhang G, Huang H, Scheres B, Xu L (2017) Non-canonical WOX11-mediated root branching contributes to plasticity in arabidopsis root system architecture. Development (Cambridge) **144**: 3126–3133

Siddique S, Matera C, Radakovic ZS, Shamim Hasan M, Gutbrod P, Rozanska E, Sobczak M, Torres MA, Grundler FMW (2014) Parasitic Worms Stimulate Host NADPH Oxidases to Produce Reactive Oxygen Species That Limit Plant Cell Death and Promote Infection. Sci Signal **7**: 1–11

Sijmons PC, Atkinson HJ, Wyss U (1994) Parasitic strategies of root nematodes and associated host cell responses. Annu Rev Phytopathol 235–59

Sijmons PC, Grundler FMW, von Mende N, Burrows PR, Wyss U (1991) Arabidopsis thaliana as a new model host for plant-parasitic nematodes. The Plant Journal **1**: 245–254

Sikora RA, Helder J, Molendijk LPG, Desaeger J, Eves-Van Den Akker S, Mahlein A-K (2023) Integrated Nematode Management in a World in Transition: Constraints, Policy, Processes, and Technologies for the Future. Annual Reviews. doi: 10.1146/annurev-phyto-021622

Smant G, Helder J, Goverse A (2018) Parallel adaptations and common host cell responses enabling feeding of obligate and facultative plant parasitic nematodes. Plant Journal **93**: 686–702

The European Commission (2023) Farm to Fork - targets - Progress. https://food.ec.europa.eu/plants/pesticides/sustainable-use-pesticides/farm-fork-targets-progress_en,

Trudgill DL (1986) Concepts of Resistance, Tolerance and Susceptibility in Relation to Cyst Nematodes. Cyst Nematodes. Springer US, Boston, MA, pp 179–189

Trudgill DL (1991) Resistance to and tolerance of plants parasitic nematodes in plants. Annu Rev Phytopathol **29**: 167–192

Trudgill DL, Cotes LM (1983) Tolerance of potato to potato cyst nematodes (Globodera rostochiensis and G. pallida) in relation to the growth and efficiency of the root system. Annals of Applied Biology **102**: 385–397

United Nations (2022) World Population Prospects 2022: Summary of Results Ten key messages.

Urano K, Maruyama K, Koyama T, Gonzalez N, Inzé D, Yamaguchi-Shinozaki K, Shinozaki K (2022) CIN-like TCP13 is essential for plant growth regulation under dehydration stress. Plant Mol Biol **108**: 257–275

Wallace HR (1987) A Perception of Tolerance. Nematologica **33**: 419–432

Wang LQ, Wen SS, Wang R, Wang C, Gao B, Lu MZ (2021) PagWOX11/12a activates PagCYP736A12 gene that facilitates salt tolerance in poplar. Plant Biotechnol J **19**: 2249–2260

Warmerdam S, Sterken MG, van Schaik C, Oortwijn MEP, Sukarta OCA, Lozano-Torres JL, Dicke M, Helder J, Kammenga JE, Goverse A, et al (2018) Genome-wide association mapping of the architecture of susceptibility to the root-knot nematode Meloidogyne incognita in Arabidopsis thaliana. New Phytologist **218**: 724–737

Wilhelm NS, Fisher JM, Graham RD (1985) The effect of manganese deficiency and cereal cyst nematode infection on the growth of barley. Plant Soil **85**: 23–32

Wyss U (1992) Observations on the feeding behaviour of Heterodera schachtii throughout development, including events during moulting. Fundam Appl Nematol **15**: 75–89

Wyss U, Grundler FMW (1992) Feeding behavior of sedentary plant parasitic nematodes. Netherlands Journal of Plant Pathology **98**: 165–173

Wyss U, Zunke U (1986) Observations on the behaviour of second stage juveniles of Heterodera schachtii inside host roots. Revue de nématologie **9**: 153–165

Xu Y, Liu H, Gao Y, Xiong R, Wu M, Zhang K, Xiang Y (2021) The TCP transcription factor PeTCP10 modulates salt tolerance in transgenic Arabidopsis. Plant Cell Rep **40**: 1971–1987

Zhang G, Zhao F, Chen L, Pan Y, Sun L, Bao N, Zhang T, Cui CX, Qiu Z, Zhang Y, et al (2019) Jasmonate-mediated wound signalling promotes plant regeneration. Nat Plants **5**: 491–497

Zhang Z, Zhao Y, Chen Y, Li Y, Pan L, Wang S, Wang P, Fan S (2023) Overexpression of TCP9-like gene enhances salt tolerance in transgenic soybean. PLoS One **18**: e0288985

Zunke U (1990a) Observations on the Invasion and Endoparasitic Behavior of the Root Lesion Nematode Pratylenchus penetrans. J Nematol **22**: 309–320

Zunke U (1990b) Ectoparasitic feeding behaviour of the root lesion nematode, Pratylenchus penetrans, on root hairs of different host plants. Revue Nematology **13**: 331–337

Chapter 2

From root to shoot; Quantifying nematode tolerance in Arabidopsis thaliana by high-throughput phenotyping of plant development

Jaap-Jan Willig[1], Devon Sonneveld[1], Joris J.M. van Steenbrugge[1], Laurens Deurhof[2], Casper C. van Schaik[1], Misghina G. Teklu[3], Aska Goverse[1], Jose L. Lozano-Torres[1], Geert Smant[1], Mark G. Sterken[1,4]

[1]Laboratory of Nematology, Wageningen University & Research, 6708PB Wageningen, the Netherlands
[2]Laboratory of Phytopathology, Wageningen University & Research, 6708PB Wageningen, the Netherlands
[3]Agrosystems Research, Wageningen University & Research, 6708PB Wageningen, the Netherlands
[4]Corresponding author

Published in Journal of Experimental Botany, Volume 74, Issue 18, 29 September 2023, Pages 5487–5499

Abstract:

Nematode migration, feeding site formation, withdrawal of plant assimilates, and activation of plant defence responses have a significant impact on plant growth and development. Plants display intraspecific variation in tolerance limits for root-feeding nematodes. Although disease tolerance has been recognised as a distinct trait in biotic interactions of mainly crops, we lack mechanistic insights. Progress is hampered by difficulties in quantification and laborious screening methods. We turned to the model plant *Arabidopsis thaliana*, since it offers extensive resources to study the molecular and cellular mechanisms underlying nematode-plant interactions. Through imaging of tolerance-related parameters the green canopy area was identified as an accessible and robust measure for assessing damage due to cyst nematode infection. Subsequently, a high-throughput phenotyping platform simultaneously measuring the green canopy area growth of 960 *A. thaliana* plants was developed. This platform can accurately measure cyst- and root-knot nematode tolerance limits in *A. thaliana* through classical modelling of tolerance limits. Furthermore, real-time monitoring provided data for a novel view of tolerance, identifying a compensatory growth response. These findings show that our phenotyping platform will enable further studies into a mechanistic understanding of tolerance to below-ground biotic stress.

Introduction:

The impact of root-parasitic nematodes on plant growth and development leads to reduced yield of food crops globally (Jones et al., 2013; Bebber et al., 2014). Interestingly, plants show intraspecific variation in their growth responses to belowground biotic stresses by nematodes (Miltner et al., 1991; Potter and Dale, 1994). In other words, plants display different disease burdens in response to similar initial nematode densities. The first measurable repression in plant growth (i.e., yield, plant height) by pathogen infection is defined as the tolerance limit (Seinhorst, 1986). The tolerance limit of plants is measured independently from resistance because tolerance and resistance are genetically and physiologically independent traits (Evans and Haydock, 1990; Teklu et al., 2022). The tolerance limit is dependent on the plant and the nematode species, and the interaction between those two. Even though nematode tolerance is known as a phenomenon for multiple decades, we lack an understanding of the underlying molecular and/or genetic mechanisms. Difficulties in quantifying and the required laborious screening methods hamper progress in this research area. Therefore, there is a need for a genetically tractable model species and a scalable screening method to better understand tolerance.

The model plant species should be able to support infections of the families of cyst nematodes (*Heteroderinae*) and root-knot nematodes (*Meloidogyninae*), as these belong to the most damaging obligate sedentary root parasites worldwide (Jones et al., 2013; Quist et al., 2015). Both genera spend most of their life cycle within roots. Cyst nematodes and root-knot nematodes cause significant damage to the root tissue by mechanical damage, large morphological changes, and loss of plant assimilates (Kyndt et al., 2013). Infective juveniles (J2s) of cyst and root-knot nematodes invade the plant root and move through different tissue layers to reach the vascular cylinder (Wyss and Zunke, 1986; Wyss et al., 1992). Cyst nematodes move brutally through cells causing significant mechanical damage, whereas root-knot nematodes move in between cells by gently pushing them aside. After reaching the

vascular cylinder, cyst and root-knot nematodes induce a redifferentiation process that leads to the formation of multinucleated feeding cells known as syncytium and giant cells, respectively. The feeding cells are hypermetabolic sink tissues and serve as the sole source of nutrients for growing nematodes throughout their entire life cycle. This leads to less nutrients available for plant growth and development. Both nematode families consist of multiple species, of which the beet cyst nematode *Heterodera schachtii* and the root-knot nematode *Meloidogyne incognita* are the best studied, and therefore considered to be model species for plant-nematode interaction studies.

Up to now, tolerance to root-parasitic nematodes is mainly studied in field crops (Seinhorst, 1986; Norshie et al., 2011; Sasanelli et al., 2013; Been et al., 2015; Moosavi, 2015), making it difficult to resolve the underlying mechanisms as to why plants differ in their tolerance limits. Knowledge of the genetic underpinnings of tolerance is important for understanding how plants differ in their tolerance limits to root-feeding nematodes. The model plant *Arabidopsis thaliana* is a rich and often-used resource to study the role of natural genetic variation, molecular, and cellular mechanisms underlying nematode-plant interactions (Grunewald et al., 2009; Absmanner et al., 2013; Lozano-Torres et al., 2014; Siddique et al., 2014; Anwer et al., 2018; Warmerdam et al., 2018; Olmo et al., 2020). It has been shown that *A. thaliana* harbours significant natural genetic variation in susceptibility to the beet cyst nematode *Heterodera schachtii* and *Meloidogyne incognita in vitro* (Anwer et al., 2018; Warmerdam et al., 2018). For instance, a quantitative trait loci allele of *ATS40-3* that was identified with a Genome Wide Association Study affects the sex ratio of *H. schachtii* in Arabidopsis (Anwer et al., 2018). Recently, we also showed that the transcription factor TCP9 modulates tolerance to *H. schachtii* via reactive oxygen species mediated processes (Willig et al., 2022). However, it remains unknown if *A. thaliana* harbours significant genetic variation in tolerance to nematodes.

So far, the Seinhorst Yield Loss Model (SYLM) is mostly used to determine the tolerance limit for plant-parasitic nematodes (Seinhorst, 1986; Norshie et al., 2011; Sasanelli et al., 2013; Been et al., 2015; Moosavi, 2015). The SYLM models the density-yield relationship by an inverted sigmoid curve where loss of yield at a given timepoint is a derivative function of damage. Yield remains stable up to a certain nematode density i.e., the tolerance limit, then declines exponentially, to end at a minimum yield level at the highest nematode density. The SYLM enables a comparison of tolerance limits of different crop varieties for a specific pathogen (Seinhorst, 1986). Importantly, herein, yield loss is dependent on the number of parasitic nematodes in the soil and not the number of successful infections detected at harvest (Seinhorst, 1986). The tolerance limit and the steepness of the decline in yield over increasing nematode densities are both agronomically important traits. Alternatively, for other pathogens, the slope of a regression of the selected host parameter against the pathogen load are made to determine if a plant is more tolerant than the other (Pagán and Garcia-Arenal, 2020). However, both linear regression and the SYLM do not account for biological responses to pathogen infection like overcompensation or compensation (i.e., increased growth speed or growth speed recovery) (Pedigo et al., 1986).

Most of the studies that measure the effect of nematode infection on crop yield rely on destructive end-point measurements (*i.e.,* crop yield (Sasanelli et al., 2013; Been et al., 2015)), leaving an information gap between start and endpoint of the experiment. Few time-series experiments were performed by measuring the effect of soybean cyst nematode *Heterodera glycines* on the root system by

using a rhizotron (Miltner et al., 1991) or by measuring the effect of *Meloidogyne chitwoodi* densities on the height of potato plants (Norshie et al., 2011). Additionally, time-series measurements were also performed on the green canopy area upon nematode infection using a phenotyping design based on microplots (Joalland et al., 2016; Joalland et al., 2017). However, this later design was limited to 70 microplots, which does accommodate large phenotyping experiments included hundreds of genotypes for multi-genotype comparisons (i.e., Genome-Wide Association Studies or mutant screens). A system that is able to monitor a larger number of individually measured plants over time could give insight in genes that modulate tolerance to root-parasitic nematodes.

Another returning hurdle in tolerance research is to determine which plant trait should be measured. Most of the studies on tolerance to root-parasitic nematodes in potato focus on yield reduction, e.g., potato yield expressed in tuber weight and quality (Been et al., 2015; Teklu et al., 2022), which depend on single destructive endpoint measurement. Others also measure the effect of nematodes foliage or plant height which are not perse destructive (Norshie et al., 2011), but these types of measurements are less often done because they are laborious. In *A. thaliana*, the green canopy growth, inflorescences, and the number of viable seeds can be used to measure tolerance to viruses (Shukla et al., 2018). Most of the screening methods are laborious and/or time-consuming. For many purposes, these kinds of measurements might be adequate, but for large scale phenotyping of multiple plant genotypes these laborious measurements hamper progress. Therefore, the chosen trait should also be easy to measure. However, it remains unknown which plant trait gives the most robust data for a high throughput design to quantify tolerance to root-parasitic nematodes in *A. thaliana*.

Here, we report on the construction and validation of a high-throughput phenotyping platform to monitor in real-time plant growth under belowground biotic stress caused by nematode infection. Initially, we tested growth parameters (e.g., root system architectural components, green canopy area, flowering, and silique formation) to robustly quantify the effect of *H. schachtii* infestation on the growth and development of the host. We found that the green canopy area of Arabidopsis is an accessible and informative trait for automated analysis of growth-responses to root-parasitic nematodes. Time-series measurements showed that daily growth rates of individual plants are congruent over plants and provided insight in biological responses of the host (*i.e.,* compensation responses) that could not be determined in previous experimental designs. Therefore, we believe that our phenotyping system will not only allow for a more accurate mechanistic studies into tolerance, but can also ultimately pinpoint genes that modulate tolerance to biotic stress by endoparasitic nematodes.

Materials and Methods:

Plant culturing

For seed sterilization, Arabidopsis seeds (Col-0, N60,000) were placed in Eppendorf tubes in a desiccator. The seeds were vapour sterilized for 3-4 hours using a mixture of hydrochloric acid (25%) and sodium hypochlorite (50 g/L). Finally, the sterile seeds were stratified for four days. For *in vitro* assays, seeds were sown on square petri dishes (120x120 mm) containing modified Knop medium (Sijmons et al., 1991). For

in vivo pot experiments, non-sterilized seeds were also stratified for four days and sowed directly on top of silversand. Seedlings were grown at 21 °C and 16-h-light/8-h-dark conditions. Seedlings growing in our high-throughput platform were grown at 19 °C and 16-h-light/8-h-dark conditions with LED light (150 lumen).

Hatching and sterilization of *Heterodera schachtii* and *Meloidogyne incognita*

H. schachtii cysts (Woensdrecht population from IRS, the Netherlands) were separated from sand and roots of infected *Brassica oleracea* plants as previously described (Baum et al., 2000). *H. schachtii* cysts were transferred into a clean Erlenmeyer containing water with 0.02% sodium azide. This mixture was gently stirred for 20 min. Later, sodium azide was removed by vigorously washing with tap water. Cysts were then placed on a hatching sieve in a glass petri dish. An antibiotic solution was added containing 1.5 mg/mL gentamycin, 0.05 mg/mL nystatin, and 3mM zinc chloride. The cysts were incubated in the dark for 4-7 days. Thereafter, nematode juveniles were collected in a 2 mL Eppendorf tube. For *in vitro* experiments, J2s were surface sterilized using a $HgCl_2$-containing solution (0.002% Triton X-100 w/v, 0.004% NaN_3 w/v, 0.004% $HgCl_2$ w/v) for 20 min. After incubation, the nematodes were collected by centrifugation and the supernatant was removed. Nematodes were washed with sterile water and spun down again. This was repeated three times. Finally, for *in vitro* experiments, the nematodes were resuspended in 0.7% gelrite (Duchefa Biochemie, Haarlem, the Netherland). For *in vivo* experiments, hatched J2s were separated from debris by centrifugation in a 70% sucrose gradient. Afterwards, the nematodes were washed by centrifugation in tap water three times. Finally, the nematodes were resuspended in tap water.

Eggs of *Meloidogyne incognita* were obtained by soaking *M. incognita* (strain 'Morelos' from INRA, Sophia Antipolis, France) with 0.05% (v/v) NaOCl for three minutes. Roots were rinsed with tap water and the eggs were collected on a 25 µM sieve. Next, the eggs were incubated in a solution of 2.4 mM NaN_3 for 20 minutes while swirling. Thereafter, the eggs were rinsed with tap water and incubated on a 25 µM sieve in a solution of 1.5 mg/mL gentamycin, 0.05 mg/mL nystatin in the dark at room temperature. After four days, hatched juveniles were collected. For *in vivo* experiments, hatched J2s were separated from debris by centrifugation in a 70% sucrose gradient. Afterwards, the nematodes were washed by centrifugation in tap water three times. Finally, the nematodes were resuspended in tap water.

Quantifying the root system architecture of nematode-infected Arabidopsis

Nine-day-old *in vitro-grown Arabidopsis thaliana* seedlings were individually inoculated with increasing densities (P_i)of surface sterilised second-stage juveniles of *H. schachtii* (from 0 to 50 juveniles per mL modified KNOP media). Roots of nematode-infected plants were scanned at 7 dpi using an Epson Perfection V800 photo scanner. Various root measurements were conducted (*i.e*. total root length, main root length, total secondary root length, and average secondary root length), collectively referred to as the root system architecture. Measurements were taken using the WinRHIZO package for Arabidopsis (WinRHIZO pro2015, Regent Instrument Inc., Quebec, Canada). The number of root tips was counted manually based on the scans made by WinRHIZO. Differences in the root length per seedling

in centimetres and the number of root tips were statistically analysed with a one-way ANOVA with *post-hoc* Tukey's HSD test in R.

Quantifying above-ground development and growth of *Heterodera schachtii* infected Arabidopsis plants

Three-week-old *Arabidopsis thaliana* seedlings were inoculated with increasing densities of *H. schachtii* (from 0 to 50 juveniles per g dry sand). During a period of 14 days post inoculation (dpi), we recorded the green canopy area, the number of flowers, the number of siliques, and the number of basal stems every second day with a video camera. By using Adobe Photoshop (Version: 22.5.6 20220204.r.749 810e0a0 x64), we manually isolated the green canopy area from the images and analysed the area manually using ImageJ. Differences per treatment per timepoint were analysed using One-Way ANOVA with *post-hoc* Tukey's HSD test in R.

High throughput analysis of the green canopy area of nematode-infected Arabidopsis

Pots filled with silver sand were placed in stainless steel frames made (Fig. S1a and d) and covered with a 3 mm thick black nonreflective foamed PVC coversheet (Fig. S1b, c and e) drilled with countersunk holes ~73 mm apart. Extra holes were drilled with a diameter of 7 mm and 4 mm away from the countersunk holes for nematode inoculations. Prior to sowing, silver sand was watered with Hyponex (1.7 mM/L $NH4^{+}$, 4.1 mM/L K^{+}, 2 mM/L Ca_2^{+}, 1.2 mM/L Mg_2^{+}, 4.3 mM/L NO_3^{-}, 3.3 mM/L SO_4^{2-}, 1.3 mM/L $H2PO_4^{-}$, 3.4 µm/L Mn, 4.7 µm/L Zn, B 14 µm/L, 6.9 µm/L Cu, 0.5 µm/L Mo, 21 µm/L Fe, pH 5.8) for five minutes. Seven days after sowing, seedlings were watered again for five minutes. Nine-day-old seedlings were inoculated with increasing densities of *H. schachtii* and *M. incognita* (0 to 100 juveniles per g dry sand). Seedlings were inoculated by first punching a hole of approximately 3.5 cm deep in the soil, into which 1 mL tap water containing a measured number of nematodes was added using a pipet. For our experiments we did not use a blocking design as it would greatly increase the chance for error when manually inoculating plants. Pictures of the Arabidopsis seedlings were taken every hour (15 pictures per day) during the light period automatically for a period of 21 days with twelve UI-1490LE-C-HQ cameras (IDS Imaging) mounted with 12mm lenses on the ceiling of the climate chamber (Cat. No. B5M12056, IDS Imaging). Because of the purple LED light, colour corrections were done using Adobe Photoshop (Version: 22.5.6 20220204.r.749 810e0a0 x64)**.** The surface area of the rosette was determined using a custom-written ImageJ macro (ImageJ 1.51f; Java 1.8.0_321 [32-bit]) (Supplementary File 1) and Java was used to make GIFs (Supplementary File 2). In the GIFs and images of individual plants, a green artefact can be observed for all plants and images which is caused by algae growth. This error is systemic and occurs for all plants, however after day 4 the impact on the green canopy area is minimum. Another point of notion is that the number of measured plants vary between experiments due to technical issues (i.e. not enough nematodes), abnormal growth (clearly smaller than the general trend within inoculum densities), or plants that died due to extremely high densities of nematodes. More information about how the experiment was performed can be found in: (DOI: dx.doi.org/10.17504/protocols.io.kqdg39167g25/v1).

Seinhorst yield loss model (SYLM)

To quantify the tolerance limit for *H. schachtii* infection in Arabidopsis we fitted the green canopy area data to the Seinhorst's Equation (1) (Seinhorst, 1986). Before fitting the model to the data, each measurement was averaged over the day and replicates for each nematode density

$$y = m + (1 - m) \times 0.95^{(Pi/T-1)} \text{ for } P_i > T$$
$$y = 1 \text{ for } P_i \leq T$$

where *y* is the relative yield defined as the ratio between the canopy surface area to the non-inoculated canopy area surface area (control), *m* is the minimum relative yield, P_i is the initial nematode density in nematodes per gram soil and *T* is the tolerance limit (nematodes per gram of soil). The assumption in the model (Seinhorst, 1986) is that below the tolerance limit plant yield is equal to a situation where $P_i = 0$ (not infected).

Using these equations the tolerance limit *T* and the minimum yield *m* were estimated (available via gitlab: https://git.wur.nl/published_papers/willig_2023_camera-setup).

Plant growth analysis using the high-throughput phenotyping platform

To analyse the growth data of the plants obtained from the high-throughput platform, custom scripts and functions were written in "R" (available via gitlab: https://git.wur.nl/published_papers/willig_2023_camera-setup). For analysis we used the median daily leaf area (cm2), which was calculated by taking the median leaf area of the daily measurements (15 per day). The data was log2-transformed before analysis for normalization. The rate of growth was determined per day per plant by (equation 2)

$$R_{x,t} = \log_2(A_{x,t-1} - A_{x,t})$$

where $R_{x,t}$ is the transformed growth rate of plant *x* at day *t* from day *t-1* to day *t* based on the median Green canopy area *Ax,t* (cm^2). Differences in growth rate were determined using a Wilcoxon Rank Sum test as implemented in the ggpubr package (https://cran.r-project.org/web/packages/ggpubr/index.html). Differences in growth rate between plants infected with either *H. schachtii* or *M. incognita* were tested using a paired t-test comparing data from the same day and density combination. Data was multiple-testing corrected using the *p.adjust* function with the *fdr* method (Benjamini and Hochberg, 1995).

Modelling growth rates

Growth models were fitted to the data using the *growthrates* package, which was used to fit a logistic growth model for the canopy area A_t (cm^2) (equation 3),

$$A_t = \frac{K \times A_0}{A_0 + (K - A_0) \times e^{(-r \times t)}}$$

where the parameters K is the maximum green canopy area (cm^2), A_0 is the initial canopy area (cm^2), and r is the intrinsic growth rate (d^{-1}) were determined as a function of time t (d). These fitted values were used to explore the relation between nematode density and the K and r. Bad fits ($p < 0.05$) were removed before analysis. We found that the relation between K (cm^2) and density could be described by the Gaussian function (equation 4)

$$K = K_B + \frac{K_\sigma}{P_\sigma} \times e^{-\left(\frac{P_i - P_M}{P_\sigma}\right)^2}$$

where P_i is the initial nematode density in nematodes per gram soil, K_B is the basal canopy size (cm^2), K_σ (nematode density / cm^2) is the normalized maximum canopy area that can be achieved over the P_i range, P_σ is the deviation around the nematode density allowing maximum growth, P_M is the nematode density at which maximum growth is achieved. Note that this allows for the maximum growth to be achieved at $P_i \geq 0$, which is not possible in the SYLM, which assumes maximum growth at $P_i = 0$.

We found that the relation between the intrinsic growth rate r (d^{-1}) and the initial nematode density P_i (number of nematodes per gram of soil) could be described by the exponential function (equation 5)

$$r = r_B + r_A \times e^{-(c_{Pi} \times P_i)}$$

where r_B is the basal growth rate (d^{-1}), r_A is the adaptive growth rate (d^{-1}), and c_{Pi} is the translation constant (gram soil per nematode density), which translates the P_i to an impact on growth rate.

Together, the function for K and r could be used to model the time series data of the entire experiment in the logistic growth model. We modelled the parameter values using *nls* and extracted confidence intervals using the *nlstools* package. In this model the tolerance limit can be defined as $2*P_M$ (where the achieved canopy area is equal to the achieved canopy area at $P_i = 0$).

Results:

Density-response relationship between plant architecture and nematode inoculation density

The impact of biotic stresses on plant growth and development can be expressed as a function of inoculation density of causal agents of disease. To determine which plant growth parameters sensitively reflect the impact of nematode challenge on *A. thaliana*, we monitored changes in root system architecture and above-ground plant features at increasing inoculation densities of the beet cyst nematode *H. schachtii*. We first quantified different root system architecture components (*i.e.,* primary root length, the number of secondary roots, and secondary root length) after inoculating *in vitro* cultured Arabidopsis plants with increasing densities (P_i) of *H. schachtii* (Fig. 1a). At the system architecture level, we found that challenging Arabidopsis with

H. schachtii at higher inoculation densities disturbs the typical regular patterning of emerging lateral roots (Fig. 1b). However, despite disturbing the lateral root patterning, the total root length did not change by increasing inoculation densities of *H. schachtii* (Fig. 1c). We did observe a decrease in primary root length around P_i 5, and higher, but this was compensated by an increase in the number of secondary roots (Fig. 1c).

Next, we monitored the impact of *H. schachtii* densities on aboveground plant growth and development of *A. thaliana* cultivated in soil by daily assessing changes in green canopy area, the number of flowers, and the number of siliques (Fig. 1d). The above-ground plant growth/development over time showed clear detrimental effects linked to increased *H. schachtii* infection pressure (Fig. S2a). At 11 days post inoculation (dpi), we observed the biggest differences in green canopy area between inoculation densities, including a tolerance limit of Arabidopsis for *H. schachtii* around 15 juveniles per gram soil (Fig. 1d and e). We also counted the number of flowers and siliques over time (Fig. S2b and c). Likewise, we also observed a density-dependent response for the number of flowers, albeit at higher inoculation densities (Fig. 1f). By contrast, we did not find a significant response in the number of siliques by inoculation density (Fig. 1g). In conclusion, both primary root length and green canopy area can be used to assess the impact of nematode-induced biotic stress on *A. thaliana.*

We tested whether the green canopy area could also be used as a proxy for belowground adaptations to nematode challenge, as repeated measurements on root system architecture requires a more artificial experimental design. To address this question, we calculated the Spearman's Rank Order Correlation Coefficient for our measurements of green canopy area and root system architecture components acquired through different experimental designs (Fig. S3). Indeed, we found that green canopy area strongly correlates with primary root length (R^2 = 0.89, P <0.0001) (Fig. S3b). Green canopy area also anticorrelated well with the number of secondary roots (R^2 = −0.63, p = 0; Fig. S3e) and total secondary root length (R^2 = −0.64, p = 0.04; Fig. S3c). As expected, we found no significant correlation between the green canopy area and average secondary root length (Fig. S3d) and total root length (Fig. S3a). Based on this analysis, we focused further on developing a high-throughput automated phenotyping platform using the green canopy area of Arabidopsis cultivated in soil to assess the impact of *H. schachtii* at different inoculation densities over time.

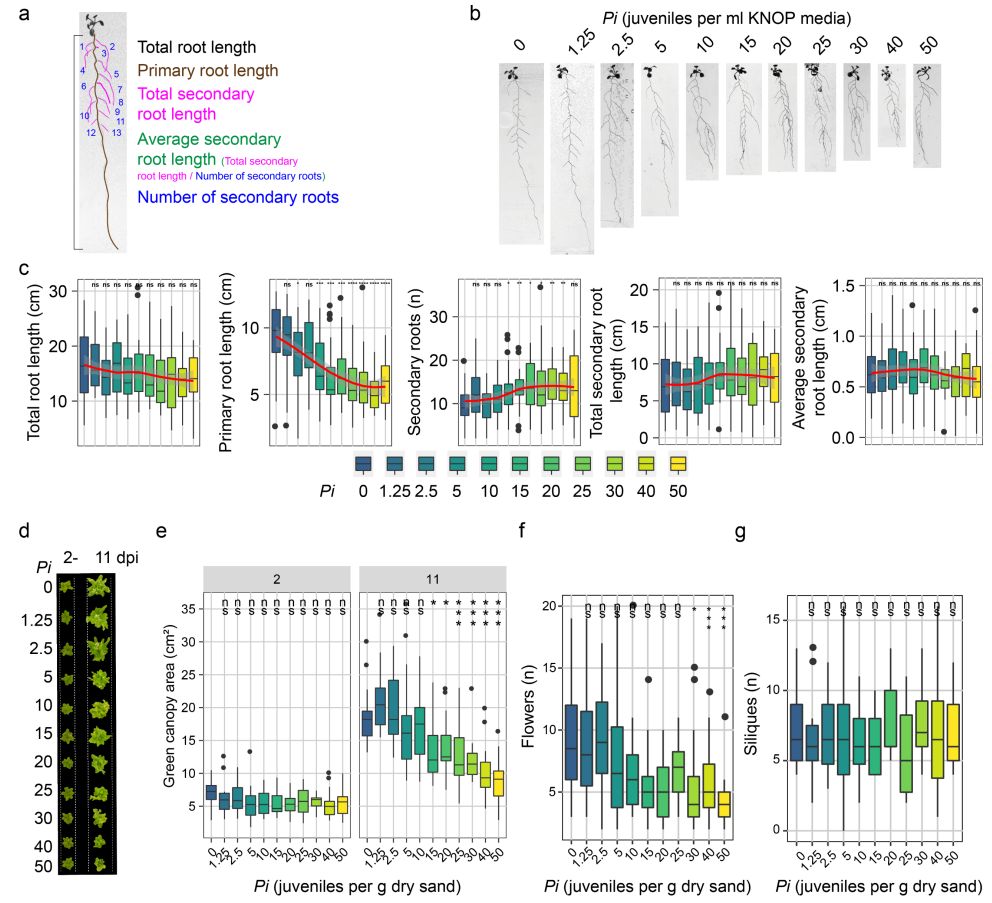

Figure 1: The primary root length and the green canopy area of Arabidopsis respond in a density-dependent manner to infection by *H. schachtii*. a-c) Nine-day-old Arabidopsis seedlings were inoculated with densities ranging from 0-50 of *H. schachtii* juveniles (ml modified KNOP media). The growth of the seedlings was monitored and measured at 7-days post-inoculation (dpi). **a)** Overview of root system architecture components that we have quantified. **b)** Representative images of Arabidopsis root system at 7 dpi. **c)** Total root length (cm), primary root length (cm), total secondary root length (cm), average secondary root length (cm), and the number of secondary roots (n). Data was analysed by one-way ANOVA with post-hoc Tukey HSD; ns= not significant, *p< 0.05, **p< 0.01, ***p<0.001 (n=24-30). D-g) Twenty-one-day-old Arabidopsis seedlings cultivated in soil were inoculated with increasing densities of second juveniles of *H. schachtii* (from 0 to 50 juveniles per g dry sand). **d)** Representative images of Arabidopsis seedlings aboveground at 2 and 11 dpi. **e)** Green canopy area (cm^2) at 2 and 11-dpi with increasing densities (Pi). **f)** Number of flowers at 11 dpi. g) Number of siliques at 11 dpi. Data was analysed by one-way ANOVA with post-hoc Tukey HSD; ns= not significant, *p< 0.05, **p< 0.01, ***p<0.001 (n=16-20).

High-throughput monitoring of density-response relationships between nematode densities and green canopy area

Our high-throughput automated monitoring platform can record and analyse changes in green canopy area of 960 Arabidopsis plants simultaneously for a period of twenty-one days (Fig. 2a). The platform design includes stainless steel frames that can hold 200 mL pots filled with soil (Fig. S1). The frames fix the pots in position and give anchor to perforated matte black cover plates which maximise the contrast of the green canopy area. The frames and cover plates match the size of a flooding table placed in a fully automated climate room. Each frame contains 160 perforated holes to sow seeds and inoculate the pots. Photographs can be made at any desired time interval by high-resolution cameras mounted at fixed positions above the cover plates. To monitor the impact of nematode challenge on green canopy area, photographs were taken at one-hour intervals for 21 days during daytime (i.e., 15 pictures per day). To collect data on individual plants, the pictures were processed by colour channel decomposition in Adobe Photoshop and analysed in ImageJ (Fig. 2a). With every experiment, which can result in 302,400 pictures of individual plants (315 pictures per plant).

To validate our system, we inoculated 480 *A. thaliana* Col-0 seedlings with increasing densities of *H. schachtii* (P_i 0 to 100 juveniles per g dry sand) and monitored their growth for a period of three weeks. The green canopy area rendered from the recordings was collected and analysed (Movie 1; Fig. 2b). We confirmed that increasing densities of *H. schachtii* decreased the growth of Arabidopsis plants. To test if changes in the green canopy area fit the SYLM, we tested our green canopy area at 21 dpi for its fit (equation 1) (Seinhorst, 1986). We found the typical inverted sigmoid curve and that our data fits well to the Seinhorst Yield Loss Model (R^2 = 0.83; Fig. 2c), indicating that there is a strong relationship between nematode densities and the green canopy area. Also, we found that the tolerance limit (*Te*) is placed around P_i 0.21 (Fig. 3c). Altogether, we concluded have developed a high-throughput system in which we can quantify the relation between green canopy size and cyst nematode inoculum densities using the Seinhorst equation for yield losses for Arabidopsis.

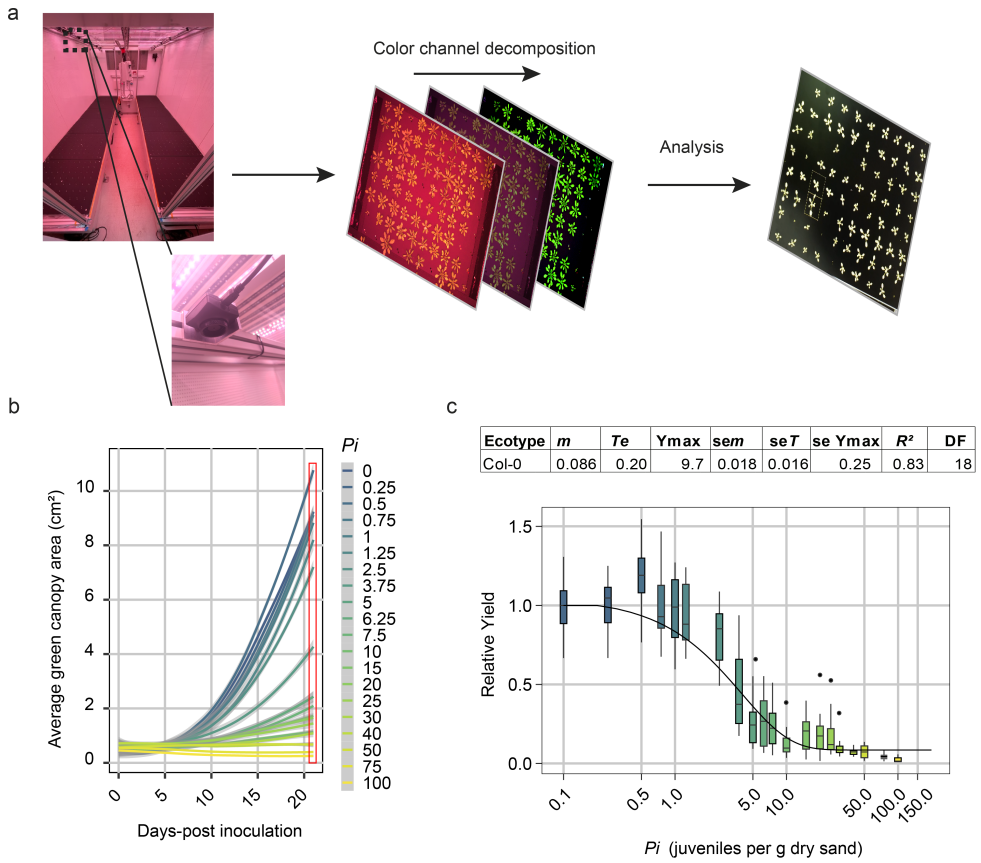

Ecotype	*m*	*Te*	Ymax	sem	seT	se Ymax	R^2	DF
Col-0	0.086	0.20	9.7	0.018	0.016	0.25	0.83	18

Figure 2: The relationship between the inoculation density (P_i) of *H. schachtii* and green canopy area (Relative Yield). Nine-day-old Arabidopsis seedlings were inoculated with 20 densities of *H. schachtii* juveniles (0 to 100 J2s per g dry sand) in 200 mL pots containing 200 grams of dry sand. **a)** Experimental setup and colour channel decomposition of photos to extract the green leaf surface from the images. **b)** Average growth curve of Arabidopsis plants inoculated with different inoculum densities of *H. schachtii* from 0-21 dpi. Line fitting was based on a LOESS regression. Red box indicates the data that is used for fitting the Seinhorst yield loss equation (n=10-24). **c)** Fitting according to the Seinhorst yield loss equation. Parameter values for Seinhorst's Eq. for the relation between initial population density (P_i) of *H. schachtii* and measured leaf surface area. P_i and tolerance limit (*Te*) are expressed in *H. schachtii* (g dry sand)$^{-1}$ while, the minimum yield (*m*) is the lowest proportion of the maximum green canopy area (cm^2) (Y_{max}) at 21dpi. The goodness of the fit of the model on the data is expressed as the coefficient of determination (R^2).

Quantifying tolerance limits on growth rates

The SYLM does not accommodate for compensation effects we observed at low inoculation densities (Fig. 2c). Based on the boxplots, the tolerance limit *Te* is between *Pi's* 1.25 and 2.5, whereas the SYLM placed it at 0.21. Another drawback of the SYLM is that data of a single timepoint of a series is tested for fit, ignoring changes over time. To take the dynamics in plant response into account, we sought an alternative way to quantify tolerance limits that uses all data collected over time (Fig. 2b). It is described that a delay in plant growth occurs at lower nematode densities and that higher nematode densities may lead to earlier cessation of growth (Seinhorst, 1986). Therefore, we extracted the growth rate (Equation 2) of plants inoculated with different nematode densities from 0 to 21 dpi to test if changes in growth rates can be used to determine tolerance limits.

First, we calculated the growth rate per day of individual plants that were inoculated with increasing *H. schachtii* densities (equation 2) (Fig. S4, S5, S6; Fig. 3a, b). Plants that were mock-inoculated showed a consistent growth rate in green canopy area between 5 and 15 dpi (Fig. 3c). Plants inoculated with P_i 0.75 or higher had a lower growth rate compared to mock-treated plants (Fig. 3c). From 15 dpi onwards, growth rates of mock-inoculated plants reached a stationary phase, while plants inoculated with nematodes (P_i 0.75 to 2.5) continued their exponential growth rate (Fig. 3d). Finally, we calculated the cumulative growth rate, which is the sum of all growth rates over time per plant (Fig. 3e), which showed that plants treated with P_i 1 or higher grew significantly slower compared to mock-inoculated plants. Based on these results, we conclude that the tolerance limit of Arabidopsis Col-0 to for *H. schachtii* is around P_i = 1.

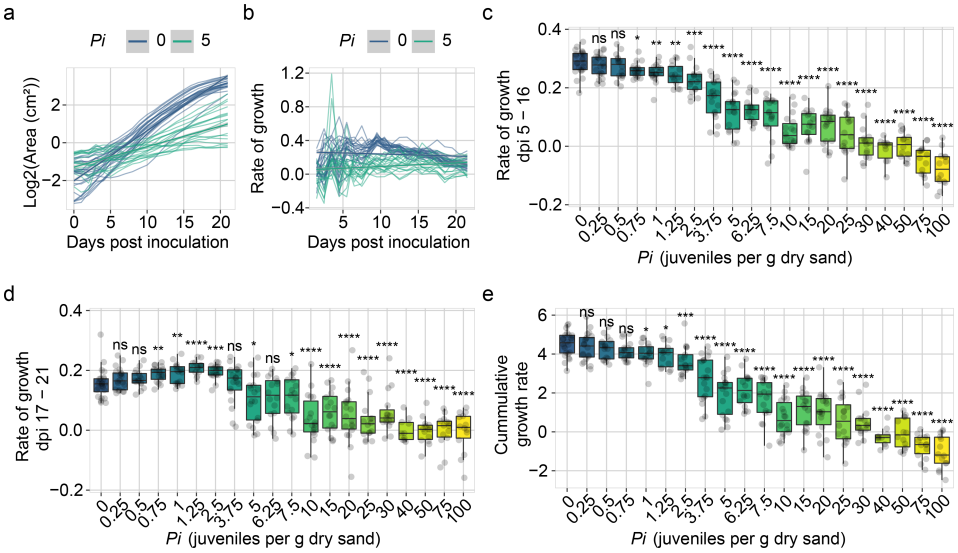

Figure 3: Quantification of tolerance limit of Col-0 to *Heterodera schachtii* based on growth rate. Nine-day old Arabidopsis seedlings were inoculated with 20 densities (P_i) of *H. schachtii* juveniles (0 to 100 juveniles per g dry sand). **a)** Green canopy area of plants treated with P_i 0 (blue line) or 5 (aquamarine line) from 0 to 21 days-post inoculation (dpi). **b)** Rate of growth of plants treated with P_i 0 (blue line) or 5 (aquamarine line) from 0 to 21 dpi was calculated using equation 2. **c)** Median rate of growth of plants inoculated with increasing P_i's growing from 5 to 16 dpi. **d)** Rate of growth (cm^2) of plants inoculated with increasing P_i's growing from 17 to 21 dpi. **e)** Cumulative growth rate of plants inoculated with increasing P_i's. **c-e)** Dots represent individual plants. Data was analysed with a Wilcoxon Rank Sum test; ns= not significant, *p< 0.05, **p< 0.01, ***p<0.001 (n=10-24).

Quantifying tolerance limit to *M. incognita*

Root-knot nematodes migrate through the roots intercellularly and therefore cause less damage than cyst nematodes. Hence, we hypothesized that the tolerance limit for *M. incognita* infections should be at a higher P_i than for *H. schachtii*. To this end, 320 nine-day old Arabidopsis seedlings were inoculated with 18 different densities (P_i 0 to 100) of *M. incognita* and monitored for 21 days. We fitted the data to the SYLM and found a *Te* of 0.57 (Fig. S7). Like we observed for *H. schachtii*-infected plants, we found that the model underestimates the *Te*. We thus also calculated the growth rates to capture the dynamics of the system (Fig. S8, Fig. 4a-e). Here, we observed that the growth rates of plants between 5 and 16 days-post inoculation were less affected by *M. incognita* than by *H. schachtii* (Fig. 4c). The growth rates of plants treated with P_i 1.25 or higher were significantly slower. From 17 to 21 dpi, we observed that plants inoculated with *M. incognita* at P_i 1 – 7.5 tended to have a higher growth rate than mock-inoculated plants (Fig. 4d). Plants inoculated with P_i 40 and 100 stopped growing altogether. Next, we calculated the cumulative growth rate, which showed that plants treated with P_i 2.5 or higher grow significantly slower compared to mock inoculated plants (Fig. 4e). Based on these results, we concluded that our high-throughput phenotyping system can also determine tolerance limits to root-knot nematodes and that the tolerance limit of *A. thaliana* Col-0 to *M. incognita* infection is around P_i 2.5.

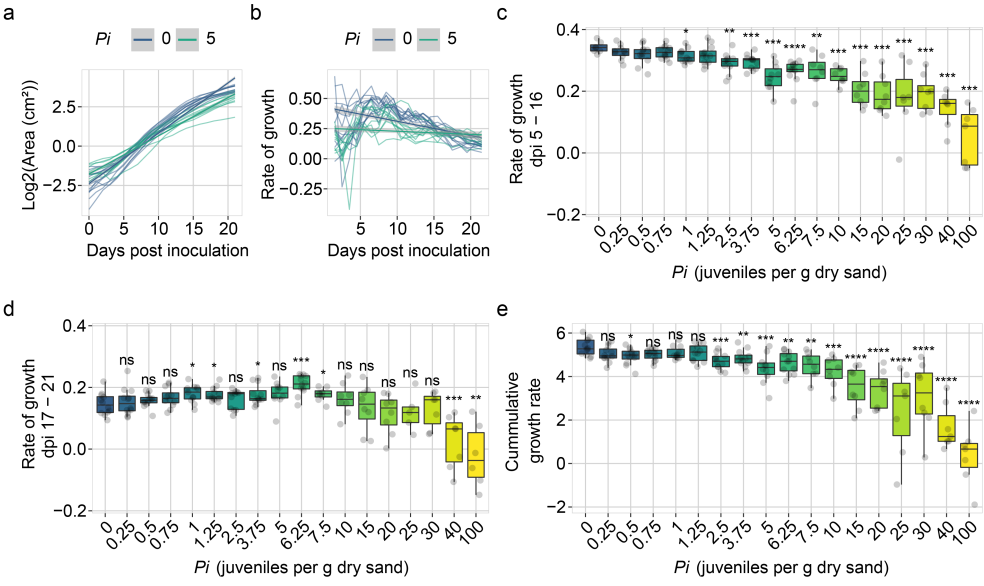

Figure 4: Quantification of tolerance limit of Col-0 to *Meloidogyne incognita* based on growth rate. Nine-day-old Arabidopsis seedlings were inoculated with 18 densities (P_i) of *M. incognita* juveniles (0 to 100 juveniles per g dry sand. **a)** Green canopy area of plants treated with P_i 0 (blue line) or 5 (aquamarine line) from 0 to 21 days-post inoculation (dpi). **b)** Rate of growth of plants treated with P_i 0 (blue line) or 5 (aquamarine line) from 0 to 21 dpi was calculated using equation 2. **c)** Rate of growth of plants inoculated with increasing P_i*'s* growing from 5 to 16 dpi. **d)** Rate of growth of plants inoculated with increasing P_i*'s* growing from 17 to 21 dpi. **e)** Cumulative growth rate of plants inoculated with increasing P_i*'s*. **c-e)** Dots represent individual plants. Data was analysed with a Wilcoxon Rank Sum test. ns= not significant, *p< 0.05, **p< 0.01, ***p<0.001 (n=10-12).

Arabidopsis Col-0 is more tolerant to *M. incognita* than to *H. schachtii*

Next, we correlated the growth rates of *M. incognita* inoculated plants to *H. schachtii* inoculated plants per timepoint and per inoculation density to determine if the growth rates of *A. thaliana* Col-0 are less affected by initial nematode densities of *M. incognita* than by *H. schachtii* (Fig. S9a and b). Both correlations based on timepoint and inoculum density between *H. schachtii* and *M. incognita* inoculated plants indicate that plants inoculated with *M. incognita* retain higher growth rates than plants inoculated with the same density of *H. schachtii*. Subsequently, we tested if there are significant differences between growth rates per P_i and per timepoint. For instance, we observed that *H. schachtii* infection has more impact on *A. thaliana* growth rates than *M. incognita* at P_i 5, especially from 5 to 10 dpi (Fig. S10a). From 11 to 21 dpi, the differences were smaller but often still significant. Then, we calculated the difference in growth rate by extracting the *H. schachtii* treated growth rates from the *M. incognita* treated growth rates per timepoint and P_i (Fig. S10b). We found that most of the growth rates of plants inoculated with *M. incognita* are higher than those of *H. schachtii* inoculated plants. Also, the largest differences in growth rates were visible from 5 to 10 dpi (Fig. S10b and c).

Pair-wise comparisons of green canopy areas between different treatments are cumbersome and drawing conclusions remain elusive. Therefore, we fitted and tested our growth dynamics of green canopy areas (Fig. 2, S7, 3, and 4) to a logistic growth model (equation 3) to determine if Arabidopsis Col-0 is more tolerant to *M. incognita* and *H. schachtii*. The logistic growth model determined the maximum canopy area and the intrinsic rate of growth. We found that the maximum canopy area K had relation with P_i that could be fitted with a Gaussian curve (equation 4) (Fig. 5a and c) and that the relation between the intrinsic growth rate r and P_i could be fitted with a hyperbolic curve (equation 5) (Fig. 5b and d). These fits allowed us to estimate the tolerance limits, which were P_i = 3.3 (95% CI: 3.0-3.7) for *H. schachtii* and 5.5 (95% CI: 4.6-6.4) for *M. incognita*. We therefore conclude that *A. thaliana* Col-0 probably is more tolerant to biotic stress by *M. incognita* infection than *H. schachtii*.

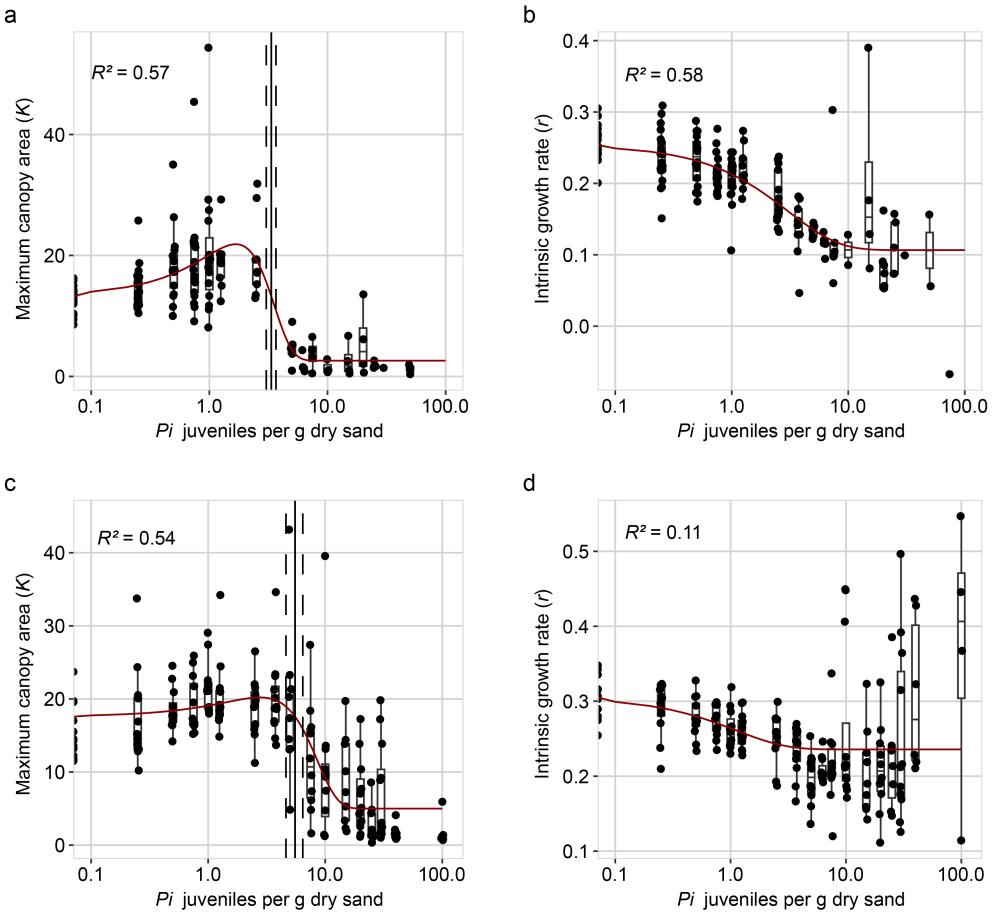

Figure 5: ***Arabidopsis thaliana* Col-0 is more tolerant to *Meloidogyne incognita* than *Heterodera schachtii*.** Fitted logistic growth rate parameters of *Arabidopsis thaliana* plants infected with *H. schachtii* or *M. incognita*. **a**) The maximum canopy area *K* per infection density of *H. schachtii*. The fitted line is from a Gaussian curve, the R^2 is from the fitted curve. **b**) The intrinsic growth rate *r* per infection density of *H. schachtii*. The fitted line is from an exponential model, the R^2 is from the fitted curve. **c**) Like (**a**) but for infections with *M. incognita*. **d**) like (**b**) but for infections with *M. incognita*. Solid line indicates the tolerance limit. Dashed line indicates the confidence interval.

Discussion:

Plants show intraspecific variation in how much damage by root-parasitic nematodes they can cope with before growth delays or ceases altogether (Potter and Dale, 1994). Unfortunately, uncovering the underlying molecular mechanisms of tolerance remains challenging and laborious since no tractable genetic model system is available. The goal of this research was twofold: (i) assess the suitability of *A. thaliana* as model for tolerance to root-parasitic nematodes and (ii) develop a high-throughput phenotyping platform to quantify and measure tolerance levels. The suitability of *A. thaliana* to measure tolerance was demonstrated with the beet cyst nematode *H. schachtii* and the root-knot nematode *M. incognita*. We present a high-throughput phenotyping platform that allows for the collection of continuous plant-growth data (here with a resolution of one data point per hour). Continuous data is an important improvement upon the end-point data which is normally used to determine tolerance levels of plants to nematode infection. Based on our findings, we believe that our phenotyping platform will enable us to uncover the underlying genetic mechanisms of tolerance.

We show that the green canopy area in *A. thaliana* is a suitable proxy to study tolerance limits and growth responses of plants to root-parasitic nematode infections in a high-throughput manner. Moreover, we were able to determine the tolerance limits of *A. thaliana* Col-0 to *M. incognita* than *H. schachtii.* The nematodes *H. schachtii* and *M. incognita* infect root tissues, but it is difficult and laborious to follow and quantify root development over time. Although we measured individual root traits, the throughput and therefore the data density were low. Similarly, although the output of the number of flowers gives a similar trend as the green canopy area and could pin-point at similar or other tolerance mechanisms, the throughput of this parameter is low compared to green canopy area measurements. Previously, it was shown that green canopies are suitable to monitor the effect of nematode infection on sugar beet (Joalland et al., 2016; Joalland et al., 2017). Therefore, we monitored green canopy area growth of individual plants in a non-destructive way by taking pictures. We showed that green canopy area is a good proxy for below-ground responses to nematode infection. Multiple root traits correlated well with the green canopy area. Furthermore, our approach allows to capture changes in growth rates in response to nematode infection over time. By identifying dynamic damage responses and compensatory growth rates of nematode-infected Arabidopsis plants, we were able to determine their tolerance limits. Even though we did not measure susceptibility (i.e. number of penetrations, feeding sites, or cysts/egg masses), tolerance measured by correlating yield to the initial density of nematodes, not the reproductive rate (P_f/ P_i) (Norshie et al., 2011; Teklu et al., 2022). Specifically, some susceptible plants (probably hosting more successful infections) are less affected than plants which are resistant (Evans, K., Franco, 1979). In other words, resistance and tolerance are genetically and physiologically different and independent traits. To our knowledge, this is the first time that tolerance limits are compared between nematode species.

We observed three distinct effects of infections by plant parasitic nematodes on plant growth-rate: an initial damage response, a growth rate-recovery at early timepoints, and a growth compensation response at later timepoints. First, we observed that plants showed an initial damage response by slowing growth rates shortly after *M. incognita* inoculation. The growth rates recovered four days later. Similar observations were made in root growth upon prolonged periods of invasion

by the cyst nematode *Heterodera avenae* (Rawsthorne and Hague, 1986). Secondly, we observed that *H. schachtii* inoculated plants grew significantly slower compared to *M. incognita* inoculated plants at 5 to 10 dpi under similar nematode inoculation densities. It is unclear whether the differential growth rates are due to differences in pathogenicity between the two nematode species, the types of damage that these two nematodes cause, or by the interaction of the nematode species and Arabidopsis. Thirdly, at the later timepoints (16-21 dpi), plants inoculated with lower dosages of *H. schachtii* and *M. incognita* showed increased growth-rates compared to mock-inoculated plants. To our knowledge, this is the first observation of – next to growth-recovery at early timepoints – growth-compensation at later stages of infection. Yield losses by nematodes could be minimized if characteristics like growth recovery and compensation are incorporated in breeding programs. However, this requires more insight in the genetic (in)dependence of these growth-response traits.

At lower nematode densities, we observed enhanced growth in the infected *A. thaliana* Col-0 plants. Earlier, we reported that at lower densities also *A. thaliana* Col-0 root-length increases at lower densities (Guarneri et al., 2023). Overcompensation, or hormesis, is a widely observed biological phenomenon, that has also been demonstrated in plants (reviewed in Agathokleous et al., 2019). It has also been shown for plant diseases (e.g. Flores & Garzon, 2013 & Di et al., 2016). However, in a quantitative relation to disease pressure on plants, including in nematode infections, hormesis has not been reported as far as we know. Rather, nematode infections are modelled using the SYLM framework (Sasanelli et al., 2013; Been et al., 2015; Moosavi, 2015). It is likely that the increased time-resolution, the high level of experimental control, and the high number of densities measured by our platform allowed measurements of this effect. It is possible that a biotic hormetic effect can be specific to nematodes, as it is well established that the initial density of nematodes relates to the damage caused (Brown, 1969; Seinhorst, 1986). In many other pathogens (e.g. viruses, fungi, bacteria) such dose-response relations are not to be expected as these replicate multiple times within a growth season whereas nematodes are comparatively slow.

There seems to be a link between the infection stages of the nematodes and the changes that we measured in growth-kinetics of host plants. The nematode infection process starts with root invasion, followed by migration through root tissue, after which feeding sites are formed leading to loss of assimilates via these feeding sites. First, we believe that the slower growth rate during the first four/five days is due to *M. incognita* and *H. schachtii* invasion and migration. A faster recovery response by the plant to *M. incognita* infection than to *H. schachtii* infection could have four reasons: 1) *M. incognita* needs less time to induce a feeding site and therefore the plant can continue growth faster, 2) *M. incognita* causes less stress due to its different way of invasion and migration, 3), *M. incognita* is a slow-moving nematode compared to *H. schachtii,* which gives the plant more time to heal the associated damage caused during root invasion and migration, or 4) the feeding site is induced at a different place in the root. Specifically, cyst nematodes can invade the root at different locations along the root axis, and subsequently migrate intracellularly through the cortex towards the vascular cylinder. Whereas root-knot nematodes invade the root at the root tip and migrate intercellularly through the cortex and the apical meristem to enter the vascular cylinder from below. (Wyss and Zunke, 1986; Wyss et al., 1992; Wyss, 1992; Kyndt et al., 2013). Finally, we measured a drop in growth speed, probably as a consequence of the loss of assimilates by nematodes feeding (Reviewed in Trudgill, 1991 & Grundler & Bockenhoff, 1997). After partial

growth recovery in response to lower nematode densities for *M. incognita* and *H. schachtii* treated plants, we observed that growth rates slowed down again around 7 dpi (Fig. S6 and S8). Mechanical or physiological damage during feeding site initiation and expansion, and consequently withdrawal of plant assimilates are important factors that contribute to reducing plant growth and delaying development (Trudgill, 1991). Being able to measure the effects of different nematode life stages (invasion/ migration and feeding) on plant growth could give new and interesting insights in how plants respond to different types of stress (i.e. mechanical damage versus loss of assimilates). Given we are able to phenotypically discriminate growth responses to different types of stresses indicates that tolerance is a complex trait. We hypothesize that tolerance is a combination of multiple (simultaneous) processes with each their own genetic architecture. Furthermore, it is possible that genotypic diversity in the root parasitic nematodes can also play a role in the tolerance response. For instance, it has been reported for various species that populations differ in infectivity and virulence on different plants (Storelli et al., 2021).

Our observation of the compensatory growth response shows that there are two limitations in the application of the SYLM on nematode-infected *A. thaliana*. First, the SYLM underestimates the tolerance limits *Te* for *H. schachtii* and *M. incognita* infections in Arabidopsis. Yet, the overall density response in our data fitted the model well. Similar observations were made previously where the *Te* strongly deviated between biological replicates (Teklu et al., 2022). We conclude that although the SYLM does not perform well at low-densities, it is suitable to predict minimum yields. Second, the SYLM is inefficient as it uses only end-point data (Seinhorst, 1986; Norshie et al., 2011; Sasanelli et al., 2013; Been et al., 2015; Moosavi, 2015), like tuber yield or shoot biomass. The SYLM does not capture the complex growth dynamics. Insight in the complex growth dynamics is necessary to separate different tolerance mechanisms.

To conclude, plants display intraspecific growth responses to nematode infection. These differences in tolerance levels are important agronomic trait of crops as they determine the level of stress that the plant can handle before growth is delayed. Due to the lack of a tractable genetic model system, the molecular mechanisms underlying tolerance remain elusive. Our high-throughput phenotyping platform is capable of monitoring the effect of nematode infection on the growth of the model plant *A. thaliana* will provide novel insights into how plants mitigate the impact of damage by nematodes and how plants try to compensate growth delays caused by the loss of assimilate by feeding nematodes. Specifically, our high-throughput phenotyping platform will provide opportunities to identify novel insights in the molecular and genetic mechanisms that underlies tolerant growth responses for instance by performing Genome-Wide Association Studies. Incorporating tolerance could provide an additional layer of protection for securing global food production besides disease resistance.

Supporting Information:

Additional Supporting Information and supplementary file with code may be found in the online version of this article.

Figure S1. Overview of experimental setup.
Figure S2. The primary root length and the green canopy area of Arabidopsis

responds in a density-dependent manner to infection by *Heterodera schachtii*.
Figure S3. Spearman correlation coefficients calculated between the average of different measurements of root components at seven-days post inoculation and green canopy area at eleven-days post inoculation.
Figure S4. Growth of Arabidopsis Col-0 plants inoculated with increasing densities of *Heterodera schachtii.*
Figure S5. Growth rate of Arabidopsis Col-0 plants inoculated with increasing densities of *Heterodera schachtii.*
Figure S6. Growth rate of Arabidopsis Col-0 plants inoculated with increasing densities of *Heterodera schachtii.*
Figure S7. The relationship between the inoculation density (P_i) of *Meloidogyne incognita* and green canopy area (Relative Yield).
Figure S8. Growth rate of Arabidopsis Col-0 plants inoculated with increasing densities of *Meloidogyne incognita.*
Figure S9. Correlations between growth rates of Arabidopsis Col-0 plants inoculated with *Heterodera schachtii* and *Meloidogyne incognita* per (a) dpi or (b) inoculum density.
Figure S10. Comparison of growth rates of Col-0 inoculated with *H. schachtii* and *M. incognita*.

Author contributions:

JJW, GS and MGS conceived the project. JJW and LD designed the high-throughput platform experiment. JJMS designed automated data collection software. JJW, DS, and CCS collected data. MGT provided scripts for SYLM analysis. Data analysis was designed by MGS with help from JJMS and data was analyzed and interpreted by JJW and MGS. JJW, GS, and MGS wrote the article. JLLT and AG provided critical feedback on the manuscript. All co-authors provided input for the submitted version.

Conflict of interest:

The authors declare no conflict of interest.

Funding statement:

This work was supported by the Graduate School Experimental Plant Sciences (EPS). JJW is funded by Dutch Top Sector Horticulture & Starting Materials (TU18152). JLLT was supported by NWO domain Applied and Engineering Sciences VENI (14250) and VIDI (18389) grants. MGS was supported by NWO domain Applied and Engineering Sciences VENI grant (17282).

Data availability:

All relevant data can be found within the manuscript, Github (https://git.wur.nl/published_papers/willig_2023_camera-setup), or protocols.io (DOI: dx.doi.org/10.17504/protocols.io.kqdg39167g25/v1). Also, the full picture dataset has been made available DOI: 10.6084/m9.figshare.23518923.

References:

Absmanner B, Stadler R, Hammes UZ (2013) Phloem development in nematode-induced feeding sites: The implications of auxin and cytokinin. Front Plant Sci **4**: 1–14

Agathokleous E, Kitao M, Calabrese EJ (2019) Hormesis: A Compelling Platform for Sophisticated Plant Science. Trends Plant Sci **24**: 318–327

Anwer MA, Anjam MS, Shah SJ, Hasan MS, Naz AA, Grundler FMW, Siddique S (2018) Genome-wide association study uncovers a novel QTL allele of AtS40-3 that affects the sex ratio of cyst nematodes in Arabidopsis. J Exp Bot **69**: 1805–1814

Baum TJ, Wubben MJ, Hardyy KA, Su H, Rodermel SR (2000) A Screen for Arabidopsis thaliana Mutants with Altered Susceptibility to Heterodera schachtii. J Nematol **32**: 166–73

Bebber DP, Holmes T, Gurr SJ (2014) The global spread of crop pests and pathogens. Global Ecology and Biogeography **23**: 1398–1407

Been TH, Teklu MG, Heve WK, Schomaker CH (2015) Damage thresholds and population dynamics of Meloidogyne chitwoodi on carrot (Daucus carota) at different seed densities. Nematology **17**: 501–514

Benjamini Y, Hochberg Y (1995) Controlling the False Discovery Rate: A Practical and Powerful Approach to Multiple Testing. Journal of the Royal Statistical Society: Series B (Methodological) **57**: 289–300

Brown EB (1969) Assessment of the damage caused to potatoes by potato cyst eelworm, Heterodera rostochiensis Woll. Annals of Applied Biology **63**: 493–502

Di YL, Cong ML, Zhang R, Zhu FX (2016) Hormetic effects of trifloxystrobin on aggressiveness of Sclerotinia sclerotiorum. Plant Dis **100**: 2113–2118

Evans, K., Franco J (1979) Tolerance to cyst-nematode attack in commercial potato cultivars and some possible mechanisms for its operation. Nematologica **25**: 153–162

Evans K, Haydock PPJ (1990) A review of tolerance by potato plants of cyst nematode attack, with consideration of what factors may confer tolerance and methods of assaying and improving it in crops. Annual applied Biology **117**: 703–740

Flores FJ, Garzon CD (2013) Detection and assessment of chemical hormesis on the radial growth in Vitro of oomycetes and fungal plant pathogens. Dose-Response **11**: 361–373

Grundler FMV, Bockenhoff A (1997) Physiology of Nematode Feeding and Feeding Sites. *In* C Fenoll, FMW Grundler, SA Ohl, eds, Cellular and Molecular Aspects of Plant-Nematode Interactions. Springer, Dordrecht, pp 107–120

Grunewald W, Cannoot B, Friml J, Gheysen G (2009) Parasitic nematodes modulate PIN-mediated auxin transport to facilitate infection. PLoS Pathog. doi: 10.1371/journal.ppat.1000266

Guarneri N, Willig J-J, Sterken MG, Zhou W, Hasan MS, Sharon L, Grundler FMW, Willemsen V, Goverse A, Smant G, et al (2023) Root architecture plasticity in response to endoparasitic cyst nematodes is mediated by damage signaling. New Phytologist **237**: 807–822

Joalland S, Screpanti C, Gaume A, Walter A (2016) Belowground biomass accumulation assessed by digital image based leaf area detection. Plant Soil **398**: 257–266

Joalland S, Screpanti C, Liebisch F, Varella HV, Gaume A, Walter A (2017) Comparison of visible imaging, thermography and spectrometry methods to evaluate the effect of Heterodera schachtii inoculation on sugar beets. Plant Methods **13**: 1–14

Jones JT, Haegeman A, Danchin EGJ, Gaur HS, Helder J, Jones MGK, Kikuchi T,

Manzanilla-López R, Palomares-Rius JE, Wesemael WML, et al (2013) Top 10 plant-parasitic nematodes in molecular plant pathology. Mol Plant Pathol 14: 946–961

Kyndt T, Vieira P, Gheysen G, de Almeida-Engler J (2013) Nematode feeding sites: Unique organs in plant roots. Planta **238**: 807–818

Lozano-Torres JL, Wilbers RHP, Warmerdam S, Finkers-Tomczak A, Diaz-Granados A, van Schaik CC, Helder J, Bakker J, Goverse A, Schots A, et al (2014) Apoplastic Venom Allergen-like Proteins of Cyst Nematodes Modulate the Activation of Basal Plant Innate Immunity by Cell Surface Receptors. PLoS Pathog. doi: 10.1371/journal.ppat.1004569

Miltner ED, Karnok KJ, Hussey RS (1991) Root Response of Tolerant and Intolerant Soybean Cultivars to Soybean Cyst Nematode. Agron J **83**: 571–576

Moosavi MR (2015) Damage of the root-knot nematode Meloidogyne javanica to bell pepper, Capsicum annuum. Journal of Plant Diseases and Protection **122**: 244–249

Norshie PM, Been TH, Schomaker CH (2011) Estimation of partial resistance in potato genotypes against Meloidogyne chitwoodi. Nematology **13**: 477–489

Olmo R, Cabrera J, Díaz-Manzano FE, Ruiz-Ferrer V, Barcala M, Ishida T, García A, Andrés MF, Ruiz-Lara S, Verdugo I, et al (2020) Root-knot nematodes induce gall formation by recruiting developmental pathways of post-embryonic organogenesis and regeneration to promote transient pluripotency. New Phytologist **227**: 200–215

Pagán I, Garcia-Arenal F (2020) Tolerance of Plants to Pathogens: A Unifying View. Annu Rev Phytopathol **58**: 77–96

Pedigo L, Hutchins SH, Higley LG (1986) Economic Injury Levels in Theory and Practice. Annu Rev Entomol **31**: 341–368

Potter JW, Dale A (1994) Wild and cultivated strawberries can tolerate or resist root-lesion nematode. HortScience **29**: 1074–1077

Quist CW, Smant G, Helder J (2015) Evolution of Plant Parasitism in the Phylum Nematoda. Annu Rev Phytopathol **53**: 289–310

Rawsthorne D, Hague NGM (1986) The effect of Heterodera avenae, on the root system of susceptible and resistant oat seedlings. Annals of Applied Biology **108**: 89–98

Sasanelli N, Vovlas N, Trisciuzzi N, Cantalapiedra-Navarrete C, Palomares-Rius JE, Castillo P (2013) Pathogenicity and host-parasite relationships of Heterodera cruciferae in cabbage. Plant Dis **97**: 333–338

Seinhorst JW (1986) Effects of nematode attack on the growth and yield of crop plants. *In* F Lamberti, CE Taylor, eds, Cyst Nematodes. Plenum Press, New York and London, pp 191–209

Shukla A, Pagán I, García-Arenal F (2018) Effective tolerance based on resource reallocation is a virus-specific defence in Arabidopsis thaliana. Mol Plant Pathol **19**: 1454–1465

Siddique S, Matera C, Radakovic ZS, Shamim Hasan M, Gutbrod P, Rozanska E, Sobczak M, Torres MA, Grundler FMW (2014) Parasitic Worms Stimulate Host NADPH Oxidases to Produce Reactive Oxygen Species That Limit Plant Cell Death and Promote Infection. Sci Signal **7**: 1–11

Sijmons PC, Grundler FMW, Mende N, Burrows PR, Wyss U (1991) Arabidopsis thaliana as a new model host for plant-parasitic nematodes. The Plant Journal **1**: 245–254

Storelli A, Kiewnick S, Daub M, Mahlein AK, Schumann M, Beyer W, Keiser A (2021) Virulence and pathogenicity of four Ditylenchus dipsaci populations on sugar beet. Eur J Plant Pathol **161**: 63–71

Teklu MG, Schomaker CH, Been TH, Molendijk LPG (2022) Tuber Yield, Quality and Infestation Levels of Potato Genotypes, Resistant to the Root-Knot Nematode, Meloidogyne chitwoodi. Potato Res **66**: 105–135

Trudgill DL (1991) Resistance to and tolerance of plants parasitic nematodes in plants. Annu Rev Phytopathol **29**: 167–192

Warmerdam S, Sterken MG, van Schaik C, Oortwijn MEP, Sukarta OCA, Lozano-Torres JL, Dicke M, Helder J, Kammenga JE, Goverse A, et al (2018) Genome-wide association mapping of the architecture of susceptibility to the root-knot nematode Meloidogyne incognita in Arabidopsis thaliana. New Phytologist 218: 724–737

Willig J-J, Guarneri N, van Steenbrugge JJM, de Jong W, Chen J, Goverse A, Lozano Torres JL, Sterken MG, Bakker J, Smant G (2022) The Arabidopsis transcription factor TCP9 modulates root architectural plasticity, reactive oxygen species-mediated processes, and tolerance to cyst nematode infections. Plant Journal **112**: 1070–1083

Wyss U (1992) Observations on the feeding behaviour of Heterodera schachtii throughout development, including events during moulting. Fundam Appl Nematol **15**: 75–89

Wyss U, Grundler FMW, Munch A (1992) The Parasitic Behaviour of Second-Stage Juveniles of Meloidogyne Incognita in Roots of Arabidopsis Thaliana. Nematologica **38**: 98–111

Wyss U, Zunke U (1986) Observations on the behaviour of second stage juveniles of Heterodera schachtii inside host roots. Revue de nématologie **9**: 153–165

Supporting information:

a b c

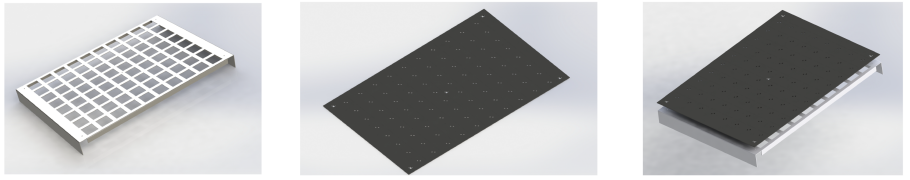

d e

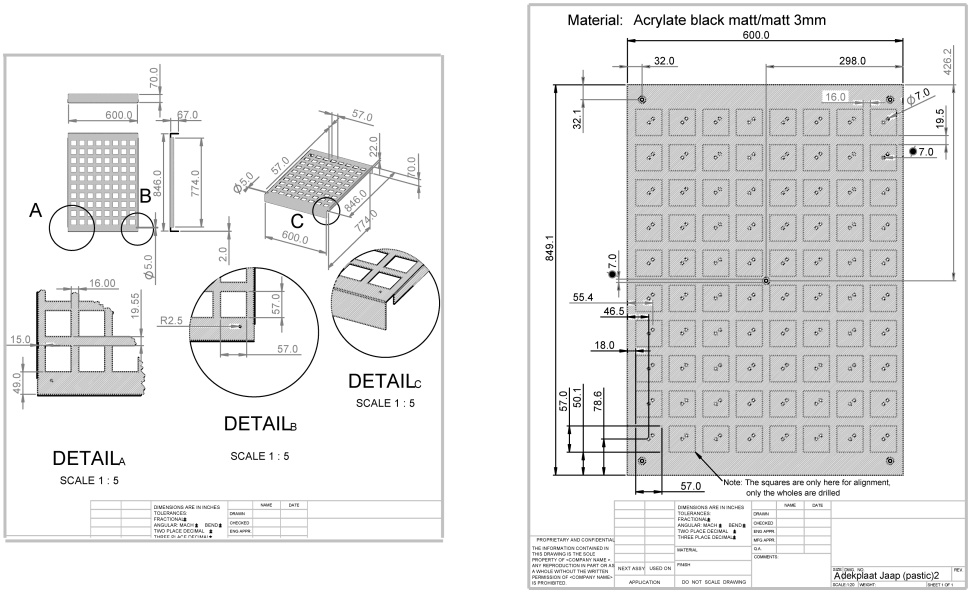

Figure S1: Overview of experimental setup. a and d) Stainless steel frames that we designed for holding pots. **b and e)** 3 mm thick black nonreflective foamed PVC coversheet drilled with countersunk holes and holes to inoculate nematodes. **c)** Black plates are attached to the aluminium frames with screws.

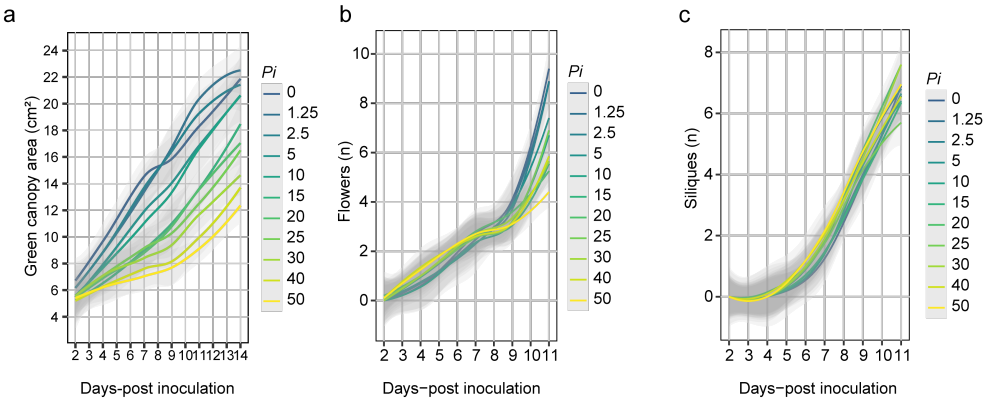

Figure S2: The primary root length and the green canopy area of Arabidopsis responds in a density-dependent manner to infection by *Heterodera schachtii*. Twenty-one-days-old Col-0 seedlings were inoculated with increasing densities of second-stage juveniles of *H. schachtii* (0-50 juveniles per g dry sand). At different timepoints, we counted the number of flowers and siliques (n=16-20). **a)** Effect of nematode inoculations on the green canopy over time. **b)** Effect of nematode inoculations on the number of flowers over time. **c)** Effect of nematode inoculations on the number of siliques over time.

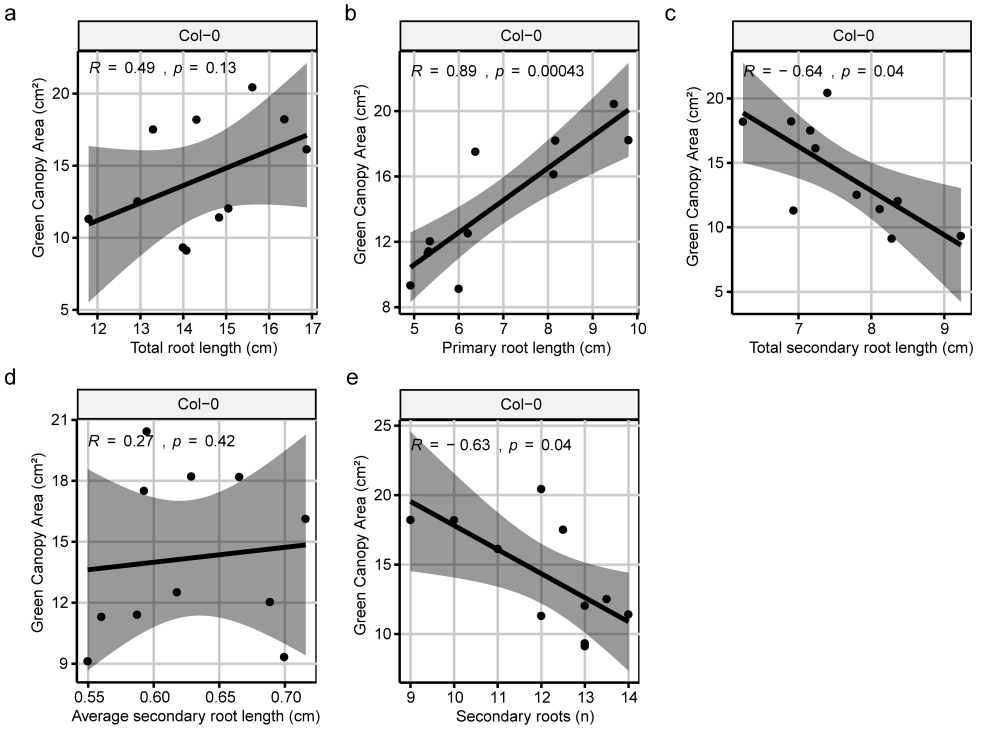

Figure S3: Spearman correlation coefficients calculated between the average of different measurements of root components at seven-days post inoculation and green canopy area at eleven-days post-inoculation. Spearman correlation coefficients were calculated on average values of 16-20 replicates of green canopy measurements and 24-30 replicates of root measurements using R software. **a)** Correlation between green canopy area and total root length. **b)** Correlation between green canopy area and primary root length. **c)** Correlation between green canopy area and total secondary root length. **d)** Correlation between green canopy area and average secondary root length. **e)** Correlation between green canopy area and the number of secondary roots.

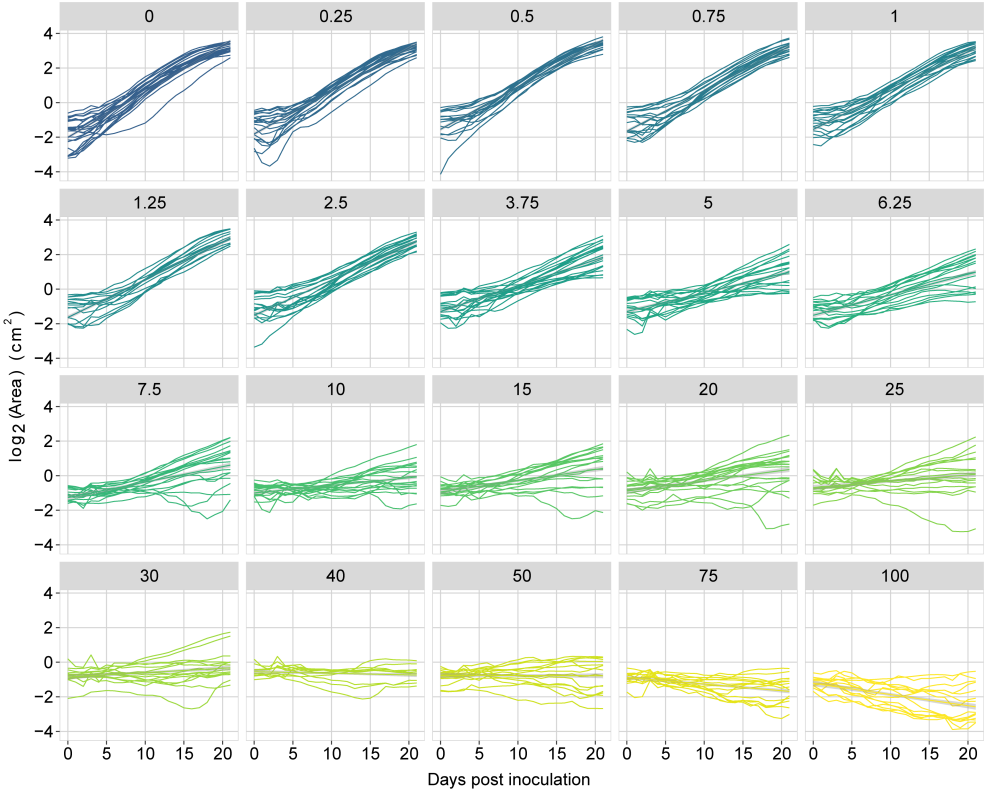

Figure S4: Growth of Arabidopsis Col-0 plants inoculated with increasing densities of *Heterodera schachtii*. Nine-day-old Arabidopsis seedlings were inoculated with 20 densities (P_i) of *H. schachtii* juveniles (0 to 100 juveniles per g dry sand). Lines represent the growth of individual plants.

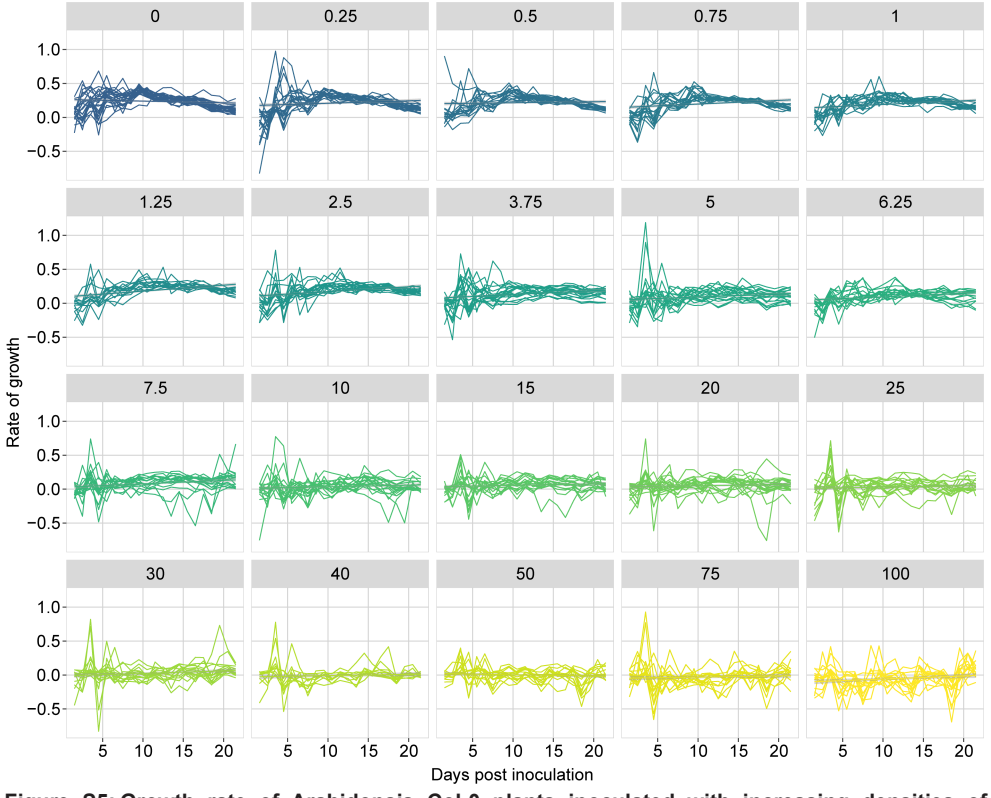

Figure S5: Growth rate of Arabidopsis Col-0 plants inoculated with increasing densities of *Heterodera schachtii*. Nine-day-old Arabidopsis seedlings were inoculated with 20 densities (P_i) of *H. schachtii* juveniles (0 to 100 juveniles per g dry sand). Lines represent the growth rates of individual plants.

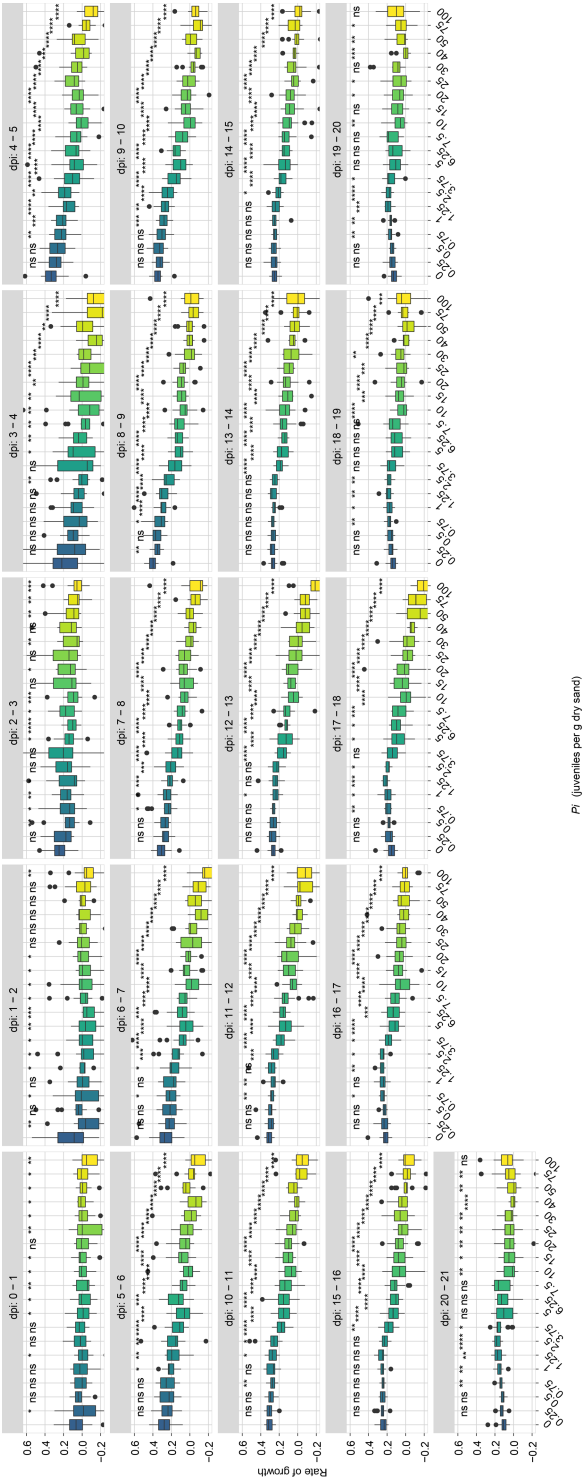

Figure S6: Growth rate of Arabidopsis Col-0 plants inoculated with increasing densities of *Heterodera schachtii*. Nine-day-old Arabidopsis seedlings were inoculated with 20 densities (P_i) of *H. schachtii* juveniles (0 to 100 juveniles per g dry sand). The growth rates of plants were calculated per day. Dots represent individual plants. Data was analysed with a Wilcoxon Rank Sum test. ns= not significant, *p< 0.05, **p< 0.01, ***p<0.001 (n=10-24).

Ecotype	*m*	*Te*	Ymax	se*m*	se*T*	se Ymax	*RSQ*	DF
Col-0	0.13	0.57	12.78	0.05	0.09	0.03	0.78	16

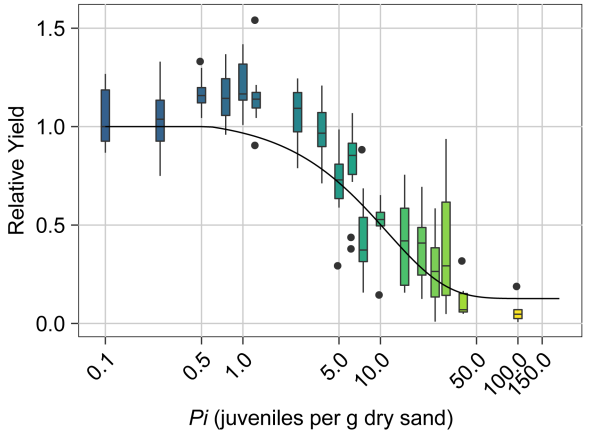

Figure S7: The relationship between the inoculation density (P_i) of *Meloidogyne incognita* and green canopy area (Relative Yield). Nine-day-old Arabidopsis seedlings were inoculated with 18 densities of *M. incognita* juveniles (0 to 20.000 J2s per pot) in 200 mL pots containing 200 grams of dry sand. Line was fitted according to the Seinhorst yield loss equation: $y = m + (1 - m)\ 0.95^{Pi/T-1}$ for $Pi > T$ and $y = 1$ for $Pi \leq T$. Parameter values for Seinhorst's Eq. for the relation between initial population density (P_i) of *H. schachtii* and measured leaf surface area. P_i and tolerance limit (T) are expressed in *M. incognita* (g dry sand)$^{-1}$ while, the minimum yield (m) is the lowest proportion of the maximum green canopy area (cm^2) (Y_{max}) at 21dpi. The goodness of the fit is expressed in the *RSQ*.

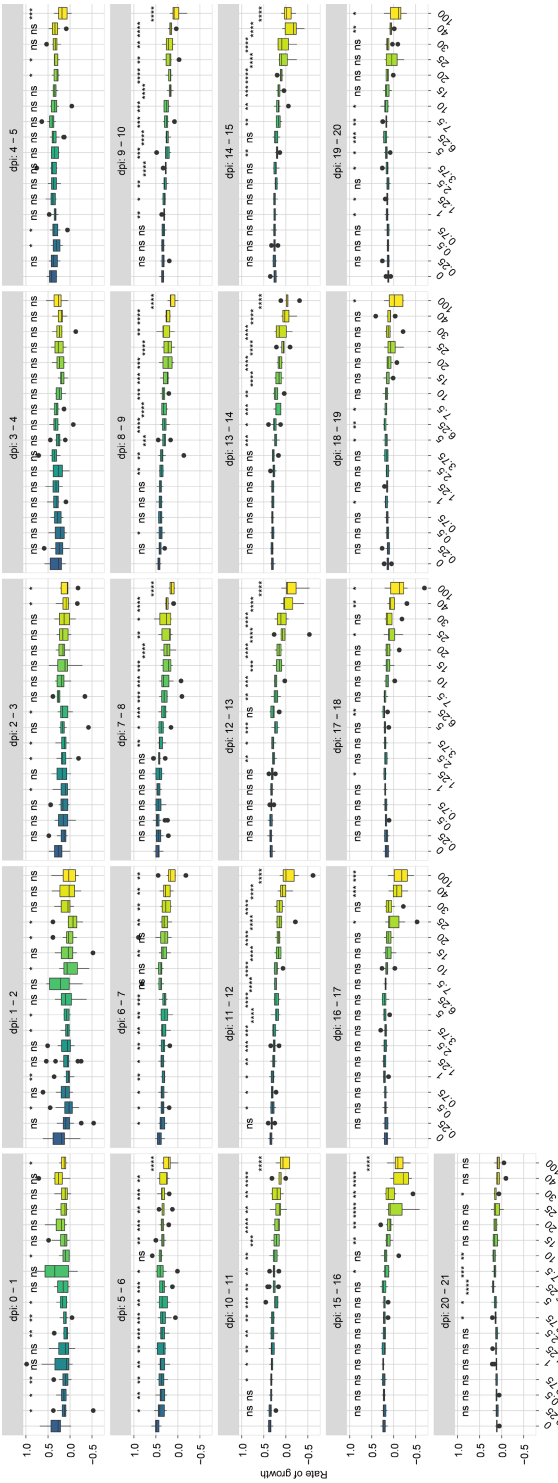

Figure S8: Growth rate of Arabidopsis Col-0 plants inoculated with increasing densities of *Meloidogyne incognita*. Nine-day-old Arabidopsis seedlings were inoculated with 18 densities (*Pi*) of *M. incognita* juveniles (0 to 100 juveniles per g dry sand). The growth rates of plants were calculated per day. Dots represent individual plants. Data was analysed with a Wilcoxon Rank Sum test. ns= not significant, *p< 0.05, **p< 0.01, ***p<0.001 (n=10-12).

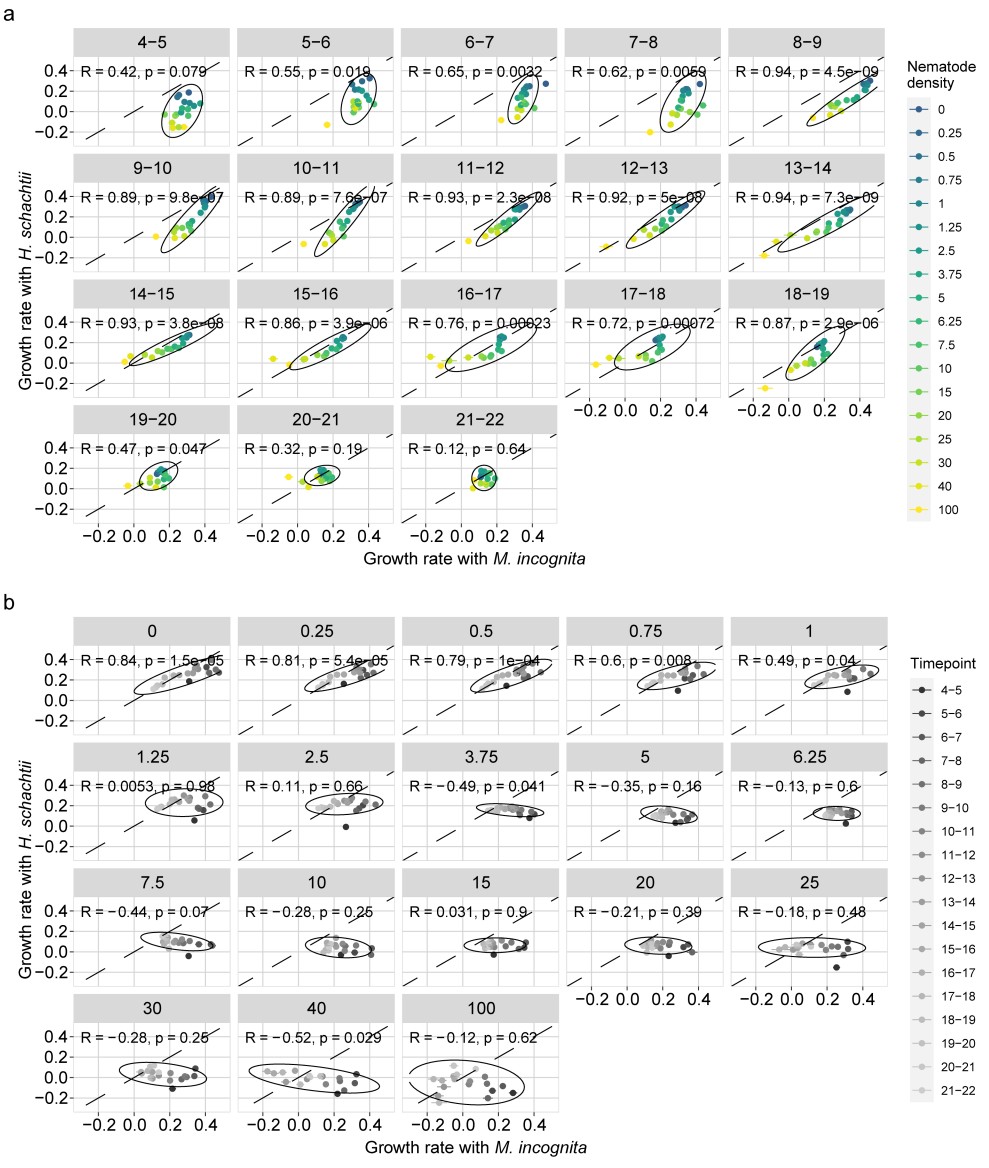

Figure S9: Correlations between growth rates of Arabidopsis Col-0 plants inoculated with *Heterodera schachtii* and *Meloidogyne incognita* per (a) dpi or (b) inoculum density. Nine-day-old Arabidopsis seedlings were inoculated with 18 densities (*Pi*) of *H. schachtii* and *M. incognita* juveniles (0 to 100 juveniles per g dry sand). The growth rates of plants were calculated per day. Dots represent the average growth rate. The correlation coefficient and p-values shown derive from a Pearson correlation.

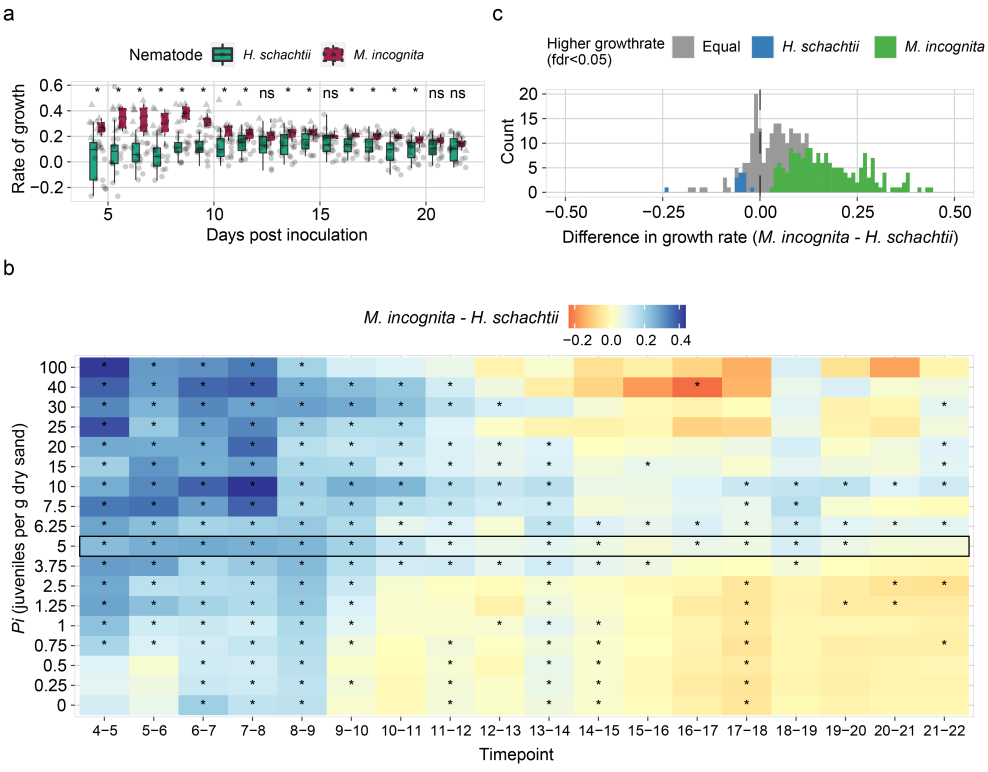

Figure S10: Comparison of growth rates of Col-0 inoculated with *H. schachtii* and *M. incognita*. Arabidopsis seedlings were inoculated with 18 densities (P_i) of *H. schachtii* juveniles or 18 P_i's of *M. incognita* (0 to 100 juveniles per g dry sand). Growth rates of green canopy areas were calculated from 0 to 22 dpi. **a)** Comparison of green canopy area growth rates of plants inoculated with P_i 5 of *H. schachtii* (full-line boxplots) and *M. incognita* (dashed-line boxplots) over time. **b)** Heatmap of the differential growth rate per P_i and timepoint. The difference in growth rate was calculated by subtracting the *H. schachtii* treated growth rates from the *M. incognita* treated growth rates per timepoint and P_i, blue indicates that *M. incognita* inoculated plants have a higher growth rate than *H. schachtii* inoculated plants and red indicates vice versa. **c)** Histogram of the number of occurrences that growth rates of *H. schachtii* and *M. incognita* inoculated plants significantly differ per P_i and timepoint. Blue represents significantly higher growth rates for *H. schachtii* inoculated plants, grey indicates no significant differences, and green represents significantly higher growth rates for *M. incognita* inoculated plants. Differences in growth rate between plants infected with either *H. schachtii* or *M. incognita* were tested using a paired t-test comparing data from the same day and density combination; ns= not significant, *p< 0.05 (n=10-24).

Chapter 3

Distinguishing tolerance from susceptibility; Genome-wide association mapping of plant responses of *Arabidopsis thaliana* to the beet cyst nematode *Heterodera schachtii*

Jaap-Jan Willig[1], Casper C. van Schaik[1], Rick Faesen[1], Dennie ten Molder[1], Mark G. Sterken[1], Geert Smant[1,2]

[1]Laboratory of Nematology, Wageningen University & Research, 6708PB Wageningen, The Netherlands
[2]Corresponding author

Abstract:

Plant-parasitic cyst nematodes inflict substantial damage to host plants by their intracellular migration through root tissue and by feeding on plant assimilates. This can lead to poor plant development and growth. However, plants show significant intraspecific variation in their growth responses to these soil-borne pathogens of which the underlying physiological and genetic mechanisms are still unknown. The recent development of a high throughput phenotyping platform allowed us to quantify aboveground growth responses of 154 *A. thaliana* ecotypes to increasing inoculation densities of the beet cyst nematode *H. schachtii*. Genome-wide association mapping of the variation in growth responses revealed two QTLs significantly linked to tolerance of Arabidopsis to *H. schachtii*. These two QTLs can be linked to 20 genes. Because the aboveground plant responses of Arabidopsis to nematodes infections can be a convolution of tolerance and susceptibility phenotypes, we also counted the number of successful infections (i.e., cysts) and mapped it to the genome of Arabidopsis. This revealed that susceptibility associated with 40 QTLs that can be linked to 209 genes. We found no overlap between the QTLs associated with the mean number of cysts per plant and the mean normalised green canopy area after inoculation with 2.5 juveniles per gram of soil. Finally, our analyses, show that aboveground growth responses to cyst nematode infections and the number of successful infections are distinct plant phenotypes. Altogether, we found ample leads for further research into tolerance genes.

Introduction:

Root-parasitic nematodes pose a significant threat to global food security. The annual damage due to plant-parasitic nematode infections in food crops accounts for more than 10% in yield loss (Jones et al., 2013; Bebber et al., 2014; Savary et al., 2019; Sikora et al., 2023). Nematode infections cause non-specific disease symptoms (e.g., aberrant root development, wilting, stunted growth), which can easily be confused with symptoms of abiotic stresses (e.g., drought and nutrient deficiency). For a long time, resistant crop cultivars and nematicides were used to control nematode outbreaks. However, since the implementation of a regulatory ban on non-selective nematicides within the EU in 2005 the diversity of parasitic nematode species challenging food crops has increased (Fuller et al., 2007; The European Commission, 2023). This diversity is too big be addressed by resistant cultivars alone due to the high specificity of major nematode resistances (Williamson and Hussey, 1996; Fuller et al., 2008). Moreover, resistance does not guarantee a high yield even when plants are lowly infected by nematodes. Some nematode-infected susceptible plants outperform resistant plants in terms of yield (Painter, 1951; Evans and Haydock, 1990a; Trudgill, 1991). This trait is known as nematode tolerance. Despite its high potential agronomic value, current knowledge of the genetics of nematode tolerance in plants is very limited. To address this knowledge gap, we focussed our research on the genetic architecture of tolerance of *Arabidopsis thaliana* to infections by the beet cyst nematode *Heterodera schachtii*.

Hitherto, scientific reports on nematode tolerance in crops are mainly observational (Fox and Spasoff, 1976; Evans and Haydock, 1990b; Trudgill, 1991; Norshie et al., 2011; Been et al., 2015; Teklu et al., 2022). Most of the work on tolerance relied on destructive end-point measurements (e.g., tuber weight or haulm height), which makes sense from a producer's point of view. However, tolerance constitutes a

complex trait with high yields likely arising from the culmination of multiple interacting physiological processes. Identifying which physiological processes contribute to tolerance and understanding how they interact to mitigate the impact of biotic stress caused by root feeding nematodes demands a closer look at plant responses (Willig et al., 2022; Guarneri et al., 2023; Willig et al., 2023). To this purpose, we developed a high throughput phenotyping platform to monitor aboveground plant responses of *A. thaliana* to increasing inoculation densities of *H. schachtii* at one-hour intervals continuously for three weeks after inoculation (Willig et al., 2023). We found that the green canopy area of Arabidopsis reflects belowground adaptations to nematode infections and that it can be used as a valid and reliable proxy to assess tolerance to root-feeding nematodes. Here, we report on the intraspecific variation in green canopy area as a measure of tolerance of 154 ecotypes of *A. thaliana* challenged with increasing inoculation densities of *H. schachtii*.

The ecotypes used for our research were drawn from the Arabidopsis collection of the 1001 Genomes Project, which provides a valuable resource for identifying natural genotypic and phenotypic variation in plants (Weigel and Mott, 2009). Genetic variation observed within this collection offers insights into the extensive diversity present within the *A. thaliana* gene pool. Representative ecotype panels of Arabidopsis have been used to resolve the genetic architecture of several complex traits (Thoen et al., 2017). For instance, genome-wide association (GWA) mapping has revealed quantitative trait loci (QTLs) in Arabidopsis associated with susceptibility to the root-knot nematode *Meloidogyne incognita* (Warmerdam et al., 2018). Likewise, it has been used to identify genomic loci in Arabidopsis associated with epigenetically regulated sex-determination in infective juveniles of *H. schachtii* (Anwer et al., 2018). At the outset of our research, we assumed that Arabidopsis would also harbour significant variation in tolerance to cyst nematode infections and that this variation can be used to identify loci in Arabidopsis associated with this trait.

We focussed our tolerance research on the beet cyst nematode *H. schachtii*, as an inducer of belowground stresses (Wyss, 1992; Grundler et al., 1994; Golinowski et al., 1996; Sobczak et al., 1997; Szakasits et al., 2009; Siddique et al., 2022). *H. schachtii* is particularly suitable for this purpose as it engages in a prolonged biotrophy with *A. thaliana*. At the start of an infection cycle, soil-borne infective juveniles of *H. schachtii* penetrate the roots of a host plant at the elongation zone, where they migrate intracellularly for several hours while causing substantial damage to host tissues (Wyss and Zunke, 1986; Wyss, 1992). Near the vascular cylinder, the juveniles inject effectors into host cells via their needle-like stylet, triggering their transformation into a syncytium (Rehman et al., 2009; Bohlmann and Sobczak, 2014). The syncytium functions as a permanent feeding structure providing juveniles access to the flow of assimilates, minerals, and water in the surrounding phloem and xylem. *H. schachtii* feeds on plant assimilates via the syncytium for several weeks. Depending on the nutrient supply, more juveniles develop into adult males, which inseminate nearby adult females to finally produce offspring. Thus, *H. schachtii* cause biotic stress on Arabidopsis by damaging host tissue, by establishing a permanent feeding structure within the vascular cylinder, and by consuming essential plant assimilates.

At present, little is known about tolerance mechanisms mitigating the impact of biotic stresses by root-feeding nematodes in plants. We hypothesize that adaptive growth responses of Arabidopsis to different types of nematode-induced stresses contribute to tolerance to cyst nematode infections. To test this hypothesis, we first asked if *A. thaliana* harbours significant aboveground variation in green canopy area as a proxy for the belowground impact of *H. schachtii* infections. Hereto, we inoculated

154 ecotypes of *A. thaliana* with six densities of *H. schachtii* and monitored the green canopy area over time for three weeks in a highly controlled climate room. As a single experiment could accommodate 960 Arabidopsis plants, we conducted in total five independent experiments over a period of three years. The image data of these runs was subsequently mapped on the genome of Arabidopsis using a total of 1,408,073 SNPs in a genome-wide association approach. Importantly, *A. thaliana* does not harbour major resistances to *H. schachtii*, which could otherwise make it difficult to specifically link aboveground plant responses to its ability to mitigate belowground stress by nematodes. Indeed, segregating resistance genes could result in different numbers of nematode per root system and thereby affect the level of belowground stress. In other words, in the latter case, the observed variation in plant responses would reflect a convolution of tolerance and susceptibility phenotypes. Nevertheless, Arabidopsis is known to harbour quantitative variation in susceptibility independent of major resistances (Anwer et al., 2018). We therefore also extracted matured cysts from soil of all inoculated Arabidopsis at the end of each experiment as an indication for plant susceptibility. This data was also mapped on the Arabidopsis genome to study if the underlying architectures of both tolerance and susceptibility are correlated. Altogether, our study sheds light on the complexity of tolerance of Arabidopsis to cyst nematode infections and provides important leads for further mechanistic studies into the underling physiological process.

Materials & Methods:

Arabidopsis thaliana ecotype selection and culturing

Ecotype selection and diversity check using principal component analysis

We randomly selected 154 accessions from the 1001 Arabidopsis genome project (Alonso-Blanco et al., 2016) (Fig. 1a). We obtained the genetic data of this population via https://1001genomes.org. The genetic diversity of this set was analysed using the kinship matrix (as generated by the A.mat function of rrBLUP (Endelman, 2011) in a principal component analysis in R (version) (Fig. 1b).

Plant culturing

Seeds of the Arabidopsis accessions were propagated in green house conditions (21°C). For *in vivo* pot experiments, Arabidopsis seeds were placed in Eppendorf tubes and stratified for 4 days. Prior to sowing, pots were filled with silver sand, covered with black coversheets, and were watered with Hyponex (1.7 mM/L NH_4^+, 4.1 mM/L K^+, 2 mM/L Ca_2^+, 1.2 mM/L Mg_2^+, 4.3 mM/L NO_3^-, 3.3 mM/L SO_4^{2-}, 1.3 mM/L $H_2PO_4^-$, 3.4 µm/L Mn, 4.7 µm/L Zn, B 14 µm/L, 6.9 µm/L Cu, 0.5 µm/L Mo, 21 µm/L Fe, pH 5.8) for five minutes. Seedlings were grown under 16 h LED light (150 µmol) at 21°C and 8 h dark at 19°C regime (Willig et al., 2023). Seven days after sowing, seedlings were watered again for five minutes. Nine-day-old seedlings were inoculated with increasing densities of *H. schachtii*.

Hatching and sterilization of *Heterodera schachtii*

H. schachtii juveniles were hatched as previously described (Willig et al., 2023). *H. schachtii* cysts (Woensdrecht population from IRS, the Netherlands) were separated from sand of infected *Brassica oleracea* plants as previously described (Baum et al., 2000). Cysts were soaked in water with 0.02% sodium azide for 20 min. Thereafter, sodium azide was removed by washing with tap water. Cysts were then incubated for 4-7 days in a solution containing 1.5 mg/mL gentamycin sulfate, 0.05 mg/mL nystatin and 3 mM $ZnCl_2$. Hatched J2s were purified by centrifugation on a 35% sucrose gradient and washed three times with tap water. Nematodes were resuspended in tap water before inoculation and subsequently inoculated.

High throughput analysis of green canopy area of nematode-infected Arabidopsis ecotypes

After seedlings were inoculated with *H. schachtii*, they were imaged and analyzed as previously described (Willig et al., 2023). In short, every hour pictures were taken of the plants (15 pictures per day) for a period of 21 days. At the end of the experiment, colour corrections were done using Adobe Photoshop (Version: 22.5.6 20220204.r.749 810e0a0 x64). The surface area of the rosette was determined using a custom-written ImageJ macro (ImageJ 1.51f; Java 1.8.0_321 [32-bit]) and Java was used to make GIFs.

Genetic variation test in growth responses and tolerance limits of twelve Arabidopsis ecotypes to *H. schachtii* infection

Before committing ourselves to the multiyear phenotyping experiment, we first wanted to obtain an initial insight in the genetic diversity in this panel. To select a diverse set of twelve ecotypes, we selected the six pairwise most divergent ecotypes among these 154 accessions based on the genetic map. Hereto, a set of twelve isolates was selected from our in-house panel based on genetic and geographical distribution: Cnt-1 (CS78782), Col-0 (CS76778), Duk (CS76824), FlyA 3 (CS76865), HS-12 (CS79015), Ler-1 (CS77021), Litva (CS76543), Lu3-30 (CS77057), NC-6 (CS77124), Panik-1 (CS77161), RLD-1 (CS76588), and Rmx-A180 (CS77218) (Fig. 1a). Nine-day old seedlings were inoculated with P_i of 0 to 50 *H. schachtii* juveniles per g dry sand. Plant growth was monitored as mentioned above. To analyse the growth data of the plants obtained from the high-throughput platform, we followed our previously published analytical pipeline using the same approach and the same functions (Willig et al., 2023); available via Gitlab: https://git.wur.nl/published_papers/willig_2023_camera-setup).

In short, the measurement used was the mean daily green canopy area (cm^2), calculated from the 15 images that were made per day. We used log_2-transformed data, where the rate of growth was determined per day per plant by (equation 1)

$$R_{x,t} = \log_2(A_{x,t-1} - A_{x,t})$$

where *R* is the transformed growth rate of plant *x* at day *t* from day *t-1* to day *t* based on the mean green canopy area *A*.

The tolerance limit was modelled using a previously described method based on fitting growth models (Willig et al., 2023). Here we fitted a logistic growth model using the *growthrates* package on the mean green canopy area *A* (cm^2) (equation 2),

$$A_t = \frac{K \times A_0}{A_0 + (K - A_0) \times e^{(-r \times t)}}$$

where *K* is the maximum green canopy area (cm^2), A_0 is the initial mean green canopy area (cm^2), and *r* is the intrinsic growth rate (t^1), which were determined as a function of time *t*. Due to the low number of replicates, we filtered the fits based on $p < 0.1$. Based on the relation between *K* and density we could identify the tolerance limit using (equation 3)

$$K = K_B + \frac{K_\sigma}{P_\sigma} \times e^{-\left(\frac{P_i - P_M}{P_\sigma}\right)^2}$$

where P_i is the initial nematode density in nematodes per gram soil, K_B is the basal canopy size ($t = 0$), K_σ is the normalized maximum canopy area that can be achieved over the P_i range, P_σ is the deviation around the nematode density allowing maximum growth, P_M is the nematode density at which maximum growth is achieved. We modelled the parameter values using *nls* and extracted confidence intervals using the *nlstools* package (Baty et al., 2015). The tolerance limit (*Te*), $2*P_M$, was determined as described in Willig et al., 2023.

Large-scale phenotyping experiment

For large-scale phenotyping, *A. thaliana* ecotypes were randomly assigned to five batches. In total, we conducted five independent experiments, in which ecotypes were exposed to six inoculation densities of *H. schachtii* ranging from a P_i of 0 to 7.5 juveniles per g dry sand. In each experiment, we included three technical replicates for each ecotype and P_i. Each ecotype was tested in at least two independent experimental runs. Cnt-1, Ler-1, Panik-1, FlyA3, NC-6, and Col-0 were tested in all six batches. For our experiments we randomized locations of ecotype but kept inoculation densities at fixed locations (to reduce the chance of errors). The measurement used was the mean daily green canopy area (cm^2), calculated from the 15 images that were made per day. Hereafter, we corrected for tolerance-independent growth differences between ecotypes by normalizing the green canopy area data to the growth of unchallenged seedlings.

At 35 days-post inoculation, shoots were removed and the pots with sand were left to dry. One week after the start of drying, sand was transferred to a paper bag and prepared for shipping to the NAK for cyst purification and collection (Randweg 114, 8304AS Emmeloord, The Netherlands). Coffee filters containing cysts were received few days/weeks later. Cysts were counted using a dissection microscope.

Hierarchical clustering analysis

Hierarchical clustering, using Euclidean distance matrices, were computed and visualized using the functions *dist* and *hclust* in R (R Core Team, 2019).To prevent cluster fragmentation (few ecotypes per cluster), we set the clustering height at 26, resulting in three large clusters containing at least 22 ecotypes.

Genome-wide association mapping of tolerance and susceptibility

To genetically map tolerance, we used the green canopy area data of the inoculation range from 0 – 2.5 to perform multiple linear regression analyses by ecotype across all time points post inoculation. To genetically map susceptibility, we used the mean number of cysts of plants inoculated with P_i 2.5. The mean regression coefficients and mean number of cysts were used as input for the GWA mapping using 1408073 SNPs using rrBLUP (Endelman, 2011). We used a kinship matrix based on all SNPs to correct for population structure, as calculated by the *A.mat* function. Second, association mapping was done, excluding SNPs with a frequency < 0.05 from analysis.

We calculated the significance threshold by determining the number of independent tests conducted in GWAS analysis using eigenvalue decomposition on the correlation matrix of the genetic map per chromosome (Li and Ji, 2005). The correlation matrix was calculated using the *cor* function, for the eigenvalues we used eigs_sym of the Rspectra package. We calculated the 1000 largest values and eigenvalues >1 were set to one. This led to an estimation of 900 independent tests conducted; which led to a corrected multiple testing threshold of $-\log_{10}(p) = 5.0$ ($p = 0.01$).

The linkage disequilibrium between significantly associated SNPs was calculated using correlation analysis. Per two locations the correlation between SNPs was calculated by Pearson correlation (using the *cor* function in R). The threshold for independence was set at $R^2 < 0.64$.

Broad-sense heritability

To estimate the amount of variation that can be explained by the genetic background of our selection of Arabidopsis ecotypes, we calculated the broad-sense heritability. The broad-sense heritability for tolerance and susceptibility was calculated using (equation 4)

$$H^2 = \frac{V_g}{V_g + V_e}$$

where H^2 is the broad-sense heritability, V_g is the genotypic variation explained by the Arabidopsis ecotypes, and V_e is residual variation. The V_g and V_e were estimated by the lme4 model $x_{norm} \sim 1 + (1|\text{ecotype})$ (Bates et al., 2015). The input data were the calculated slopes of the inoculation range from 0 – 2.5 per ecotype, and the average number of cysts found per Arabidopsis ecotype. The significance was determined by permutation analysis (1,000 times) where the trait values (calculated slopes or mean number of cysts) were randomly assigned to the ecotypes. Over

these permutated values, the variation captured by ecotypes and residuals were the calculated. The result obtained were used as the by-chance-distribution and an FDR = 0.05 threshold was taken.

Cross-correlating tolerance and susceptibility

Correlations between normalized median green canopy areas and the number of cysts that were collected from plants was calculated using Spearman correlation coefficient. The confidence interval of the inoculum density-response curves was calculated by loess regression (as per default in geom_smooth) in R. Cross correlations were confirmed using a PERMANOVA test using 1,000 permutations and the Manhattan method.

Results:

Aboveground variation in Arabidopsis growth response to nematode infections

Before committing to a large-scale multiyear phenotyping effort, we first asked if *A. thaliana* displays any significant intraspecific variation in aboveground plant responses to cyst nematode infections. To address this question, we selected twelve Arabidopsis ecotypes from our GWA panel based on a principal component analysis using single nucleotide polymorphisms which illustrates the genetic diversity (Fig. 1a and b). Next, nine-days-old seedlings of the twelve ecotypes were inoculated with ten different densities (P_i) of second stage juveniles of *H. schachtii* (P_i ranging from 0 to 50 juveniles per gram of soil). Thereafter, for three weeks, RGB pictures were taken at one-hour intervals and images were processed to capture the green canopy area per plant (Fig. S1). This demonstrated that the twelve *A. thaliana* ecotypes responded differently in aboveground growth while being exposed to increasing numbers of infective juveniles of *H. schachtii*.

We could roughly distinguish three differentiating patterns in the response of the green canopy area to increasingly higher inoculation densities of *H. schachtii* for the twelve ecotypes. In the first pattern, the ecotypes did not respond to increasing inoculation densities up until a threshold, above which the green canopy area declined. The ecotypes fitting this pattern showed variation in the range of inoculation densities wherein they remain unresponsive. Examples of this response pattern are the ecotypes Ler1 (Fig. 1c), Lu3-30 (Fig. S2e), and Litva (Fig. S2g). In the second response pattern, the green canopy area became bigger at low inoculation densities as compared to unchallenged plants (e.g., Col-0 and Panik 1 in Fig. 1c, and NC-6 in Fig. S2k). This phenomenon of enhanced growth at low inoculation densities is described in the literature as overcompensation or hormesis (Agathokleous et al., 2019; Willig et al., 2023). The ecotypes fitting this pattern differed in how much the growth of the green canopy area was stimulated by low inoculation densities. A third response pattern differentiating the ecotypes is the smallest green canopy area achieved at increasing inoculation densities. We found minor differences in this so-called minimum yield parameter, which is a function of the range of inoculation densities wherein the green canopy area showed a linear decline (Fig. S2). All ecotypes showed variation in this density range and in the minimum green canopy area.

Next, to quantify the differences in green canopy areas by ecotype, we estimated for each of the twelve ecotypes the tolerance limit (*Te*) after modelling the maximum green canopy area (*K*) (Fig. S2) and the intrinsic growth rate (*r*) (Fig. S3) using all data collected from 21 days of imaging. The tolerance limit approximates the P_i above which the maximum green canopy area becomes less than that of unchallenged plants (Willig et al., 2023). Our analysis revealed a large variation in tolerance limits among the twelve ecotypes, with a thirty-fold difference between the most and the least tolerant ecotype (Fig. 1c; Table 1). Notably, the calculated maximum green canopy area of some ecotypes generated a relatively poor fit (R^2) in a logistic growth model (e.g., Col-0 and Panik-1), because they performed better at low inoculation density than when unchallenged by *H. schachtii* (Fig. S2). Altogether, based on our findings we concluded that our GWAS panel of Arabidopsis most likely harboured sufficient quantitative variation in tolerance to *H. schachtii* to justify a multiyear phenotyping effort.

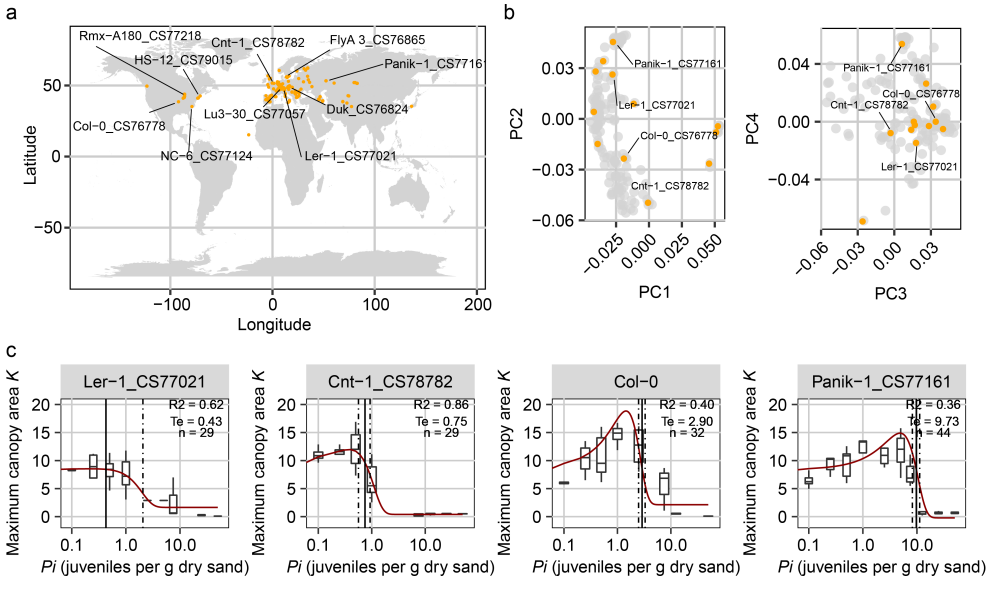

Figure 1: **Variation in tolerance limits of *Arabidopsis thaliana* ecotypes to *Heterodera schachtii* infection. a)** Geographical distribution of our inhouse Arabidopsis ecotype panel (n = 154) and selection of twelve ecotypes. **b)** Principal component analysis of our inhouse Arabidopsis ecotypes using single nucleotide polymorphisms. Yellow dots indicate the twelve selected Arabidopsis ecotypes. **c)** Nine-day-old *Arabidopsis thaliana* seedlings were inoculated with 10 densities (P_i) of *H. schachtii* juveniles (0 to 50 juveniles per g dry sand). The green canopy area was imaged for a period of 21 days and fitted to a logistic growth rate model. The maximum canopy area *K* per inoculation density of *H. schachtii* of ecotypes Cnt-1, Ler-1, Col-0, and Panik-1. Other ecotypes that are tested can be found in Fig. S1. The fitted line is from a Gaussian curve. The fitted line is from a hyperbolic curve. Solid line indicates the tolerance limit. Dashed line indicates the confidence interval. R^2 is the goodness of fit, *Te* is the tolerance limit, n is the total number of plants used for fitting the curve. Model output can be found in Table 1.

Table 1: Output of logistic growth rate model for twelve *Arabidopsis thaliana* ecotypes. Nine-day-old *Arabidopsis thaliana* seedlings were inoculated with 10 densities (P_i) of *H. schachtii* juveniles (0 to 50 juveniles per g dry sand. The green canopy area was imaged for a period of 21 days and fitted to a logistic growth rate model. *Te* is the tolerance limit in expressed in P_i, CI is the confidence interval of *Te*, R^2 (*K* model) represents the goodness from the fitted curve for the maximum green canopy area, and R^2 (*r* model) represents the goodness from the fitted curve for the intrinsic growth rate.

Ecotype	*Te*	CI	R^2 (*K*)	R^2 (*r*)
Ler-1_CS77021	0.43	-1.21 - 2.07	0.62	0.21
Cnt-1_CS78782	0.75	0.57 - 0.93	0.86	0.00
RLD-1_CS76588	0.85	-0.50 - 2.20	0.85	0.50
Rmx-A180_CS77218	1.24	0.55 - 1.94	0.77	0.00
Lu3-30_CS77057	1.66	0.65 - 2.67	0.65	0.05
Col-0_CS76778	2.90	2.48 - 3.30	0.40	0.43
Litva_CS76543	3.13	1.27 - 4.99	0.61	0.49
HS-12_CS79015	3.38	0.49 - 6.27	0.80	0.72
FlyA 3_CS76865	4.75	1.63 - 7.88	0.46	0.57
Duk_CS76824	4.77	3.58 - 5.96	0.47	0.00
NC-6_CS77124	6.83	5.39 - 8.28	0.50	0.56
Panik-1_CS77161	9.73	8.25 - 11.21	0.36	0.56

Majority of Arabidopsis ecotypes show tolerance responses

To be able to identify genetic loci associated with aboveground plant growth responses of *A. thaliana* to *H. schachtii*, we expanded our phenotyping effort to 154 ecotypes (Fig. 1a). Our platform can accommodate 960 Arabidopsis seedlings (Willig et al., 2023), because of which we conducted the experiment in batches. In total, we conducted five independent experiments over a period of three years. Each ecotype from our GWA panel was tested in at least two independent experimental runs. Six ecotypes (i.e., Cnt-1, Ler-1, Panik-1, FlyA3, NC-6, and Col-0) were included in every experiment to able to correct for possible batch effects between experiments. Furthermore, instead of challenging the Arabidopsis seedlings with ten inoculation densities ranging from 0 to 50 infective juveniles per gram of soil, we inoculated the seedlings with six densities ranging from 0 to 7.5 infective juveniles per gram of soil. As was shown in our pilot experiment, the tolerance limits of almost all ecotypes fall within this range (Table 1). The data of four ecotypes had to be excluded from further analysis because of poor germination efficiency. Furthermore, we corrected for tolerance-independent growth differences between ecotypes by normalizing the green canopy area data to the growth of unchallenged seedlings.

In total, we collected almost 1.5 million RGB images capturing the green canopy area of 154 ecotypes, at six inoculation densities, of 3 replicates at 21 different timepoints post inoculation. To reduce this overwhelmingly large data set into growth response patterns, we first performed a hierarchical cluster analysis of all ecotypes based on similarity in responses to *H. schachtii* at 21 dpi only (threshold *Height* was set to 26). We identified three major clusters, the largest of which harbours 73 ecotypes which remained unresponsive to increasing inoculation densities of *H. schachtii* (Fig. 3a). The second largest cluster harbours 55 ecotypes showing a decline in green canopy area from the lowest inoculation density onwards (Fig. 3b and c). The smallest cluster contains 22 ecotypes showing overcompensation to *H. schachtii* inoculation first and thereafter a decline in green canopy area.

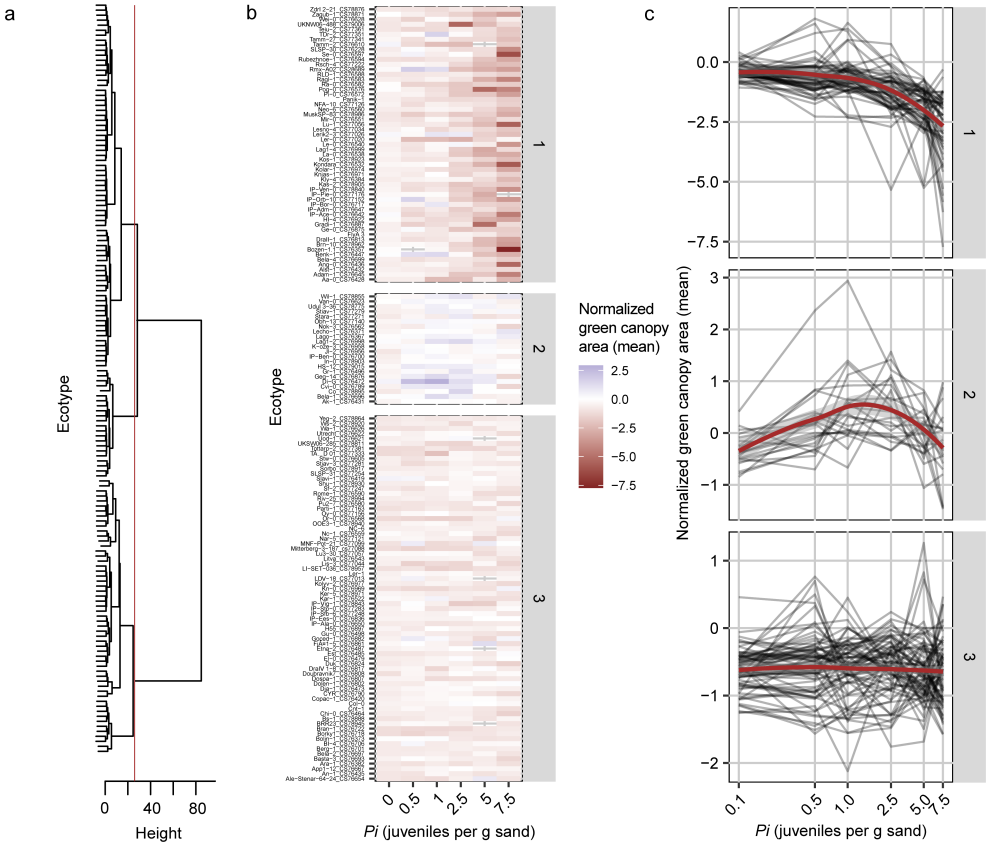

Figure 3: **Growth responses of *A. thaliana* to *H. schachtii* can be captured in three clusters.** One hundred fifty nine-day-old *Arabidopsis thaliana* ecotypes were inoculated with six densities (P_i) of *H. schachtii* juveniles (0 to 7.5 juveniles per g dry sand). The green canopy area was imaged for a period of 21 days. **a)** Dendogram of hierarchical cluster analysis (McQuitty's method) on similarities (Euclidean distance) between growth responses of Arabidopsis ecotypes to *H. schachtii* using the mean normalized green canopy area. The clustering height was set to 26, resulting in three clusters. **b)** Heatmap of three largest clusters of normalized mean green canopy area of *A. thaliana* plants after *H. schachtii* inoculation. Colouring indicates mean normalized green canopy area (cm^2). **c)** Three clusters of growth response of infected *A. thaliana* plants. Black lines indicate the mean normalized green canopy area (cm^2) of a single *A. thaliana* ecotype. Red line indicates the average normalized green canopy area of all *A. thaliana* ecotypes in a cluster.

Two QTLs for tolerance to *H. schachtii* in Arabidopsis

In our cluster analysis of the data at 21 dpi, we observed the starkest contrast between the three clusters within the range of 0 and 2.5 juveniles per gram of soil. We therefore used the data of this inoculation range to perform multiple linear regression analyses by ecotype across all time points post inoculation. The mean regression coefficients of overcompensating ecotypes are expected to be positive in this analysis. The mean regression coefficients of tolerant ecotypes are close to zero, whereas intolerant ecotypes display a negative mean regression coefficient. Figure 4a shows the variation in the mean regression coefficients (i.e., slope) of 154 ecotypes by density range 0 – 2.5 juveniles per gram soil by time point post inoculation. We found significant variation in growth responses among the Arabidopsis ecotypes, much of which can be explained by genetic variation in Arabidopsis (broad sense heritability R2 = 40%, FDR < 0.001). This data was subsequently used to identify genomic loci in Arabidopsis associated with the mean regression coefficient using linear mixed models in a GWA mapping approach. Only SNPs with a minor allele frequency above 0.05 were included, totalling to 1,408,073 SNPs. We identified significant associations between four SNPs and tolerance to *H. schachtii* in Arabidopsis (threshold for significance $-\log_{10}(P) > 5$; Fig. 4b). Assuming that the linkage disequilibrium (LD) decays within 10 kb (Kim et al., 2007), we aggregated the four SNPs into two QTLs located on two chromosomes (Table 2), which are linked to 20 unique genes. As expected, through analysis, we found a strong LD between SNPs located on chromosome 3 (Fig. S4). A lower LD was observed between the SNPs located on chromosome 5. In conclusion, allelic variation in at least 2 genome locations is linked to quantitative variation in tolerance to *H. schachtii* in our population of Arabidopsis ecotypes.

The genetic architecture of susceptibility to *H. schachtii* in Arabidopsis

The aboveground plant responses of Arabidopsis to nematodes infections can be a convolution of tolerance and susceptibility phenotypes. To assess if the 154 Arabidopsis ecotypes in our GWAS panel also differ in susceptibility to *H. schachti*, we extracted matured cysts from the soil at 35 days after inoculation with 2.5 juveniles per gram of soil. We found significant variation in offspring size among the Arabidopsis ecotypes ranging from 0 to 13 cysts per plant, much of which can be explained by genetic variation in Arabidopsis (broad sense heritability R2 = 31%, FDR < 0.001). Next, we analysed the data of cyst counts in a GWA approach to identify significantly associating SNPs in the genome of Arabidopsis. We identified significant associations between 78 SNPs and susceptibility to *H. schachtii* in Arabidopsis (threshold for significance $-\log_{10}(P) > 5$; Fig. 5b). Similar as we did for acquiring the tolerance QTLs, we aggregated the 78 SNPs into 40 QTLs located on five chromosomes (Table S1), which are linked to 209 unique genes. As expected, through analysis, we found strong LDs between SNPs located on chromosome 3, 4, and 5 (Fig. S5). Lower LDs were observed between the SNPs located on chromosome 1, 2, and 3. In conclusion, allelic variation in at least 28 genome locations are linked to quantitative variation in susceptibility to *H. schachtii* in our population of Arabidopsis ecotypes. Importantly, we found no overlap between the QTLs associated with the mean number of cysts per plant and the mean normalised green canopy area after inoculation with 2.5 juveniles per gram of soil.

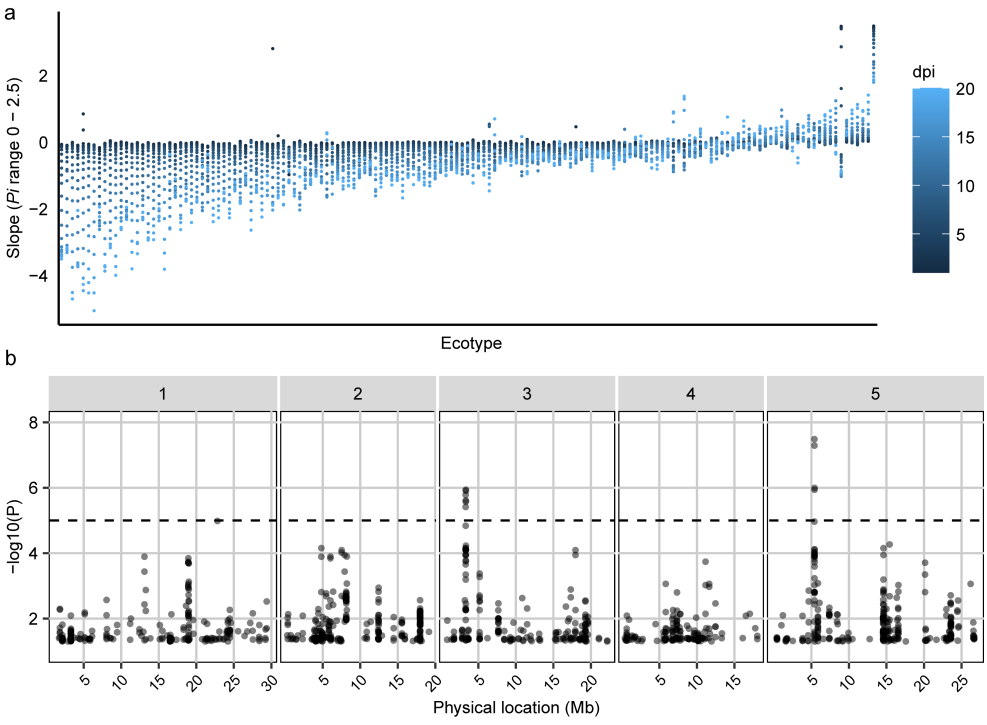

Figure 4: **Quantitative variation in tolerance to the cyst nematode *Heterodera schachtii* is associated with five/two loci in the *Arabidopsis thaliana* genome.** One hundred fifty nine-day-old *Arabidopsis thaliana* ecotypes were inoculated with 4 densities (P_i) of *H. schachtii* juveniles (0 to 2.5 juveniles per g dry sand). The green canopy area was imaged for a period of 21 days. **a)** Mean regression coefficients were calculated by performing linear regressions of the mean normalised green canopy area across the P_i range. **b)** Manhattan plot of significant associations between 1.408.073 single nucleotide polymorphisms (SNPs) and (**a**) the regression coefficients of density P_i ranges 0 to 2.5. Dashed horizontal line indicates threshold for significance in genome-wide association mapping set at $-\log_{10}(P) = 5$ (a). Number 1-5 in grey rectangles mark the five chromosomes of *A. thaliana*.

Table 2: Four single nucleotide polymorphisms (SNPs) significantly associated with tolerance to *Heterodera schachtii* aggregate into two quantitative trait loci (QTLs) located on two chromosomes of Arabidopsis

QTL	Chr.	Position	SNP[a]	-Log$_{10}$(*P*)[c]	gene_AraID	Symbol
1	3	3,319,104	G:T	5.783	AT3G10610	RPS17C
					AT3G10630	
					AT3G10650	AtNUP1
					AT3G10600	CAT7
					AT3G10590	
					AT3G10640	VPS60.1
					AT3G10595	
					AT3G10605	
		3,339,456	T:C	5.940	AT3G10690	GYRA
					AT3G10700	GalAK
					AT3G10680	SLI1
					AT3G10670	ABCI6
					AT3G10660	ATCPK2
3	5	5,404,504	T:A	7.486	AT5G16520	
					AT5G16550	
					AT5G16560	KAN1
					AT5G16540	ZFN3
					AT5G16530	PIN5
		5,416,765	T:C	5.996	AT5G16580	BGLU2
					AT5G16570	GLN1;4

The genetic architecture of susceptibility to *H. schachtii* in Arabidopsis

The aboveground plant responses of Arabidopsis to nematodes infections can be a convolution of tolerance and susceptibility phenotypes. To assess if the 154 Arabidopsis ecotypes in our GWAS panel also differ in susceptibility to *H. schachti*, we extracted matured cysts from the soil at 35 days after inoculation with 2.5 juveniles per gram of soil. We found significant variation in offspring size among the Arabidopsis ecotypes ranging from 0 to 13 cysts per plant, much of which can be explained by genetic variation in Arabidopsis (broad sense heritability R2 = 31%, FDR < 0.001). Next, we analysed the data of cyst counts in a GWA approach to identify significantly associating SNPs in the genome of Arabidopsis. We identified significant associations between 78 SNPs and susceptibility to *H. schachtii* in Arabidopsis (threshold for significance -log$_{10}$(P) > 5; Fig. 5b). Similar as we did for acquiring the tolerance QTLs, we aggregated the 78 SNPs into 40 QTLs located on five chromosomes (Table S1), which are linked to 209 unique genes. As expected, through analysis, we found strong LDs between SNPs located on chromosome 3, 4, and 5 (Fig. S5). Lower LDs were observed between the SNPs located on chromosome 1, 2, and 3. In conclusion, allelic variation in at least 28 genome locations are linked to quantitative variation in susceptibility to *H. schachtii* in our population of Arabidopsis ecotypes. Importantly, we found no overlap between the

QTLs associated with the mean number of cysts per plant and the mean normalised green canopy area after inoculation with 2.5 juveniles per gram of soil.

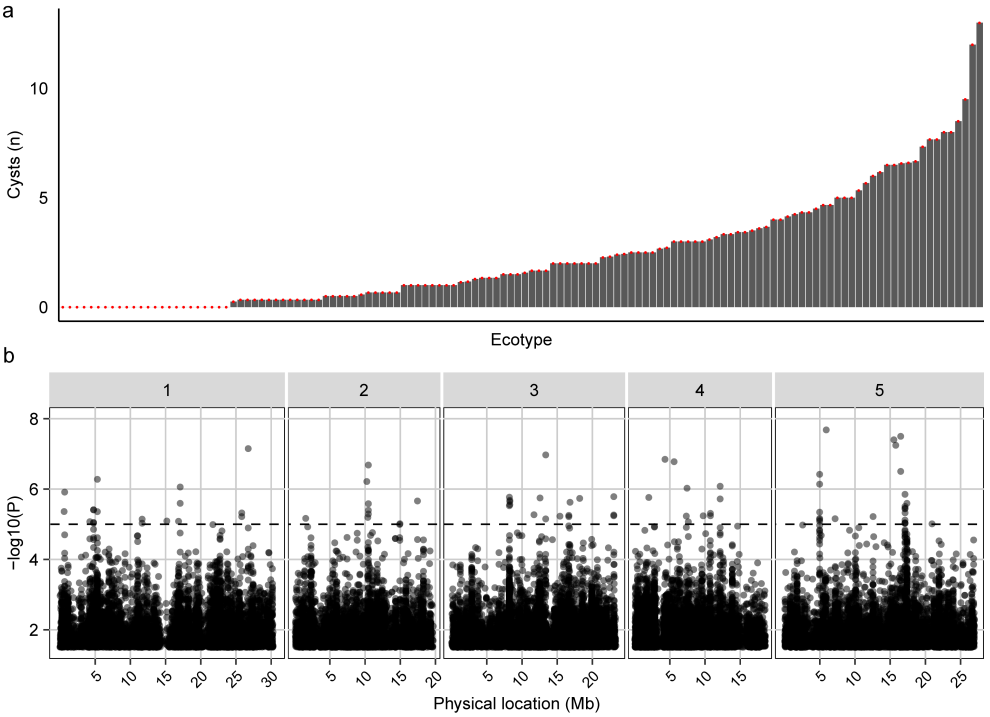

Figure 5: **Quantitative variation in susceptibility to the cyst nematode *Heterodera schachtii* associates with genomic variation in *Arabidopsis thaliana*.** One hundred fifty nine-day-old *Arabidopsis thaliana* ecotypes were inoculated with a density of 2.5 *H. schachtii* juveniles per g dry soil. Cysts were extracted from the soil at 35 dpi. **a)**. Mean number of cysts per plant per ecotype. **b)** Manhattan plot of significant associations between 1.408.073 single nucleotide polymorphisms (SNPs) and (**a**) the mean number of cysts per plant. Dashed horizontal line indicates threshold for significance in genome-wide association mapping set at $-\log_{10}(P) = 5$ (a). Number 1-5 in grey rectangles mark the five chromosomes of *A. thaliana*.

Aboveground plant response and nematode reproduction are distinct phenotypes

To investigate if aboveground plant responses to cyst nematode offspring are at least partly distinct phenotypes, we performed a Spearman correlation analysis on the green canopy area at 21 dpi and cyst counts by inoculation density. Ecotypes with zero cysts were excluded from the analysis, leaving us with 106 ecotypes. First, we tested for correlation between the normalized mean green canopy areas and the number of cysts of plants inoculated with the six densities ranging from 0 to 7.5 infective juveniles per gram of soil (Fig. 6a), revealing that there is no correlation between aboveground plant responses and nematode offspring (Spearman's correlation coefficient = -0.056, $P = 0.003$). Next, we performed Spearman correlation analysis on ecotype level. This revealed a wide variation in correlation coefficients, ranging from 0.6 to -0.84 (Fig. 6b), indicating that there is variation in ecotype

responses to successful infections. Multiple ecotypes exhibited positive slopes, indicative of enhanced growth during infection, with some even tolerating up to 30 cysts per plant (Fig. S6). Conversely, a larger portion of ecotypes, demonstrated negative slopes, suggesting compromised growth in the presence of cysts. Next, by performing a PERMANOVA test, we identified that Arabidopsis ecotype accounts for the highest amount of the variance in growth responses to nematode infection (39%). Inoculation densities and cyst formation only account for 4% and 0.2% of the variance, respectively. In summary, based on our analysis we conclude that tolerance and susceptibility are independent phenotypes.

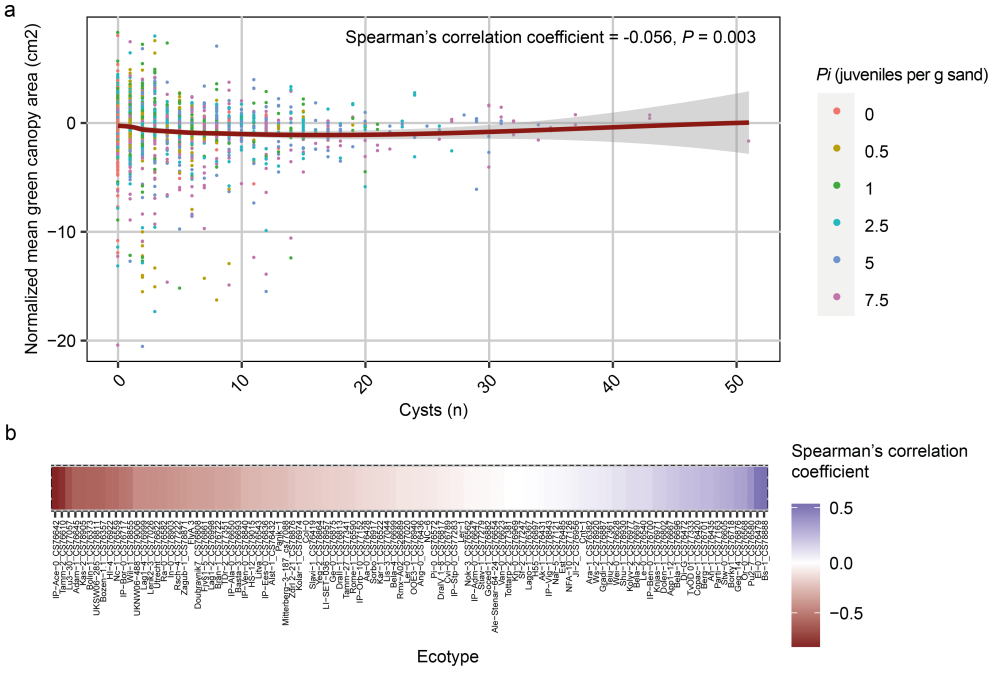

Figure 6: **Aboveground plant response to *H. schachtii* and offspring size are independent Arabidopsis phenotypes.** One hundred fifty nine-day-old *Arabidopsis thaliana* ecotypes were inoculated with six densities of *H. schachtii* (0 to 7.5 juveniles per g dry sand). The green canopy area was monitored for 21 days, with 15 images per day. Data in this figure only includes the mean per plant at 21dpi. Cysts were extracted from soil at 35 dpi. **a)**. Normalized green canopy area was plotted against the number of cysts per plant, irrespective of ecotypes. **b)** Heatmap of Spearman's correlation coefficients generated by correlating the mean green canopy area on 21 dpi *vs* the counted cysts per plant. Colouring indicates decline or increase in normalized mean green canopy area (cm^2) when more cysts are found.

Discussion:

In this study, we aimed to uncover the genetic underpinnings of tolerance to cyst nematode infections in a representative population of *A. thaliana* ecotypes. Using a GWAS approach, we mapped the aboveground growth responses as a proxy of tolerance to increasing inoculation densities of *H. schachtii* on the Arabidopsis genome. We identified two loci in Arabidopsis associated with tolerance to *H. schachtii*. Here, we define tolerance as the ability to mitigate the impact of biotic stress. However, the aboveground plant response of Arabidopsis could also partly reflect the level of biotic stress on the root system (i.e., the number of nematodes

inside the root). We therefore also mapped the number of successful infections per plant (i.e., matured cysts) on the genome of Arabidopsis. We identified 40 loci associated with this indicator of plant susceptibility. Importantly, the Arabidopsis loci associated with tolerance do not overlap with the loci associated with susceptibility to cyst nematode infections. Furthermore, the variance observed in the number of matured cysts per plant explains only 0.2% of the variation in aboveground plant responses in our Arabidopsis panel. We therefore conclude that the aboveground plant response indeed reflects the ability of Arabidopsis to mitigate biotic stress by cyst nematodes, and that this phenotype is distinct from susceptibility of Arabidopsis to cyst nematode infections.

Our data shows that Arabidopsis harbours significant quantitative variation in tolerance to cyst nematode infections. We only mapped the aboveground plant response to the lowest inoculation densities (i.e., P_i 0 – 2.5 juveniles per gram of soil) to provide a proof of concept. This led us to two tolerance loci in Arabidopsis, which suggests a relatively simple underlying genetic architecture. However, we expect to find more tolerance loci by further mapping plant responses to lower and higher inoculation density ranges (i.e., P_i 0 – 0.5 or 0 – 7.5 juveniles per gram of soil). Notably, the two tolerance loci identified in this study explain 40% of the observed phenotypic variance at low inoculation densities. This suggests that a significant portion of the observed variation might be attributed to alleles with minor allele frequencies below 0.05, which were excluded from the GWA mapping. Moreover, others have used a less stringent threshold for significant associations in GWA mapping (e.g., $-\log_{10}(P) > 4$; El-Soda et al., 2015; Kloth et al., 2016; Kooke et al., 2016; Davila Olivas et al., 2017) to explore the genetic framework governing responses to abiotic stresses in Arabidopsis. Similarly relaxing the stringency for our dataset would lead to nine additional loci significantly associating with the growth responses of Arabidopsis to *H. schachtii*, but this would also increase the risk of pursuing false positives in follow-up research.

Based on our observations on the aboveground plant responses of Arabidopsis to cyst nematode infections we classified the Arabidopsis ecotypes as intolerant, tolerant, and overcompensating. Two third of the Arabidopsis ecotypes are either tolerant or overcompensating in their responses to cyst nematodes, whereas one third of the ecotype panel showed a decline in aboveground plant growth even at the lowest inoculation density. This demonstrates that most Arabidopsis ecotypes in our panel adapt to mitigate the impact of biotic stress on the root system, or even benefit from it. Interestingly, we observed not much variation in the minimum green canopy area (i.e., minimum yield) at the highest inoculation densities, which was in many cases close to zero. These findings contrast with the large differences in minimum yield observed between crop cultivars exposed to high inoculation densities of cyst nematodes (Jindo et al., 2023). Under field conditions cyst nematodes can induce severe reduction in above ground growth of crops, but even at high population densities infected plants rarely die. An explanation for this discrepancy in minimum yield between Arabidopsis and crop plants might be the difference in plant size (e.g., root diameter) relative to size of the nematodes. As compared to crops, such as potato and tomato, the root architecture of Arabidopsis is simple and harbours not much structural redundancy within tissue. This means that damage by invading cyst nematode is more likely to have a devasting impact in Arabidopsis than in crop plants under similar infection conditions (i.e., inoculation densities).

In total, we identified 40 QTLs significantly associating with the number of matured cysts per plant at 35 days after inoculation with 2.5 juveniles per gram of

soil. Together, these QTLs explain only 31% of the observed phenotypic variance. Nevertheless, the picture of susceptibility of Arabidopsis to cyst nematodes arising from our data is of high complexity. This contrasts with earlier reports on GWA mapping of plant susceptibility of Arabidopsis to cyst nematode infections identifying only one QTL (Anwer et al., 2018). In this latter study the authors focused on male-to-female ratio at 14 days after inoculation as an indicator of plant susceptibility. Furthermore, this work was done in a more artificial setup with *in vitro* cultivated plants, while we collected our data from inoculation assays in soil. Still, we identified members of the *XTH* genes family in Arabidopsis (i.e., *XTH1* and *XTH2*) in our experimental design which was also identified by Anwer *et al.,* (2018) (Table S1). Furthermore, we found two members of the *WRKY* transcription factor family, which are known to contribute to resistance against nematodes (Amjad Ali et al., 2014). Finally, we found *PIN3* which is involved in polar auxin transport as candidate susceptibility gene for *H. schachtti* infections in Arabidopsis. This is in agreement with previous studies showing that cyst nematode modulate *PIN3* mediated later auxin transport during syncytium formation (Grunewald et al., 2009). We therefore conclude that our GWA mapping approach provides insight in the complexity of the genetic architecture of susceptibility of Arabidopsis to cyst nematodes infections, revealing many novel candidate susceptibility genes.

We view tolerance and susceptibility as two separate plant traits, which are distinct but not independent. While susceptibility determines the level of biotic stress (i.e., the number of successful infections), tolerance reflects the ability of plants to mitigate the impact of stress at a particular level. Our analyses show that aboveground growth responses to cyst nematode infections and the number of successful infections are indeed distinct plant phenotypes. By performing a Spearman correlation coefficient test we found no correlation between the green canopy area of Arabidopsis plants at 21 days after inoculation and the number of matured cysts 35 days after inoculation. Some of the ecotypes performed even better when more juveniles developed to mature cysts. In fact, only 0.2% of the variance in aboveground plant responses in our Arabidopsis panel can be explained by the number of matured cysts. Our findings seem to contradict a recent report on plant tolerance to cyst nematode infections (Sielemann et al., 2023). However, in this latter work tolerance was defined as a form of quantitative susceptibility focusing on nematode development and reproduction. By contrast, we define tolerance differently and with our work we aimed to understand the underpinning of variation in plant development and growth at a given level nematode-induced stress.

In conclusion, the overarching hypothesis of our research entails that phenotypic plasticity of root system architecture is key to plant tolerance to belowground biotic stressors, such as plant parasitic nematodes. In this study we used aboveground plant responses as a proxy for the impact of belowground biotic stress and to genetically map these responses on the genome of Arabidopsis. Our data provides ample leads for further research into tolerance genes, some of which we expect to play a role in root system architecture. For instance, one of the candidate tolerance genes identified in this study encodes the auxin transporter PIN5, which modulates intracellular auxin homeostasis and thereby plant development (Mravec et al., 2009). Recently, PIN5 was found to be involved in mediating root meristem size and root growth (Di Mambro et al., 2019), which could support our hypothesis. Nonetheless, further research is needed to establish if tolerance of Arabidopsis to cyst nematode infections can be causally linked to specific genes, such as *PIN5*.

Supporting information:

Additional Supporting Information and supplementary file with code may be found in the online version of this article.

Figure S1. Green canopy area growth of *Arabidopsis thaliana* ecotypes infected with *Heterodera schachtii*.
Figure S2. Maximum project green canopy area of *Arabidopsis thaliana* ecotypes infected with *Heterodera schachtii*
Figure S3. Intrinsic growth rates of *Arabidopsis thaliana* ecotypes infected with *Heterodera schachtii*
Figure S4. Linkage disequilibrium (LD) between four SNPs in Arabidopsis significantly associated with tolerance to *H. schachtii* in Arabidopsis.
Figure S5. Linkage disequilibrium (LD) between 78 SNPs in Arabidopsis significantly associated with susceptibility to *H. schachtii* in Arabidopsis
Figure S6. Aboveground plant response to *H. schachtii* and offspring size are independent Arabidopsis phenotypes
Table S1. Seventy eight single nucleotide polymorphisms (SNPs) significantly associated with tolerance to *Heterodera schachtii* aggregate into forty quantitative trait loci (QTLs) located on five chromosomes of Arabidopsis

Author contributions:

JJW and GS conceived the project. Experiments were designed by JJW, MGS, and GS. JJW, RF, and CvS performed the experiments. Data analysis was designed, analyzed, and interpreted by JJW, DtM, GS, and MGS. JJW, MGS, and GS wrote the article. All co-authors provided input for the submitted version.

Conflict of interest:

The authors declare no conflict of interest.

Funding statement:

This work was supported by the Graduate School Experimental Plant Sciences (EPS). JJW is funded by Dutch Top Sector Horticulture & Starting Materials (TU18152). MGS was supported by NWO domain Applied and Engineering Sciences VENI grant (17282).

References:

Agathokleous E, Kitao M, Calabrese EJ (2019) Hormesis: A Compelling Platform for Sophisticated Plant Science. Trends Plant Sci **24**: 318–327

Alonso-Blanco C, Andrade J, Becker C, Bemm F, Bergelson J, Borgwardt KMM, Cao J, Chae E, Dezwaan TMM, Ding W, et al (2016) 1,135 Genomes Reveal the Global Pattern of Polymorphism in Arabidopsis thaliana. Cell **166**: 481–491

Amjad Ali M, Wieczorek K, Kreil DP, Bohlmann H (2014) The beet cyst nematode Heterodera schachtii modulates the expression of WRKY transcription factors in syncytia to favour its development in Arabidopsis roots. PLoS One. doi: 10.1371/journal.pone.0102360

Anwer MA, Anjam MS, Shah SJ, Hasan MS, Naz AA, Grundler FMW, Siddique S (2018) Genome-wide association study uncovers a novel QTL allele of AtS40-3 that affects the sex ratio of cyst nematodes in Arabidopsis. J Exp Bot **69**: 1805–1814

Bates D, Mächler M, Bolker BM, Walker SC (2015) Fitting linear mixed-effects models using lme4. J Stat Softw. doi: 10.18637/jss.v067.i01

Baty F, Ritz C, Charles S, Brutsche M, Flandrois J-P, Delignette-Muller M-L (2015) A Toolbox for Nonlinear Regression in R: The Package nlstools.

Baum TJ, Wubben MJ, Hardyy KA, Su H, Rodermel SR (2000) A Screen for Arabidopsis thaliana Mutants with Altered Susceptibility to Heterodera schachtii. J Nematol **32**: 166–73

Bebber DP, Holmes T, Gurr SJ (2014) The global spread of crop pests and pathogens. Global Ecology and Biogeography **23**: 1398–1407

Been TH, Teklu MG, Heve WK, Schomaker CH (2015) Damage thresholds and population dynamics of Meloidogyne chitwoodi on carrot (Daucus carota) at different seed densities. Nematology **17**: 501–514

Bohlmann H, Sobczak M (2014) The plant cell wall in the feeding sites of cyst nematodes. Front Plant Sci **5**: 1–10

Davila Olivas NH, Kruijer W, Gort G, Wijnen CL, van Loon JJA, Dicke M (2017) Genome-wide association analysis reveals distinct genetic architectures for single and combined stress responses in Arabidopsis thaliana. New Phytologist **213**: 838–851

El-Soda M, Kruijer W, Malosetti M, Koornneef M, Aarts MGM (2015) Quantitative trait loci and candidate genes underlying genotype by environment interaction in the response of Arabidopsis thaliana to drought. Plant Cell Environ **38**: 585–599

Endelman JB (2011) Ridge Regression and Other Kernels for Genomic Selection with R Package rrBLUP. Plant Genome **4**: 250–255

Evans K, Haydock PPJ (1990a) A review of tolerance by potato plants of cyst nematode attack, with consideration of what factors may confer tolerance and methods of assaying and improving it in crops. Annual applied Biology **117**: 703–740

Evans K, Haydock PPJ (1990b) A review of tolerance by potato plants of cyst nematode attack, with consideration of what factors may confer tolerance and methods of assaying and improving it in crops. 703–740

Fox JA, Spasoff L (1976) Resistance and tolerance of tobacco to Heterodera solanacearum. J Nematol 8:

Fuller VL, Lilley CJ, Urwin PE (2008) Nematode resistance. New Phytologist **180**: 27–44

Fuller VL, Lilley CJ, Urwin PE (2007) Nematode resistance. New Phytologist 243–255

Golinowski W, Grundler FMW, Sobczak M (1996) Changes in the structure of Arabidopsis thaliana during female development of the plant-parasitic nematode Heterodera schachtii. Protoplasma **194**: 103–116

Grundler F, Böckenhoff A, Schmidt K-P, Sobczak M, Golinowski W, Wyss U (1994) Arabidopsis thaliana and Heterodera schachtii: a versatile model to characterize the interaction between host plants and cyst nematodes. *In* BD eds Lamberti F, De Giorgi C, ed, Advances in Molecular Plant Nematology. Springer US, Boston, pp 171–180

Grunewald W, Cannoot B, Friml J, Gheysen G (2009) Parasitic nematodes modulate PIN-mediated auxin transport to facilitate infection. PLoS Pathog. doi: 10.1371/journal.ppat.1000266

Guarneri N, Willig J-J, Sterken MG, Zhou W, Hasan MS, Sharon L, Grundler FMW, Willemsen V, Goverse A, Smant G, et al (2023) Root architecture plasticity in response to endoparasitic cyst nematodes is mediated by damage

signaling. New Phytologist **237**: 807–822

Jindo K, Teklu MG, van Boheeman K, Njehia NS, Narabu T, Kempenaar C, Molendijk LPG, Schepel E, Been TH (2023) Unmanned Aerial Vehicle (UAV) for Detection and Prediction of Damage Caused by Potato Cyst Nematode G. pallida on Selected Potato Cultivars. Remote Sens (Basel). doi: 10.3390/rs15051429

Jones JT, Haegeman A, Danchin EGJ, Gaur HS, Helder J, Jones MGK, Kikuchi T, Manzanilla-López R, Palomares-Rius JE, Wesemael WML, et al (2013) Top 10 plant-parasitic nematodes in molecular plant pathology. Mol Plant Pathol **14**: 946–961

Kim S, Plagnol V, Hu TT, Toomajian C, Clark RM, Ossowski S, Ecker JR, Weigel D, Nordborg M (2007) Recombination and linkage disequilibrium in Arabidopsis thaliana. Nat Genet **39**: 1151–1155

Kloth KJ, Wiegers GL, Busscher-Lange J, Van Haarst JC, Kruijer W, Bouwmeester HJ, Dicke M, Jongsma MA (2016) AtWRKY22 promotes susceptibility to aphids and modulates salicylic acid and jasmonic acid signalling. J Exp Bot **67**: 3383–3396

Kooke R, Kruijer W, Bours R, Becker F, Kuhn A, van de Geest H, Buntjer J, Doeswijk T, Guerra J, Bouwmeester H, et al (2016) Genome-wide association mapping and genomic prediction elucidate the genetic architecture of morphological traits in arabidopsis. Plant Physiol **170**: 2187–2203

Li J, Ji L (2005) Adjusting multiple testing in multilocus analyses using the eigenvalues of a correlation matrix. Heredity (Edinb) **95**: 221–227

Di Mambro R, Svolacchia N, Dello Ioio R, Pierdonati E, Salvi E, Pedrazzini E, Vitale A, Perilli S, Sozzani R, Benfey PN, et al (2019) The Lateral Root Cap Acts as an Auxin Sink that Controls Meristem Size. Current Biology **29**: 1199-1205.e4

Mravec J, Skůpa P, Bailly A, Hoyerová K, Křeček P, Bielach A, Petrášek J, Zhang J, Gaykova V, Stierhof YD, et al (2009) Subcellular homeostasis of phytohormone auxin is mediated by the ER-localized PIN5 transporter. Nature **459**: 1136–1140

Norshie PM, Been TH, Schomaker CH (2011) Estimation of partial resistance in potato genotypes against Meloidogyne chitwoodi. Nematology **13**: 477–489

Painter RH (1951) Insect resistance in crop plants.

R Core Team (2019) R: A language and environment for statistical computing. R Foundation for Statistical Computing, Vienna, Austria

Rehman S, Butterbach P, Popeijus H, Overmars H, Davis EL, Jones JT, Goverse A, Bakker J, Smant G (2009) Identification and Characterization of the Most Abundant Cellulases in Stylet Secretions from Globodera rostochiensis. Phytopathology **99**: 194–202

Savary S, Willocquet L, Pethybridge SJ, Esker P, McRoberts N, Nelson A (2019) The global burden of pathogens and pests on major food crops. Nat Ecol Evol **3**: 430–439

Siddique S, Radakovic ZS, Hiltl C, Pellegrin C, Baum TJ, Beasley H, Bent AF, Chitambo O, Chopra D, Danchin EGJ, et al (2022) The genome and lifestage-specific transcriptomes of a plant-parasitic nematode and its host reveal susceptibility genes involved in trans-kingdom synthesis of vitamin B5. Nat Commun. doi: 10.1038/s41467-022-33769-w

Sielemann K, Pucker B, Orsini E, Elashry A, Schulte L, Viehöver P, Müller AE, Schechert A, Weisshaar B, Holtgräwe D (2023) Genomic characterization of a nematode tolerance locus in sugar beet. BMC Genomics. doi: 10.1186/s12864-023-09823-2

Sikora RA, Helder J, Molendijk LPG, Desaeger J, Eves-Van Den Akker S, Mahlein A-K (2023) Integrated Nematode Management in a World in Transition: Constraints, Policy, Processes, and Technologies for the Future.

Annual Reviews. doi: 10.1146/annurev-phyto-021622
Sobczak M, Golinowski W, Grundler FMW (1997) Changes in the structure of Arabidopsis thaliana roots induced during development of males of the plant parasitic nematode Heterodera schachtii. Eur J Plant Pathol **103**: 113–124
Szakasits D, Heinen P, Wieczorek K, Hofmann J, Wagner F, Kreil DP, Sykacek P, Grundler FMW, Bohlmann H (2009) The transcriptome of syncytia induced by the cyst nematode Heterodera schachtii in Arabidopsis roots. Plant Journal **57**: 771–784
Teklu MG, Schomaker CH, Been TH, Molendijk LPG (2022) Tuber Yield, Quality and Infestation Levels of Potato Genotypes, Resistant to the Root-Knot Nematode, Meloidogyne chitwoodi. Potato Res **66**: 105–135
The European Commission (2023) Farm to Fork - targets - Progress. https://food.ec.europa.eu/plants/pesticides/sustainable-use-pesticides/farm-fork-targets-progress_en,
Thoen MPM, Davila Olivas NH, Kloth KJ, Coolen S, Huang PP, Aarts MGM, Bac-Molenaar JA, Bakker J, Bouwmeester HJ, Broekgaarden C, et al (2017) Genetic architecture of plant stress resistance: multi-trait genome-wide association mapping. New Phytologist **213**: 1346–1362
Trudgill DL (1991) Resistance to and tolerance of plants parasitic nematodes in plants. Annu Rev Phytopathol **29**: 167–192
Warmerdam S, Sterken MG, van Schaik C, Oortwijn MEP, Sukarta OCA, Lozano-Torres JL, Dicke M, Helder J, Kammenga JE, Goverse A, et al (2018) Genome-wide association mapping of the architecture of susceptibility to the root-knot nematode Meloidogyne incognita in Arabidopsis thaliana. New Phytologist **218**: 724–737
Weigel D, Mott R (2009) The 1001 genomes project for Arabidopsis thaliana. Genome Biol **10**: 107
Williamson VM, Hussey RS (1996) Nematode pathogenesis and resistance in plants. Plant Cell **8**: 1735–1745
Willig J-J, Guarneri N, van Steenbrugge JJM, de Jong W, Chen J, Goverse A, Lozano Torres JL, Sterken MG, Bakker J, Smant G (2022) The Arabidopsis transcription factor TCP9 modulates root architectural plasticity, reactive oxygen species-mediated processes, and tolerance to cyst nematode infections. Plant Journal **112**: 1070–1083
Willig J-J, Sonneveld D, van Steenbrugge JJM, Deurhof L, van Schaik CC, Teklu MG, Goverse A, Lozano-Torres JL, Smant G, Sterken MG (2023) From root to shoot; Quantifying nematode tolerance in Arabidopsis thaliana by high-throughput phenotyping of plant development. J Exp Bot erad266
Wyss U (1992) Observations on the feeding behaviour of Heterodera schachtii throughout development, including events during moulting. Fundam Appl Nematol **15**: 75–89
Wyss U, Zunke U (1986) Observations on the behaviour of second stage juveniles of Heterodera schachtii inside host roots. Revue de nématologie **9**: 153–165

Supporting information:

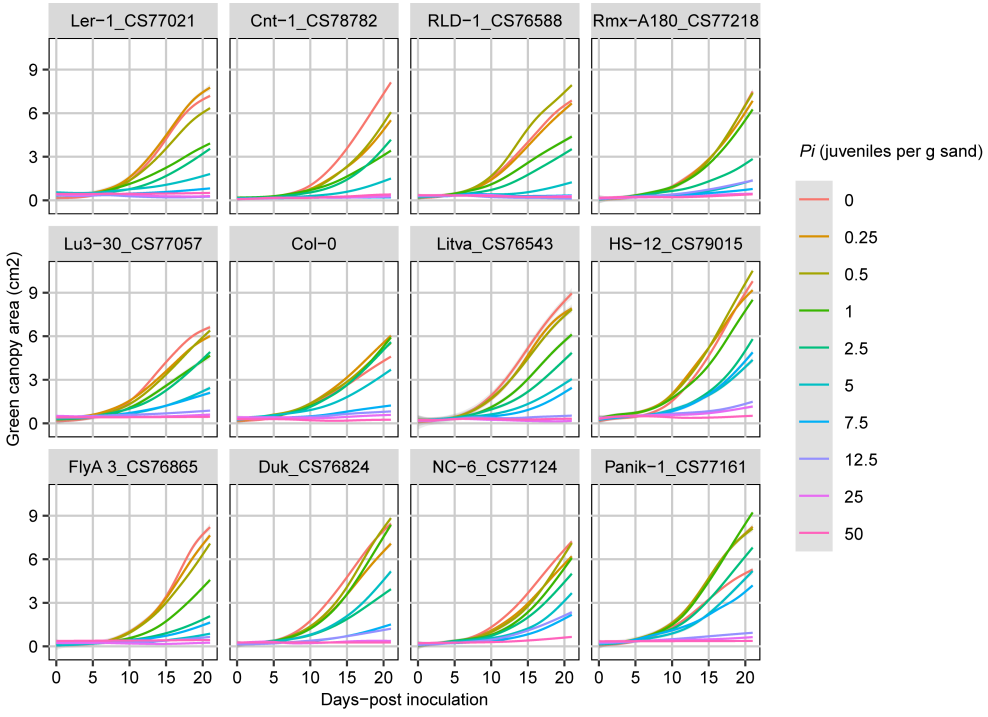

Figure S1: **Green canopy area growth of *Arabidopsis thaliana* ecotypes infected with *Heterodera schachtii*.** Nine-day-old *Arabidopsis thaliana* seedlings were inoculated with 10 densities (P_i) of *H. schachtii* juveniles (0 to 50 juveniles per g dry sand. The green canopy area was imaged for a period of 21 days.

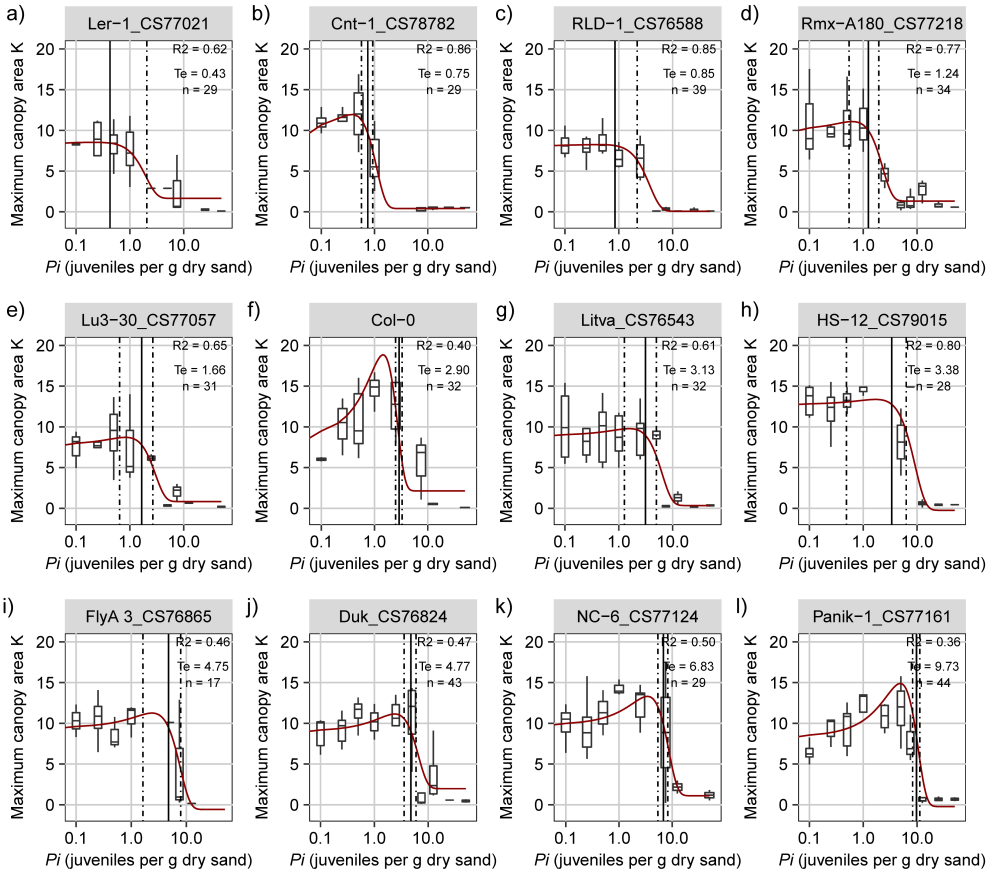

Figure S2: **Maximum project green canopy area of *Arabidopsis thaliana* ecotypes infected with *Heterodera schachtii*. a-l)** Nine-day-old *Arabidopsis thaliana* seedlings were inoculated with 10 densities (P_i) of *H. schachtii* juveniles (0 to 50 juveniles per g dry sand. The green canopy area was imaged for a period of 21 days and fitted to a gaussian curve model. Solid line indicates the tolerance limit. Dashed line indicates the confidence interval.

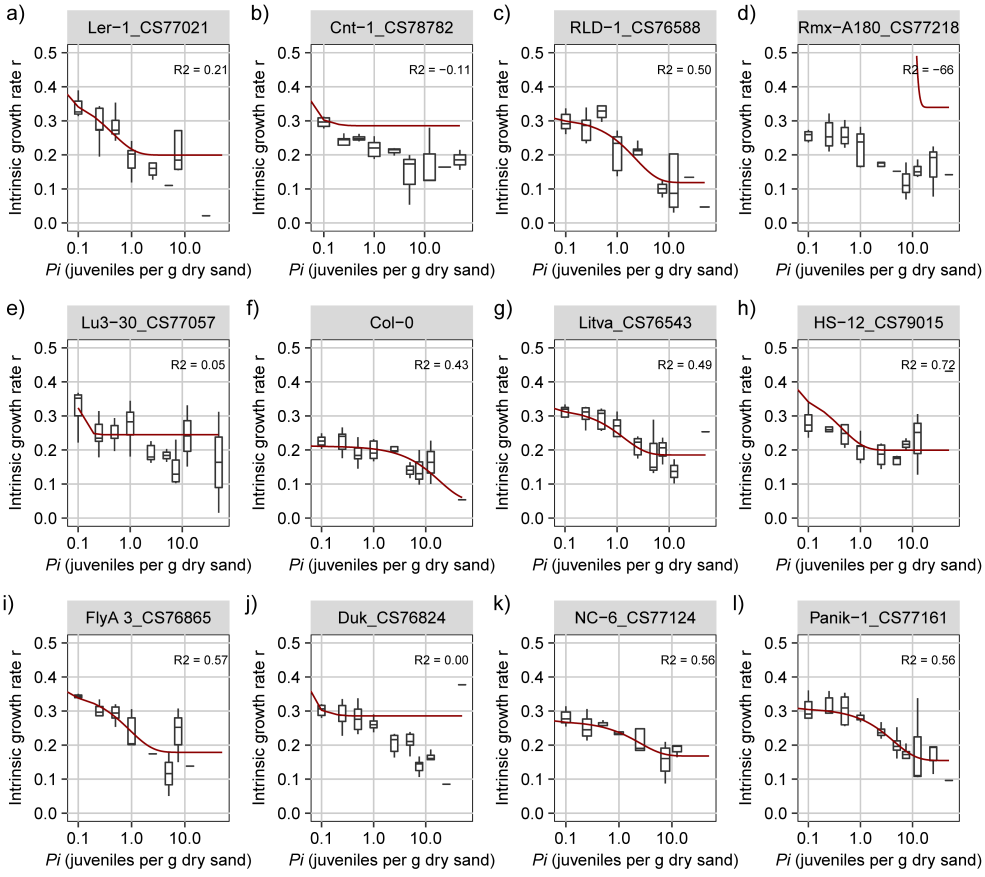

Figure S3: **Intrinsic growth rates of *Arabidopsis thaliana* ecotypes infected with *Heterodera schachtii*. a-l)** Nine-day-old *Arabidopsis thaliana* seedlings were inoculated with 10 densities (P_i) of *H. schachtii* juveniles (0 to 50 juveniles per g dry sand. The green canopy area was imaged for a period of 21 days and fitted to a logistic growth rate model.

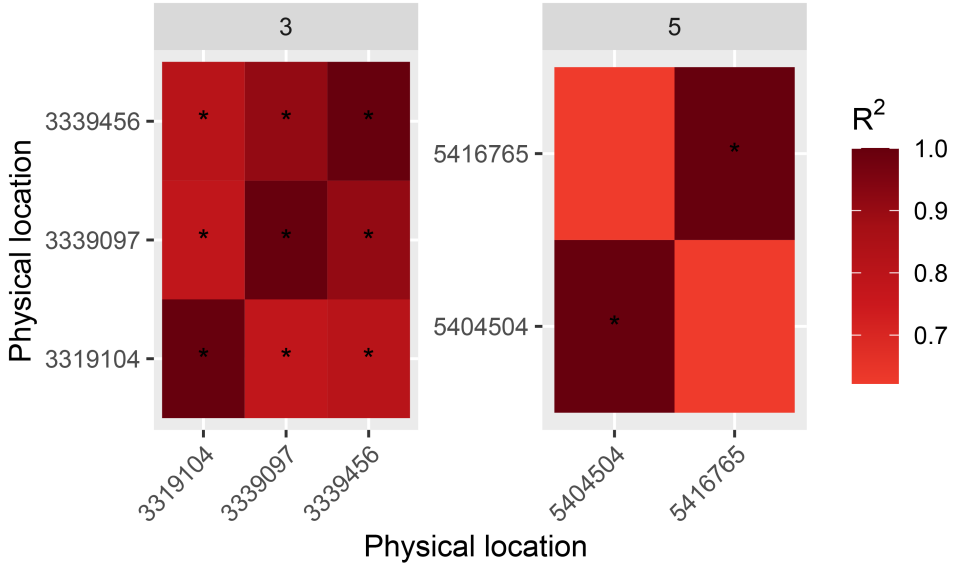

Figure S4: **Linkage disequilibrium (LD) between four SNPs in Arabidopsis significantly associated with tolerance to *H. schachtii* in Arabidopsis.**

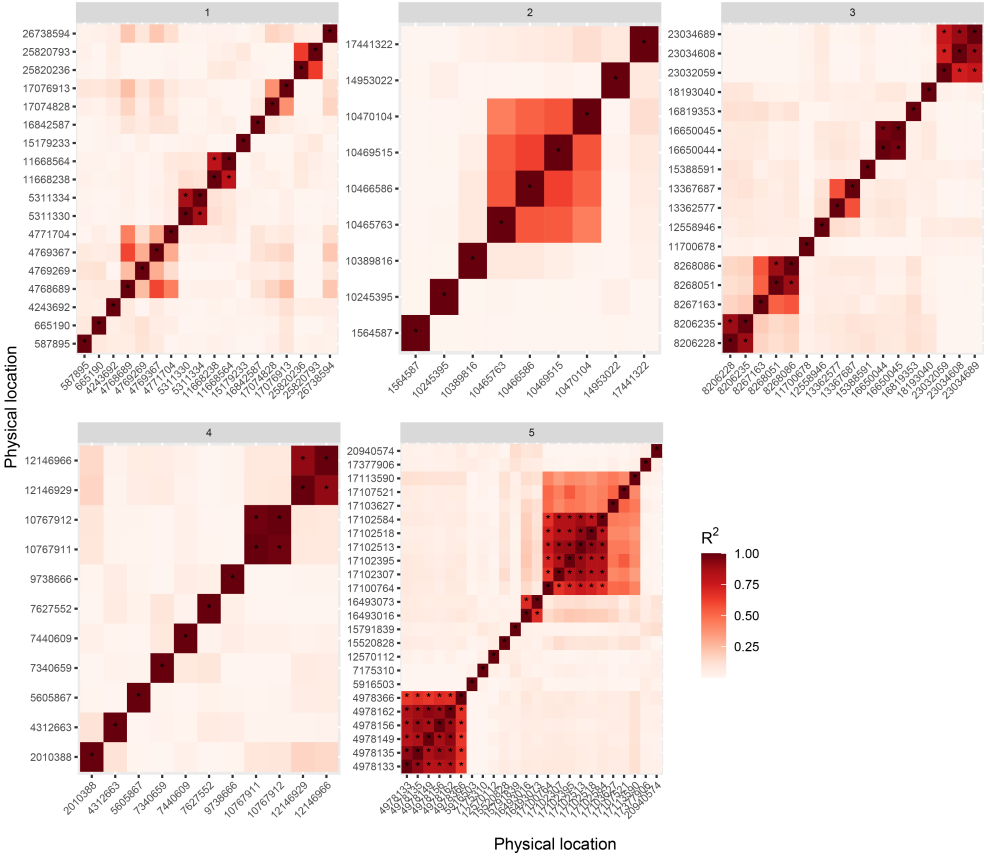

Figure S5: **Linkage disequilibrium (LD) between 78 SNPs in Arabidopsis significantly associated with susceptibility to *H. schachtii* in Arabidopsis.**

Table S1: Seventy eight single nucleotide polymorphisms (SNPs) significantly associated with tolerance to *Heterodera schachtii* aggregate into forty quantitative trait loci (QTLs) located on five chromosomes of Arabidopsis

QTL	Chr.	Position	SNP[a]	-Log$_{10}$(*P*)[c]	gene_AraID	Symbol
1	1	587895	A:G	5.362	AT1G02680	TAF13
					AT1G02690	IMPA-6
					AT1G02700	
					AT1G02720	GATL5
					AT1G02730	CSLD5
2	1	665190	C:G	5.915	AT1G02910	LPA1
					AT1G02920	GSTF7
					AT1G02930	GSTF6
					AT1G02940	ATGSTF5
					AT1G02950	ATGSTF4
					AT1G02960	
					AT1G02965	
					AT1G02970	WEE1
	1	4243692	G:C	5.074	AT1G12430	ARK3
					AT1G12440	SAP1
					AT1G12450	
					AT1G12460	
					AT1G12470	VPS18
3	1	4768689	A:T	5.035	AT1G13930	
					AT1G13940	
					AT1G13950	ELF5A-1
					AT1G13960	WRKY4
	1	4771704	A:G	5.052	AT1G13970	
4	1	5311330	A:T	6.278	AT1G15420	
					AT1G15430	
					AT1G15440	PWP2
					AT1G15460	BOR4
					AT1G15470	
					AT1G15480	
					AT1G15490	
5	1	11668238	T:C	5.030	AT1G32337	
					AT1G32340	NHL8
					AT1G32350	AOX3

					AT1G32360	
					AT1G32361	ATL81
					AT1G32370	TOM2B
6	1	16842587	G:A	5.085	AT1G44350	ILL6
					AT1G44414	
					AT1G44446	CAO
7	1	17074828	A:T	5.595	AT1G45130	BGAL5
					AT1G45145	TRX5
					AT1G45150	
					AT1G45160	
8	1	25820236	A:C	5.322	AT1G68730	
					AT1G68740	PHO1-H1
					AT1G68750	PPC4
					AT1G68760	NUDT1
					AT1G68765	IDA
9	1	26738594	G:T	7.151	AT1G70900	
					AT1G70910	DEP
					AT1G70920	ATHB-X
					AT1G70940	PIN3
	2	1564587	A:G	5.168	AT2G04480	
					AT2G04495	
					AT2G04500	
					AT2G04515	
10	2	10245395	G:T	6.216	AT2G24080	
					AT2G24090	RPL35
					AT2G24100	
					AT2G24120	RPOT3
11	2	10389816	A:G	5.196	AT2G24420	
					AT2G24430	ANAC038
					AT2G24440	
					AT2G24460	
					AT2G24470	
					AT2G24490	RPA2A
12	2	10465763	T:C	5.397	AT2G24610	ATCNGC14
					AT2G24615	
					AT2G24625	

					AT2G24630	CSLC8
	2	10466586	A:T	6.684	AT2G24640	UBP19
13	2	14953022	G:A	5.015	AT2G35605	
					AT2G35610	XEG113
					AT2G35612	CEP4
					AT2G35615	
					AT2G35620	FEI2
14	2	17441322	T:A	5.663	AT2G41800	
					AT2G41810	
					AT2G41820	PXC3
					AT2G41830	
15	3	8206228	A:T	5.527	AT3G23060	
					AT3G23070	CFM3A
					AT3G23080	
					AT3G23090	
	3	8267163	C:T	5.647	AT3G23160	
					AT3G23165	LCR42
					AT3G23167	LCR39
					AT3G23170	
					AT3G23172	
					AT3G23175	
					AT3G23180	
16	3	11700678	T:G	5.271	AT3G29791	
17	3	12558946	T:A	5.748	AT3G30823	
18	3	13362577	G:A	5.152	AT3G32400	FH17
					AT3G32410	
19	3	15388591	A:T	5.230	AT3G43470	
20	3	16650044	C:T	5.253	AT3G45390	LECRK12
					AT3G45400	
					AT3G45410	LECRK13
					AT3G45420	LECRK14
	3	16819353	A:T	5.625	AT3G45780	PHOT1
					AT3G45790	
21	3	18193040	C:T	5.736	AT3G49055	
					AT3G49060	PUB32
					AT3G49070	

					AT3G49080	RPS9M
					AT3G49100	SRP9
					AT3G49110	PER33
22	3	23032059	C:T	5.264	AT3G62200	
					AT3G62210	EDA32
					AT3G62220	
					AT3G62230	
					AT3G62240	
					AT3G62250	RPS27AC
					AT3G62260	
	3	23034608	A:C	5.241	AT3G62270	BOR2
23	4	4312663	C:T	6.846	AT4G07455	
24	4	5605867	G:A	6.779	AT4G08780	PER38
					AT4G08790	NLP2
					AT4G08800	
25	4	7340659	T:C	5.233	AT4G12370	
					AT4G12380	
					AT4G12382	
					AT4G12390	PME1
					AT4G12400	HOP3
					AT4G12410	
					AT4G12420	SKU5
26	4	7440609	C:G	6.025	AT4G12545	AIR1B
					AT4G12550	AIR1
					AT4G12560	CPR1
					AT4G12570	UPL5
					AT4G12580	
27	4	7627552	A:G	5.069	AT4G13050	FATA2
					AT4G13060	
					AT4G13070	
					AT4G13075	RALFL30
					AT4G13080	XTH1
					AT4G13090	XTH2
					AT4G13095	LCR37
					AT4G13100	
28	4	9738666	A:G	5.240	AT4G17460	HAT1

					AT4G17470	
					AT4G17480	
					AT4G17483	
29	4	10767911	A:G	5.243	AT4G19800	
					AT4G19810	ChiC
					AT4G19820	
					AT4G19830	FKBP17-1
					AT4G19840	PP2A1
					AT4G19850	ATPP2-A2
30	4	12146929	A:G	5.720	AT4G23180	CRK10
					AT4G23190	CRK11
					AT4G23200	CRK12
					AT4G23210	CRK13
					AT4G23220	CRK14
31	5	4978133	T:C	6.140	AT5G15300	PCMP-E40
					AT5G15310	ATMYB16
					AT5G15320	
					AT5G15330	ATSPX4
					AT5G15340	PCMP-H91
					AT5G15350	ENODL17
					AT5G15360	
32	5	5916503	C:T	7.683	AT5G17870	PSRP6
					AT5G17880	CSA1
					AT5G17890	DAR4
					AT5G17900	
33	5	7175310	C:T	5.158	AT5G21100	
					AT5G21105	
					AT5G21120	EIL2
					AT5G21125	
34	5	12570112	C:T	5.219	AT5G33300	
35	5	15520828	A:C	7.402	AT5G38730	
					AT5G38740	AGL77
					AT5G38750	
					AT5G38760	
					AT5G38770	GDU7
					AT5G38780	

36	5	15791839	T:A	7.245	AT5G39440 AT5G39450 AT5G39460 AT5G39470 AT5G39471 AT5G39480	SnRK1.3
37	5	16493016	G:A	7.500	AT5G41180 AT5G41190 AT5G41200 AT5G41210 AT5G41220 AT5G41240 AT5G41250	 AGL75 GSTT1 GSTT3 GSTT2 GT20
38	5 5 5	17100764 17107521 17113590	C:T C:T C:T	5.042 5.457 5.325	AT5G42650 AT5G42655 AT5G42660 AT5G42670 AT5G42680 AT5G42690 AT5G42700	CYP74A
39	5	17377906	C:A	5.595	AT5G43280 AT5G43285 AT5G43290 AT5G43300 AT5G43310 AT5G43320	DCI1 LURE1.1 WRKY49 GDPD3 CKL8
40	5	20940574	T:C	5.012	AT5G51540 AT5G51545 AT5G51550 AT5G51560 AT5G51570	OCT1 LPA2 EXL3 HIR4

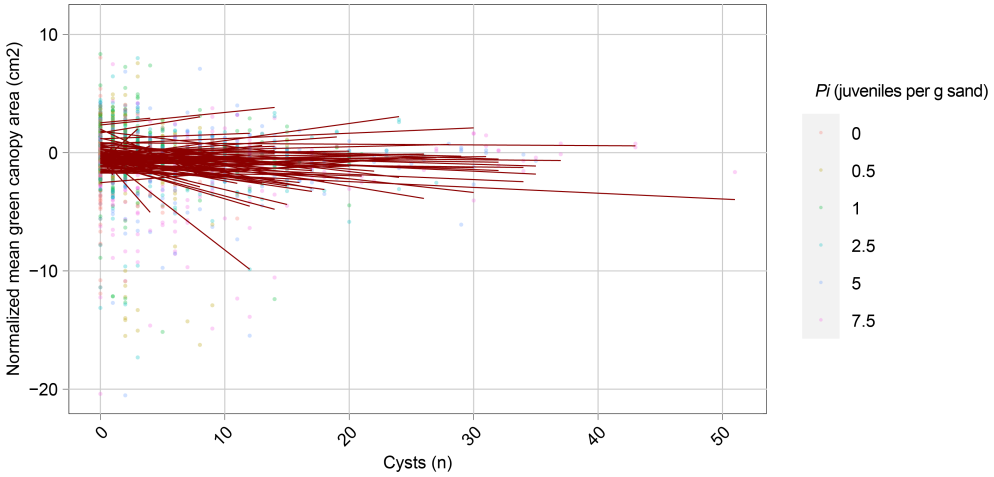

Figure S6: **Aboveground plant response to *H. schachtii* and offspring size are independent Arabidopsis phenotypes.** Hundred fifty nine-day-old *Arabidopsis thaliana* ecotypes were inoculated with six densities of *H. schachtii* (0 to 7.5 juveniles per g dry sand). The green canopy area was monitored for 21 days, with 15 images per day. Data in this figure only includes the mean per plant at 21dpi. Cysts were extracted from soil at 35 dpi. To illustrate the different responses between ecotypes we performed linear regressions between the mean green canopy area and the number of cysts per ecotype.

Chapter 4

Root architecture plastcity in response to endoparasitic cyst nematodes is mediated by damage signaling

Nina Guarneri[1,‖], Jaap-Jan Willig[1,‖], Mark G. Sterken[1], Wenkun Zhou[2,3], M. Shamim Hasan[4], Letia Sharon[4], Florian M. W. Grundler[4], Viola Willemsen[2], Aska Goverse[1], Geert Smant[1,‡], and Jose L. Lozano-Torres[1,‡]

[1] - Laboratory of Nematology, Wageningen University & Research, 6708 PB Wageningen, the Netherlands
[2] - Laboratory of Molecular Biology, Cluster of Plant Developmental Biology, Wageningen University & Research, 6708 PB Wageningen, the Netherlands
[3] - State Key Laboratory of Plant Physiology and Biochemistry, College of Biological Sciences, China Agricultural University, Beijing, 100193 China
[4] - Institute of Crop Science and Resource Conservation (INRES), Molecular Phytomedicine, University of Bonn, INRES, 53115 Bonn, Germany

‖ - these authors contributed equally
‡ - these authors contributed equally

Published in New Phytologist, Volume 237, Issue 3, February 2023, Pages 807-8222023, Pages 5487–5499

Abstract:

Plant root architecture plasticity in response to biotic stresses has not been thoroughly investigated. Infection by the endoparasitic cyst nematodes induces root architectural changes that involve the formation of secondary roots at infection sites. However, the molecular mechanisms regulating secondary root formation in response to cyst nematode infection remain largely unknown. We first assessed whether secondary roots form in a nematode-density dependent manner by challenging wildtype Arabidopsis plants with increasing numbers of cyst nematodes (*Heterodera schachtii*). Next, by using jasmonate-related reporter lines and knock-out mutants, we tested if tissue damage by nematodes triggers jasmonate-dependent secondary root formation. Finally, we verified whether damage-induced secondary root formation depends on local auxin biosynthesis at nematode infection sites. Intracellular host invasion by H. schachtii triggers a transient local increase in jasmonates, which activates the expression of *ERF109* in a COI1-dependent manner. Knock-out mutations in COI1 and ERF109 disrupt the nematode-density dependent increase of secondary roots observed in wildtype plants. Furthermore, ERF109 regulates secondary root formation upon *H. schachtii* infection via local auxin biosynthesis. Host invasion by *H. schachtii* triggers secondary root formation via the damage-induced jasmonate-dependent ERF109 pathway. This points at a novel mechanism underlying plant root plasticity in response to biotic stress.

Introduction:

Plants utilize root plasticity as a key strategy to survive in a changing soil environment. Remodeling of root systems allows plants to cope with nutrient deficiencies, drought, salinity, and other abiotic stresses (Koevoets et al., 2016). However, little is known about root architecture plasticity in response to soil-borne biotic stresses. Infections by cyst nematodes are known to induce elaborate root architectural changes in host plants. Secondary roots form locally at cyst nematode infection sites (Grymaszewska & Golinowski, 1991; Goverse et al., 2000; Lee et al., 2011). Furthermore, the ability to form secondary roots in response to nematode infection can result in better maintenance of shoot growth in some potato and soybean cultivars (Trudgill & Cotes, 1983; Miltner et al., 1991). Nevertheless, the molecular mechanisms regulating secondary root formation in response to belowground herbivory are not well understood.

Cyst nematodes are microscopic root endoparasites that cause large agricultural losses worldwide. These nematodes can persist in the soil in a dormant state for many years (Jones et al., 2013). Exudates from host roots trigger hatching of dormant second-stage juveniles (J2s) and guide their migration to the root surface. Here, the J2s penetrate the root epidermis of the differentiation or mature root zone by piercing plant cell walls with their needle-like oral stylet and by secreting plant cell wall degrading enzymes (Bohlmann & Sobczak, 2014). Subsequently, juveniles migrate intracellularly within the cortex, leaving behind a trail of destruction (Wyss & Zunke, 1986; Grundler et al., 1994). Plant cell wall fragments released during nematode migration can act as damage-associated molecular patterns triggering defense signaling in the host (Shah et al., 2017). Nematode migration also activates biosynthesis and signaling of the defense hormone jasmonate (JA) (Kammerhofer et al., 2015). Upon successful arrival at the vascular cylinder, cyst nematodes utilize stylet-secreted effectors to manipulate plant developmental pathways to transform

host cells into permanent feeding sites (Gheysen & Mitchum, 2011). Together with permanent feeding site development, multiple de novo formed secondary roots emerge in clusters at nematode infection sites (Grymaszewska & Golinowski, 1991; Goverse et al., 2000; Lee et al., 2011).

Nematode feeding sites are characterized by the local accumulation of the plant hormone auxin (Karczmarek et al., 2004; Grunewald et al., 2009). Auxin transport and auxin-insensitive Arabidopsis mutants infected by cyst nematodes show smaller females and smaller feeding sites, respectively (Goverse et al., 2000; Grunewald et al., 2009). Additionally, auxin is an important regulator of secondary root formation. Oscillations of auxin maxima at the root tip determine the formation of lateral roots in a regularly spaced pattern along the primary root (Fukaki & Tasaka, 2009). However, these oscillations are not required for the de novo formation of secondary roots. Ectopic induction of local auxin biosynthesis in pericycle cells via an inducible promoter is sufficient to trigger de novo secondary root formation (Dubrovsky et al., 2008). Auxin accumulation in multiple neighboring pericycle cells can lead to the formation of secondary root clusters (Dubrovsky et al., 2008). The spatial co-occurrence of nematode feeding sites and secondary root clusters often corresponds to overlapping regions of auxin accumulation (Karczmarek et al., 2004; Absmanner et al., 2013). This suggests that secondary roots could be induced as the sole consequence of the auxin that accumulates during nematode feeding site development (Goverse et al., 2000). Alternatively, damage caused by nematode infection might also lead to local auxin accumulation and secondary root formation.

Tissue damage triggers auxin accumulation and de novo root formation via the JA-dependent ERF109 transcription factor in leaf explants (Liu et al., 2014; Chen et al., 2016; Hu & Xu, 2016; Zhang et al., 2019). Herein, JA accumulates at the site of wounding within a few hours of leaf detachment and triggers expression of the transcription factor ERF109 via the JA receptor COI1. ERF109 binds to the promoter of the auxin biosynthesis gene ASA1, which induces root formation in a process referred to as de novo root organogenesis. Direct interaction of JAZ proteins inhibits ERF109 expression in a negative feedback loop to avoid wound hypersensitivity (Zhang et al., 2019). Sterile mechanical injury in primary roots of Arabidopsis can trigger auxin accumulation at the wounding site and subsequent secondary root formation (Sheng et al., 2017). However, whether this occurs via the same damage signaling pathway as de novo root organogenesis from leaf explants is unknown. Furthermore, mechanical injury is an artificial condition and therefore it remains unclear whether the JA-dependent ERF109 pathway is involved in the regulation of secondary root formation also upon naturally occurring damage by herbivory or pathogen penetration.

Previously, we showed that components of the JA-dependent ERF109 pathway are induced by root-knot nematode (Meloidogyne spp.) infection (Zhou et al., 2019). Differently from cyst nematodes, root-knot nematodes penetrate roots at the elongation zone and migrate towards the root apical meristem by moving in between cells. Although this type of migration creates minimum tissue damage, root-knot nematode invasion of the root apical meristem induces expression of the ERF109 transcription factor. This eventually promotes tissue regeneration and reduces the inhibitory effect of nematode infection on primary root growth (Zhou et al., 2019). Thus, wound signaling can mediate primary root growth compensation in response to damage by stealthily migrating root-knot nematodes. However, further research is needed to understand whether JA-dependent wound signaling regulates root architectural changes to compensate for tissue destruction by the more damaging

cyst nematodes in the differentiation and mature root zones.
In this study, we hypothesized that local tissue damage by cyst nematode host invasion causes secondary root formation at infection sites via the JA-dependent ERF109 pathway. By challenging Arabidopsis seedlings with increasing numbers of J2s of the beet cyst nematode Heterodera schachtii, we found that secondary root formation is induced at infection sites in a nematode-density dependent manner. With time course confocal microscopy of JA biosensors and ERF109 reporter lines in Arabidopsis, we provide evidence that secondary root formation is preceded by the transient and local JA-dependent expression of ERF109. Moreover, the nematode-density dependent increase in secondary roots is abolished in coi1-2 and erf109 knock-out mutants. By selectively applying the auxin biosynthesis chemical inhibitor L-kynurenine (L-kyn) to shoots and roots, we further found that the ERF109-mediated formation of secondary roots is dependent on local auxin biosynthesis. We therefore conclude that tissue damage by host invading cyst nematodes induces secondary root formation by altering local auxin biosynthesis via the JA-dependent ERF109 pathway. Altogether, our results show that damage signaling via the JA-dependent ERF109 pathway regulates root architectural plasticity in response to cyst nematode infection.

Material & Methods:

Plant material and growth conditions

The Arabidopsis (Arabidopsis thaliana) lines Col-0, pAOS::YFPN (Poncini et al., 2017), DR5::GUS/Col-0, and DR5::GUS/erf109 (Cai et al., 2014), p35S::JAS-VENUS/p35S::H2B-RFP (Larrieu et al., 2015) and pERF109::GFP/Col-0 (Zhou et al., 2019) were used. The erf109 mutant was chosen because of the extensive characterization in previous research (Cai et al., 2014; Kong et al., 2018; Zhang et al., 2019; Ye et al., 2020). The weak allele coi1-2 mutant (Xu et al., 2002) was used since it allows for propagation of homozygous plants and therefore does not need pre-selection with MeJA, which could interfere with the ERF109 pathway. pERF109::GFP/coi1-2 was obtained through crossing followed by selection of homozygous plants on selective ½ MS medium containing 15 µg ml-1 hygromycin B (Melford Laboratories Ltd.) and 20 µg ml-1 MeJA (Sigma-Aldrich). Arabidopsis plants were vertically grown in sterile conditions on modified Knop medium (Sijmons et al., 1991) in a growth chamber with a 16 h: 8 h, light: dark photoperiod at 21°C.

Nematode sterilization

Heterodera schachtii (Woensdrecht population from IRS, the Netherlands) cysts were extracted from sand of Brassica oleracea infected plants as previously described (Baum et al., 2000) and incubated for seven days in a solution containing 1.5 mg ml-1 gentamycin sulfate, 0.05 mg ml-1 nystatin and 3mM ZnCl2. Hatched second-stage juveniles (J2s) were purified by centrifugation on a 35% sucrose gradient and surface sterilized for 15 minutes in a solution containing 0.16 mM HgCl2, 0.49 mM NaN3, and 0.002% Triton X-100. After washing three times with sterile tap water, H. schachtii J2s were re-suspended in a sterile 0.7% Gelrite (Duchefa Biochemie) solution. A similar concentration of Gelrite solution was used as mock treatment.

Inoculation density-response curve

Individual Arabidopsis seeds were sown in square Petri dishes. Nine-day-old seedlings were inoculated with 0 (mock), 50, 100, 200, 350, or 500 H. schachtii J2s. Specifically, two 5 µl drops of solution (with J2s or mock) were pipetted at opposite sides of each seedling while keeping the Petri dishes vertical. This allowed for a homogeneous smear of J2s along the whole length of the root. At 7 days post inoculation (dpi), scans were made of whole seedlings using an Epson Perfection V800 photo scanner. The root architecture (total root length, primary root length, total secondary root length) was measured using the WinRHIZO package for Arabidopsis (Regent Instrument Inc.). For the coi1-2 mutant, primary root length was measured manually because of the convoluted root system. The number of root tips was counted manually based on the scans. Furthermore, nematodes within the roots were stained with acid fuchsin and counted as previously described (Warmerdam et al., 2018). For comparisons between genotypes, the background effect of the mutation on the root architecture was corrected by normalizing each measured component in infected seedlings to the average respective component in mock-inoculated roots. Additionally, the presence of clusters and the number of secondary roots per cluster were scored using a binocular.

Histology and microscopy

Four-day-old Arabidopsis seedlings were inoculated with either 15 H. schachtii J2s or mock solution. The choice of using younger seedlings like previously done by Zhou et al. (2019) was made to reduce the damage inflicted to the seedling during sample preparation for microscopy. Root architecture was inspected using an Olympus SZX10 binocular with a 1.5x objective and 2.5x magnification. Pictures were taken with an AxioCam MRc5 camera (Zeiss). For confocal and brightfield microscopy, single-nematode infection sites were selected for observation. For histochemical staining of β-glucuronidase (GUS) activity, seedlings were incubated in a GUS staining solution as previously described (Zhou et al., 2019) for four hours. Stained seedlings were mounted in a chloral hydrate clearing solution (12 M chloral hydrate, 25% glycerol) and inspected with an Axio Imager.M2 light microscope (Zeiss) via a 20x objective. Differential interference contrast (DIC) images were taken with an AxioCam MRc5 camera (Zeiss). GUS saturation was quantified as previously described (Beziat et al., 2017) using Fiji software (Schindelin et al., 2012). For confocal laser scanning microscopy, seedlings were mounted either in water or in 10 µg ml-1 propidium iodide and imaged using a Zeiss LSM 710 system via 10x and 40x objectives. The following wavelengths were used: 600–640 nm for PI, 500-540 nm for GFP, 520-560 nm for YFP, and 590-680 nm for RFP. For pAOS::YFPN and JAS9-VENUS reporters, the fluorescent signal was imaged at the focal plane displaying the xylem vessels, where the nematode head is found. For the pERF109::GFP reporter, Z-stacks of six 13µm-slices were made of the entire root depth. Images were taken using the ZEN 2009 software (Zeiss) and processed using Fiji software. To make the fluorescence more visible, the brightness was enhanced for all the representative pictures in the same way using Adobe Photoshop 2021. Fluorescence intensity was quantified using the Fiji software. Specifically, the region of interest was selected using a set threshold and then the integrated density was measured. Z-Stacks were projected using the maximum intensity method.

Auxin biosynthesis inhibition

For split-plate assays, we used the method described in Matosevich et al. (2020). For the L-kyn split plate assay the following four treatment combinations were prepared: MM (modified Knop medium and 0.02% DMSO), KK (modified Knop medium, 10 µM L-kynurenine (Sigma-Aldrich) and 0.02% DMSO), MK (L-kyn only in the root), and KM (L-kyn only in the shoot). The Yucasin split plate assay is described in Fig. S1. Four-day-old Arabidopsis seedlings were inoculated with 15 H. schachtii J2s. Sixteen hours post inoculation (hpi), when J2s are still migrating through the root, seedlings were transferred to the treatment plates, so that the shoot and the hypocotyl were in contact with the medium in the upper half of the plate and the nematode-infected root was on the medium in the lower half of the plate. For microscopy, seedlings were collected at 3 dpi and GUS staining was performed. For root architecture inspection, scans were made of whole seedlings at 7 dpi using an Epson Perfection V800 photo scanner. The total number of secondary roots per plant was counted based on the scans. Additionally, the presence of clusters and the number of secondary roots per cluster were scored using an Olympus SZX10 binocular.

Reverse transcription-quantitative real-time PCR

For reverse transcription-quantitative real-time PCR (RT-qPCR) analysis, several hundred root segments (~0.2 cm) harboring nematode infection sites or similar root segments of mock-inoculated 12-day old seedlings of Arabidopsis were collected at 12 hpi. Attention was paid not to include root tips and secondary root primordia. Subsequently, RNA extraction and qPCR were performed as previously described (Chopra et al., 2021; Hasan et al., 2022). ERF109 was amplified using the primers CTTATGATCGAGCCGCGATT and TCCTCCGTTCCATTGCTCTG (Cai et al., 2014; Zhou et al., 2019). Three independent biological replicates of the experiment were performed, with three technical replicates per each biological replicate. Relative expression of ERF109 was calculated based on the endogenous control 18S rRNA (Pfaffl, 2001). The average ERF109 expression in the mock-inoculated wildtype roots of the first biological replicate was used as a reference to normalize the average expression in the other samples (Hasan et al., 2022).

Statistical analysis

Statistical analyses were performed using the R software version 3.6.3 (Windows, x64). Correlation between variables was calculated using Spearman Rank-Order Correlation coefficient. Significance of the differences between samples was calculated as indicated in the figure legends. The confidence interval of the inoculum density-response curves was calculated by loess regression (as per default in geom_smooth) in R.

Results:

H. schachtii infection induces local formation of secondary roots in a nematode density-dependent manner

To test if tissue damage by invading nematodes in roots triggers the formation of secondary roots, we analyzed root branching upon penetration by increasing numbers of nematodes. We inoculated seedlings with 0, 50, 100, 200, 350, or 500 J2s of H. schachtii and counted both the number of nematodes that penetrated the roots and the total number of secondary roots at 7 dpi (Fig. 1). Here, the total number of secondary roots in infected seedlings was normalized to the average respective number in uninfected roots. We found that the number of nematodes that penetrated the roots increased by inoculum density for up to 350 J2s per plant, whereafter it remained the same (Fig. 1a). Furthermore, we observed that the number of penetrated nematodes correlated positively with the total number of secondary roots per plant (Fig. 1b). Next, we investigated if the clustering of secondary roots around nematode infections sites also correlates with the inoculum density (Fig. 1c,d). For this, we challenged Arabidopsis with four inoculum densities (0, 50, 100, and 350) to establish an incremental increase in the number of nematode infection sites per plant. Infection sites were identified by the local discoloration of root tissue due to cell necrosis along the migratory tract of the nematode (Grundler et al., 1994). Roots were counted as clusters when more than one secondary root emerged in proximity of an infection site. Also, we counted the number of secondary roots per cluster. We found that uninfected seedlings showed a typical pattern of lateral roots regularly distributed along the primary root (Fig. 1c). However, in infected seedlings clusters of secondary roots emerged close to nematode infection sites in an inoculum density-dependent manner (Fig. 1c,d). Interestingly, also the number of secondary roots per cluster significantly increased at inoculum density 350 compared to 50 (Fig. 1c,e). Moreover, higher inoculation densities caused more extensive discoloration at the infection sites indicating higher levels of tissue damage. Altogether, these observations showed that infection by H. schachtii triggers local density-dependent formation of secondary roots.

H. schachtii host invasion induces JA biosynthesis and signaling

Artificially induced tissue damage can trigger the formation of roots via JA-dependent signaling pathways. For instance, wounding induces JA-dependent *de novo* root organogenesis in leaf explants (Zhang et al., 2019). Infective juveniles of *H. schachtii* invade the host by destructive thrusts of the oral stylet and release of plant cell wall degrading enzymes causing extensive cell damage during host invasion (Grundler *et al.*, 1994; Tytgat et al., 2002; Vanholme et al., 2007). We hypothesized that secondary root formation in proximity of *H. schachtii* infection sites might be regulated by JA, in response to tissue damage associated with nematode host invasion. To test our hypothesis, we investigated whether JA biosynthesis and signaling were activated during *H. schachtii* infection using the JA biosynthesis reporter line *pAOS::YFP*$_N$ (Poncini *et al.*, 2017) and the JA signaling biosensor *JAS9-VENUS* (*p35S::JAS9-VENUS/p35S::H2B-RFP*) (Larrieu *et al.*, 2015) (Fig. 2). We chose three timepoints that reflect the early parasitic stages of intracellular host invasion (12 hpi), permanent

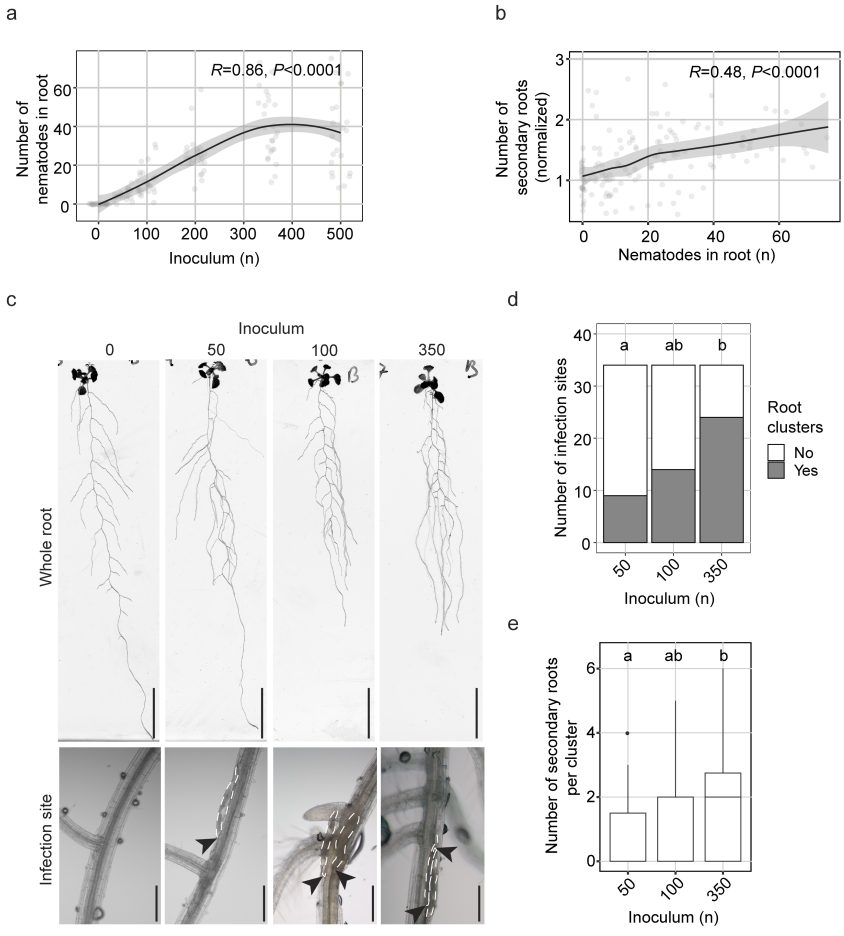

Figure 1: Secondary roots form locally at *Heterodera schachtii* infection sites in a nematode density-dependent manner. Nine-day-old Arabidopsis Col-0 seedlings were inoculated with increasing numbers of *H. schachtii* second-stage juveniles (J2s), ranging from 0 (mock) to 500 J2s per seedling. At 7 days post inoculation (dpi), scans were made of the root systems and the total number of secondary roots per plant was counted. Fuchsin staining was performed to count the number of J2s that had penetrated the roots. Additionally, the presence of clusters and the number of secondary roots per cluster was scored. **a)** Number of nematodes that successfully penetrated the roots per inoculum. **b)** Number of secondary roots formed per number of nematodes inside the roots. The total number of secondary roots in infected seedlings was normalized to the average respective component in uninfected roots and correlated with the number of nematodes inside the roots. Data from three independent biological repeats of the experiment was combined. Correlation (*R*) between two variables was calculated using Spearman's Rank-Order Correlation coefficient (n=30, *P*<0.0001). Grey area indicates the 95% confidence interval. **c)** Representative pictures of whole roots and infection sites in Col-0 seedlings inoculated with 0 (mock), 50, 100, and 350 J2s. Scale bars in whole root and infection site pictures are 2 cm and 200 µm, respectively. Black arrowheads indicate the nematodes head; white dotted lines outline the nematodes body. **d)** The proportions of secondary root clusters close to infection sites in Arabidopsis seedlings inoculated with 50, 100, and 350 J2s. Statistical significance was calculated by a Pairwise Z-test (n=34, *P*<0.05). (e) Number of secondary roots within each root cluster in Arabidopsis seedlings inoculated with 50, 100, and 350 J2s. Statistical significance was calculated by pairwise Wilcoxon test followed by false discovery rate correction for multiple comparisons (n=34, *P*<0.001). For boxplots, the horizontal line represents the median, the whiskers indicate the maximum/minimum range and the black dots represent the outliers. Different letters indicate statistically different groups.

feeding site initiation (24 hpi), and permanent feeding site expansion (168 hpi) (Tytgat et al., 2002; Hewezi et al., 2014; Kammerhofer et al., 2015; Marhavy et al., 2019). Importantly, to avoid interference of signals due to the presence of multiple nematodes at one infection site, we selected single-nematode infection sites for our observations. We found that infection with *H. schachtii* significantly induces transient expression of *pAOS::YFP*$_N$, with the highest level of expression at 12 hpi (Fig. 2a-d). Likewise, *JAS9-VENUS* showed a strong JA signaling activity (i.e., low VENUS/RFP ratio) in infected roots at 12 hpi, which decreased over time to the level of uninfected root tissue at 168 hpi (Fig. 2e-h). These observations demonstrated that both JA biosynthesis and JA signaling are strongly induced

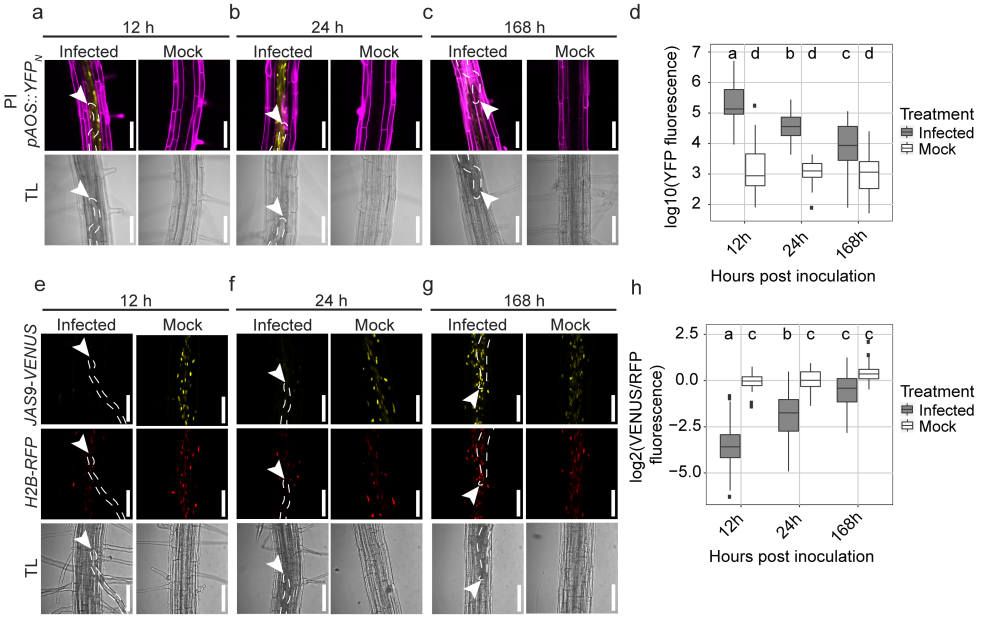

Figure 2: Transient induction of jasmonate (JA) biosynthesis and signaling at *Heterodera schachtii* infection sites. Four-day-old Arabidopsis seedlings were either inoculated with 15 *H. schachtii* second-stage juveniles (J2s) or mock-inoculated. At 12, 24, and 168 hours post inoculation (hpi) seedlings were mounted in 10 µg ml^{-1} propidium iodide (PI) and then imaged using a fluorescent confocal microscope. Single-nematode infection sites were selected for observation. **a-c)** Representative pictures of infected and non-infected roots expressing the JA biosynthesis marker *pAOS::YFP*$_N$. To make the fluorescence more visible, the brightness was enhanced for all the representative pictures in the same way. **d)** Quantification of YFP intensity in the *pAOS::YFP*$_N$ line. Values represent the $\log_{10}$ of the YFP integrated density. **e-g)** Representative pictures of infected and non-infected roots expressing the JA biosensor *p35S::JAS9-VENUS/p35S::H2B-RFP*. To make the fluorescence more visible, the brightness was enhanced for all the representative pictures in the same way. **h)** Quantification of the JA signaling repressor motif *JAS9*. Values represent the $\log_2$ of the fluorescence ratio between *JAS9-VENUS* and *H2B-RFP* raw integrated densities. Data from three independent biological repeats of the experiment was combined. Significance of differences between fluorescent intensities in nematode-infected and non-infected seedlings over the different timepoints was calculated by ANOVA followed by Tukey's HSD test for multiple comparisons (n=30, P<0.0001). For boxplots, the horizontal line represents the median, the whiskers indicate the maximum/minimum range and the black dots represent the outliers. Different letters indicate statistically different groups. White arrowheads indicate the nematode head; white dotted lines outline the nematode body. TL=transmission light. Scale bar is 100 µm.

during and shortly after *H. schachtii* host invasion close to the nematode infection site. We therefore concluded that tissue damage caused by *H. schachtii* during intracellular host invasion triggers local JA biosynthesis and signaling in Arabidopsis.

COI1-mediated JA signaling regulates ERF109 expression upon *H. schachtii* infection

Root tip resection or wounding in leaf explants induce *ERF109* expression in a COI1-dependent manner (Zhang et al., 2019; Zhou et al., 2019). To determine if *H. schachtii*-induced JA signaling also triggers *ERF109* expression, we monitored *pERF109::GFP* expression within single-nematode infection sites in the *coi1-2* mutant and wildtype Arabidopsis Col-0 plants during the early stages of infection by *H. schachtii* (Fig. 3). Similar to what we observed for JA biosynthesis and signaling, *ERF109* expression was induced at early timepoints (12 and 24 hpi) of *H. schachtii* infection around the migratory track of the nematodes in wildtype Col-0 (Fig. 3a-c). Moreover, in the *coi1-2* mutant, *pERF109::GFP* fluorescence was significantly reduced compared to wildtype Arabidopsis (Fig. 3d). Nevertheless, we observed a slight increase in fluorescence in *coi1-2* mutant over time, which reached the fluorescence levels detected in Col-0 at 168 hpi. The fluorescence detected in wildtype Col-0 and *coi1-2* mutant at 168 hpi might be caused by tissue autofluorescence from the cell walls of the permanent feeding sites (Hoth et al., 2005). Since *pERF109::GFP* has a nuclear-cytoplasmic localization (Zhou et al., 2019) due to GFP diffusion into the nucleus (Hanson & Kohler, 2001), autofluorescence from cell walls in syncytia cannot be easily distinguished from the cytoplasmic part of the *pERF109::GFP* signal. However, after quantifying only nuclear-localized *pERF109::GFP*, the initially observed fluorescence in the nematode-infected wildtype Col-0 and *coi1-2* mutant plants at 168 hpi was not detected anymore, pointing at autofluorescence as the most plausible cause (Fig. S2). To independently verify a COI1-dependent regulation of *ERF109* expression, we also performed a RT-qPCR on ERF109 transcripts in root segments containing nematode infection sites collected from *coi1-2* and wildtype Col-0 at 12 hpi. Consistent with the observed regulation of *pERF109::GFP* fluorescence, we found significantly fewer transcripts of *ERF109* in *coi1-2* compared to wildtype Col-0 (Fig. 3e). We therefore concluded that *H. schachtii* induces *ERF109* expression during host invasion in a JA-dependent manner.

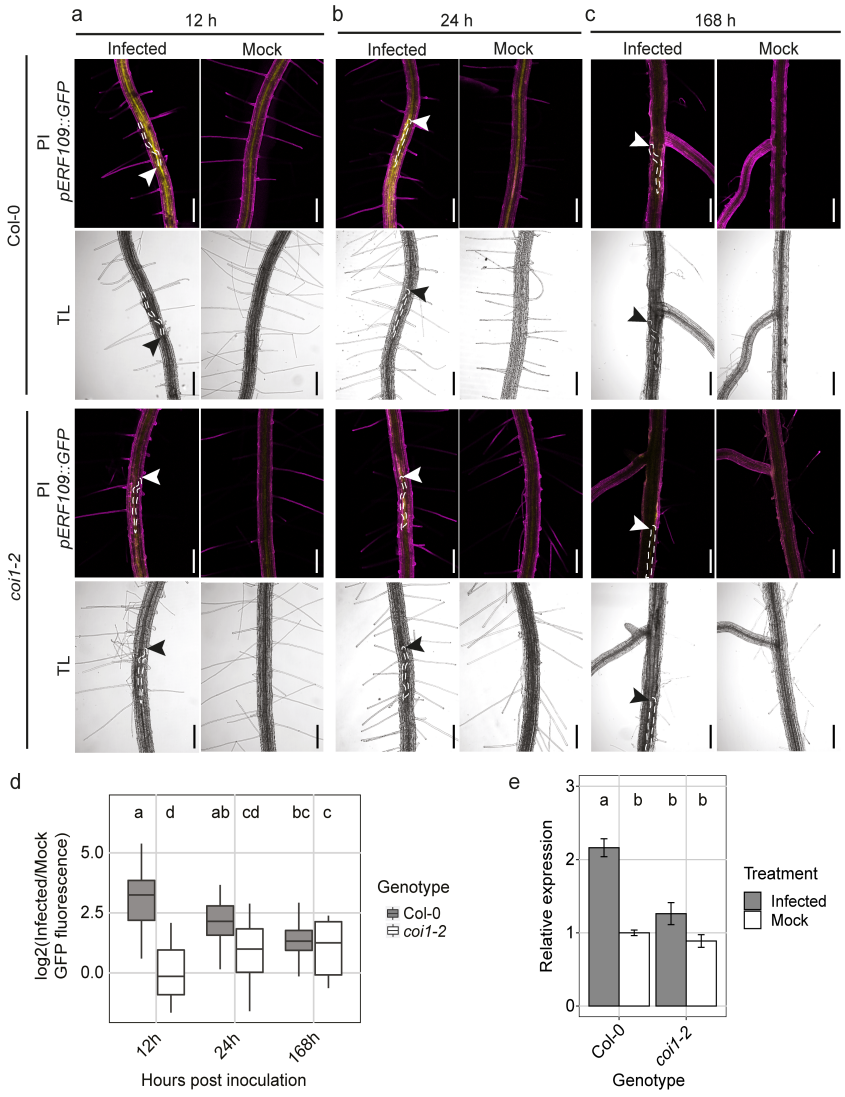

Figure 3: *ERF109* expression upon *Heterodera schachtii* host invasion is dependent on COI1-mediated jasmonate (JA) signaling. a-d) Four-day-old Arabidopsis seedlings were either inoculated with 15 *H. schachtii* second-stage juveniles (J2s) or mock-inoculated. At 12, 24, and 168 hours post inoculation (hpi) seedlings were mounted in 10 µg ml^{-1} propidium iodide (PI) and then imaged using a fluorescent confocal microscope. Single-nematode infection sites were selected for observation. **a-c)** Representative pictures of infected and mock-inoculated seedlings expressing the *pERF109::GFP* construct in either wildtype Col-0 or mutant *coi1-2* background at 12 hpi (**a**), 24 hpi (**b**), and 168 hpi (**c**). To make the fluorescence more visible, the brightness was enhanced for all the representative pictures in the same way. **d)** Quantification of *pERF109::GFP* fluorescent intensity induced by infection of Col-0 and *coi1-2* roots. Values represent $\log_2$ of the fluorescence ratio between the GFP integrated density of infected and non-infected roots. Data from two independent biological repeats of the experiment was combined. Significance of differences between fluorescent intensities in Col-0 and *coi1-2* roots over the different timepoints was calculated by ANOVA followed by Tukey's HSD test for multiple comparisons (n=20, P<0.05). For boxplots, the horizontal line represents the median and the whiskers indicate the maximum/minimum range. Different letters indicate statistically different groups. White and black arrowheads

indicate the nematode head; white dotted lines outline the nematode body. TL=transmission light. Scale bar is 200 µm. **e)** 12-day-old Col-0 and *coi1-2* Arabidopsis plants were inoculated with *H. schachtii.* At 12 hpi, RNA was extracted from root segments of ~ 0.2 cm harboring nematode infection sites or similar root segments of mock-inoculated seedlings. Data represents three independent biological replicates with three technical replicates per biological replicate. Relative expression of *ERF109* was first calculated based on the endogenous control *18s rRNA* and then normalized to the mock-inoculated wildtype samples in the first biological replicate. Significance of differences between *ERF109* relative expression in Col-0 and *coi1-2* infected roots was calculated by ANOVA followed by Tukey's HSD test for multiple comparisons (n=3 biological replicates, $P<0.01$). Different letters indicate statistically different groups. Error bars represent standard error of the mean.

COI1 and ERF109 regulate secondary root formation upon *H. schachtii* infection

Next, we asked if the activation of JA-dependent expression of *ERF109* is required for the formation of secondary roots during *H. schachtii* infections. If this holds true, the nematode density-dependent increase in secondary roots observed for wildtype Col-0 should be altered in both *coi1-2* and *erf109* mutants. To test this, we performed the same density-response experiment as shown in figure 1a and b. At 7 dpi, the number of nematodes that had successfully penetrated the roots did not differ significantly between wildtype Col-0 and the *erf109* mutant (Fig. 4). In contrast, the number of nematodes was significantly higher in roots of the *coi1-2* mutant compared to wildtype Arabidopsis plants, indicating a role of COI1 in plant susceptibility to penetration by *H. schachtii* (Fig. 4b). However, it must be noted that the uninfected *coi1-2* mutant had a much larger root system compared to wildtype Arabidopsis Col-0 (Fig. S3), which also may influence the number of nematode penetrations. Nevertheless, while nematode infections in wildtype Arabidopsis induced the formation of secondary roots, no such increase was observed for *erf109* and *coi1-2* mutants (Fig. 4c). In conclusion, both COI1 and ERF109 regulate the density-dependent induction of secondary root formation by *H. schachtii*. This induction of secondary root formation is independent from plant susceptibility to nematode penetration.

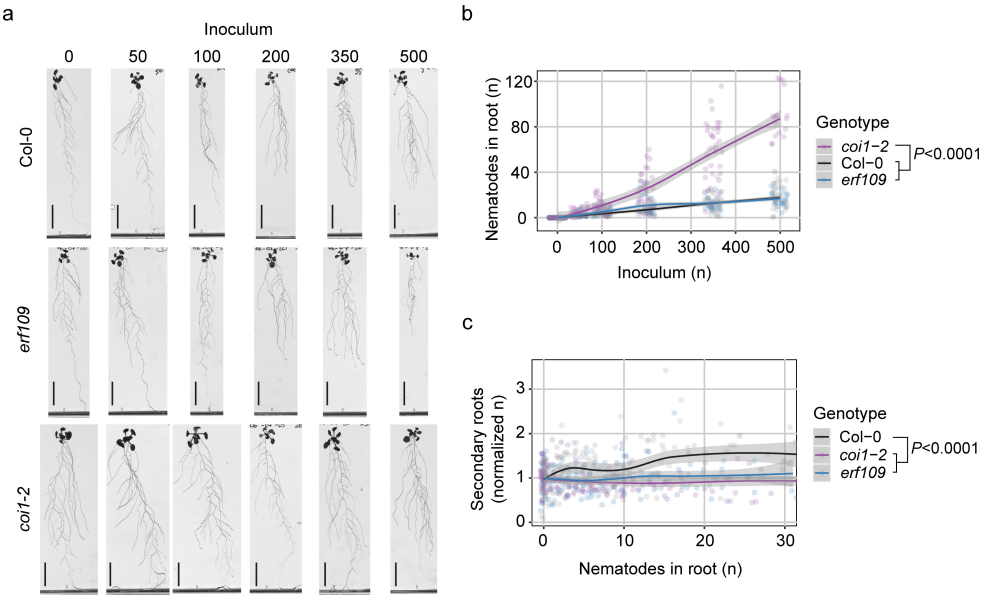

Figure 4: ERF109 and COI1 regulate the nematode density-dependent secondary root formation that is triggered by *Heterodera schachtii* infections. Nine-day-old wildtype Col-0, *erf109,* and *coi1-2* seedlings were inoculated with increasing numbers of *H. schachtii* second-stage juveniles (J2s), ranging from 0 (mock) to 500 J2s per seedling. At 7 days post inoculation, scans were made of the root systems and the number of secondary roots per plant was counted. Fuchsin staining was performed to count the number of J2s that had penetrated the roots. **a)** Representative pictures of wildtype Col-0, *erf109,* and *coi1-2* infected seedlings at 7 dpi. **b)** Number of nematodes that successfully penetrated the roots per inoculum. **c)** Secondary roots formed per number of nematodes inside the roots. The total number of secondary roots in infected seedlings was normalized to the average respective component in mock-treated roots. Data of three independent biological repeats of the experiment was combined. Significance of differences between genotypes was calculated by ANOVA followed by Tukey's HSD test for multiple comparisons (n=30, *P*<0.0001). Grey area indicates the 95% confidence interval. Scale bar is 2 cm.

ERF109-mediated induction of secondary root formation compensates for primary root growth inhibition by *H. schachtii*

The induction of secondary root formation by cyst nematodes might compensate for a possible inhibition of root growth by nematode invasion. To test this hypothesis, we investigated whether the total length of the entire root system, the primary root length, and the total length of the secondary roots were altered in the infected *erf109* mutant compared to wildtype Col-0 (Fig. 5). To eliminate the background effect of the mutation on the root architecture, we normalized each measured component in infected seedlings to the average respective component in uninfected roots. We found that the total length of the root system of wildtype Col-0 at increasing numbers of nematodes remains similar to that of uninfected plants (i.e., close to 1 in Fig. 5a). In contrast, the total length of the entire root system in the *erf109* mutant decreased by nematode density as compared to uninfected plants. As the total length of the root system is the sum of the lengths of the primary roots and the secondary roots, we also analyzed these components separately. The primary root length of both wildtype Col-0 and the *erf109* mutant declined by nematode density (Fig. 5b). This decline was slightly but significantly exacerbated by the *erf109* mutation. However, we found

a more striking difference in the total length of the secondary roots between wildtype Col-0 and the *erf109* mutant (Fig. 5c). In wildtype Col-0, we observed a significant increase in the total length of the secondary roots by nematode density, sufficient to compensate for the loss in primary root length. However, we observed no significant increase in the total length of the secondary roots by nematode density in the *erf109* mutant, which explains why the total length of the root system by nematode density remained stable for wildtype Col-0, but not for the *erf109* mutant. Based on our data, we conclude that ERF109-mediated formation of secondary roots compensates for primary root growth inhibition by *H. schachtii*.

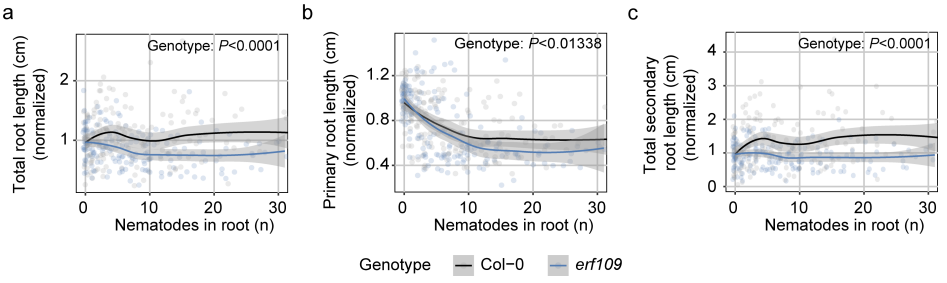

Figure 5: ERF109-mediated secondary root formation allows for maintenance of total root length despite primary root growth inhibition by *Heterodera schachtii*. Nine-day-old Col-0 and erf109 Arabidopsis seedlings were inoculated with increasing *H. schachtii* densities ranging from 0 (mock) to 500 second-stage juveniles (J2s) per seedling. At 7 days post inoculation, scans were made of the root systems and the root length was measured using WinRHIZO. Total, primary, and secondary root length was normalized to the average respective component in mock-treated roots. Fuchsin staining was performed for counting the number of J2s that penetrated the roots. **a)** Total root length per number of nematodes in the roots. **b)** Primary root length per number of nematodes in the roots. **c)** Total secondary root length per number of nematodes in the roots. Data from three independent biological repeats of the experiment was combined. Significance of differences between genotypes was calculated by ANOVA (n=30). Grey area indicates the 95% confidence interval.

ERF109 regulates local auxin biosynthesis at the nematode infection site

ERF109 mediates JA-induced secondary root formation by directly binding to the promoter of auxin biosynthesis genes *ASA1* and *YUC2* (Cai et al., 2014). We hypothesized that ERF109 regulates secondary root formation by inducing local auxin biosynthesis at the nematode infection site. Thus, we used a split plate assay containing growth media with and without L-kyn to chemically inhibit auxin biosynthesis in the shoots and/or the roots of infected wildtype and *erf109* plants (Fig. 6). The local accumulation of auxin was monitored using the *DR5::GUS* reporter (Fig. 6a). When seedlings were grown on regular medium or when auxin biosynthesis was inhibited by L-kyn only in the shoots, *DR5::GUS* was expressed at nematode infection sites in wildtype Col-0 seedlings. However, when auxin biosynthesis was inhibited in both shoots and roots or only in the roots by treatment with L-kyn, no *DR5::GUS* expression was observed (Fig. 6b,c). This suggested that auxin accumulation at nematode infection sites was dependent on local auxin biosynthesis in the roots. Importantly, we observed that the auxin accumulation at nematode infection sites via root-localized auxin biosynthesis was disrupted in the *erf109* mutant. Indeed,

DR5::GUS expression was significantly lower at the nematode infection sites in *erf109* seedlings compared to wildtype Col-0 when auxin biosynthesis was permitted in the root (Fig. 6b,c). To determine if the differences in *DR5::GUS* between the two Arabidopsis genotypes were only local at the nematode infection site or systemic throughout the root system, we also looked at *DR5::GUS* expression in root tips (Fig. 6d, S4). In contrast to nematode infection sites, when auxin biosynthesis was inhibited only in the shoots, we observed no difference between *erf109* and wildtype Col-0 in *DR5::GUS* expression in the root tip (Fig. 6d, S4). Since L-kyn has been shown to also inhibit ethylene-induced auxin biosynthesis (He *et al.*, 2011) we also performed the experiment using the auxin biosynthesis inhibitor Yucasin (Yuc). Due to the higher concentration of DMSO used to dissolve Yuc, an overall lower frequency of *DR5:GUS* staining was observed. Nevertheless, the Yuc split plate assay showed the same trend as the L-kyn experiment (Fig. S1). From these results, we concluded that ERF109 regulates local auxin biosynthesis at infection sites of *H. schachtii*.

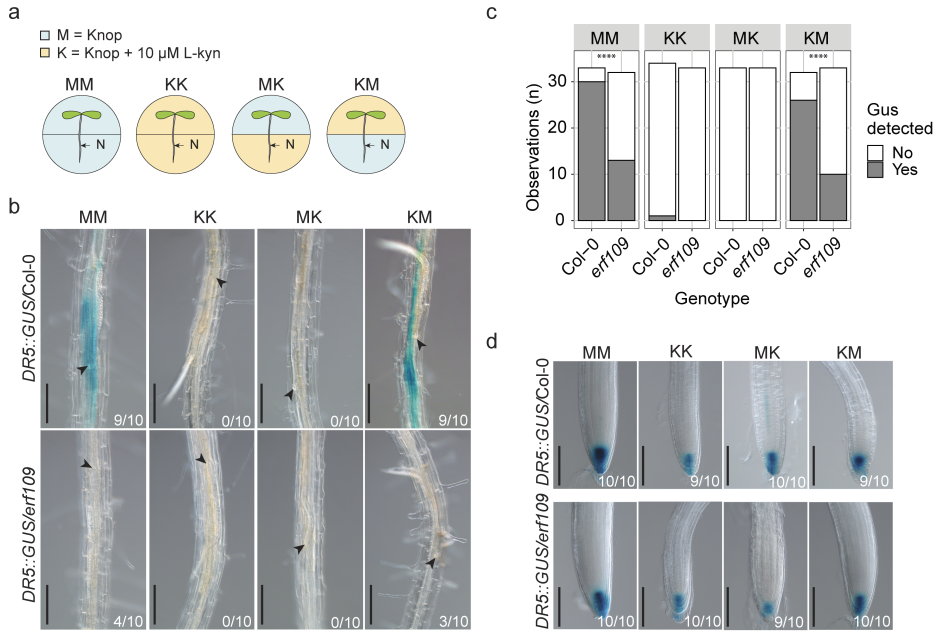

Figure 6: ERF109 regulates local auxin biosynthesis at *Heterodera schachtii* infection sites. Four-day-old Arabidopsis Col-0 and *erf109* seedlings expressing the auxin *DR5::GUS* reporter were infected with 15 *H. schachtii* second-stage juveniles (J2s). At 16 hours post inoculation, seedlings were transferred to treatment plates. Four treatment combinations were prepared: MM (modified Knop medium and 0.02% DMSO), KK (modified Knop medium, 10µM L-kyn and 0.02% DMSO), MK (L-kyn only in the root), KM (L-kyn only in the shoot). At 3 days post inoculation GUS staining assay was performed for 4 hours and seedlings were imaged. Single-nematode infection sites were selected for observation. **a)** Experimental design with Arabidopsis seedlings transferred to split plates with modified Knop medium either with or without L-kyn. N = nematode. **b)** *DR5::GUS* expression at nematode infection sites in wildtype Col-0 and *erf109* roots in the four different treatment combinations with or without L-kyn applied to shoots and/or roots. **c)** Number of observations with (Yes) or without (No) GUS staining at the nematode infection sites in roots of wildtype Col-0 and *erf109* plants. Statistical significance was calculated by a Pairwise Z-test (n=33, ****, $P<0.0001$). **d)** *DR5::GUS* expression in the root tips of Col-0 and *erf109* roots. Black arrowheads indicate the nematode head. Frequencies at the bottom right corner indicate how many times GUS staining was observed in one of the three independent biological repeats of the experiment. Scale bar is 200 µm.

ERF109-induced secondary root formation upon *H. schachtii* infection is dependent on local auxin biosynthesis

We found that ERF109 regulates local auxin biosynthesis at *H. schachtii* infection sites. This raised the question if the ERF109-mediated secondary root formation upon *H. schachtii* infection is dependent on this local biosynthesis of auxin. To test this, we inoculated four-day-old wildtype Col-0 and *erf109* seedlings with either 15 *H. schachtii* J2s or a mock solution. At 16 hpi, seedlings were transferred to the four previously described split-plates containing medium with and without 10 µM L-kyn (Fig. 6a). At 7 dpi, the total number of secondary roots was scored. As expected, the different treatment combinations with and without L-kyn in the shoots and/or roots led to a different number of lateral roots in the uninfected roots (Fig. S5). Therefore, to calculate the number of additional secondary roots induced by nematode infection, the number of secondary roots in infected roots was normalized to the average respective component in uninfected roots. Additionally, we scored how often a cluster of roots occurs in proximity of an infection site and the number of secondary roots per cluster (Fig. 7). When auxin biosynthesis was inhibited in both shoots and roots or only in the roots no additional secondary roots formed in infected Col-0 wildtype seedlings (Fig. 7a,b). Consistently, no clusters of secondary roots were found at nematode infection sites (Fig. 7c-e). However, inhibition of auxin biosynthesis in the shoots alone led to a significant reduction in the total number of secondary roots in infected seedlings (Fig. 7a, b) as well as in the number of clusters and the number of secondary roots per cluster compared to when auxin biosynthesis was permitted in both shoots and roots (Fig. 7c-e; treatment MM versus KM). Thus, secondary root formation upon *H. schachtii* infection is dependent on local auxin biosynthesis, although polar auxin transport from the shoots might still play a role. Furthermore, the mutation in *erf109* strongly affected secondary root formation when auxin biosynthesis was permitted in the roots. Indeed, a significant decrease in the number of additional secondary roots, the number of clusters of secondary roots, and the number of secondary roots per cluster was observed for *erf109* when compared to wildtype Col-0 (Fig. 7). Altogether, we concluded that ERF109-dependent secondary root formation upon *H. schachtii* infection relies at least partially on local auxin biosynthesis.

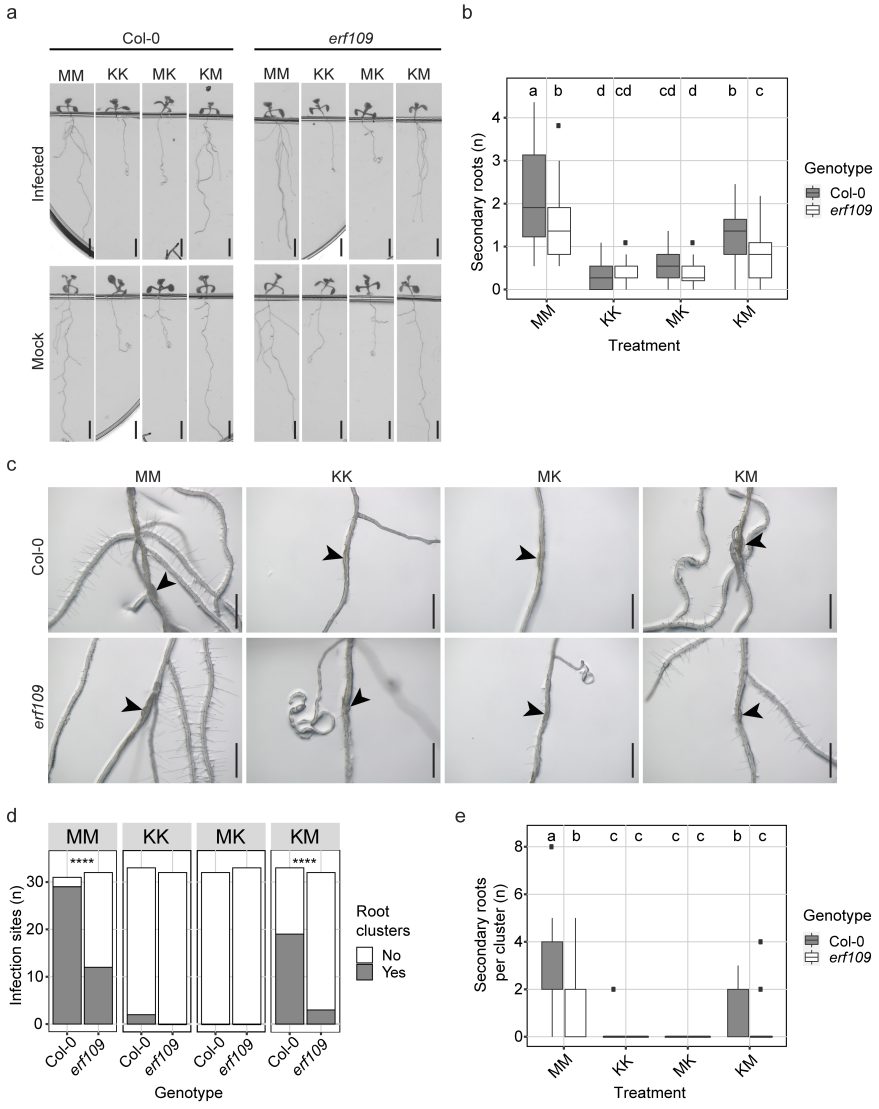

Figure 7: ERF109-dependent local auxin biosynthesis regulates secondary root formation upon *Heterodera schachtii* infection. Four-day-old Arabidopsis Col-0 and *erf109* seedlings were either infected with 15 *H. schachtii* second-stage juveniles (J2s) or mock-inoculated. At 16 hours post inoculation, seedlings were transferred to treatment plates. Four treatment combinations were prepared: MM (modified Knop medium and 0.02% DMSO), KK (modified Knop medium, 10µM L-kyn and 0.02% DMSO), MK (L-kyn only in the root), KM (L-kyn only in the shoot). At 7 days post inoculation, scans were made of the root systems and the total number of secondary roots per plant was counted. Additionally, the presence of clusters and the number of secondary roots per cluster was scored. **a)** Representative pictures of wildtype Col-0 and *erf109* mutant seedlings. (Figure legend continues on the page).
b) Number of secondary roots in infected versus non-infected roots of wildtype Col-0 and *erf109* seedlings. Data of two independent biological repeats of the experiment was combined. Significance of differences in secondary roots between the different treatment combinations was calculated by ANOVA followed by Tukey's HSD test for multiple comparisons (n=43-45, $P<0.05$). **c)** Representative images of nematode infection sites in wildtype Col-0 and *erf109* mutant. **d)** Number of secondary root clusters that are associated with *H. schachtii* infection sites. Data of two independent biological repeats of the

experiment was combined. Statistical significance was calculated by a Pairwise Z-test n=31-33, ****, *P*<0.0001). **e)** Number of secondary roots per cluster. Data of two independent biological repeats of the experiment was combined. Significance of differences between secondary roots within a cluster was calculated by Aligned Rank Transform for non-parametric factorial ANOVA followed by Tukey's HSD test for multiple comparisons (n=31-33, *P*<0.0001). For boxplots, the horizontal line represents the median, the whiskers indicate the maximum/minimum range and the black dots represent the outliers. Difference in letters indicates statistically different groups. Black arrowheads indicate the infection site. Scale bar is 0.5 cm.

Discussion:

Root architecture plasticity in response to stress by soil-borne pathogens and pests is a largely unexplored field of research. Root parasitism by cyst nematodes is often associated with formation of secondary roots in proximity of infection sites (Grymaszewska & Golinowski, 1991; Goverse et al., 2000; Lee et al., 2011). However, the molecular mechanisms regulating secondary root formation in response to cyst nematode infection have thus far remained unclear. Here, we provide evidence for a model wherein formation of secondary roots near H. schachtii infection sites is triggered by tissue damage caused by nematode invasion. This response is regulated by the JA-dependent ERF109-activated local biosynthesis of auxin.

Our data demonstrates that secondary root formation is most likely initiated by tissue damage brought about by cyst nematode infections. The number of secondary roots induced by H. schachtii correlated positively with the number of nematodes that penetrated the roots. This increase in the number of secondary roots may be simply due to an increase in the number of infection sites. However, we also observed more nematodes within infection sites at higher inoculation densities, which correlated well with the number of secondary roots per infection site. This may mean that infection sites containing multiple nematodes developed a higher number of secondary roots per cluster compared to single-nematode associated infection sites. Moreover, we saw more extensive root tissue damage (i.e., root discoloring) at infection sites harboring multiple nematodes. We therefore consider tissue damage by infective juveniles inside roots as the likely cause of enhanced local secondary root formation.

Tissue damage in Arabidopsis leaf explants triggers de novo root organogenesis in a JA-dependent manner (Zhang et al., 2019). We found that intracellular host invasion by H. schachtii transiently induces JA biosynthesis and signaling, and that the JA receptor mutant coi1-2 is defective in secondary root formation upon H. schachtii infection. Our results are in line with whole transcriptome analyses of root segments of Arabidopsis harboring migrating juveniles of H. schachtii at 10 hpi, which also showed that JA biosynthesis and signaling genes are upregulated during host invasion (Kammerhofer et al., 2015; Mendy et al., 2017). In contrast, recent reports indicate that host invasion by H. schachtii does not activate the JA signaling biosensor JAZ10::NLS-3xVENUS in Arabidopsis roots (Marhavy et al., 2019). The discrepancy between our observations with the JAS9-VENUS biosensor and the observations with the JAZ10::NLS-3xVENUS biosensor might be due to differences in sensitivity of both sensor constructs. As compared to JAZ10::NLS-3xVENUS, the JAS9-VENUS biosensor is particularly sensitive to biologically active JA (JA-isoleucine) enabling the visualization of local JA signaling in response to stress in Arabidopsis roots at a high spatiotemporal resolution (Larrieu et al., 2015). Furthermore, JAS9-VENUS has been used to monitor the dynamics of JA signaling in response to single-cell ablation and intercellular migration of the less-damaging root-knot nematodes in Arabidopsis roots (Zhou et al., 2019). Therefore, based on

the activity of the JAS9-VENUS biosensor in our experiments, we conclude that the tissue damage associated with host invasion triggers a JA signal in cells close to the infection site of H. schachtii. Moreover, the transient nature of the JA signal suggests that the damage trigger decreases after nematode host invasion, or that JA signaling is actively suppressed by H. schachtii when infective juveniles become sedentary.

JA signaling during H. schachtii migration also results in activation of plant defense responses (Kammerhofer et al., 2015). We observed that the coi1-2 mutant is more susceptible to penetration by H. schachtii, which is in line with previous findings showing a negative effect of exogenous JA on H. schachtii penetration rate (Kammerhofer et al., 2015). However, after nematode penetration, COI1 does not affect the rate at which J2s induce a permanent feeding site (Marhavy et al., 2019). Altogether, these findings suggest that JA signaling both negatively regulates host penetration rate by H. schachtii and mediates secondary root formation at H. schachtii infection sites.

The damage-induced formation of secondary roots by H. schachtii appears to be regulated by the JA-dependent expression of ERF109. We found that the expression of ERF109, which showed the same transient induction pattern as the JA biosynthesis reporter AOS and JAS9-VENUS biosensor, was abrogated in coi1-2 mutant. Moreover, the erf109 mutant was as defective as the coi1-2 mutant in the density-dependent secondary root formation upon H. schachtii infection. Consistently with our data, ERF109 expression showed a COI1-dependent transient expression upon wounding in leaf explants (Zhang et al., 2019). Furthermore, the erf109 mutation also disrupted the induction of secondary root formation by exogenous application of JA (Cai et al., 2014). Altogether, our findings show that tissue damage by invading nematodes triggers a JA signal, which induces the ERF109-dependent formation of secondary roots.

Next, our data provides evidence that damage-induced activation of ERF109 regulates formation of secondary roots via local auxin biosynthesis. The local accumulation of auxin at nematode infection sites (i.e., expression of the auxin reporter DR5::GUS) was strongly reduced in the erf109 mutant compared to wildtype plants. However, when auxin biosynthesis was blocked in whole seedlings or only in roots, the local accumulation of auxin at nematode infection sites was completely abolished in both the erf109 mutant and wildtype Arabidopsis. Taken together, this demonstrates that auxin accumulation at nematode infection sites is at least partially dependent on ERF109-regulated local auxin biosynthesis. Importantly, the patterns observed for local accumulation of auxin at nematode infection sites matched the patterns of secondary root formation in absence or presence of the auxin biosynthesis inhibitor. The inhibition of auxin biosynthesis in the roots, but not in the shoots, abolished the formation of secondary roots upon nematode infection. Previously, ERF109 was shown to regulate secondary root formation by binding the promoter of auxin biosynthesis genes upon exogenous application of JA (Cai et al., 2014). Here, our data shows that tissue damage by nematodes activates JA signaling and subsequently induces ERF109, which on its turn regulates secondary root formation via local biosynthesis of auxin.

After blocking auxin biosynthesis in the shoots, we observed auxin accumulation and formation of secondary roots at nematode infection sites, which indicates that polar auxin transport from the shoots is not required for secondary root formation at nematode infection sites. Nevertheless, we noted a quantitative effect of the inhibition of auxin biosynthesis in shoots, leading to the formation of fewer secondary root clusters and fewer secondary roots per cluster as compared

to untreated plants. This implies that polar auxin transport from the shoots may still play a complementary role in secondary root formation at nematode infection sites, albeit below the detection levels of the DR5::GUS reporter. Polar auxin transport from the shoots and further redistribution in root tissue results from the coordinated activities of auxin influx and efflux carrier proteins (Petrasek & Friml, 2009). Lee et al. (2011) showed that H. schachtii induces the formation of secondary roots in double aux1lax3 and quadruple aux1lax1lax2lax3 influx carrier mutants, which are otherwise unable to form secondary roots. This suggests that the accumulation of auxin and subsequent formation of secondary roots may be regulated independently of the activity of these influx carriers. There is ample evidence that auxin efflux carriers (i.e., PIN proteins) are important for the susceptibility of Arabidopsis to infections of H. schachtii (Grunewald et al., 2009). However, if and how they might contribute to the accumulation of auxin underlying the damage-induced formation of secondary roots needs further investigation.

Here, we demonstrate that ERF109-mediated local adaptations in root architecture compensate for primary root growth inhibition in response to nematode infection. In wildtype Arabidopsis, increasing densities of J2s led to a decline in the length of infected primary roots. However, this reduction in length of infected primary roots did not result into a smaller root system, because of an increase in the total length of secondary roots. Our data shows that these adaptations in root architecture depend on the transient and local activation of ERF109 by JA at nematode infection sites. Consistently, the JA signaling mutant coi1-2 showed a similar impairment as erf109 in compensating primary root length inhibition by an increase in total secondary root length (Fig. S6). Nevertheless, since COI1 also affects plant susceptibility to nematode penetration more complex defense versus growth trade-offs may influence root growth in the coi1-2 mutant. Importantly, loss of function mutations in ERF109 do not alter the susceptibility of Arabidopsis to H. schachtii penetration, but instead affect root architecture plasticity in response to nematode infection. Further research is needed to understand whether ERF109-mediated compensatory adaptations in root architecture could mediate tolerance of Arabidopsis to infections by H. schachtii.

It was previously shown that meristem damage caused by M. incognita root tip penetration triggers regeneration via JA- and ERF109-mediated damage signaling (Zhou et al., 2019). Here, we show that H. schachtii penetration of the mature root zone causes damage-induced secondary root formation, which compensates for primary root growth inhibition. Therefore, we consider root tip regeneration and secondary root formation as two different outcomes of the same compensatory mechanism in response to tissue damage in different root zones.

Furthermore, we show the first case of a naturally occurring and biotic stress that triggers damage signaling-mediated secondary root formation. Primary roots can form two types of secondary roots (Sheng et al., 2017). One type, referred to as lateral root, forms during the physiological post-embryogenic development of plants and is regulated by ARF7 and ARF19 auxin response factors. The other type is induced by sterile mechanical injury of the mature root zone, soil penetration, or osmotic stress, and is dependent on the transcription factor WOX11. Sterile mechanical injury causes a different type of root tissue damage compared to a biotic stress such as cyst nematodes (Marhavy et al., 2019). Sterile mechanical injury damages many root cells at one time. Instead, cyst nematode host invasion causes the rupture of multiple single cells one after the other over the course of many hours (Wyss & Zunke, 1986). Thus, our results provide biological relevance for a

mechanism so far only observed upon artificial conditions.
As a natural trigger for damage signaling, H. schachtii can be used to further elucidate the pathway leading to secondary root formation. ERF109 was previously found to be responsive to reactive oxygen species (ROS) (Kong et al., 2018). It would be interesting to test whether ROS mediate ERF109-dependent secondary root formation upon H. schachtii infection. Furthermore, follow-up research could investigate if damage receptors activated during H. schachtii migration (Shah et al., 2017) act upstream of ERF109. The root-knot nematode M. javanica triggers expression of LBD16, a downstream target of both WOX11, and ARF7 and ARF19 (Cabrera et al., 2014; Olmo et al., 2017). Moreover, M. javanica infection of primary roots induces secondary root formation independently from ARF7 and ARF19 (Olmo et al., 2017). This suggests that nematode-induced secondary root formation could be regulated by WOX11. However, whether WOX11-mediated secondary root formation acts downstream of the ERF109-damage signaling pathway remains unknown.

In summary, we showed that H. schachtii triggers the formation of secondary roots via JA- and ERF109-mediated damage signaling (Fig. 8). Furthermore, ERF109-mediated secondary root formation compensates for primary root growth inhibition associated with H. schachtii infection. Thus, damage signaling-induced formation of secondary roots points at a novel mechanism underlying plant root architecture plasticity to biotic stress. Further research is needed to investigate whether damage-induced root architecture plasticity can contribute to plant tolerance to belowground herbivory.

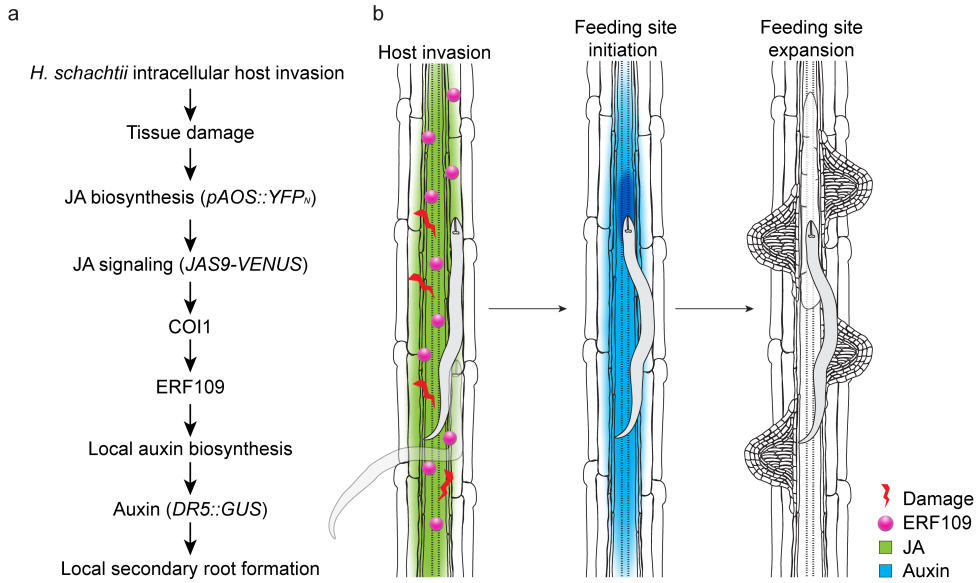

Figure 8: Model of the pathway regulating *Heterodera schachtii*-induced secondary root formation. **a)** Intracellular invasion of host roots by *H. schachtii* causes tissue damage, which triggers jasmonate (JA) biosynthesis (*pAOS::YFP*$_N$). JA signaling (*JAS9-VENUS*) via COI1 induces expression of *ERF109*, which leads to auxin accumulation (*DR5::GUS*) via local auxin biosynthesis. ERF109-mediated local auxin biosynthesis finally results in the formation of secondary roots at *H. schachtii* infection sites. **b)** Graphical model illustrating the pathway investigated in this paper.

Supporting information:

Figure S1. Yuc split plate assay showing that ERF109 regulates local auxin biosynthesis at the nematode infection site.
Figure S2. Induction of *pERF109::GFP* nuclear fluorescence by *Heterodera schachtii* host invasion is disrupted in the *coi1-2* Arabidopsis mutant.
Figure S3. The root architecture of uninfected coi1-2 and erf109 Arabidopsis plants differs from wildtype Col-0 plants.
Figure S4. *DR5::GUS* expression at the root tip does not differ between infected wildtype Col-0 and *erf109* seedlings when auxin biosynthesis is inhibited only in the shoot.
Figure S5. The number of lateral roots in non-infected wildtype Col-0 and *erf109* mutant seedlings is affected by L-kyn treatment.
Figure S6. COI1-mediated secondary root formation allows for maintenance of total root length despite primary root growth inhibition by *Heterodera schachtii.*

Author contributions:

We thank Hang Liu for the help provided with data collection as part of his MSc Thesis at Wageningen University. This work was supported by the Graduate School Experimental Plant Sciences (EPS). WZ was funded by EMBO long-term fellowship (ALTF 784-2014) and the National Natural Science Foundation of China (32070874). JJW was funded by Dutch Top Sector Horticulture & Starting Materials (TU18152). MGS was supported by NWO domain Applied and Engineering Sciences VENI grant (17282). JLLT was supported by NWO domain Applied and Engineering Sciences VENI (14250) and VIDI (18389) grants. No conflict of interest declared.

Author contributions:

JLLT, GS, NG, JJW, AG, WZ, and VW conceived the project. NG, JJW, MSH and LS designed the experiments and performed data collection. WZ and VW provided most of the Arabidopsis mutants and granted access to the confocal microscope. WZ performed the crossing to obtain the pERF109::GFP/coi1-2 Arabidopsis line, while homozygous plants were selected by both WZ and NG. Data was analyzed and interpreted by NG, JJW, MSH and MGS. NG, JLLT, GS, and JJW wrote the article with inputs from AG, MGS, VW, WZ, MSH, LS and FMWG.

Funding statement:

This work was supported by the Graduate School Experimental Plant Sciences (EPS). JJW is funded by Dutch Top Sector Horticulture & Starting Materials (TU18152). MGS was supported by NWO domain Applied and Engineering Sciences VENI grant (17282).

Data availability:

The data that supports the findings of this study are available in the supplementary material of this article.

References:

Absmanner B, Stadler R, Hammes UZ. 2013. Phloem development in nematode-induced feeding sites: the implications of auxin and cytokinin. *Front Plant Sci* **4**: 241.

Baum TJ, Wubben MJ, Hardyy KA, Su H, Rodermel SR. 2000. A screen for *Arabidopsis thaliana* mutants with altered susceptibility to *Heterodera schachtii*. *J Nematol* **32**(2): 166-173.

Beziat C, Kleine-Vehn J, Feraru E. 2017. Histochemical staining of beta-glucuronidase and its spatial quantification. *Methods Mol Biol* **1497**: 73-80.

Bohlmann H, Sobczak M. 2014. The plant cell wall in the feeding sites of cyst nematodes. *Front Plant Sci* **5**: 89.

Cabrera J, Diaz-Manzano FE, Sanchez M, Rosso MN, Melillo T, Goh T, Fukaki H, Cabello S, Hofmann J, Fenoll C, et al. 2014. A role for *LATERAL ORGAN BOUNDARIES-DOMAIN 16* during the interaction Arabidopsis-*Meloidogyne* spp. provides a molecular link between lateral root and root-knot nematode feeding site development. *New Phytol* **203**(2): 632-645.

Cai XT, Xu P, Zhao PX, Liu R, Yu LH, Xiang CB. 2014. Arabidopsis ERF109 mediates cross-talk between jasmonic acid and auxin biosynthesis during lateral root formation. *Nat Commun* **5**: 5833.

Chen L, Tong J, Xiao L, Ruan Y, Liu J, Zeng M, Huang H, Wang JW, Xu L. 2016. YUCCA-mediated auxin biogenesis is required for cell fate transition occurring during *de novo* root organogenesis in Arabidopsis. *J Exp Bot* **67**(14): 4273-4284.

Chopra D, Hasan MS, Matera C, Chitambo O, Mendy B, Mahlitz SV, Naz AA, Szumski S, Janakowski S, Sobczak M, et al. 2021. Plant parasitic cyst nematodes redirect host indole metabolism via NADPH oxidase-mediated ROS to promote infection. *New Phytol* **232**(1): 318-331.

Dubrovsky JG, Sauer M, Napsucialy-Mendivil S, Ivanchenko MG, Friml J, Shishkova S, Celenza J, Benkova E. 2008. Auxin acts as a local morphogenetic trigger to specify lateral root founder cells. *Proc Natl Acad Sci U S A* **105**(25): 8790-8794.

Fukaki H, Tasaka M. 2009. Hormone interactions during lateral root formation. *Plant Mol Biol* **69**(4): 437-449.

Gheysen G, Mitchum MG. 2011. How nematodes manipulate plant development pathways for infection. *Curr Opin Plant Biol* **14**(4): 415-421.

Goverse A, Overmars H, Engelbertink J, Schots A, Bakker J, Helder J. 2000. Both induction and morphogenesis of cyst nematode feeding cells are mediated by auxin. *Mol Plant Microbe Interact* **13**(10): 1121-1129.

Grundler FMW, Böckenhoff A, Schmidt K-P, Sobczak M, Golinowski W, Wyss U 1994. *Arabidopsis thaliana* and *Heterodera schachtii*: a versatile model to characterize the interaction between host plants and cyst nematodes. In: Lamberti F, De Giorgi C, Bird DM eds. *Advances in Molecular Plant Nematology*. Boston, MA: Springer US, 171-180.

Grunewald W, Cannoot B, Friml J, Gheysen G. 2009. Parasitic nematodes modulate PIN-mediated auxin transport to facilitate infection. *PLoS Pathog* **5**(1): e1000266.

Grymaszewska G, Golinowski W. 1991. Structure of syncytia Induced by *Heterodera avenae* Woll. in roots of susceptible and resistant wheat (*Triticum aestivum L.*). *Journal of Phytopathology* **133**(4): 307-319.

Hanson MR, Kohler RH. 2001. GFP imaging: methodology and application to investigate cellular compartmentation in plants. *J Exp Bot* **52**(356): 529-539.

Hasan MS, Chopra D, Damm A, Koprivova A, Kopriva S, Meyer AJ, Muller-Schussele S, Grundler FMW, Siddique S. 2022. Glutathione contributes to plant defence against parasitic cyst nematodes. *Mol Plant Pathol* **23**(7): 1048-

1059.
He W, Brumos J, Li H, Ji Y, Ke M, Gong X, Zeng Q, Li W, Zhang X, An F, et al. 2011. A small-molecule screen identifies L-kynurenine as a competitive inhibitor of TAA1/TAR activity in ethylene-directed auxin biosynthesis and root growth in Arabidopsis. *Plant Cell* **23**(11): 3944-3960.
Hewezi T, Piya S, Richard G, Rice JH. 2014. Spatial and temporal expression patterns of auxin response transcription factors in the syncytium induced by the beet cyst nematode *Heterodera schachtii* in Arabidopsis. *Mol Plant Pathol* **15**(7): 730-736.
Hoth S, Schneidereit A, Lauterbach C, Scholz-Starke J, Sauer N. 2005. Nematode infection triggers the de novo formation of unloading phloem that allows macromolecular trafficking of green fluorescent protein into syncytia. *Plant Physiol* **138**(1): 383-392.
Hu X, Xu L. 2016. Transcription factors WOX11/12 directly activate WOX5/7 to promote root primordia initiation and organogenesis. *Plant Physiol* **172**(4): 2363-2373.
Jones JT, Haegeman A, Danchin EG, Gaur HS, Helder J, Jones MG, Kikuchi T, Manzanilla-Lopez R, Palomares-Rius JE, Wesemael WM, et al. 2013. Top 10 plant-parasitic nematodes in molecular plant pathology. *Mol Plant Pathol* **14**(9): 946-961.
Kammerhofer N, Radakovic Z, Regis JM, Dobrev P, Vankova R, Grundler FM, Siddique S, Hofmann J, Wieczorek K. 2015. Role of stress-related hormones in plant defence during early infection of the cyst nematode *Heterodera schachtii* in Arabidopsis. *New Phytol* **207**(3): 778-789.
Karczmarek A, Overmars H, Helder J, Goverse A. 2004. Feeding cell development by cyst and root-knot nematodes involves a similar early, local and transient activation of a specific auxin-inducible promoter element. *Mol Plant Pathol* **5**(4): 343-346.
Koevoets IT, Venema JH, Elzenga JT, Testerink C. 2016. Roots withstanding their environment: exploiting root system architecture responses to abiotic atress to improve crop tolerance. *Front Plant Sci* **7**: 1335.
Kong X, Tian H, Yu Q, Zhang F, Wang R, Gao S, Xu W, Liu J, Shani E, Fu C, et al. 2018. PHB3 maintains root stem cell niche identity through ROS-responsive AP2/ERF transcription factors in Arabidopsis. *Cell Rep* **22**(5): 1350-1363.
Larrieu A, Champion A, Legrand J, Lavenus J, Mast D, Brunoud G, Oh J, Guyomarc'h S, Pizot M, Farmer EE, et al. 2015. A fluorescent hormone biosensor reveals the dynamics of jasmonate signalling in plants. *Nat Commun* **6**: 6043.
Lee C, Chronis D, Kenning C, Peret B, Hewezi T, Davis EL, Baum TJ, Hussey R, Bennett M, Mitchum MG. 2011. The novel cyst nematode effector protein 19C07 interacts with the Arabidopsis auxin influx transporter LAX3 to control feeding site development. *Plant Physiol* **155**(2): 866-880.
Liu J, Sheng L, Xu Y, Li J, Yang Z, Huang H, Xu L. 2014. WOX11 and 12 are involved in the first-step cell fate transition during de novo root organogenesis in Arabidopsis. *Plant Cell* **26**(3): 1081-1093.
Marhavy P, Kurenda A, Siddique S, Denervaud Tendon V, Zhou F, Holbein J, Hasan MS, Grundler FM, Farmer EE, Geldner N. 2019. Single-cell damage elicits regional, nematode-restricting ethylene responses in roots. *EMBO J* **38**(10).
Matosevich R, Cohen I, Gil-Yarom N, Modrego A, Friedlander-Shani L, Verna C, Scarpella E, Efroni I. 2020. Local auxin biosynthesis is required for root regeneration after wounding. *Nat Plants* **6**(8): 1020-1030.
Mendy B, Wang'ombe MW, Radakovic ZS, Holbein J, Ilyas M, Chopra D, Holton N, Zipfel C, Grundler FM, Siddique S. 2017. Arabidopsis leucine-rich repeat receptor-like kinase NILR1 is required for induction of innate immunity to

parasitic nematodes. *PLoS Pathog* **13**(4): e1006284.
Miltner E, Karnok KJ, Hussey RS. 1991. Root response of tolerant and intolerant soybean cultivars to soybean cyst nematode. *Agronomy Journal* **83**: 571-576.
Olmo R, Cabrera J, Moreno-Risueno MA, Fukaki H, Fenoll C, Escobar C. 2017. Molecular transducers from roots are triggered in Arabidopsis leaves by root-knot nematodes for successful feeding site formation: a conserved post-embryogenic *de novo* organogenesis program? *Front Plant Sci* **8**: 875.
Petrasek J, Friml J. 2009. Auxin transport routes in plant development. *Development* **136**(16): 2675-2688.
Pfaffl MW. 2001. A new mathematical model for relative quantification in real-time RT-PCR. *Nucleic Acids Res* **29**(9): e45.
Poncini L, Wyrsch I, Denervaud Tendon V, Vorley T, Boller T, Geldner N, Metraux JP, Lehmann S. 2017. In roots of *Arabidopsis thaliana*, the damage-associated molecular pattern AtPep1 is a stronger elicitor of immune signalling than flg22 or the chitin heptamer. *PLoS One* **12**(10): e0185808.
Schindelin J, Arganda-Carreras I, Frise E, Kaynig V, Longair M, Pietzsch T, Preibisch S, Rueden C, Saalfeld S, Schmid B, et al. 2012. Fiji: an open-source platform for biological-image analysis. *Nat Methods* **9**(7): 676-682.
Shah SJ, Anjam MS, Mendy B, Anwer MA, Habash SS, Lozano-Torres JL, Grundler FMW, Siddique S. 2017. Damage-associated responses of the host contribute to defence against cyst nematodes but not root-knot nematodes. *J Exp Bot* **68**(21-22): 5949-5960.
Sheng L, Hu X, Du Y, Zhang G, Huang H, Scheres B, Xu L. 2017. Non-canonical WOX11-mediated root branching contributes to plasticity in Arabidopsis root system architecture. *Development* **144**(17): 3126-3133.
Sijmons PC, Grundler FMW, von Mende N, Burrows PR, Wyss U. 1991. *Arabidopsis thaliana* as a new model host for plant-parasitic nematodes. *The Plant Journal* **1**(2): 245-254.
Trudgill DL, Cotes LM. 1983. Tolerance of potato to potato cyst nematodes (*Globodera rostochiensis* and *G. pallida*) in relation to the growth and efficiency of the root system. *Annals of Applied Biology* **102**(2): 385-397.
Tytgat T, De Meutter J, Vanholme B, Claeys M, Verreijdt L, Gheysen G, Coomans A. 2002. Development and pharyngeal gland activities of *Heterodera schachtii* infecting *Arabidopsis thaliana* roots. *Nematology* **4**(8): 899-908.
Vanholme B, W VANT, Vanhouteghem K, J DEM, Cannoot B, Gheysen G. 2007. Molecular characterization and functional importance of pectate lyase secreted by the cyst nematode *Heterodera schachtii*. *Mol Plant Pathol* **8**(3): 267-278.
Warmerdam S, Sterken MG, van Schaik C, Oortwijn MEP, Sukarta OCA, Lozano-Torres JL, Dicke M, Helder J, Kammenga JE, Goverse A, et al. 2018. Genome-wide association mapping of the architecture of susceptibility to the root-knot nematode Meloidogyne incognita in Arabidopsis thaliana. *New Phytol* **218**(2): 724-737.
Wyss U, Zunke U. 1986. Observations on the behavior of second-stage juveniles of *Heterodera schachtii* inside host root. *Revue de Nematologie* **9**.
Xu L, Liu F, Lechner E, Genschik P, Crosby WL, Ma H, Peng W, Huang D, Xie D. 2002. The SCF(COI1) ubiquitin-ligase complexes are required for jasmonate response in Arabidopsis. *Plant Cell* **14**(8): 1919-1935.
Ye BB, Shang GD, Pan Y, Xu ZG, Zhou CM, Mao YB, Bao N, Sun L, Xu T, Wang JW. 2020. AP2/ERF Transcription Factors Integrate Age and Wound Signals for Root Regeneration. *Plant Cell* **32**(1): 226-241.
Zhang G, Zhao F, Chen L, Pan Y, Sun L, Bao N, Zhang T, Cui CX, Qiu Z, Zhang Y, et al. 2019. Jasmonate-mediated wound signalling promotes plant regeneration. *Nat Plants* **5**(5): 491-497.
Zhou W, Lozano-Torres JL, Blilou I, Zhang X, Zhai Q, Smant G, Li C, Scheres

B. 2019. A jasmonate signaling network activates root stem cells and promotes regeneration. *Cell* **177**(4): 942-956 e914.

Supporting information:

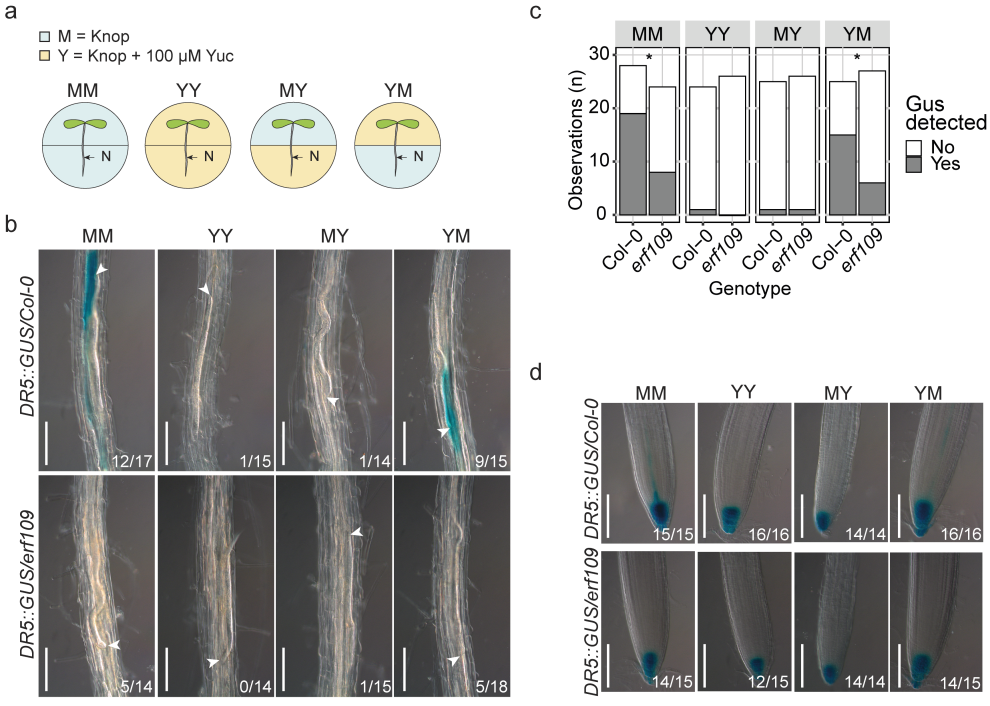

Figure S1: Yuc split plate assay showing that ERF109 regulates local auxin biosynthesis at the nematode infection site. Four-day-old Arabidopsis Col-0 and *erf109* seedlings expressing the auxin *DR5::GUS* reporter were infected with 15 *Heterodera schachtii* second-stage juveniles (J2s). At 16 hours post inoculation, seedlings were transferred to treatment plates. Four treatment combinations were prepared: MM (modified Knop medium and 0.2% DMSO), YY (modified Knop medium, 100µM Yuc and 0.2% DMSO), MK (Yuc only in the root), YM (Yuc only in the shoot). At 3 days post inoculation GUS staining assay was performed for 4 hours and seedlings were imaged. Single-nematode infection sites were selected for observation. **a)** Experimental design with Arabidopsis seedlings transferred to split plates with modified Knop medium either with or without Yuc. N = nematode. **b)** *DR5::GUS* expression at nematode infection sites in wildtype Col-0 and erf109 roots in the four different treatment combinations with or without Yuc applied to shoots and/or roots. **c)** Number of observations with (Yes) or without (No) GUS staining at the nematode infection sites in roots of wildtype Col-0 and *erf109* plants. Statistical significance was calculated by a Pairwise Z-test (n=33, *, P<0.05). **d)** *DR5::GUS* expression in the root tips of Col-0 and *erf109* roots. White arrowheads indicate the nematode head. Frequencies at the bottom right corner indicate how many times GUS staining was observed in one of the three independent biological repeats of the experiment. Scale bar is 200 µm.

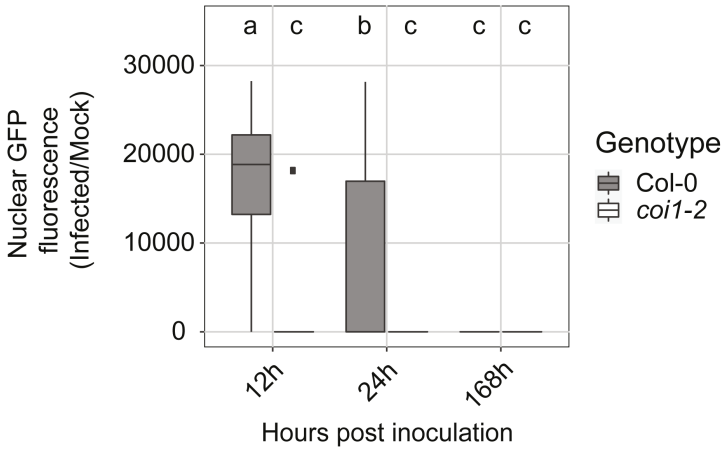

Figure S2: Induction of *pERF109::GFP* nuclear fluorescence by *Heterodera schachtii* host invasion is disrupted in the *coi1-2* Arabidopsis mutant. Four-day-old Arabidopsis seedlings were either inoculated with 15 *H. schachtii* second-stage juveniles (J2s) or mock inoculated. At 12, 24, and 168 hpi seedlings were mounted in 10 µg ml-1 propidium iodide and then imaged. Nuclei were selected and the integrated density was measured using Fiji software. Ratio of the nuclear GFP fluorescence between infected and non-infected seedlings of wildtype Col-0 and *coi1-2* mutant. Significance of differences between fluorescent intensity in Col-0 and *coi1-2* roots over the different timepoints was calculated by Aligned Rank Transform for non-parametric factorial ANOVA followed by Tukey's HSD test for multiple comparisons (n=30, P<0.001). For boxplots, the horizontal line represents the median, the whiskers indicate the maximum/minimum range and the black dots represent the outliers. Difference in letters indicates statistically different groups.

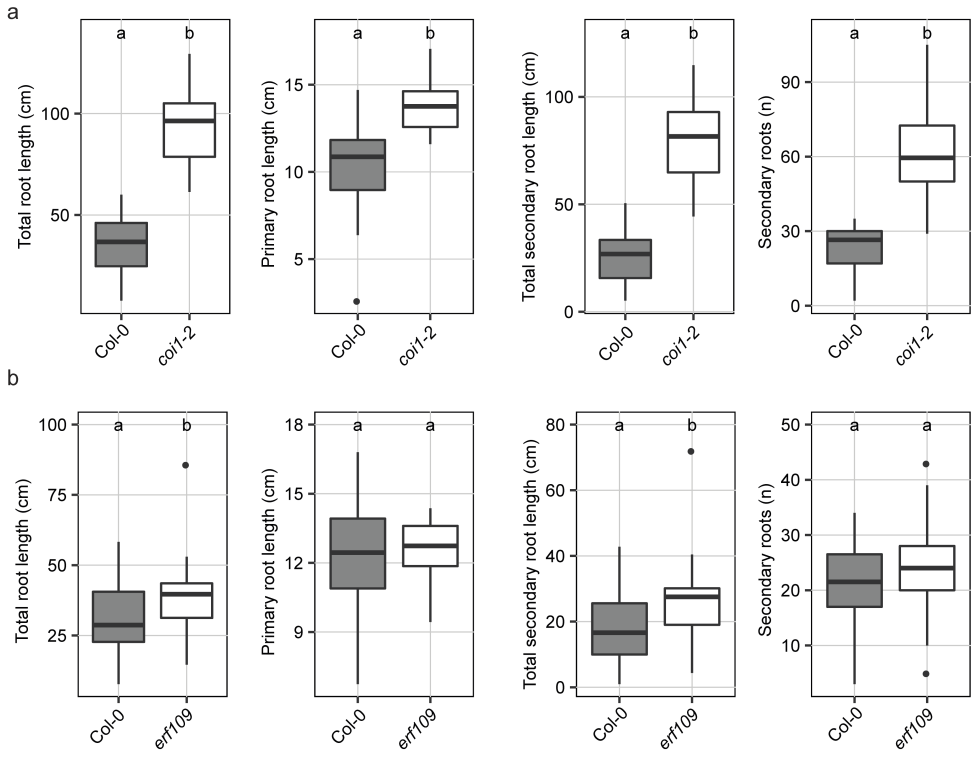

Figure S3: The root architecture of uninfected *coi1-2* and *erf109* Arabidopsis plants differs from wildtype Col-0 plants. Scans of the roots of 16-day-old plants were made and the total root length was measured using WinRHIZO. For the experiment including *coi1-2* (**a**) the primary root was measured manually using ImageJ because of the complex root system of the mutant. For the experiment including *erf109* (**b**) the primary root length was automatically measured by WinRHIZO. Total secondary root length was calculated by subtracting the primary root length from the total root length. Data from three independent biological repeats of the experiment was combined. Significance of differences between genotypes was calculated by Student's T test (n=30, $P<0.05$). For boxplots, the horizontal line represents the median, the whiskers indicate the maximum/minimum range and the black dots represent the outliers. Different letters indicate statistically different groups.

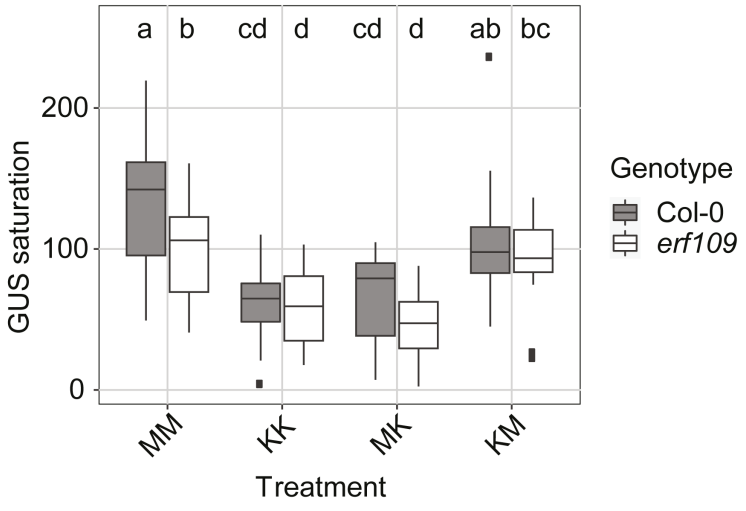

Figure S4: *DR5::GUS* expression at the root tip does not differ between infected wildtype Col-0 and *erf109* seedlings when auxin biosynthesis is inhibited only in the shoot. Four-day-old wildtype Arabidopsis Col-0 and *erf109* mutant seedlings expressing the auxin *DR5::GUS* reporter were infected with 15 *Heterodera schachtii* second-stage juveniles (J2s). At 16 hours post inoculation, seedlings were transferred to treatment plates in a split-plate design. Four treatment combinations were prepared in split-plate assay: MM (modified Knop medium and 0.02%DMSO), KK (modified Knop medium, 10µM L-kyn and 0.02% DMSO), MK (L-kyn only in the root), KM (L-kyn only in the shoot). At 3 days post inoculation GUS staining was performed for 4 hours and seedlings were imaged. GUS saturation was measured as mean grey value using Fiji software. Data of two independent biological replicates was combined. Significance was calculated by ANOVA followed by Tukey's HSD test (n=20, $P<0.05$). For boxplots, the horizontal line represents the median, the whiskers indicate the maximum/minimum range and the black dots represent the outliers. Difference in letters indicates statistically different groups.

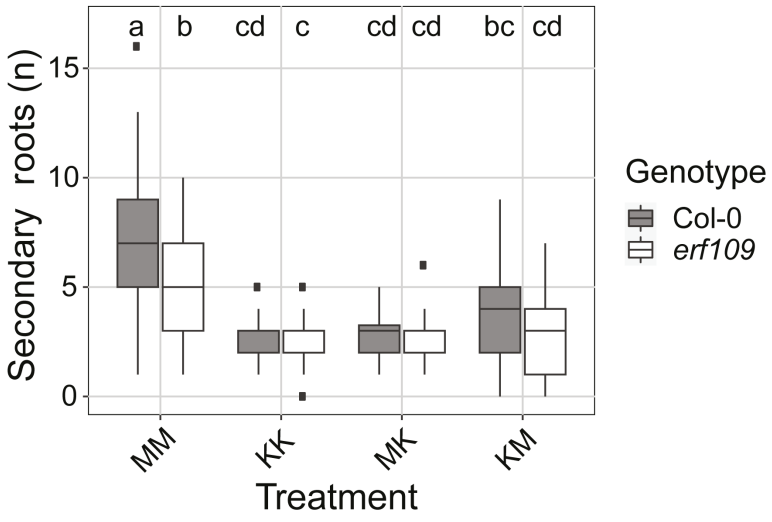

Figure S5: The number of lateral roots in non-infected wildtype Col-0 and *erf109* mutant seedlings is affected by L-kyn treatment. Four-day-old Arabidopsis wildtype Col-0 and *erf109* seedlings were either infected with 15 *Heterodera schachtii* second-stage juveniles (J2s) or mock inoculated. At 16 hours post inoculation, seedlings were transferred to treatment plates in a split-plate design. Four treatment combinations were prepared: MM (modified Knop medium and 0.02% DMSO), KK (modified Knop medium, 10µM L-kyn and 0.02% DMSO), MK (L-kyn only in the root), KM (L-kyn only in the shoot). At 7 days post inoculation, scans were made of the root systems and the total number of secondary roots per plant was counted. Data of two independent biological repeats of the experiment was combined. Significance of differences in secondary roots between the different treatment combinations was calculated by ANOVA followed by Tukey's HSD test for multiple comparisons (n=43-45, $P<0.001$). For boxplots, the horizontal line represents the median, the whiskers indicate the maximum/minimum range and the black dots represent the outliers. Difference in letters indicates statistically different groups.

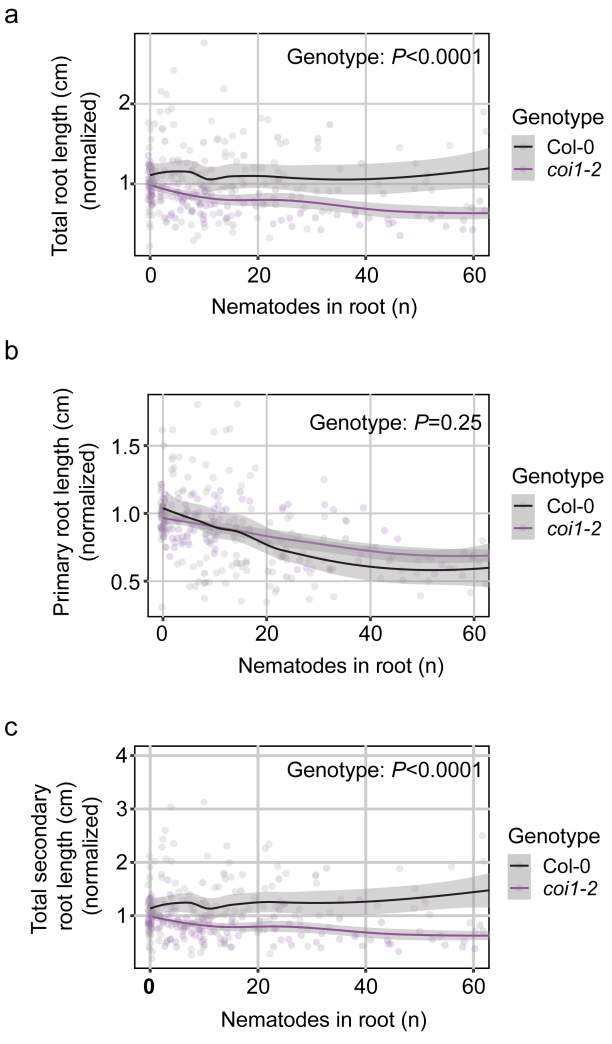

Fig. S6 COI1-mediated secondary root formation allows for maintenance of total root length despite primary root growth inhibition by *Heterodera schachtii*. Nine-day-old Col-0 and *coi1-2* Arabidopsis seedlings were inoculated with increasing *H. schachtii* densities ranging from 0 (mock) to 500 second-stage juveniles (J2s) per seedling. At 7 days post inoculation, scans were made of the root systems and the root length was measured using WinRHIZO. Total, primary, and secondary root length was normalized to the average respective component in mocktreated roots. Fuchsin staining was performed for counting the number of J2s that penetrated the roots. **a)** Total root length per number of nematodes in the roots. **b)** Primary root length per number of nematodes in the roots. **c)** Total secondary root length per number of nematodes in the roots. Data from three independent biological repeats of the experiment was combined. Significance of differences between genotypes was calculated by ANOVA (n=30). Grey area indicates the 95%. confidence interval.

Chapter 5
Transcription factor WOX11 modulates tolerance to cyst nematodes via adventitious lateral root formation

Jaap-Jan Willig[1‖], Nina Guarneri[1‖], Thomas van Loon[1], Sri Wahyuni [1], Ivan E. Astudillo-Estévez[1#], Lin Xu[2], Viola Willemsen[3], Aska Goverse[1], Mark G. Sterken[1], José L. Lozano-Torres[1], Jaap Bakker[1], Geert Smant[1]

[1]Laboratory of Nematology, Wageningen University & Research, 6708 PB Wageningen, the Netherlands
[2]National Key Laboratory of Plant Molecular Genetics, CAS Center for Excellence in Molecular Plant Sciences, Institute of Plant Physiology and Ecology, Chinese Academy of Sciences, Shanghai 200032, China
[3]Cluster of Plant Developmental Biology, Cell and Developmental Biology, Wageningen University & Research, 6708 PB Wageningen, the Netherlands

- Present address: Instituto de Microbiología, Universidad San Francisco de Quito, Quito, Ecuador
‖ - These authors have contributed equally.

Published in Plant Physiology, Volume 195, Issue 1, May 2024, Pages 799-811

Abstract:

The transcription factor *WUSCHEL-RELATED HOMEOBOX 11* (WOX11) in Arabidopsis initiates the formation of adventitious lateral roots upon mechanical injury in primary roots. Root-invading nematodes also induce *de novo* root organogenesis leading to excessive root branching, but it is not known if this symptom of disease involves mediation by WOX11 and if it benefits the plant. Here, we show with targeted transcriptional repression and reporter gene analyses in Arabidopsis that the beet cyst nematode *Heterodera schachtii* activates WOX11-adventitious lateral rooting from primary roots close to infection sites. The activation of WOX11 in nematode-infected roots occurs downstream of jasmonic acid-dependent damage signaling via *ETHYLENE RESPONSIVE FACTOR109*, linking adventitious lateral root formation to nematode damage to host tissues. By measuring different root system components, we found that WOX11-mediated formation of adventitious lateral roots compensates for nematode-induced inhibition of primary root growth. Our observations further demonstrate that WOX11-mediated rooting reduces the impact of nematode infections on aboveground plant development and growth. Altogether, we conclude that the transcriptional regulation by WOX11 modulates root system plasticity under biotic stress, which is one of the key mechanisms underlying tolerance of Arabidopsis to cyst nematode infections.

Introduction:

Soil-borne infections by cyst nematodes affect above- and below-ground plant development and growth, sometimes resulting in large yield losses in agriculture (Jones et al., 2013). Biotic stress induced by cyst nematodes in roots of host plants occurs at different stages of their infection cycle. Firstly, the infective second stage juveniles (J2s) invade host roots and migrate intracellularly through the epidermis and cortex, causing extensive damage to root tissue. Secondly, after becoming sedentary, cyst nematodes take up large amounts of plant assimilates during feeding from modified plant cells, which therefore develop strong metabolic sink activity (Gheysen and Mitchum, 2011; Jones et al., 2013; Bebber et al., 2014). As a response to nematode infections, plants remodel their root system by forming additional secondary roots (Goverse et al., 2000; Olmo et al., 2020; Willig et al., 2022; Guarneri et al., 2023). The *de novo* formation of secondary roots in response to endoparasitism by nematodes might be a mechanism to compensate for primary root growth inhibition caused by nematode infection (Guarneri et al., 2023). However, whether such a form of root system plasticity contributes to overall plant tolerance to cyst nematode infections remains to investigated.

Depending on where and how secondary roots are formed, they are either classified as lateral roots or adventitious lateral roots (Sheng et al., 2017). During post-embryonic development in Arabidopsis, periodic oscillations of auxin maxima at the root tip prime cells to form lateral roots that emerge in a regular acropetal pattern from the growing primary root (Fukaki and Tasaka, 2009; van den Berg et al., 2016). The emergence of lateral roots is controlled by AUXIN RESPONSE FACTOR (ARF)7 and ARF19, which directly regulate *LATERAL ORGAN BOUNDARIES DOMAIN* (*LBD)16* and other *LBD* genes (Okushima et al., 2007). In contrast, adventitious lateral roots do not follow an acropetal pattern as they emerge in between and

opposite of existing lateral roots. Moreover, adventitious lateral roots emerge in response to tissue damage, and their formation is regulated by a separate pathway mediated by the transcription factor WUSCHEL-RELATED HOMEOBOX (WOX)11 (Liu et al., 2014; Hu and Xu, 2016; Sheng et al., 2017). After cutting the primary root, local accumulation of auxin activates *WOX11* transcriptional activity through auxin response elements in its promotor region (Liu et al., 2014). Subsequently, WOX11 induces the expression of *LBD16* but also the expression of other *WOX* genes (Hu and Xu, 2016; Sheng et al., 2017). Ultimately, this leads to the *de novo* formation of secondary roots close to the injury site (Cai et al., 2014; Liu et al., 2014; Hu and Xu, 2016; Sheng et al., 2017). Cyst nematode infection in primary roots of Arabidopsis triggers the formation of secondary roots which does not follow an acropetal patterning (Guarneri et al., 2022). Instead, secondary roots often form clusters at nematode infection sites. As to whether the formation of these secondary roots depends on the WOX11-mediated pathway and whether they should thus be classified as adventitious lateral roots is still a knowledge gap.

We have recently demonstrated that the formation of secondary roots near nematode infection sites involves damage-induced jasmonic acid (JA) signalling (Guarneri et al., 2023). Tissue damage caused by intracellular migration of infective juveniles of *H. schachtii* induces the biosynthesis of JA, which activates the transcription factor *ETHYLENE RESPONSIVE FACTOR* (ERF)109 via the JA receptor *CORONATINE INSENSITIVE* (COI)1. ERF109, in turn, can trigger local biosynthesis of auxin by directly binding to the promoters of auxin biosynthesis genes *ASA1* and *YUC2* (Cai et al., 2014). Indeed, our data showed that COI1/ERF109-mediated formation of secondary roots from nematode-infected primary roots depends on local biosynthesis and accumulation of auxin (Guarneri et al., 2023). WOX11-mediated formation of adventitious lateral roots upon root injury also involves local accumulation of auxin (Liu et al., 2014). However, it remains to be demonstrated if WOX11 becomes activated by COI1- and ERF109-mediated damage signalling in nematode-infected roots.

Several recent reports in the literature point at a role for WOX11-mediated root plasticity in modulating plant responses to abiotic stresses. For instance, *WOX11*, designated as *PagWOX11/ WOX12a*, in poplar mediates changes in root system architecture in response to drought and salt stress (Wang et al., 2020; Wang et al., 2021). Overexpression and dominant repression of this gene in poplar plants alters the number of adventitious roots formed under high saline conditions (Liu et al., 2022). Likewise, the loss-of-function mutant *wox11* in rice exhibits reduced root system development in response to drought as compared to wildtype plants (Cheng et al., 2016). Based on these findings, WOX11-mediated root plasticity is thought to enhance plant tolerance to abiotic stress. However, whether WOX11-mediated root plasticity is also involved in mitigating the impact of biotic stresses on the root system is not known.

In this study, we first addressed whether cyst nematode-induced secondary roots qualify as damage-induced adventitious lateral roots. Hereto, we monitored *de novo* secondary root formation in Arabidopsis seedlings of the double mutant *arf7/arf19* and the WOX11 transcriptional repressor mutant *35S:WOX11-SRDX* in the *arf7/arf19* background (Hiratsu et al., 2003) infected with *H. schachtii.* Next, we asked whether the regulation of *WOX11* in nematode-infected Arabidopsis roots occurs downstream of JA-dependent damage signalling through COI1 and ERF109. To answer this question we performed a time course experiment measuring *pWOX11::GFP* expression with confocal microscopy in wild-type, *coi1-2*, and *erf109*

infected mutant seedlings. Third, we assessed if WOX-11-mediated root system plasticity compensates for the inhibition of primary root growth upon cyst nematode infection. For this, we measured different components of root system architecture of nematode-infected WOX11 transcriptional repressor mutant and wildtype Arabidopsis plants. Last, we tested if WOX11-mediated root system plasticity contributes to the overall tolerance of Arabidopsis to cyst nematode infections. To this end, we compared the aboveground plant growth and development of cyst nematode-infected *35S:WOX11-SRDX* mutants and wildtype Arabidopsis for a period of three weeks after inoculation. Based on our data, we propose a model wherein the formation of WOX11-mediated adventitious lateral roots enhances tolerance of Arabidopsis to biotic stress by cyst nematode infections.

Material & Methods:

Plant material and culturing

The Arabidopsis (Arabidopsis thaliana) lines wild-type Col-0 (N60.000), 35S:WOX11-SRDX/arf7-1/19-1, arf7-1/19-1, LBD16pro:LBD16-GUS and 35S:WOX11-SRDX/LBD16pro:LBD16-GUS (Sheng et al., 2017), pWOX11::GFP, pWOX11::GFP-coi1-2, pWOX11::GFP-erf109, coi1-2 and erf109 were used. For in vitro experiments, seeds were vapor sterilized for 3-4 hours using a mixture of hydrochloric acid (25%) and sodium hypochlorite (50 g/L). Finally, sterile seeds were stratified for 4 days at 4 °C, after which they were sown on square Petri dishes (120x120 mm) containing modified Knop medium (Sijmons et al., 1991) in a growth chamber with a 16-h-light/8-h-dark photoperiod at 21°C. For in vivo pot experiments, seeds were stratified for 4 days and sown on silver sand in 200 mL pots. Seedlings were grown at 19 °C and 16-h-light/8-h-dark conditions with LED light (150 lumen), as previously described in (Willig et al., 2023).

Hatching and sterilization of *Heterodera schachtii*

H. schachtii cysts (Woensdrecht population from IRS, the Netherlands) were separated from sand of infected *Brassica oleracea* plants as previously described (Baum et al., 2000). Cysts were transferred into a clean Erlenmeyer containing water with 0.02% sodium azide. This mixture was gently stirred for 20 min. Later, sodium azide was removed by washing with tap water. Cysts were then incubated for 4-7 days in a solution containing 1.5 mg/mL gentamycin sulfate, 0.05 mg/mL nystatin and 3 mM $ZnCl_2$. Hatched J2s were purified by centrifugation on a 35% sucrose gradient, transferred to a 2 mL Eppendorf tube and surface sterilized for 15 minutes in a solution containing 0.16 mM $HgCl_2$, 0.49 mM NaN_3, and 0.002% (v/v) Triton X-100. After washing the J2s three times with sterile tap water, *H. schachtii* J2s were re-suspended in a sterile 0.7% Gelrite (Duchefa Biochemie, Haarlem, the Netherland) solution. A similar concentration of Gelrite solution was used as mock treatment.
For *in vivo* pot experiments, J2s were hatched and collected in a similar way as described above. Non-sterile J2s were purified by centrifugation on a 35% sucrose gradient and washed three times with tap water. Nematodes were resuspended in tap water for specific inoculation densities.

Quantifying root system architecture of nematode-infected Arabidopsis

Seven-day-old *35S:WOX11-SRDX/arf7-1/19-1* and *arf7-1/19-1* Arabidopsis seedlings were inoculated with either 90 *H. schachtii* J2s or a mock solution. Root architecture was inspected at 7 dpi using an Olympus SZX10 binocular with a 1.5x objective and 2.5x magnification. Scans were made of whole seedlings using an Epson Perfection V800 photo scanner. Pictures of nematode infections were taken with a AxioCam MRc5 camera (Zeiss) and the ZEN 3.2 blue edition software (Zeiss). Nine-day-old *35S:WOX11-SRDX* and wild-type Col-0 seedlings, grown on 120x120 mm square Petri dishes were inoculated with 0 (mock), 0.5, 1.0, 2.5, 5.0, and 7.5 *H. schachtii* J2s per mL of modified Knop medium as previously described (Guarneri et al., 2023). Inoculations were done with two 5 µl drops that were pipetted at opposite sides of each seedling while keeping the petri dishes vertical. At 7 dpi, scans were made of whole seedlings using an Epson Perfection V800 photo scanner. The architecture (i.e., total root length, primary root length, total secondary root length) was measured using the WinRHIZO package for Arabidopsis (WinRHIZO pro2015, Regent Instrument Inc., Quebec, Canada). The number of root tips was counted manually based on the scans.

Acid fuchsine staining of nematodes

Nematodes within the roots were stained with acid fuchsin and counted as previously described (Warmerdam et al., 2018). For comparisons between genotypes, the background effect of the mutation on the root architecture was corrected by normalizing each measured root architecture component in infected seedlings to the median respective component in mock-inoculated roots.

Histology and brightfield microscopy

Four-day-old Arabidopsis seedlings were inoculated with 20 *H. schachtii* J2s or a mock solution. For histochemical staining of β-glucuronidase (GUS) activity, seedlings were incubated in a GUS staining solution (1 mg/mL X-GlcA in 100 mM phosphate buffer pH 7.2, 2 mM potassium ferricyanide, 2 mM potassium ferrocyanide, and 0.2 % Triton X-100) at 37 °C (Zhou et al., 2019) for 3 hours. Stained seedlings were mounted in a chloral hydrate clearing solution (12 M chloral hydrate, 25% glycerol) and inspected with an Axio Imager nM2 light microscope (Zeiss) via a 20x objective. Differential interference contrast (DIC) images were taken with an AxioCam MRc5 camera (Zeiss) and the ZEN 3.2 blue edition software (Zeiss).

Confocal laser microscopy of single *H. schachtii* infection sites

Four-day-old Arabidopsis seedlings were inoculated with roughly five sterile *H. schachtii* J2s in 10 µL 0.7% Gelrite. Single nematode infection sites were selected for observation at 2, 3, 4, and 7 dpi. Infection sites were inspected using a Zeiss LSM 710 confocal laser scanning microscope and a 40x objective. After a single infection site was located, a Z-stack of ten 13 µm-slices was made. Z-stacks were taken using the ZEN 2009 software (Zeiss). The imaging settings in ZEN 2009 were as follows: Laser 488 at 50%, Pinhole 41.4 µm, eGFP 645 nm, TPMT 217 nm. Z-stacks were processed with ImageJ Version 1.53 to quantify the fluorescence integrated density. The post-processing in ImageJ of one individual image was as follows: Firstly, an

auto-scaled compressed-hyper-Z-stack was created of the 10 layers made with the confocal microscope by using the Z-compression function at max intensity (Supplemental Fig. S4). Secondly, a duplicate of the original Z-stack was created, and a Gaussian filter with a sigma value of 2.0 was applied to this duplicate. This duplicate was subtracted from the original image by using the image calculator function. Thirdly, the image threshold limits were set to a specific range ranging from 0 to 100 depending on the quality of the image. The same threshold limits were applied on all images that were taken on the same day. Lastly, the particles were analysed using Analyse Particles at size 0-Infinity and circularity 0.00-1.00.

High throughput analysis of the green canopy area of nematode-infected Arabidopsis plants

Plants were imaged and analyzed as previously described (Willig et al., 2023). Prior to sowing, pots, were filled with silver sand, covered with black coversheets, and were watered with Hyponex (1.7 mM/L NH_4^+, 4.1 mM/L K^+, 2 mM/L Ca_2^+, 1.2 mM/L Mg_2^+, 4.3 mM/L NO_3^-, 3.3 mM/L SO_4^{2-}, 1.3 mM/L H2PO_4^-, 3.4 µm/L Mn, 4.7 µm/L Zn, B 14 µm/L, 6.9 µm/L Cu, 0.5 µm/L Mo, 21 µm/L Fe, pH 5.8) for five minutes. Seven days after sowing, seedlings were watered again for five minutes. Nine-day-old seedlings were inoculated with increasing densities of *H. schachtii* (0 to 10 juveniles per g dry sand). For our experiments we did not use a blocking design as it would greatly increase the chance for error when manually inoculating plants. Every hour, pictures were taken of the plants (15 pictures per day) for a period of 21 days. At the end of the experiment, colour corrections were done using Adobe Photoshop (Version: 22.5.6 20220204.r.749 810e0a0 x64)**.** The surface area of the rosette was determined using a custom-written ImageJ macro (ImageJ 1.51f; Java 1.8.0_321 [32-bit]) and Java was used to make GIFs.

Plant growth analysis and tolerance modelling using a high-throughput phenotyping platform

To analyse the growth data of the plants obtained from the high-throughput platform, we followed the same approach and used the same functions as in our previously published analytical pipeline (Willig et al., 2023); available via Gitlab: https://git.wur.nl/published_papers/willig_2023_camera-setup).

In short, the measurement used was the median daily leaf area (cm^2), calculated from the 15 daily measurements. We used log_2-transformed data, where the rate of growth was determined per day per plant by (equation 1)

$$R_{x,t} = \log_2(A_{x,t-1} - A_{x,t})$$

where $R_{x,t}$ is the transformed growth rate of plant *x* at day *t* from day *t-1* to day *t* based on the median Green canopy area *Ax,t*.

The tolerance limit was modelled using a previously described method based on fitting growth models (Willig et al., 2023). Here we fitted a logistic growth model using the *growthrates* package on the median daily leaf area A_t (cm^2) (equation 2),

$$A_t = \frac{K \times A_0}{A_0 + (K - A_0) \times e^{(-r \times t)}}$$

where K is the maximum green canopy area (cm^2), A_0 is the initial canopy area (cm^2), and r is the intrinsic growth rate (d^{-1}), which were determined as a function of time t (d) ($p < 0.1$).

Based on the relation between K and density we could identify the tolerance limit (equation 3)

$$K = K_B + \frac{K_\sigma}{P_\sigma} \times e^{-\left(\frac{P_i - P_M}{P_\sigma}\right)^2}$$

where P_i is the initial nematode density in nematodes per gram soil, K_B is the basal canopy size, K_σ is the normalized maximum canopy area that can be achieved over the P_i range, P_σ is the deviation around the nematode density allowing maximum growth, P_M is the nematode density at which maximum growth is achieved. We modelled the parameter values using *nls* and extracted confidence intervals using the *nlstools* package (Baty et al., 2015). The tolerance limit, $2*P_M$, could such be determined (as in (Willig et al., 2023)).

Statistical analyses

Statistical analyses were performed using the R software version 3.6.3 (Windows, x64). The R packages used are *tidyverse* (https://CRAN.R-project.org/package=tidyverse), *ARTool* (https://CRAN.R-project.org/package=ARTool) and *multcompView* (https://CRAN.R-project.org/package=multcompView). Correlation between variables was calculated using Spearman Rank-Order Correlation coefficient. For binary data, significance of the differences between proportions was calculated by a Pairwise Z-test. For normally distributed data, significance of the differences among means was calculated by ANOVA followed by Tukey's HSD test for multiple comparisons. A non-parametric pairwise Wilcoxon test followed by false discovery rate correction for multiple comparisons was used for data with other distributions and one grouping factor. For the high-throughput platform data we used the Wilcoxon test as implemented in the *ggpubr* package (https://cran.r-project.org/web/packages/ggpubr/index.html). The confidence interval of the inoculum density-response curves was calculated by LOESS regression (as per default in *geom_smooth*) in R.

Results:

Cyst nematodes induce the formation of adventitious lateral roots

Our earlier work showed that *H. schachtii* induces the *de novo* formation of secondary roots between or across fully developed lateral roots near nematode infection sites (Guarneri et al., 2023). Here, we hypothesized that these secondary roots are adventitious lateral roots, the formation of which depends on WOX11-

mediated transcriptional regulation (Fig. 1a). To test this hypothesis, we inoculated *H. schachtii* on the lateral root-deficient *arf7-1/19-1* double mutant, which is unable to form acropetal lateral roots, and the transcription repressor mutant *35S:WOX11-SRDX/arf7-1/19-1* (Hiratsu et al., 2003), which is unable to form neither acropetal nor adventitious lateral roots (Fig. 1b-d). Importantly, we observed no difference in the number of nematodes per plant between *arf7-1/19-1* and *35S:WOX11-SRDX/arf7-1/19-1* (Fig. 1c), indicating that both Arabidopsis lines were exposed to similar levels of biotic stress. However, significantly fewer *35S:WOX11-SRDX/arf7-1/19-1* plants showed secondary root formation upon inoculation with *H. schachtii* inoculation compared to *arf7-1/19-1* mutant plants (Fig. 1b, d and Supplemental Fig. S1). From this, we concluded that the induction of secondary roots by *H. schachtii* is mediated by WOX11 and that these secondary roots therefore qualify as adventitious lateral roots.

WOX11-mediated formation of adventitious lateral roots from primary roots of Arabidopsis involves the downstream transcriptional activation of *LBD16* (Fig. 1a) (Sheng et al., 2017). To test if WOX11 activates *LBD16* in nematode-infected Arabidopsis roots, we monitored the expression of *LBD16* fused to *GUS* in wildtype (*LBD16pro:LBD16-GUS*) and *35S:WOX11-SRDX* (*35S:WOX11-SRDX/LBD16pro:LBD16-GUS*) seedlings inoculated with *H. schachtii* (Fig. 1e and f). We found that *LBD16* was highly expressed in nematode infection sites in the wildtype, but not in the *35S:WOX11-SRDX* background. This demonstrates that *H. schachtii* activates *LBD16* expression in a WOX11-dependent manner. Based on these observations, we concluded that cyst nematode infections activate the WOX11/LBD16-mediated pathway to form adventitious lateral roots from primary roots.

Emergence of adventitious lateral roots correlates with damage in primary roots

Previously, we showed that increasing nematode inoculation densities result in more tissue damage in Arabidopsis leading to a higher number of secondary roots emerging from infected primary roots (Guarneri et al., 2023). To test the hypothesis that WOX11 mediates this quantitative relationship between inoculation density and the number of secondary roots emerging from cyst nematode-infected primary roots (Fig. 2a), we inoculated nine-day-old seedlings of *35S:WOX11-SRDX* and wildtype plants with increasing densities of *H. schachtii* (Fig. 2b). At 7 dpi, the number of nematodes that had successfully penetrated the roots was counted after staining with acid fuchsin (Fig. 2c). The number of infective juveniles in *35S:WOX11-SRDX* plants by inoculation density was significantly higher compared to wild-type Col-0 plants. This indicates that the transcriptional regulation by WOX11 in wild-type Arabidopsis plants reduces susceptibility to penetration by *H. schachtii*. Next, we counted the number of secondary roots to determine whether this correlates with the number of nematodes inside the roots. It should be noted that uninfected *35S:WOX11-SRDX* plants have more secondary roots than wild-type Col-0 plants (Supplemental Fig. S2). To correct for this background effect of the SRDX-transcriptional repressor construct on root system architecture, we normalized the total number of secondary roots in infected seedlings to the average respective number in uninfected seedlings (Fig. 2d). As expected, after normalization, the number of secondary roots emerging from primary roots increased with the number of successful invasions of *H. schachtii* in wild-type Arabidopsis. However, no such correlation was observed in *35S:WOX11-SRDX* plants. We therefore concluded that the density-dependent adaptations in

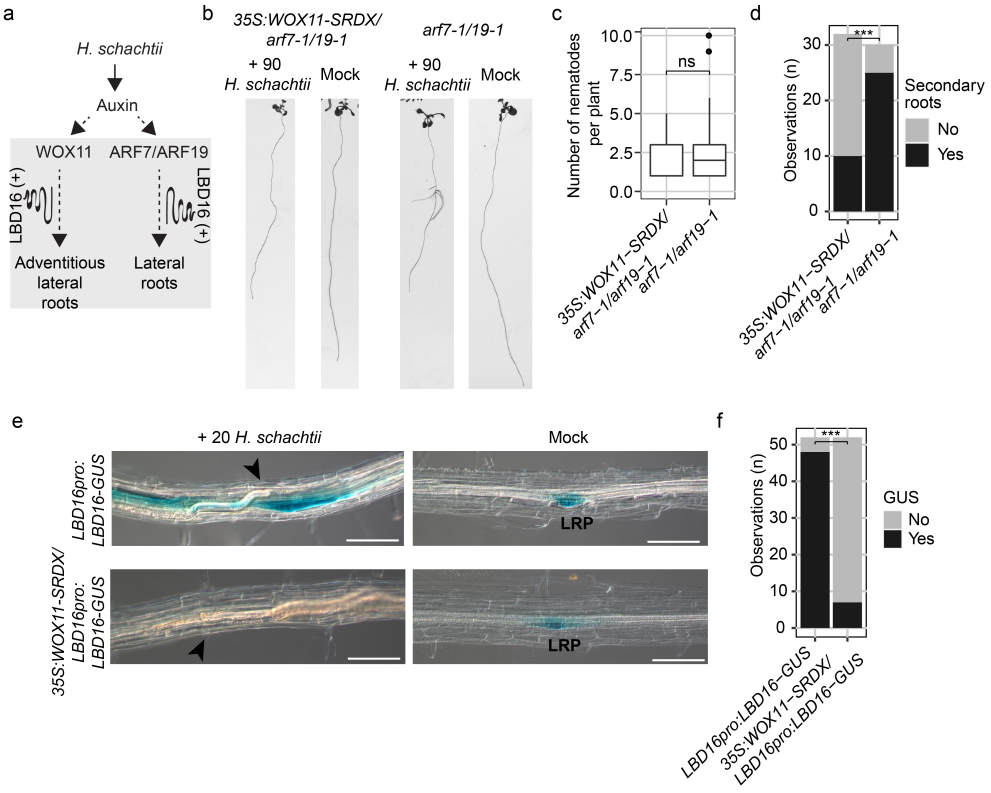

Figure 1: *Heterodera schachtii* induces adventitious lateral root formation in a WOX11- and LBD16-dependent manner. a) Schematic diagram of *H. schachtii*-and WOX11-mediated adventitious lateral root emergence. Grey area indicates the tested part of the pathway. Curling line and '+' indicate involvement of multiple proteins, including LBD16. **b-d)** Seven-day old *35S:WOX11-SRDX/arf7-1/19-1* and *arf7-1/arf19-1* mutant seedlings were inoculated with 90 *H. schachtii* juveniles or with mock solution. At 7dpi, scans were made of the root system. **a)** Representative pictures of *35S:WOX11-SRDX/arf7-1/19-1* and *arf7-1/arf19-1* mutant seedlings inoculated with 90 *H. schachtii* or with mock solution. **b)** Number of juveniles that invaded the primary roots. **d)** Number of seedlings that show secondary roots (Yes) that are associated with *H. schachtii* infection sites or no secondary roots at all (No). Data from three independent biological repeats of the experiment was combined. Statistical significance was calculated by a Pairwise Z-test n=30-32, ***: p<0.001). **e-f)** Four-day-old Arabidopsis seedlings expressing the *LBD16pro:LBD16-GUS* and *35S:WOX11-SRDX/LBD16pro:LBD16-GUS* reporters were inoculated with 20 *H. schachtii* juveniles. At 4dpi, GUS expression was stained for 3 hours and seedlings were imaged **e)** *LBD16pro:LBD16-GUS* and *35S:WOX11-SRDX/LBD16pro:LBD16-GUS* expression at nematode infection sites in roots. Black arrowheads indicate the nematode head. LRP indicates lateral root primordia. Scale bar = 100 µm. **f)** Number of observations with (Yes) or without (No) GUS staining at the nematode infection site in roots of wild-type Col-0 seedlings. Data from three independent biological repeats of the experiment were combined. Statistical significance was calculated by a Pairwise Z-test n=52, ***: p<0.001).

root system architecture to increasing levels of damage in nematode-infected roots are brought about by WOX11-mediated formation of adventitious lateral roots.

COI1 and ERF109 modulate damage-induced activation of *WOX11* at nematode infection sites

De novo formation of secondary roots on nematode-infected primary roots of Arabidopsis is mediated by damage-induced activation of JA signaling via COI1 and ERF109 (Guarneri et al., 2023). In this study we tested whether COI1 and ERF109 are required for the regulation of *WOX11* in nematode-infection sites (Fig. 3a). Hereto, we imaged nucleus-localized *pWOX11::GFP* expression within single-nematode infection sites in the *coi1-2* and *erf109* mutants and wild-type Col-0 at 2, 3, 4, and 7 dpi (Fig. 3 and Supplemental Fig. S3). Cyst nematode infection typically causes tissue autofluorescence in Arabidopsis roots (Hoth et al., 2005). To filter out this autofluorescence from the fluorescent signal emitted by the GFP construct, we subtracted a Gaussian blurred image from the original images (Supplemental Fig. S4). Hereafter, we observed a gradual increase in the *pWOX11::GFP*-derived fluorescent signal in nematode infection sites over time in *coi1-2, erf109,* and wild-type Col-0 (Fig. S3a-f), with wild-type Col-0 showing the strongest increase (Supplemental Fig. S3f). For instance, at 4 dpi, wild-type Col-0 plants showed significantly more nuclear GFP fluorescence in and around nematode feeding sites compared to *coi1-2* and *erf109* in the processed images (Fig. 3b-d). We, therefore, concluded that two key components of the damage-induced JA signalling pathway, COI1 and ERF109, modulate *WOX11* expression in infection sites of *H. schachtii* in Arabidopsis.

COI1 and ERF109 modulate damage-induced activation of *WOX11* at nematode infection sites

De novo formation of secondary roots on nematode-infected primary roots of Arabidopsis is mediated by damage-induced activation of JA signaling via COI1 and ERF109 (Guarneri et al., 2023). In this study we tested whether COI1 and ERF109 are required for the regulation of *WOX11* in nematode-infection sites (Fig. 3a). Hereto, we imaged nucleus-localized *pWOX11::GFP* expression within single-nematode infection sites in the *coi1-2* and *erf109* mutants and wild-type Col-0 at 2, 3, 4, and 7 dpi (Fig. 3 and Supplemental Fig. S3). Cyst nematode infection typically causes tissue autofluorescence in Arabidopsis roots (Hoth et al., 2005). To filter out this autofluorescence from the fluorescent signal emitted by the GFP construct, we subtracted a Gaussian blurred image from the original images (Supplemental Fig. S4). Hereafter, we observed a gradual increase in the *pWOX11::GFP*-derived fluorescent signal in nematode infection sites over time in *coi1-2, erf109,* and wild-type Col-0 (Fig. S3a-f), with wild-type Col-0 showing the strongest increase (Supplemental Fig. S3f). For instance, at 4 dpi, wild-type Col-0 plants showed significantly more nuclear GFP fluorescence in and around nematode feeding sites compared to *coi1-2* and *erf109* in the processed images (Fig. 3b-d). We, therefore, concluded that two key components of the damage-induced JA signalling pathway, COI1 and ERF109, modulate *WOX11* expression in infection sites of *H. schachtii* in Arabidopsis.

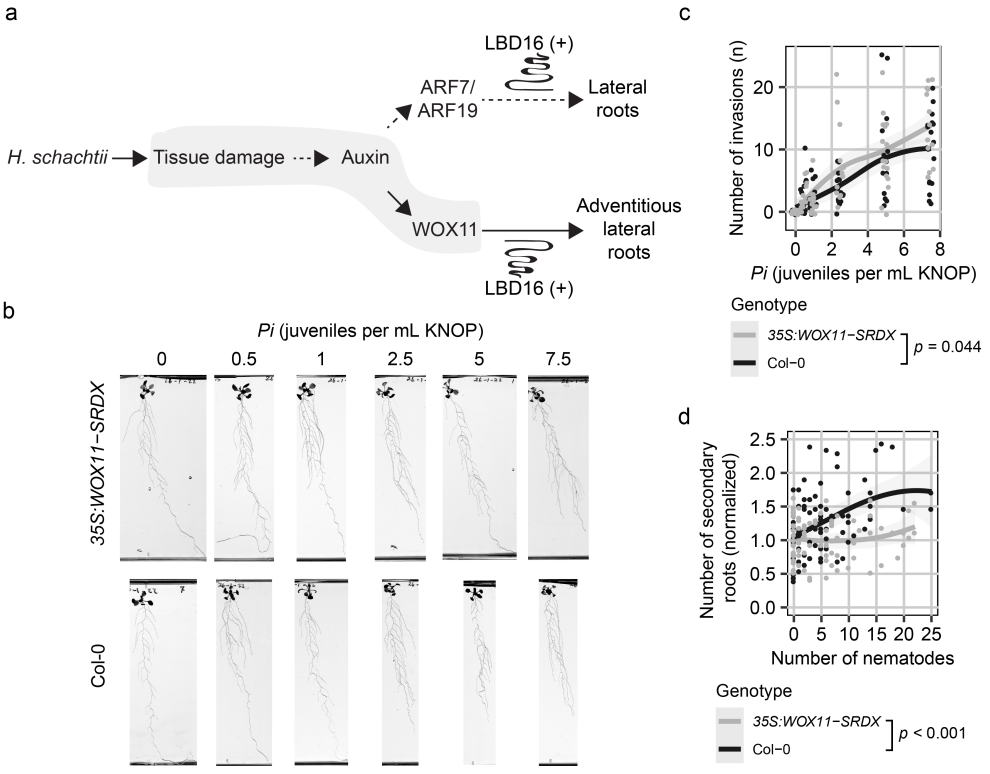

Figure 2: WOX11 is required in *Heterodera schachtii* induced adventitious lateral root formation in a density-dependent manner. a) Schematic diagram of *H. schachtii*-and WOX11-mediated adventitious lateral roots emergence. Grey area indicates the tested part of the pathway. Curling line and '+' indicate the involvement of multiple proteins, including LBD16. **b-d)** Nine-day-old *35S:WOX11-SRDX* and wild-type Col-0 seedlings were inoculated with nematode densities (P_i) ranging from 0-7.5 *H. schachtii* J2s (mL modified KNOP media). Roots were scanned and nematodes were counted after acid fuchsin staining at 7 dpi. b) Representative images of Arabidopsis root systems at 7dpi. **c)** Number of nematodes that successfully penetrated the roots per plant. **d)** Secondary roots formed per number of nematodes inside the roots. The total number of secondary roots of infected seedlings was normalized to the median respective component in mock-inoculated roots. Data from two independent biological repeats of the experiment were combined. Significance of differences between genotypes was calculated by analysis of variance (n=14-18). Grey area indicates the 95% confidence interval.

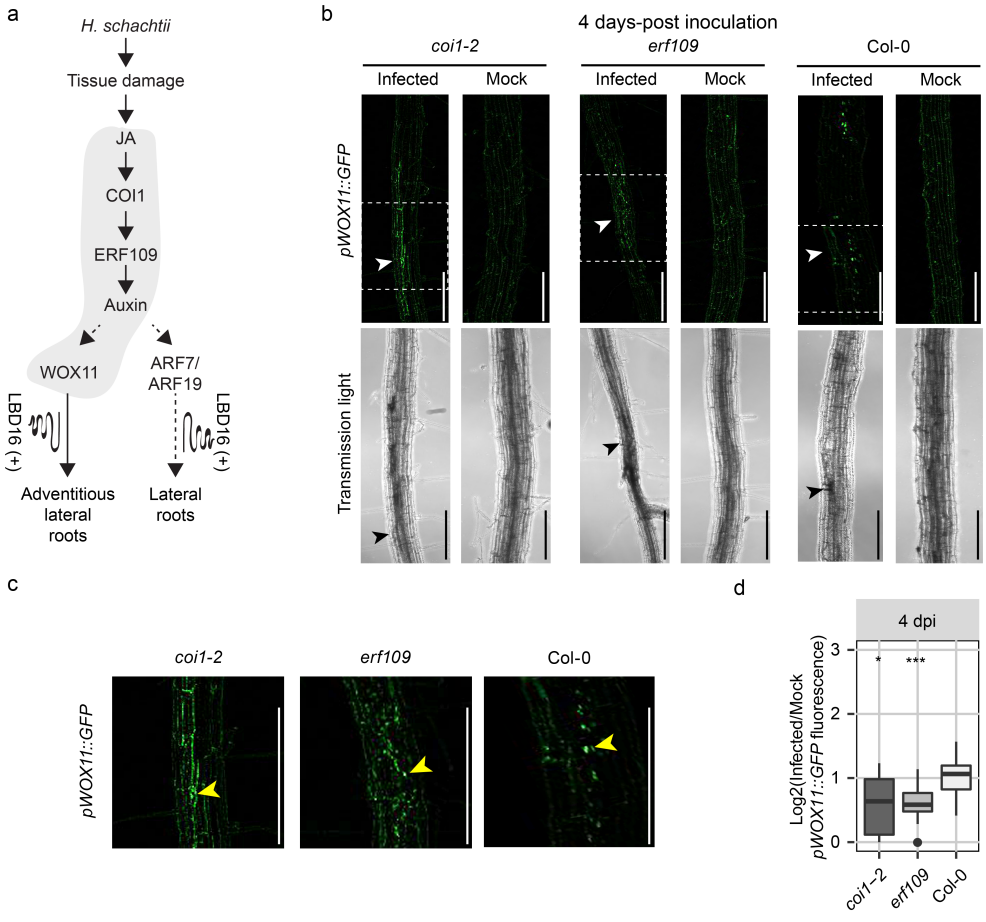

Figure 3: COI1 and ERF109 modulate *WOX11* expression upon *H. schachtii* infection. a) Schematic diagram of *H. schachtii*-and WOX11-mediated adventitious lateral root emergence. Grey area indicates the tested part of the pathway. Curling line and '+' indicate involvement of multiple proteins, including LBD16. **b-c)** Four-day-old Arabidopsis seedlings were either inoculated with 10 *H.* schachtii second-stage juveniles (J2s) or with mock solution. At 4 dpi, seedlings were mounted in water and then imaged using a fluorescent confocal microscope. Single-nematode infection sites were selected for observation. Images are original. **b)** Representative pictures of infected and mock-inoculated seedlings expressing the *pWOX11::GFP* construct with nuclear localization signal in either wild-type Col-0, mutant *coi1-2*, or mutant *erf109* background at 4 dpi. To make the fluorescence more visible, the brightness was enhanced for all the representative pictures in the same way. **c)** Zoomed parts of original images fluorescent signal that are indicated by dashed white box in panel **(b)**. Yellow arrowhead indicates true fluorescent signal of *pWOX11::GFP* in the nucleus. **d)** Quantification of *pWOX11::GFP* fluorescent intensity induced by infection in wild-type Col-0, *coi1-2,* and *erf109* roots. Values represent $\log_2$ of the fluorescence ratio between the GFP integrated density of infected and noninfected roots. Scale bar: 200 µm. Data from three independent biological repeats of the experiment were combined. Significance of differences between fluorescent intensities in Co-0, *coi1-2,* and *erf109* per timepoint was calculated by a Wilcoxon Rank Sum test. ns = not significant, *p< 0.05, **p< 0.01, ***p<0.001 (n=15).

Formation of adventitious lateral roots compensates for nematode-induced primary root growth inhibition

Next, we asked whether WOX11-mediated adventitious lateral roots formation compensates for the inhibition of primary root growth due to nematode infections (Fig. 4a). To this end, we quantified root system architecture components (i.e., total root length, primary root length, total secondary root length, and average secondary root length) of nematode-infected roots of both *35S:WOX11-SRDX* and wildtype Col-0 plants (Fig. 2). Initially, we noticed that our measurements of root system architecture components followed a parabolic function with the minimum values at the infection rate of 15 juveniles per root, suggesting the existence of two density dependent counteracting mechanisms (Supplemental Fig. S5). We, therefore, analysed our data for the lower (Fig. 4) and higher infection rates separately (Supplemental Fig. S5). For plants infected with 0 to 15 juveniles per root, we found that the total root length was significantly more reduced by nematode infection in *35S:WOX11-SRDX* mutant plants than in wild-type Col-0 plants (Fig. 4b and d). Interestingly, the growth of the primary root was not different between *35S:WOX11-SRDX* mutant plants and wild-type plants upon infection with cyst nematodes (Fig. 4c). However, the total length of the secondary roots of nematode-infected *35S:WOX11-SRDX* mutant plants was significantly smaller as compared to wild-type Col-0 plants (Fig. 4d). As the average secondary root length did not significantly differ between *35S:WOX11-SRDX* and wild-type Arabidopsis plants, WOX11 affects the root system architecture by increasing the number of secondary roots but not by extending secondary root growth (Supplemental Fig. 5e). For plants infected with 15 to 25 juveniles per plant, we observed no significant differences for the total root length (Supplemental Fig. S5b) between wild-type Col-0 and *35S:WOX11-SRDX*. Likewise, we found no differences in the primary root length (Supplemental Fig. S5c), total secondary root length (Supplemental Fig. S5d), and average secondary root length (Fig. S5e). Based on our analyses, we concluded that WOX11-mediated formation of adventitious lateral roots compensates for nematode-induced inhibition of primary root growth at lower infection rates.

WOX11 modulates tolerance to cyst nematode infections

The growth of the green canopy area over time reflects the tolerance of Arabidopsis to biotic stress by root-feeding cyst nematodes (Willig et al., 2023). To assess if WOX11-mediated *de novo* formation of adventitious lateral roots modulates tolerance of Arabidopsis to cyst nematode infection, we monitored the growth of the green canopy area of *35S:WOX11-SRDX* mutant and wild-type Col-0 seedlings for a period of 21 days after inoculation with different numbers of *H. schachtii* (Fig. 5a and b). At the end of the experiment, the green canopy area of the *35S:WOX11-SRDX* mutant was smaller at higher inoculation densities of *H. schachtii* as compared to wild-type Col-0 plants (Fig. 5c and d). Notably, the first significant reduction in green canopy area of *35S:WOX11-SRDX* plants by nematode infection was observed at inoculation densities between P_i 2.5 and 5 J2s per gram sand, while in wild-type Col-0 plants we observed a first significant reduction in green canopy area at P_i 7.5 J2s per gram sand. To quantify more exactly the difference in tolerance of *35S:WOX11-SRDX* and wildtype Col-0 plants, we fitted the growth rates of individual plants (Supplemental Fig. S6 and S7) to a logistic growth model. From this, we calculated the maximum projected green canopy area and determined the tolerance limit with

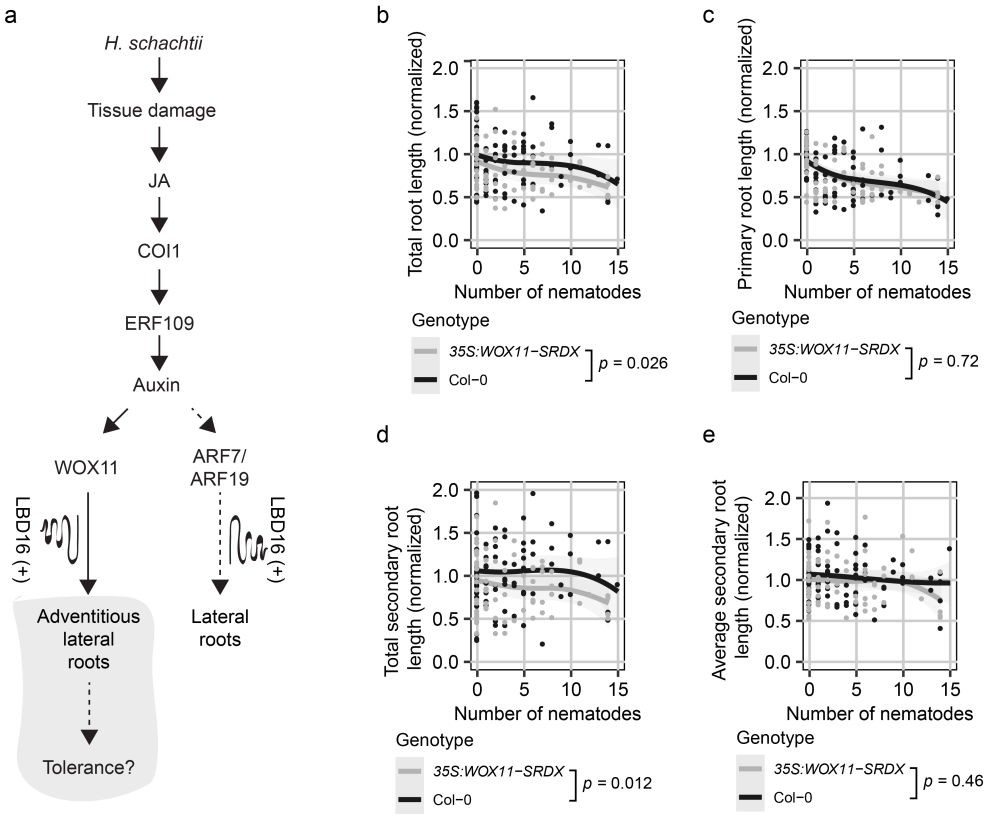

Figure 4: Formation of adventitious lateral roots compensates for nematode-induced primary root growth inhibition. a) Schematic diagram of *H. schachtii*-and WOX11-mediated adventitious lateral root emergence. Grey area indicates the tested part of the pathway. Curling line and '+' indicate involvement of multiple proteins, including LBD16. **b-d)** Nine-day old *35S:WOX11-SRDX* and wild-type Col-0 seedlings were inoculated densities (P_i) ranging from 0-7.5 *H. schachtii* J2s (mL modified KNOP media). Roots were scanned and nematodes were counted after fuchsine staining at 7 dpi. Root architectural components of infected seedlings were normalized to the median respective component in mock-treated roots. Data of two independent biological repeats of the experiment was combined. **b)** Representative images of Arabidopsis root system at 7dpi. **b)** Total root length per number of nematodes inside the roots. **c)** Primary root length per number of nematodes inside the roots. **d)** Total secondary root length per number of nematodes inside the roots. **e)** Average secondary root length per number of nematodes inside the roots. Data from two independent biological repeats of the experiment were combined. Significance of differences between genotypes was calculated by analysis of variance (n=14-18). Grey area indicates the 95% confidence interval of the LOESS fit.

95% confidence interval (95% CI) (Fig. 5e). The relationship between maximum canopy area *K* and the P_i fitted a Gaussian curve, based on which we estimated the tolerance limit for *35S:WOX11-SRDX* at P_i = 2.25 (95% CI: 0.67-3.83) and for wild-type Col-0 at P_i = 4.84 (95% CI: 3.8-5.89). This difference in tolerance limits led us to conclude that WOX11 modulates tolerance of Arabidopsis to cyst nematode infections.

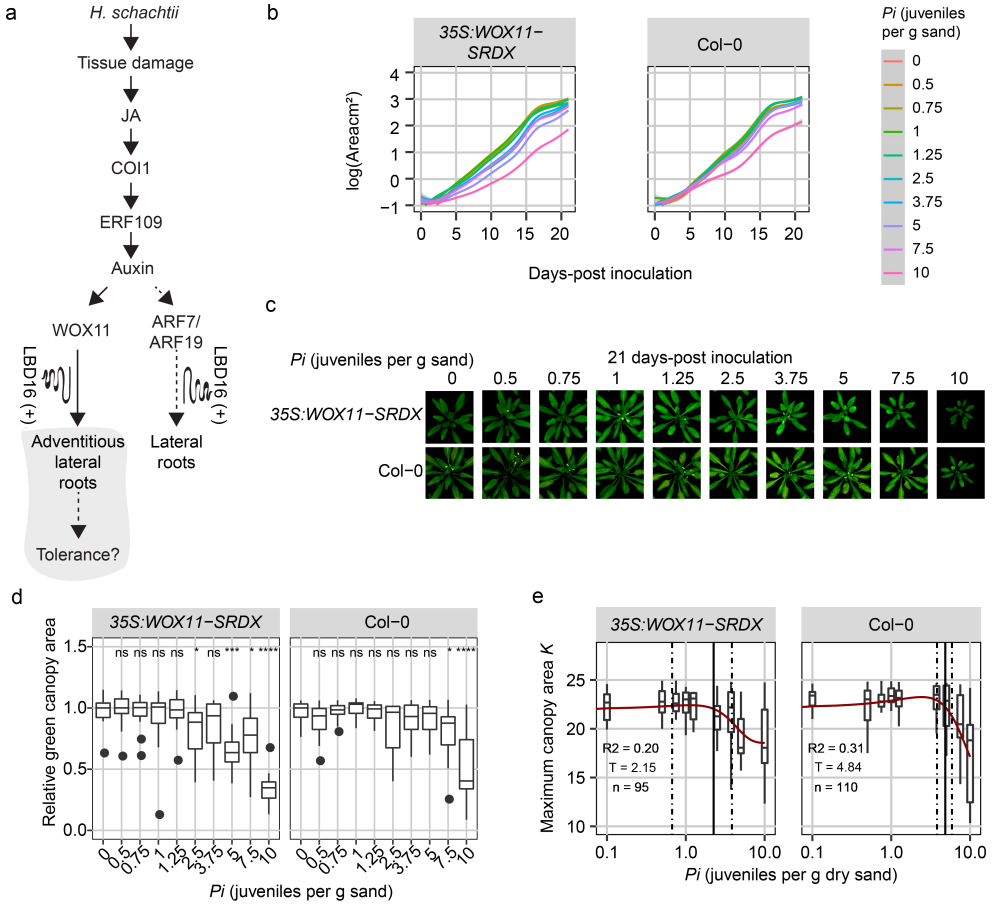

Figure 5: WOX11 is involved in tolerance to cyst nematode infection. a) Schematic diagram of *H. schachtii*-and WOX11-mediated adventitious lateral root emergence. Grey area indicates the tested part of the pathway. Curling line and '+' indicate involvement of multiple proteins, including LBD16. Nine-day-old Arabidopsis seedlings were inoculated with 10 densities (P_i) of *H. schachtii* juveniles (0 to 10 J2s per g dry sand) in 200 mL pots containing 200 grams of dry sand. **b)** Average growth curve of Arabidopsis plants inoculated with different inoculum densities of *H. schachtii* from 0-21 dpi. Line fitting was based on a LOESS regression. **c)** Representative images of plants inoculated with *H. schachtii* at 21-days post inoculation. **d)** Relative green canopy area at 21 dpi. For the relative green canopy area, all values were normalized to the median of the measurements of the corresponding mock-inoculated plants. Data was analysed with a Wilcoxon Rank Sum test; ns= not significant, *p< 0.05, **p< 0.01, ***p<0.001 (n=10-18 plants per treatment). **e)** The maximum canopy area *K* per inoculation density of *H. schachtii*. The fitted line is from a Gaussian curve. Solid line indicates the tolerance limit. Dashed line indicates the confidence interval. R^2 is the goodness of the fit, *T* is the tolerance limit, and n is the number of plants used for fitting the data.

Discussion:

Excessive root branching is a classical symptom of nematode disease in plants of which the underlying causes nor the functions are well understood. Recently, we showed that endoparasitic cyst nematodes activate a JA-dependent damage signaling pathway leading to local auxin biosynthesis and subsequent *de novo* formation of secondary roots near infection sites (Guarneri et al., 2023). At the outset of this study, it was not clear if nematode-induced secondary roots emerge from primary roots following the canonical auxin-dependent pathway for the formation of acropetal lateral roots, or if they emerge following a different pathway. Our current data supports the alternative hypothesis wherein the emergence of secondary roots in response to nematode damage follows the non-canonical WOX11-dependent pathway leading to the formation of adventitious lateral roots. This induction of adventitious lateral roots near nematode infection sites compensates for the inhibition of primary root growth by root-feeding cyst nematodes. We further show that the WOX11-mediated plasticity of root system architecture contributes to the tolerance of Arabidopsis to cyst nematode infections.

Our observations demonstrate that WOX11 modulates *de novo* root organogenesis near cyst nematode infection sites. Both WOX11- and ARF7/ARF19-mediated rooting pathways are activated by auxin, but they form a divergence point in the differentiation of adventitious lateral root primordia from lateral root primordia. WOX11 responds to auxin signals brought about by external cues, such as wounding (Sheng et al., 2017), and mediates tissue repair and regeneration mechanisms (Liu et al., 2014). In contrast, the auxin signals activating ARF7/ARF19 are thought to be developmentally regulated following endogenous rooting cues. Interestingly, both WOX11- and ARF7/ARF19-mediated root organogenesis pathways converge on LBD16 (Okushima et al., 2007; Sheng et al., 2017; Zhang et al., 2023). Our findings indeed show that cyst nematodes induce expression of *LBD16* in a WOX11-dependent manner. However, this observation contradicts earlier work wherein *LBD16* expression was not observed in Arabidopsis infected with *H. schachtii* at similar timepoints after inoculation (Cabrera et al., 2014). It should be noted that we used a different $LBD16_{pro}$*:LBD16-GUS* reporter line containing a much larger genomic region upstream of *LBD16* (Sheng *et al.*, 2017) compared to previous studies (Okushima et al., 2007; Cabrera et al., 2014). This extended promoter region included in the $LBD16_{pro}$*:LBD16-GUS* line harbours multiple WOX11-binding sites, which are absent in previously used *LBD16-GUS* reporter lines and which may thus explain the differences in observed *LBD16* expression in cyst nematode-infected Arabidopsis roots.

Our data further shows that both COI1 and ERF109 modulate WOX11 expression in response to cyst nematode infection, which positions WOX11 downstream of ERF109 within the JA-dependent damage signalling pathway. JA-dependent damage signaling induces local auxin biosynthesis, which drives the production of secondary roots (Guarneri et al., 2023). Auxin has been shown to directly activate WOX11 expression, and as such WOX11 connects stress-induced auxin signaling to the establishment of adventitious lateral root founder cells (Sheng et al., 2017). ERF109 most likely modulates WOX11 activity by regulating local YUCCA-mediated biosynthesis of auxin (Cai et al., 2014). However, even in the absence of ERF109 (i.e., *erf109* mutant) we observed some *WOX11-GFP* expression in nematode infection sites. This agrees with our earlier observations demonstrating

that besides damage-induced local biosynthesis of auxin, auxin transported from the shoots towards nematode infection sites also contributes to local stress-induced auxin maxima (Guarneri et al., 2023). WOX11 may thus integrate local and systemic auxin-based stress response mechanisms leading to formation of adventitious lateral roots in nematode-infected Arabidopsis.

In our *in vitro* bioassays, WOX11 affected the number of secondary roots emerging from nematode-infected primary roots, but not the average secondary root length. Furthermore, we found that WOX11-mediated adventitious rooting compensated for the inhibition of primary root growth due to nematode infections, which implies that WOX11 mitigates the impact of nematode infections by adapting root system branching. This fits in the current model of wound-induced formation of secondary roots, wherein the activation of WOX11 initiates the cell fate transition of protoxylem cells into adventitious root founder cells (Liu et al., 2014). WOX11 expression is thought to be specific for adventitious root founder cells, where it activates, together with its close homolog WOX12, LBD16- and WOX5-mediated divisions to initiate the formation adventitious root primordia (Liu et al., 2014; Hu and Xu, 2016). During these divisions the expression of WOX11 decreases, because of which it affects the number of secondary roots but is less likely to alter secondary root growth.

Based on the green canopy area as a proxy for measuring the overall impact of belowground stress on plant fitness, we conclude that WOX11-mediated root system plasticity also contributes to the tolerance of Arabidopsis to cyst nematode infections. The estimated tolerance limit of *35S:WOX11-SRDX* plants for cyst nematode infections was significantly lower than for wild-type Col-0 plants. Others have shown that homologs of Arabidopsis WOX11 in rice, apple, and poplar enhance plant tolerance to abiotic stresses, such as drought and low nitrate conditions, by regulating adventitious lateral root formation (Cheng et al., 2016; Wang et al., 2020; Wang et al., 2021; Tahir et al., 2022). Furthermore, WOX11 functions as a key regulator in the regeneration of primary roots after mechanical injury by inducing the formation of adventitious lateral roots at the cut site (Sheng et al., 2017). Our study provides a first example of WOX11-mediated mitigation of the impact of belowground biotic stress.

WOX11-mediated adventitious rooting may contribute to tolerance of Arabidopsis to biotic stress by restoring the capacity of the root system to take up and transport water and minerals. Cyst nematodes modify host cells within the vascular cylinder into a permanent feeding structure, which interrupts the continuity of surrounding xylem vessels (Golinowski et al., 1996; Sobczak et al., 1997; Levin et al., 2020). As cyst nematodes develop, their feeding structures expand, consuming a larger part of the vascular cylinder while further impeding the flow of water and minerals (Bohlmann and Sobczak, 2014). This is the reason why aboveground symptoms of cyst nematodes infections are often confused for drought stress. Local and systemic auxin-based stress signals may thus activate WOX11-mediated adventitious lateral rooting to maintain the flow of water and minerals to the xylem vessels above infection sites (Levin et al., 2020). At lower inoculation densities, WOX11-meditated adventitious lateral root formation from cyst nematode infected primary roots may suffice to sustain normal Arabidopsis development and growth resulting in a more tolerant phenotype.

Recent research suggests that the cellular processes targeted by transcriptional activity of WOX11 includes the modulation of reactive oxygen species (ROS)-homeostasis. In poplar, PagWOX11/12a has been shown to regulate the

expression of enzymes involved in scavenging ROS under salt stress conditions (Wang et al., 2021). In crown root meristem cells of rice, WOX11 modulates ROS-mediated post-translational modifications (i.e., protein acetylation) of proteins required for crown root development (Xu et al., 2022). ROS are required for the induction of adventitious root formation from Arabidopsis explants (Shin et al., 2022). There is also evidence that ROS modulate auxin levels during the initiation of adventitious roots from Arabidopsis explants (Huang et al., 2020). Moreover, we have recently linked tolerance of Arabidopsis to cyst nematode infections, ROS-mediated processes, and root system plasticity (Willig et al., 2022). However, further research is needed to investigate if WOX11 influences ROS-related processes, or vice versa, in infection sites of cyst nematodes in Arabidopsis roots, and if such a mechanism plays a role in WOX11-mediated root plasticity and tolerance to nematode infections.

Supporting information:

Additional Supporting Information and supplementary file with code may be found in the online version of this article.

Figure S1. Primordia formed in response to *H. schachtii* infection in *arf7-1/19-1* mutant seedlings.
Figure S2. Root architecture comparison between *35S:WOX11-SRDX* seedlings and wild-type Col-0 seedlings.
Figure S3. COI1 and ERF109 contribute to *WOX11* expression upon *H. schachtii* infection.
Figure S4. Noise removal process using Gaussian Blur option in ImageJ.
Figure S5. Adventitious lateral roots increase the total secondary root length upon nematode infection.
Figure S6. Growth rates of *coi1-2, erf109,* and *35S:WOX11-SRDX*, and wild-type Col-0 plants over time.
Figure S7. Growth rates of *coi1-2, erf109,* and *35S:WOX11-SRDX* plants are more affected during *H. schachtii* than wild-type.

Funding:

This work was supported by the Graduate School Experimental Plant Sciences (EPS). JJW is funded by Dutch Top Sector Horticulture & Starting Materials (TU18152). JLLT was supported by NWO domain Applied and Engineering Sciences VENI (14250) and VIDI (18389) grants. MGS was supported by NWO domain Applied and Engineering Sciences VENI grant (17282).

Acknowledgements:

We thank Prof. Viola Willemsen for providing the pWOX11::GFP, pWOX11::GFP-coi1-2, pWOX11::GFP-erf109 reporter lines, and Lin Xu for providing the 35S:WOX11-SRDX/arf7-1/19-1, arf7-1/19-1, LBD16pro:LBD16-GUS and 35S:WOX11-SRDX/LBD16pro:LBD16-GUS mutant lines.

Author contributions:

JJW, NG, JB, and GS conceived the project. JJW, NG, TvL, SW, IEAE designed and performed the experiments. MGT provided scripts for SYLM analysis. Data analysis was designed analyzed and interpreted by JJW, NG, and MGS. JJW, NG, and GS wrote the article. VW performed crosses of *coi1-2, erf109* with wildtype plants expressing *pWOX11::GFP.* VW and LX provided Arabidopsis mutant and reporter lines. VW, LX, AG, MGS, and JLLT provided critical feedback on the manuscript. All co-authors provided input for the submitted version.

Conflict of interest:

The authors declare no conflict of interest.

References:

Baty F, Ritz C, Charles S, Brutsche M, Flandrois J-P, Delignette-Muller M-L (2015) A Toolbox for Nonlinear Regression in R: The Package nlstools.

Bebber DP, Holmes T, Gurr SJ (2014) The global spread of crop pests and pathogens. Global Ecology and Biogeography **23**: 1398–1407

van den Berg T, Korver RA, Testerink C, ten Tusscher KHWJ (2016) Modeling halotropism: A key role for root tip architecture and reflux loop remodeling in redistributing auxin. Development (Cambridge) **143**: 3350–3362

Bohlmann H, Sobczak M (2014) The plant cell wall in the feeding sites of cyst nematodes. Front Plant Sci **5**: 1–10

Cabrera J, Fernando ED, Melillo T, Fukaki H, Cabello S, Hofmann J, Fenoll C, Escobar C, Díaz-Manzano FE, Sanchez M, et al (2014) A role for LATERAL ORGAN BOUNDARIES-DOMAIN 16 during the interaction Arabidopsis-Meloidogyne spp. provides a molecular link between lateral root and root-knot nematode feeding site development. New Phytologist **203**: 632–645

Cai XT, Xu P, Zhao PX, Liu R, Yu LH, Xiang C Bin (2014) Arabidopsis ERF109 mediates cross-talk between jasmonic acid and auxin biosynthesis during lateral root formation. Nat Commun. doi: 10.1038/ncomms6833

Cheng S, Zhou DX, Zhao Y (2016) WUSCHEL-related homeobox gene WOX11 increases rice drought resistance by controlling root hair formation and root system development. Plant Signal Behav. doi: 10.1080/15592324.2015.1130198

Fukaki H, Tasaka M (2009) Hormone interactions during lateral root formation. Plant Mol Biol **69**: 437–449

Gheysen G, Mitchum MG (2011) How nematodes manipulate plant development pathways for infection. Curr Opin Plant Biol **14**: 415–421

Golinowski W, Grundler FMW, Sobczak M (1996) Changes in the structure of Arabidopsis thaliana during female development of the plant-parasitic nematode Heterodera schachtii. Protoplasma **194**: 103–116

Goverse A, Overmars H, Engelbertink J, Schots A, Bakker J, Helder J (2000) Both induction and morphogenesis of cyst nematode feeding cells are mediated by auxin. Molecular Plant-Microbe Interactions **13**: 1121–1129

Guarneri N, Willig J-J, Sterken MG, Zhou W, Hasan MS, Sharon L, Grundler FMW, Willemsen V, Goverse A, Smant G, et al (2023) Root architecture plasticity in response to endoparasitic cyst nematodes is mediated by damage signaling. New Phytologist **237**: 807–822

Hiratsu K, Matsui K, Koyama T, Ohme-Takagi M (2003) Dominant repression of

target genes by chimeric repressors that include the EAR motif, a repression domain, in Arabidopsis. Plant Journal **34**: 733–739

Hoth S, Schneidereit A, Lauterbach C, Scholz-Starke J, Sauer N (2005) Nematode infection triggers the de novo formation of unloading phloem that allows macromolecular trafficking of green fluorescent protein into syncytia. Plant Physiol **138**: 383–392

Hu X, Xu L (2016) Transcription Factors WOX11/12 Directly Activate *WOX5/7* to Promote Root Primordia Initiation and Organogenesis. Plant Physiol **172**: 2363–2373

Huang A, Wang Y, Liu Y, Wang G, She X (2020) Reactive oxygen species regulate auxin levels to mediate adventitious root induction in Arabidopsis hypocotyl cuttings. J Integr Plant Biol **62**: 912–926

Jones JT, Haegeman A, Danchin EGJ, Gaur HS, Helder J, Jones MGK, Kikuchi T, Manzanilla-López R, Palomares-Rius JE, Wesemael WML, et al (2013) Top 10 plant-parasitic nematodes in molecular plant pathology. Mol Plant Pathol **14**: 946–961

Levin KA, Tucker MR, Bird DMK, Mather DE (2020) Infection by cyst nematodes induces rapid remodelling of developing xylem vessels in wheat roots. Sci Rep. doi: 10.1038/s41598-020-66080-z

Liu J, Sheng L, Xu Y, Li J, Yang Z, Huang H, Xu L (2014) *WOX11* and *12* Are Involved in the First-Step Cell Fate Transition during de Novo Root Organogenesis in *Arabidopsis*. Plant Cell **26**: 1081–1093

Liu R, Wen SS, Sun TT, Wang R, Zuo WT, Yang T, Wang C, Hu JJ, Lu MZ, Wang LQ (2022) PagWOX11/12a positively regulates the PagSAUR36 gene that enhances adventitious root development in poplar. J Exp Bot **73**: 7298–7311

Okushima Y, Fukaki H, Onoda M, Theologis A, Tasaka M (2007) ARF7 and ARF19 regulate lateral root formation via direct activation of LBD/ASL genes in Arabidopsis. Plant Cell **19**: 118–130

Olmo R, Cabrera J, Díaz-Manzano FE, Ruiz-Ferrer V, Barcala M, Ishida T, García A, Andrés MF, Ruiz-Lara S, Verdugo I, et al (2020) Root-knot nematodes induce gall formation by recruiting developmental pathways of post-embryonic organogenesis and regeneration to promote transient pluripotency. New Phytologist **227**: 200–215

Sheng L, Hu X, Du Y, Zhang G, Huang H, Scheres B, Xu L (2017) Non-canonical WOX11-mediated root branching contributes to plasticity in arabidopsis root system architecture. Development (Cambridge) **144**: 3126–3133

Shin SY, Park SJ, Kim HS, Jeon JH, Lee HJ (2022) Wound-induced signals regulate root organogenesis in Arabidopsis explants. BMC Plant Biol. doi: 10.1186/s12870-022-03524-w

Sobczak M, Golinowski W, Grundler FMW (1997) Changes in the structure of Arabidopsis thaliana roots induced during development of males of the plant parasitic nematode Heterodera schachtii. Eur J Plant Pathol **103**: 113–124

Tahir MM, Tong L, Fan L, Liu Z, Li S, Zhang X, Li K, Shao Y, Zhang D, Mao J (2022) Insights into the complicated networks contribute to adventitious rooting in transgenic MdWOX11 apple microshoots under nitrate treatments. Plant Cell Environ **45**: 3134–3156

Wang LQ, Li Z, Wen SS, Wang JN, Zhao ST, Lu MZ (2020) WUSCHEL-related homeobox gene PagWOX11/12a responds to drought stress by enhancing root elongation and biomass growth in poplar. J Exp Bot **71**: 1503–1513

Wang LQ, Wen SS, Wang R, Wang C, Gao B, Lu MZ (2021) PagWOX11/12a activates PagCYP736A12 gene that facilitates salt tolerance in poplar. Plant Biotechnol J **19**: 2249–2260

Warmerdam S, Sterken MG, van Schaik C, Oortwijn MEP, Sukarta OCA, Lozano-Torres JL, Dicke M, Helder J, Kammenga JE, Goverse A, et al (2018) Genome-wide association mapping of the architecture of susceptibility to

the root-knot nematode Meloidogyne incognita in Arabidopsis thaliana. New Phytologist **218**: 724–737

Willig J-J, Guarneri N, van Steenbrugge JJM, de Jong W, Chen J, Goverse A, Lozano Torres JL, Sterken MG, Bakker J, Smant G (2022) The Arabidopsis transcription factor TCP9 modulates root architectural plasticity, reactive oxygen species-mediated processes, and tolerance to cyst nematode infections. Plant Journal **112**: 1070–1083

Willig J-J, Sonneveld D, van Steenbrugge JJM, Deurhof L, van Schaik CC, Teklu MG, Goverse A, Lozano-Torres JL, Smant G, Sterken MG (2023) From root to shoot; Quantifying nematode tolerance in Arabidopsis thaliana by high-throughput phenotyping of plant development. J Exp Bot erad266

Xu Q, Wang Y, Chen Z, Yue Y, Huang H, Wu B, Liu Y, Zhou DX, Zhao Y (2022) ROS-stimulated protein lysine acetylation is required for crown root development in rice. J Adv Res. doi: 10.1016/j.jare.2022.07.010

Zhang T, Ge Y, Cai G, Pan X, Xu L (2023) WOX-ARF modules initiate different types of roots. Cell Rep. doi: 10.1016/j.celrep.2023.112966

Supporting information:

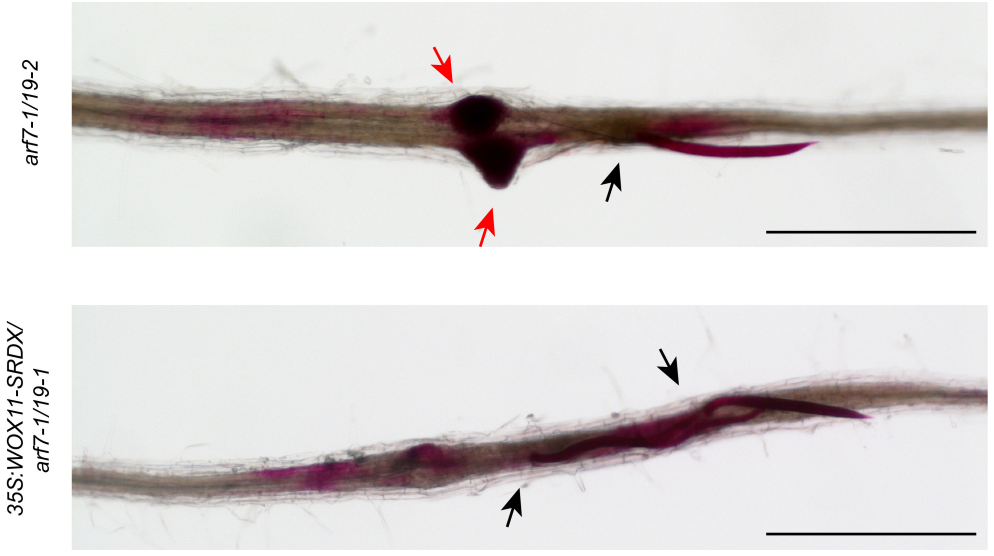

Figure S1: Primordia formed in response to *H. schachtii* infection in *arf7-1/19-1* mutant seedlings. Seven-day-old *35S:WOX11-SRDX/arf7-1/19-1* and *arf7-1/arf19-1* mutant seedlings were inoculated with 90 *H. schachtii* juveniles or with mock solution. At 7 dpi nematodes were stained with fuchsin and imaged using a dissection microscope. Black arrowheads indicate head of the nematode. Red arrowheads indicate primordia. Scale bar: 500 µm.

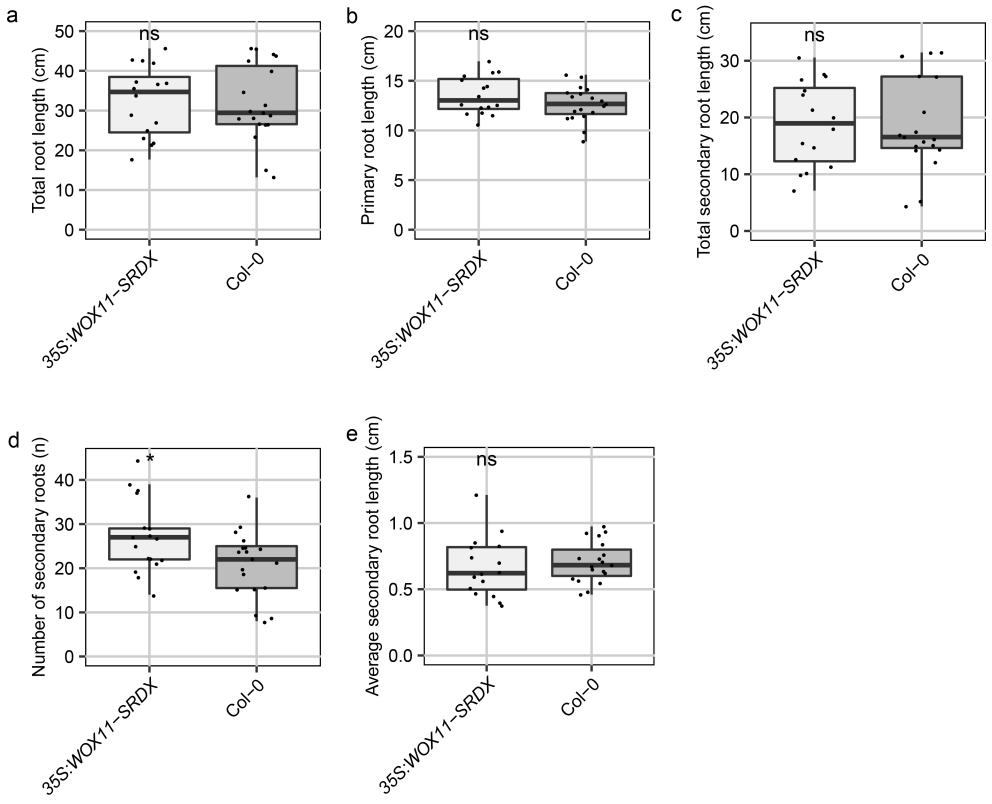

Figure S2: Root architecture comparison between *35S:WOX11-SRDX* seedlings and wild-type Col-0 seedlings. *35S:WOX11-SRDX* and wild-type Col-0 seedlings were grown on modified KNOP medium for 16 days. Roots were scanned and root architectural components were measured. **a)** Total root length. **b)** Primary root length. **c)** Total secondary root length. **d)** Number of secondary roots. **e)** Average secondary root length. Data from two independent biological repeats of the experiment were combined. Significance of differences between genotypes was calculated by a Unpaired Two-Samples Wilcoxon Test. (n = 14-18).

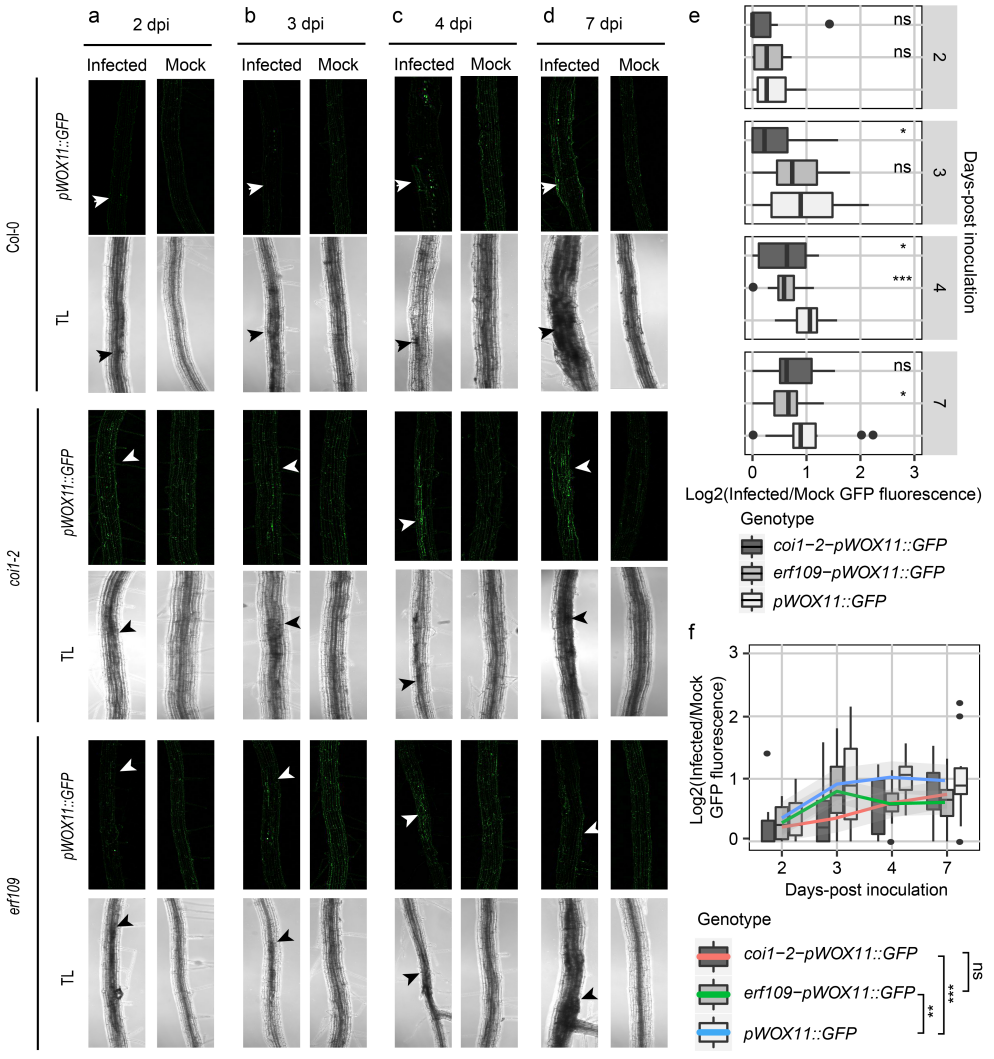

Figure S3: COI1 and ERF109 contribute to *WOX11* expression upon *H. schachtii* infection. a-f) Four-day-old Arabidopsis seedlings were either inoculated with 10 *H.* schachtii second-stage juveniles (J2s) or with mock solution. At 2, 3, 4, and 7 dpi, seedlings were mounted and then imaged using a fluorescent confocal microscope. Single-nematode infection sites were selected for observation. **a-d)** Representative pictures of infected and mock-inoculated seedlings expressing the *pWOX11::GFP* construct in either wild-type Col-0, mutant *coi1-2*, or mutant *erf109* background at **(a)** 2 dpi, **(b)** 3 dpi, **(c)** 4 dpi, and **(d)** 7 dpi. To make the fluorescence more visible, the brightness was enhanced for all the representative pictures in the same way. **e)** Quantification of *pWOX11::GFP* fluorescent intensity induced by infection of wild-type Col-0, *coi1-2,* and *erf109* roots. Values represent $\log_2$ of the fluorescence ratio between the GFP integrated density of infected and noninfected roots. Data from three independent biological repeats of the experiment were combined. Significance of differences between fluorescent intensities in Co-0, *coi1-2,* and *erf109* per timepoint was calculated by a Wilcoxon Rank Sum test. ns = not significant, *p< 0.05, **p< 0.01, ***p<0.001 (n=15). **(f)** Values represent $\log_2$ of the fluorescence ratio between the GFP integrated density of infected and noninfected roots. Significance of differences between genotypes was calculated by analysis of variance. Grey area indicates the 95% confidence interval of the loess fit.

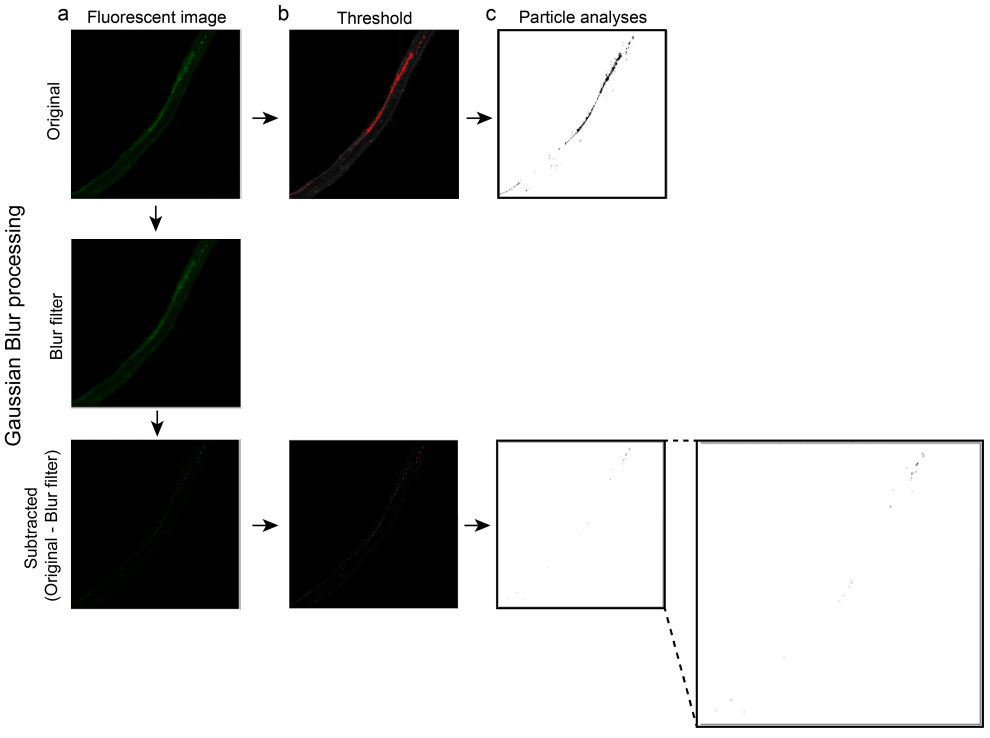

Figure S4: Noise removal process using Gaussian Blur option in ImageJ. a) The original images, which gave a lot of noise in the practical analyses (**c**) after setting the threshold (**b**) was duplicated and blurred using the Gaussian blur option in ImageJ. The blurred image was subtracted from the original image and the particles were analysed.

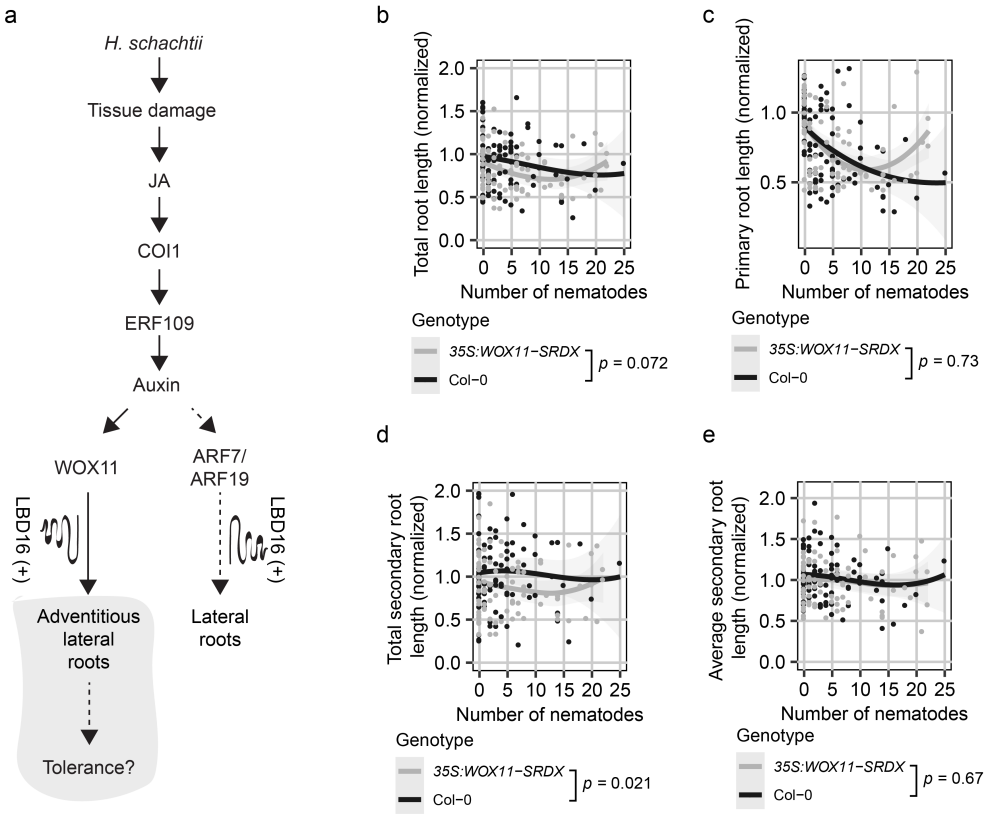

Figure S5: Adventitious lateral roots increase the total secondary root length upon nematode infection. a) Schematic diagram of *H. schachtii*- and WOX11-mediated adventitious lateral root emergence. Grey area indicates the tested part of the pathway. Curling line and '+' indicate involvement of multiple proteins, including LBD16. **b-e)** Nine-day old *35S:WOX11-SRDX* and wild-type Col-0 seedlings were inoculated with densities (P_i) ranging from 0-7.5 *H. schachtii* J2s (per mL modified KNOP media). Roots were scanned and nematodes were counted after fuchsine staining at 7 dpi. Root architectural components of infected seedlings were normalized to the median respective component in mock-treated roots. Data of two independent biological repeats of the experiment were combined. **b)** Total root length per number of nematodes inside the roots. **c)** Primary root length per number of nematodes inside the roots. **d)** Total secondary root length per number of nematodes inside the roots. **e)** Average secondary root length per number of nematodes inside the roots. Data from two independent biological repeats of the experiment were combined. Significance of differences between genotypes was calculated by analysis of variance (n=14-18). Grey area indicates the 95% confidence interval of the loess fit.

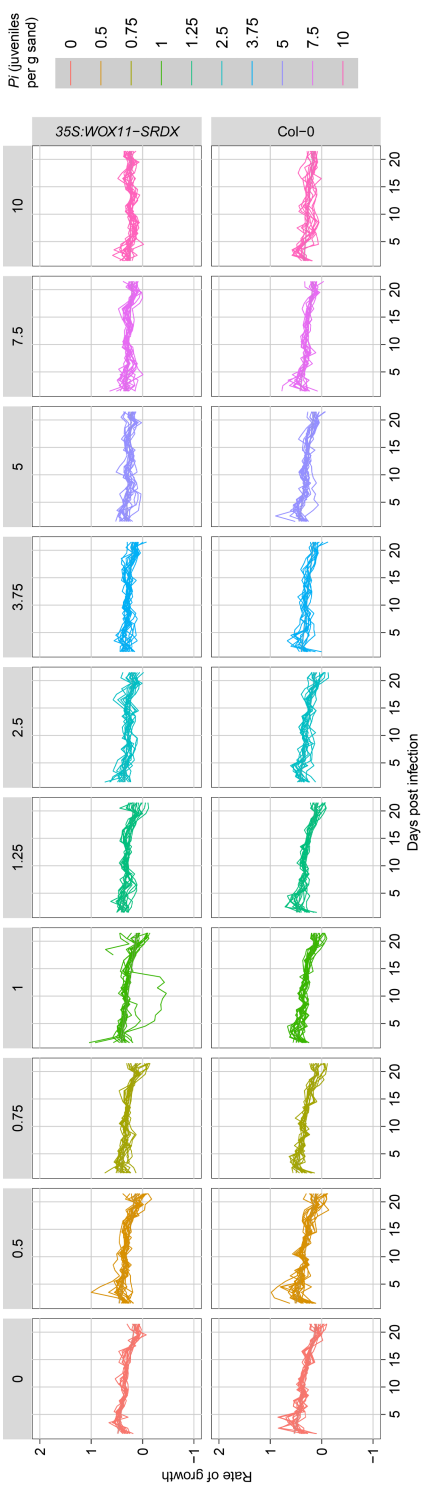

Figure S6: Growth rates of *35S:WOX11-SRDX* and wild-type Col-0 plants over time. Nine-day-old Arabidopsis seedlings (*35S:WOX11-SRDX* and wild-type Col-0) were inoculated with 10 densities (P_i) of *H. schachtii* juveniles (0 to 2000 juveniles per g dry sand). The growth rates of plants were calculated per day. Lines represent individual plants (n=10-18 plants per treatment).

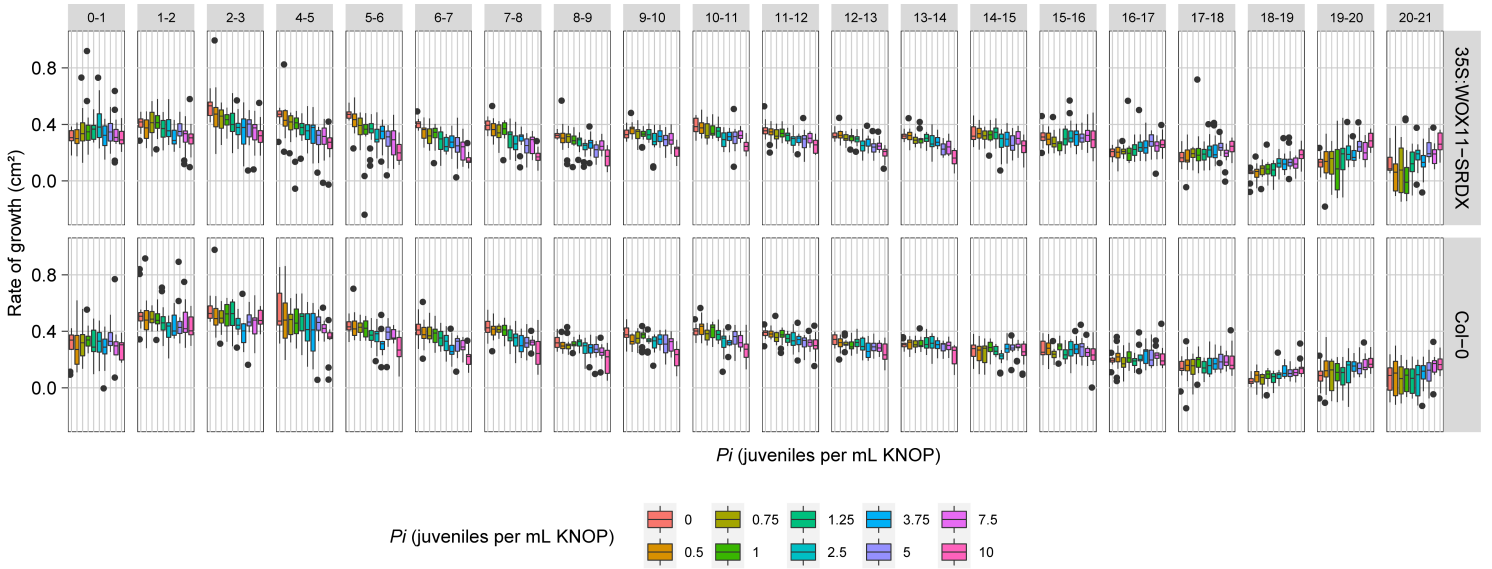

Figure S7: Growth rates of *35S:WOX11-SRDX* plants are more affected during *H. schachtii* than wild-type Col-0. Nine-day-old Arabidopsis seedlings (*35S:WOX11-SRDX* and wild-type Col-0) were inoculated with 10 densities (P_i) of *H. schachtii* juveniles (0 to 2000 juveniles per g dry sand). The growth rates of plants were calculated per day. Boxplots represent data of x plants, the dots represent outlier measurements (1.5 times the interquartile range). (n = 10-18 plants per treatment).

Chapter 6

The Arabidopsis transcription factor TCP9 modulates root architectural plasticity, ROS-mediated processes, and tolerance to cyst nematode infections

Jaap-Jan Willig[1], Nina Guarneri[1], Joris J.M. van Steenbrugge[1], Willem de Jong[1], Jingrong Chen[1], Aska Goverse[1], José L. Lozano Torres[1], Mark G. Sterken[1], Jaap Bakker[1], Geert Smant[1,2]

[1]Laboratory of Nematology, Wageningen University & Research, 6708 PB Wageningen, the Netherlands

Published in The Plant Journal, Volume 112, Issue 4, November 2022, Pages 1070-1083

Abstract:

Infections by root feeding nematodes have profound effects on root system architecture and consequently shoot growth of host plants. Plants harbour intraspecific variation in their growth responses to belowground biotic stresses by nematodes, but the underlying mechanisms are not well understood. Here, we show that the transcription factor TEOSINTE BRANCHED/CYCLOIDEA/PROLIFERATING CELL FACTOR-9 (TCP9) modulates root system architectural plasticity in *Arabidopsis thaliana* in response to infections by the endoparasitic cyst nematode *Heterodera schachtii*. Young seedlings of *tcp9* knock-out mutants display a significantly weaker primary root growth inhibition response to cyst nematodes than wildtype Arabidopsis. In older plants, *tcp9* reduces the impact of nematode infections on the emergence and growth of secondary roots. Importantly, the altered growth responses by *tcp9* are most likely not caused by less biotic stress on the root system, because TCP9 does not affect the number of infections, nematode development, and size of the nematode-induced feeding structures. RNA sequencing of nematode-infected roots of the *tcp9* mutants revealed differential regulation of enzymes involved in reactive oxygen species (ROS) homeostasis and responses to oxidative stress. We also found that root and shoot growth of *tcp9* mutants is less sensitive to exogenous hydrogen peroxide and that ROS accumulation in nematode infection sites in these mutants is reduced. Altogether, these observations demonstrate that TCP9 modulates root system architectural plasticity to nematode infections via ROS-mediated processes. Our study further points at a novel regulatory mechanism contributing to the tolerance of plants to root feeding nematodes by mitigating the impact of belowground biotic stresses.

Introduction:

Plant roots are intermittently exposed to various abiotic stresses, such as drought, but also to biotic stresses, such as herbivory by root-parasitic nematodes. Plants utilize root system architectural plasticity to cope with such changing environmental conditions in the soil (Koevoets et al., 2016; Karlova et al., 2021). For instance, secondary roots are formed at the water-contact side of the roots to adapt root system architecture to the heterogenous distribution of water in the soil (Karlova et al., 2021). Likewise, root feeding by plant parasitic nematodes results in the formation of secondary roots in the proximity of permanent nematode-induced feeding structures (Goverse et al., 2000; Lee et al., 2011). Earlier work has shown that plants harbour intraspecific variation in their root growth responses to belowground biotic stress by these cyst nematodes, which correlates with the overall level of tolerance to nematode infections (Trudgill and Cotes, 1983; Miltner et al., 1991). However, the genetic and molecular mechanisms governing root system architectural plasticity in response to biotic stress during nematode infections in plants are not well understood.

The impact of root feeding cyst nematodes on plant development and growth leads to large global agricultural losses. This is partly because cyst nematodes can persist in a dormant state in the soil in the absence of host plants for many years (Jones et al., 2013). Hatching of infective juveniles of cyst nematodes primarily occurs in response to root exudates of host plants. These root exudates also provide guidance for the migration of cyst nematodes to the root surface, where

they penetrate the root epidermis at the differentiation or maturation zone. Host invasion by cyst nematodes involves piercing of plant cell walls with a needle-like oral stylet and concomitant secretion of plant cell wall degrading enzymes (Rehman et al., 2009). Once inside the root cortex, infective juveniles migrate intracellularly towards the vascular cylinder, while causing extensive tissue damage. After arriving at the vascular cylinder, they deliver stylet secreted effectors into a host cell to initiate the formation of a permanent feeding site by manipulating plant cell differentiation and growth. Throughout the course of several weeks, this permanent feeding site expands further inside the vascular cylinder by local cell wall degradation and subsequent fusion of neighbouring host cells. The permanent feeding site, hereafter named syncytium, provides cyst nematodes access to the flow of assimilates in the plant, which are essential for nematode development and reproduction. Thus, biotic stress on plant root systems during cyst nematode infections is caused by tissue damage during host invasion and loss of assimilates by feeding nematodes.

Members of the *TEOSINTE BRANCHED1/CYCLOIDEA/ PROLIFERATING CELL FACTOR1* (TCP) transcription factor family convert environmental signals into adaptive growth responses in plants (Danisman, 2016). In Arabidopsis, the TCP family consists of 24 members and is divided over two groups, named class I and II, based on sequence variation in a conserved TCP domain of about 60 residues (Li, 2015). Class I and II TCPs differ in composition of the nuclear localization signal, the length of the second helix in the basic helix-loop-helix region, and the presence of a positively charged arginine-rich domain (Cubas et al., 1999). The basic region in the TCP domain is required for binding to GC-rich motifs in *cis*-regulatory elements in DNA sequences upstream of genes that are transcriptionally regulated by TCPs (Kosugi and Ohashi, 2002). Moreover, TCPs are able to form homo- and heterodimers, mostly between different members of the same class, which further contributes to functional diversity within the TCP family (Viola et al., 2011; Danisman et al., 2012). Because both class I and II TCP factors can bind to partially overlapping *cis*-acting regulatory elements, it is thought that members of the two classes might act antagonistically (Danisman et al., 2012). However, recent reports do not support a strict functional distinction of class I and class II TCP into transcriptional activators and repressors, respectively (Kubota et al., 2017; Lucero et al., 2017; Wang et al., 2020).

Several TCP transcription factors have been shown to drive adaptations in root system architecture in response to abiotic stress. For instance, in Arabidopsis, TCP20 regulates preferential secondary root growth in response to nitrates in a process called root foraging (Guan et al., 2014). To this end, TCP20 interacts with NIN-like protein (NLP) transcription factors NLP6 and NLP7 to support root meristem growth under nitrogen starvation (Guan et al., 2014). Likewise, TCP13 regulates leaf and root growth in Arabidopsis in response conditions simulating drought (Urano et al., 2022). Furthermore, heterologous expression of *PeTCP10* of bamboo (*Phyllostachys edulis*) in transgenic Arabidopsis induces secondary root growth under treatments simulating drought conditions (Liu et al., 2020) and salt stress (Xu et al., 2021). In a similar experimental design, *OsTCP19*, a class I TCP from rice, also makes plants more tolerant to salt stress (Mukhopadhyay and Tyagi, 2015). A subset of TCP transcription factors involved in root development and growth is controlled by the microRNA miR319 (Baulies et al., 2022), which together may form a regulatory module tuning plant responses to abiotic stresses (Zhou et al., 2013; Fang et al., 2021).

As members of the TCP family in Arabidopsis regulate root system

architectural changes in response to abiotic stresses, we reasoned that they might also be involved in root plasticity under biotic stress. To test this hypothesis, we first analysed the expression of TCP family members during early stages of infection of the beet cyst nematode *Heterodera schachtii* in Arabidopsis. As *TCP9* was found to be strongly upregulated in association with nematode infections, we further focused our study on this class I TCP transcription factor. Hereto, we investigated the impact of TCP9 on root plasticity during cyst nematode infections by monitoring the primary root growth inhibition response and secondary root formation shortly after inoculation with infective juveniles. Next, we tested if the aberrant root phenotypes observed for *tcp9* mutants could be caused by a loss of susceptibility to nematode infections, and therefore lower levels of biotic stress on the root system. To pinpoint possible mechanisms underlying the impact of TCP9 on root system architectural plasticity, we used RNA sequencing of nematode-infected roots of *tcp9* mutants at early stages of infection by *H. schachtii*. The TCP9-regulated gene expression patterns that we observed herein pointed at changes in ROS-mediated processes. We therefore subsequently analysed if ROS accumulates differently in nematode infection sites in the *tcp9* mutants and if root and shoot growth of these mutants responds differently to exogenously applied hydrogen peroxide as compared to wildtype Arabidopsis plants. Altogether, our data provides insights into a novel mechanism underlying root architecture plasticity in response to biotic stress by endoparasitic cyst nematodes.

Materials and Methods:

Plant culturing

For seed sterilization, Arabidopsis seeds (Col-0, *tcp9*, *tcp20*, *tcp9tcp20* (Danisman et al., 2012) were placed in Eppendorf tubes in a desiccator. The seeds were vapour sterilized for 3-4 hours using a mixture of hydrochloric acid (25%) and sodium hypochlorite (50 g/L). Finally, the sterile seeds were stratified for 4 days. For *in vitro* assays, seeds were sown on square petri dishes (120x120 mm) or 12-well plates containing modified Knop medium (Sijmons et al., 1991). Seedlings were grown at 21 °C and 16-h-light/8-h-dark conditions. For *in vivo* pot experiments, Arabidopsis seeds (Col-0, *tcp9*, *tcp20*, *tcp9tcp20*) were placed in Eppendorf tubes and stratified for 4 days and sown in 200 mL pots containing Lentse potgrond (Lensi B.V. Bleiswijk).

Nematode hatching and sterilization

H. schachtii cysts (Woensdrecht population from IRS, the Netherlands) were collected from sand of *Brassica oleracea* infected plants as previously described (Baum et al., 2000). *H. schachtii* cysts were rinsed and transferred into a clean Erlenmeyer. Water was added to a maximum volume of 100 ml containing 0.02% sodium azide. This mixture was stirred for 20 min. Later, sodium azide was vigorously removed by washing with tap water. Cysts were then placed on a hatching sieve in a glass petri dish. An antibiotic solution was added containing 1.5 mg/mL gentamycin, 0.05 mg/mL nystatin and 3mM zinc chloride. The cysts were incubated in the dark for 4-7 days. Eventually, nematode juveniles were collected in a 2 mL Eppendorf tube. The J2s were surface sterilized with HgCl2 solution (0.002% Triton X-100 w/v, 0.004% NaN3 w/v, 0.004% HgCl2 w/v) for 20 min. After incubation, the nematodes were spun down and the supernatant was removed. Nematodes were washed with sterile

water and spun down again. This was repeated three times. Finally, the nematodes were resuspended in 0.7% gelrite (Duchefa Biochemie, Haarlem, the Netherland).

Root architecture assay

Four- or nine-day old seedlings were inoculated with either 0 (negative control; mock), 15 or 200 sterile second stage *H. schachtii* juveniles (J2) in 5 µL gelrite (Baum et al., 2000). At 4- or 7 dpi, seedlings were scanned and analysed using WhinRHIZO (WinRhizo pro2015; Regent Instruments Inc., Ville de Québec, Canada). To compare the effect of nematode infection on the root system component between genotypes we normalized the values of nematode infected seedlings to the median of the corresponding root system component of mock treated seedlings.

Fuchsin staining

To determine how many *H. schachtii* juveniles entered the root at 4 dpi, Arabidopsis seedlings were transferred to a 2.5% bleach solution for five minutes and afterwards washed and incubated in water for 10 minutes. The roots were placed in fuchsine solution (15 mL:500 µL fuchsine stock; 0.35 g acid fuchsin, 25 ml glacial acetic acid, 75ml water). The solution was boiled for one minute in a microwave and cooled down to room temperature. Subsequently, the roots were washed with water and stored in 40% glycerol. Using a stereo microscope, the number of juveniles were counted.

Nematode infection assay

14-day old Arabidopsis seedlings in a 12-well plate were inoculated with ~250 sterile *H. schachtii* juveniles in 5µL gelrite (Baum et al., 2000). At 14- and 28 dpi, the number of J3 stage nematodes, male and female nematodes were counted. The counting and imaging were done under a light microscope (ZEISS microscopes and cameras, ZEN 3.2 (Blue edition)). ImageJ (1.53c) was used to measure the size of the females and the feeding sites.

RNAseq analysis

Experimental setup and RNA isolation

To check the expression of TCPs during cyst nematode infection, four-day old *A. thaliana Col-0* seedlings were inoculated with 200 sterile *H. schachtii* juveniles in modified Knop's medium. To understand how TCP9 transcriptionally regulates root growth responses during cyst nematode infections, four-day old *A. thaliana* seedlings of Col-0, *tcp9*, *tcp20*, and the double mutant *tcp9tcp20* were inoculated with 80 sterile *H. schachtii* juveniles in modified Knop's medium. Root tissue was harvested and snap frozen in liquid nitrogen. Root tissue was ground in liquid nitrogen and total RNA was extracted with the Maxwell® 16 LEV plant RNA kit (Promega) in the Maxwell 16 AS2000 instrument (Promega), following the manufacturer's instructions. Three biological replicates of ~80 plants/sample per condition were generated.

RNAseq and quantification

The RNA was sequenced at BGI using the DNBseq platform. Approximately 50 million paired reads of 150bp were generated per sample. Raw reads were deposited at ArrayExpress under E-MTAB-11649. Code used for the analysis has been reposited under https://git.wur.nl/published_papers/willig_2022_tcp.

Reads were aligned to the TAIR10 genome of *A. thaliana* (Berardini et al., 2015) using hisat2 v2.1.0 with option –dta enabled (Kim et al., 2015). Transcripts were predicted and quantified as TPM (transcripts per kilobase million) using stringtie v2.2.0 based on the TAIR10 reference gene annotations using the –e option (Pertea et al., 2016). To check the expression of TCPs at different time points in Col-0 inoculated with *H. schachtii*, we calculated gene expression levels with RSEM (Version: v1.2.12) using default parameters (#Add Ref https://bmcbioinformatics.biomedcentral.com/articles/10.1186/1471-2105-12-323) and determined differentially expressed genes using DEseq2 (Add Ref: https://genomebiology.biomedcentral.com/articles/10.1186/s13059-014-0550-8) with a fold Change >= 2.00 and adjusted P-value <= 0.05.

Presence of TCP9 and TCP20 mutations

To visually confirm the *tcp9*-, *tcp20*- and double knockout mutants, samples of RNAseq reads mapped to the TAIR10 genome were visualised in the JBrowse genome browser (Buels et al., 2016), along with the TAIR10 reference gene annotations. We used Col-0_72_-_2 (S2) as control, tcp9_72_-_3 (S5) for the *tcp9* mutant, tcp20_72_-1 (S38) for the *tcp20* mutant, and tcp9/20_72_-_1 (S42) for the *tcp9tcp20* double mutant. Screenshots were taken at the genomic loci of the *TCP9* (AT2G45685) and *TCP20* (A0A178VAT1) genes on the TAIR10 genome.

RNAseq analysis

Data was analyzed using “R” (v. 3.5.3 x64) in Rstudio (R Core Team, 2019). For analysis, the dplyr and tidyr packages were used for data organization (Wickham, H. F., R.; Henry, L; Müller, 2018a; Wickham, H. F., R.; Henry, L; Müller, 2018b) and plots were generated using ggplot2 (Hadley Wickham, 2009). Before analysis, the TPM values were filtered and transformed (Diaz-Granados et al., 2019). First, the *A. thaliana* gene-expression was filtered for reads detected in all samples, resulting in 28,600 detected genes (out of 48,359 protein coding genes in the TAIR11 assembly). We did not notice a batch-effect over the biological replicates. In subsequent analyses either log-transformed or the raw TPM values were used.

Principal component analysis

To understand the sources of variance in the gene expression data principal component analysis was used.

To ensure equal weight on the differences in expression, the gene expression data *E* was transformed by:

$$R_{i,j} = \log_2(\frac{E_{TPM,i,j}}{\overline{E_{TPM,i}}})$$

where *R* is the $\log_2$ ratio with the mean of gene *i* and sample *j*, E_{TPM} is the expression measured as TPM and $\overline{E_{TPM}}$ is the mean expression of gene *i* over all samples. This procedure was followed for both species (for *H. schachtii* only on the infected samples). The expression data was analysed using the *prcomp* function. The first four axes of both species were examined.

Linear model on A. thaliana expression

To understand the role of time, treatment, presence of the *tcp9* mutation, and presence of the *tcp20* mutation on gene expression in *A. thaliana*, we used various linear models, where differential expression of the genes was determined by comparison to the wild-type reference genotype Col-0. For each combination of genotype (*tcp9, tcp20, tcp9tcp20*), timepoint (24, 48, or 72 hours), and treatment (mock or inoculated with *H. schachtii*) the following model was fitted

$$E_{TPM,log2} = G + e$$

Where $E_{TPM,log2}$ is the $\log_2$-normalized expression and G is genotype (Col-0 versus the selected mutant genotype). This led to 18 comparisons. To determine the amount of differentially expressed genes (DEG) per comparison, we first selected for effect-size (|effect| > 1.5) and set the threshold for the p-value to < 0.01, to determine the false-positive rate, we used the *p.adjust* function with the *fdr* method (Benjamini and Hochberg, 1995). We found that this selection had a median FDR = 0.066 (see Table S1). This led to the identification of 21-244 DEGs per comparison (see Table S1 & S2).

Enrichment analysis

Gene enrichment analyses were conducted using the TAIR10 GO annotations. Groups were selected on minimum three genes representing one group and with minimum two genes in overlap (FDR <0.01) (see Table S3).

DAB staining

Sterile *H. schachtii* juveniles were inoculated onto 4-day old Arabidopsis seedlings that were grown in square petri dishes. Three days after inoculation, Arabidopsis roots were stained with DAB staining solution in the dark for 3 hours (Siddique et al., 2014). Later the DAB staining solution was replaced by a bleaching solution (ethanol: acetic acid: glycerol = 3: 1: 1). Finally, the DAB staining on the roots was visualized

with a Zeiss, Axio Imager.A2 microscope via 10x and 20x objectives. Significance of the differences between proportions was calculated by a in Fischer's exact test.

Root architecture assay of H_2O_2 treated seedlings

We first tested which concentration of H_2O_2 is the most informative. To this end, six-day old wildtype Col-0 seedlings that were grown in a square petri dish were transferred to a 24-well plate containing sterile liquid Knop media which contained either 0, 100, 200, or 300 µM H_2O_2. Eight-days after growth, the roots of seedlings were scanned and analysed using WhinRHIZO Statistical significance of the pairwise differences between mock and nematode infection groups were tested using a two-way ANOVA with Tukey correction (Fig. S1). Seedlings treated with 200 µM H_2O_2 gave the most informative result. Therefore, we decided to continue with only the treatments 0 (mock) and 200 µM H_2O_2. To determine if there are differences between *tcp9*, *tcp20*, *tcp9tcp20* and wildtype Col-0 seedlings we followed the same procedure. To compare if genotypes were less affected by H_2O_2 treatment, we normalized the values of H_2O_2 treated plants to the median of mock treated plants.

Shoot growth assay of H_2O_2 treated plants

Nine-day old Arabidopsis seedlings that were grown in Lentse potgrond were exposed to 200 µM H_2O_2 that was applied by spraying (Sewelam et al., 2013). Mock-treated plants were both sprayed with water. At 21 dpi, the green canopy area was imaged using a sony α33 camera equiped with a 28mm lens. By using the 'Color Threshold' and 'Analyze Particles' tools in ImageJ, we calculated the green canopy area. To compare the effect of spraying H_2O_2 on the shoot system, we normalized the values of H_2O_2 treated plants to the median of the mock sprayed plants.

Statistical analysis

Statistical analyses were performed using the R software version 3.6.3 (Windows, x64). The R packages used are tidyverse (https://CRAN.R-project.org/package=tidyverse), ARTool (https://CRAN.R-project.org/package=ARTool) and multcompView (https://CRAN.R-project.org/package=multcompView). For normally distributed data, significance of the differences among means was calculated by a one-way or two-way ANOVA followed by Tukey's HSD test for multiple comparisons. A non-parametric pairwise Wilcoxon test followed by false discovery rate correction for multiple comparisons was used for non-normally distributed data with one grouping factor.

Results:

TCPs are differentially regulated during *H. schachtii* infection

To investigate if members of the *TCP* transcription factor family are differentially regulated during early stages of nematode infection, we assessed their expression levels in whole root systems of Arabidopsis infected with *H. schachtii* using RNA sequencing. We inoculated four-day old seedlings with infective *H. schachtii*

juveniles and analysed the root transcriptome at 6, 12, 24, 48, 72, and 120 hours post inoculation (hpi). We found that nine TCP family members were differentially expressed in nematode-infected roots at one or more timepoints post inoculation (Fig. 1). Of the class I TCPs, *TCP8, TCP9*, and *TCP20* were up-regulated, whereas *TCP7*, *TCP14,* and *TCP21* were down-regulated. Of the class II TCPs, only *TCP13* was upregulated throughout this entire time series, whereas both *TCP2* and *TCP24* were downregulated at the 120 hpi. Our data thus showed that *TCP* transcription factors might indeed be involved in regulating plant responses during the onset of parasitism by *H. schachtii*.

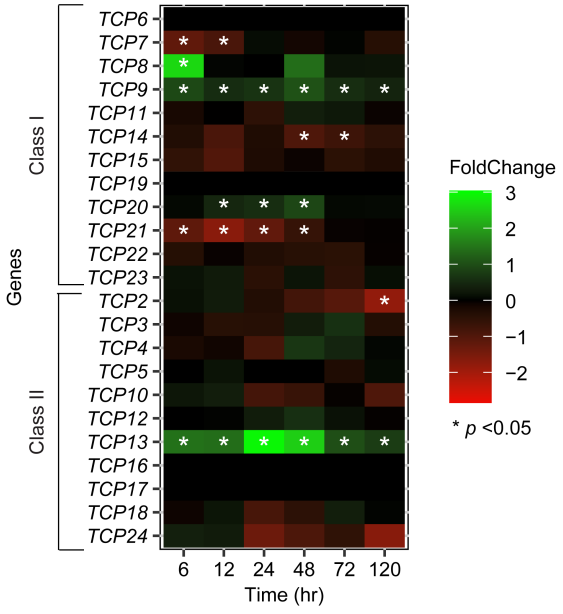

Figure 1: Members of *TCP* gene family are differentially regulated in whole roots of nematode-infected Arabidopsis seedlings. Relative expression level of TCPs as determined by RNA sequencing of whole roots of Arabidopsis seedlings either inoculated with 200 infective juveniles of *H. schachtii* or mock inoculated. Samples were collected at 6, 12, 24, 48, 72, and 120 hours post inoculation. Heatmap shows the Log2 Fold Change of *TCP* gene expression of normalized read counts per gene in nematode-inoculated seedlings versus mock-inoculated seedlings at different timepoints. Green indicates up-regulation and red indicates down-regulation. Asterisk (*) indicates significantly different expression level in nematode- versus mock-inoculated seedlings (*p< 0.05).

TCP9 modulates root system architecture during *H. schachtii* infection

Both *TCP9* and *TCP13* were significantly upregulated throughout all early stages of infection by *H. schachtii* in Arabidopsis. Since the function of TCP13 has recently been studied in more detail (Hur et al., 2019; Urano et al., 2022), we decided to further focus our research on a possible role for TCP9 in root plasticity responses to biotic stress by *H. schachtii*. TCP9 can alter root growth in Arabidopsis , but if it does so in response to abiotic and biotic stress is unknown. We also included TCP20 in our study, because it transcriptionally regulates *TCP9* expression and forms a functional dimer with TCP9 (Danisman et al., 2012; Wang et al., 2015). First, we challenged

four-day old seedlings of the Arabidopsis loss-of-function single mutants *tcp9, tcp20*, and the double mutant *tcp9tcp20* with infective juveniles of *H. schachtii* to monitor changes in primary root growth at 4 dpi. Notably, at this young age the root system of Arabidopsis seedlings only consists of a primary root. We found that primary root growth of all three *tcp* mutants and wildtype Arabidopsis seedlings was inhibited after inoculation with *H. schachtii* (Fig. 2a and b). Because we noticed differences in primary root growth for *tcp20* and *tcp9tcp20* in mock-inoculated seedlings (Fig. S2), we also calculated the relative growth of the primary root compared to mock-inoculated plants of the same genotype (Fig. 2c). This showed that the relative growth of the primary root of both *tcp9* and the *tcp9tcp20* mutants was significantly less affected (and thus closer to 1) by cyst nematodes than of the *tcp20* mutant and wildtype Arabidopsis.

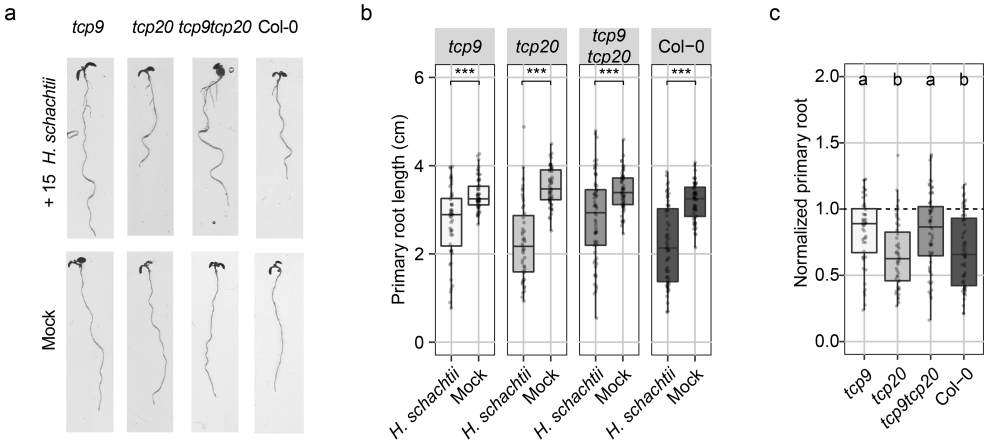

Figure 2: Primary root growth of young *tcp9* mutant seedlings is less affected by cyst nematode infections. Four-day old Arabidopsis seedlings (*tcp9, tcp20, tcp9tcp20* and wild-type Col-0) were inoculated with 15 juveniles of *H. schachtii* or a mock-solution. **a)** Representative pictures of seedlings either nematode- or mock-inoculated at 4-days post inoculation (dpi). **b)** Primary root length (cm) of wildtype and mutant Arabidopsis seedlings at 4 dpi. Data was analysed with a two-way ANOVA with a post hoc Tukey HSD test (n=60). ns= not significant, *p< 0.05, **p< 0.01, ***p<0.001. **c)** Impact of nematode infection on primary root growth calculated as the primary root length of nematode-inoculated seedlings divided by the median value of mock-inoculated seedlings of the same genotype. Data was analysed with a multiple comparison one-way ANOVA with a post hoc Tukey HSD test. Letters indicate different levels of significance. This experiment was performed three times with similar outcomes and pooled for data analysis.

Next, we tested if TCP9 also affects growth of other root system architecture components in response to *H. schachtii*. Hereto, we inoculated nine-day old Arabidopsis seedlings having a more elaborate root system with *H. schachtii*, and measured different root architecture components (i.e., total root length, primary root length, number of secondary roots, total secondary root length) at 7 dpi (Fig. 3a). All measurements were transformed to relative values by normalizing the data to the median of the corresponding measurement in mock-inoculated plants. We found that the total relative root length of only the *tcp9* mutant was significantly less affected (and closer to 1) by inoculation with *H. schachtii* compared to wildtype Col-0 plants (Fig. 3b). Remarkably, the relative growth of the primary root of the *tcp9* mutants was still slightly but no longer significantly different from wild type Arabidopsis (Fig.

3c). However, the number (Fig. 3d) and the total length of the secondary roots (Fig. 3e) were less affected by *H. schachtii* in the *tcp9* mutant as compared to wildtype Arabidopsis Col-0. We therefore concluded that TCP9 modulates the plasticity of the root system architecture in response to *H. schachtii* in Arabidopsis.

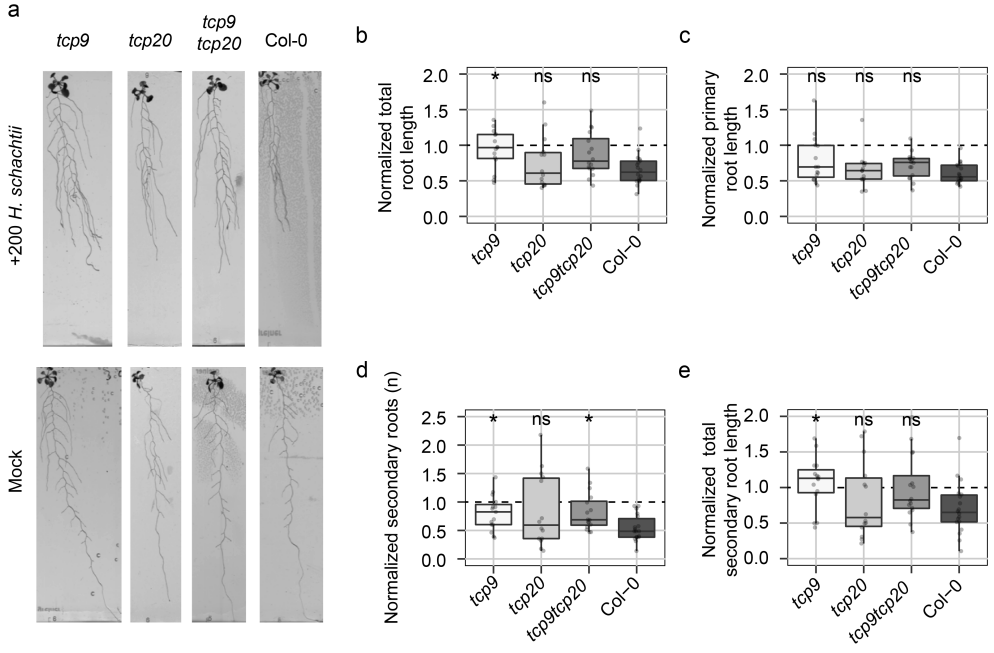

Figure 3: Root system architecture of *tcp9* mutants responds less to cyst nematode infections. Nine-day old Arabidopsis seedlings (*tcp9, tcp20, tcp9tcp20* and wild-type Col-0) were inoculated with 200 or 0 (Mock) infective juveniles of *H. schachtii*. **a)** Representative pictures of seedlings at 7-days post inoculation (dpi). For data analysis, all values were normalized to the median of the measurements of the corresponding mock-inoculated plants at 7 dpi. **b)** Total root length of wildtype and mutant Arabidopsis seedlings. **c)** Primary root length of wildtype and mutant Arabidopsis seedlings. **d)** Number of secondary roots of wildtype and mutant Arabidopsis seedlings. **e)** Total secondary root length of wildtype and mutant Arabidopsis seedlings. This experiment was performed two times with similar outcomes. All data was pooled and analysed with a Pairwise Wilcoxon Rank Sum Test (n=15-20). ns= not significant, *p< 0.05.

TCP9 does not affect susceptibility of Arabidopsis to *H. schachtii*

Next, we asked if the root growth response of the *tcp9* mutants upon nematode infections was different, because of loss of susceptibility to *H. schachtii*. In other words, we reasoned that a weaker response in root system architecture of *tcp9* and *tcp9tcp20* mutants could be due to a smaller number of nematodes inside the roots, and therefore a lower level of biotic stress on the root system. However, we observed no significant differences in the number of nematodes per plant between any of the mutant lines and wildtype Arabidopsis at 4 dpi (Fig. 4a).

To assess further if TCP9 affects the development of feeding nematodes, we monitored their progression through different development stages inside plants for 28 dpi. We observed that parasitic second stage juveniles did not moult significantly faster into third stage juveniles in any of the mutants compared to wildtype Arabidopsis plants (Fig. 4b). Furthermore, as the supply of nutrients to feeding cyst nematodes can affect the differentiation of juveniles into either males or females,

we also examined if TCP9 affects the sex determination of *H. schachtii*. To this end, we counted the number of males, females, and the total number of individuals at 28 dpi. We observed no significant difference in the number of males or females in any of the mutant lines as compared to wildtype Arabidopsis (Fig. 4c-e). We therefore concluded that TCP9 does not affect normal development of *H. schachtii*.

Differences in plant susceptibility to parasitic nematodes can also appear in the size of the feeding females. To test if TCP9 indirectly regulates female growth, we measured the maximum surface area of adult females in the two-dimensional focal plane of a dissecting microscope (Fig. 4f). The surface area of adult females in none of the mutants was significantly different compared to wildtype Arabidopsis plants (Fig. 4g). Then, we asked if the size of nematode-induced syncytium could be affected by TCP9. After measuring the maximum surface area of individual syncytia of feeding adult females, we found no significant difference between the *tcp* mutants and wildtype Arabidopsis plants either (Fig. 4h). Altogether, we concluded that TCP9 does not affect susceptibility of Arabidopsis to infections by *H. schachtii* and that lower levels of biotic stress are not the cause of the altered root growth responses in nematode-infected *tcp9* mutants.

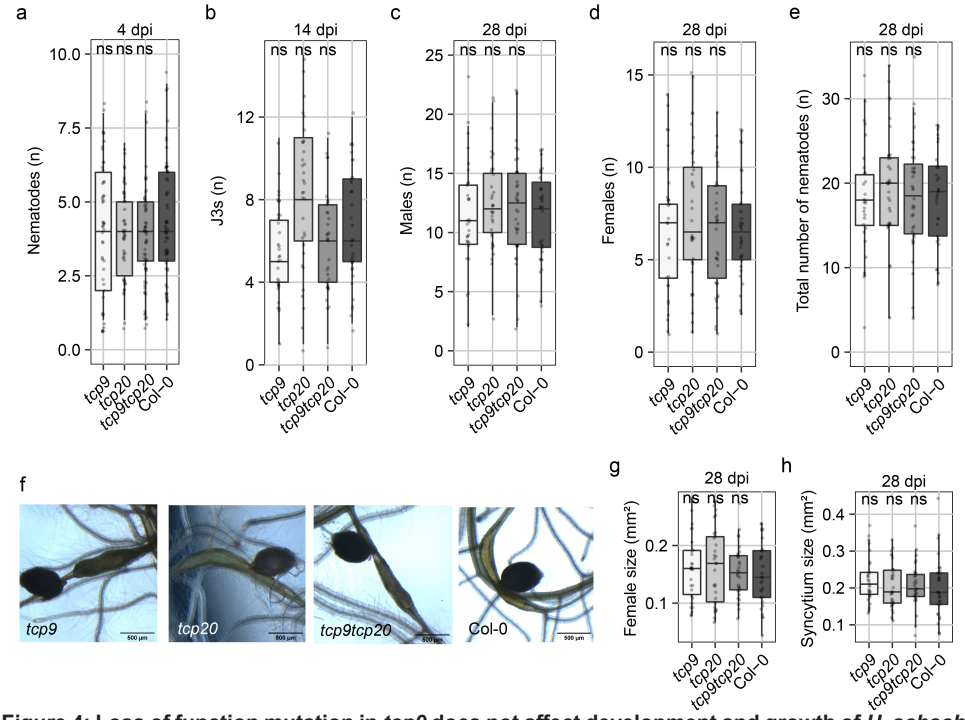

Figure 4: Loss of function mutation in *tcp9* does not affect development and growth of *H. schachtii* in Arabidopsis. a) Number of juveniles per root system on *tcp* mutants (*tcp9, tcp20, tcp9tcp20)* and wildtype Arabidopsis plants (Col-0) at 4-day post inoculation (dpi) (n=60). **b)** The number of third stage juveniles of *H. schachtii* at 14 dpi. **c)** The number of males of *H. schachtii* at 28 dpi. **d)** The number of females at 28 dpi. **e)** The total number nematodes at 28 dpi. **f)** Representative images of syncytia and adult females at 28dpi. Scale bar represents 500 µm. **g)** The maximum two-dimensional surface area of adult *H. schachtii* females in a single focal plane of the dissection microscope at 28 dpi. **h)** The maximum two-dimensional surface area of syncytia at 28 dpi. This experiment was performed three times with similar outcomes. Data was pooled and analysed with one-way ANOVA with a post hoc Tukey HSD test. ns= not significant, *p< 0.05, **p< 0.01, ***p<0.001 (n=30-36).

TCP9 regulates the expression of genes involved in ROS-related processes

TCP9 functions as a transcription factor and to understand how it modulates root growth responses, we analysed changes in the root transcriptome upon infection with *H. schachtii* in both wildtype and different mutant Arabidopsis plants. To this end, we performed a time-series experiment for which we inoculated four days old Arabidopsis seedlings of the *tcp9*, *tcp20*, and *tcp9tcp20* mutants and wildtype Arabidopsis plants with *H. schachtii* or a mock solution. Whole roots were sampled at 24, 48, and 72 hpi and subsequently subjected to RNA sequencing. A principal component analysis of the sequence data revealed that most of the overall variance in gene expression was captured by infection with *H. schachtii* (21.9%) and by time post inoculation (9.5%; Fig. 5a). The overall variance in gene expression captured by plant genotype was small. Nonetheless, to specifically map the effect of the *tcp9, tcp20* and the *tcp9tcp20* mutations on gene expression, we used a linear model including presence of infection, time after inoculation, and plant genotype as factors (Table S1 and S2). We found a relatively small number of genes in *tcp9, tcp20* and *tcp9tcp20* mutants with a significantly different expression at different timepoints post inoculation (Fig. 5b and Table S1). This showed that the mutations in *TCP9* (Fig. S3) and *TCP20* (Fig. S4) most likely have a minor impact on the root transcriptome during *H. schachtii* infection. Notably, the knock-out mutation in *TCP9*, both in *tcp9* and *tcp9tcp20*, had its biggest impact at 48 hpi. Gene Ontology (GO) term enrichment analysis of the set of differentially expressed genes in nematode-infected *tcp9*, *tcp20*, and *tcp9tcp20* mutants revealed a significant overrepresentation of reactive oxygen species (ROS)-related processes associated with absence of *TCP9* (Table S3). For instance, fourteen Arabidopsis genes annotated as being involved in oxidation-reduction process (GO:0055114) were downregulated in *tcp9* at 48 hpi (False Discovery Rate = 7.57E-05; Fig. 5d; Table S4). Likewise, four out of nine Arabidopsis genes annotated as having oxidoreductase activity (GO:0016491) were also down-regulated in *tcp9* (False Discovery Rate = 0.0046). Based on these observations, we concluded that the TCP9-modulated root growth responses during nematode infections most likely involve ROS-related processes.

TCP9 alters sensitivity of Arabidopsis to exogenous H_2O_2

To test if the TCP9-mediated root growth responses indeed involve ROS-mediated processes, we first transferred six-day old seedlings of the *tcp9*, *tcp20*, and *tcp9tcp20* mutants and wildtype Arabidopsis to liquid media containing 200 µM hydrogen peroxide (H_2O_2). Eight days after the transfer, we calculated the relative total root length of the seedlings by normalizing the data to the median of the corresponding measurement in mock-treated plants. This showed that the relative total root length of *tcp9* mutant was least affected by H_2O_2 in the media (and thus closer to 1; Fig. 6a and b). Notably, the relative total root length of the *tcp20* and *tcp9tcp20* mutants was slightly, but not significantly, less affected by hydrogen peroxide than wildtype Arabidopsis seedlings.

Root growth responses to belowground biotic stress by cyst nematodes has been shown to correlate with the aboveground plant growth (Trudgill and Cotes, 1983; Miltner et al., 1991), which could also be mediated by ROS regulation (Labudda et al., 2018). To assess if TCP9 regulates sensitivity to ROS aboveground, we sprayed nine-day old seedlings with 200 µM hydrogen peroxide. Twenty-one

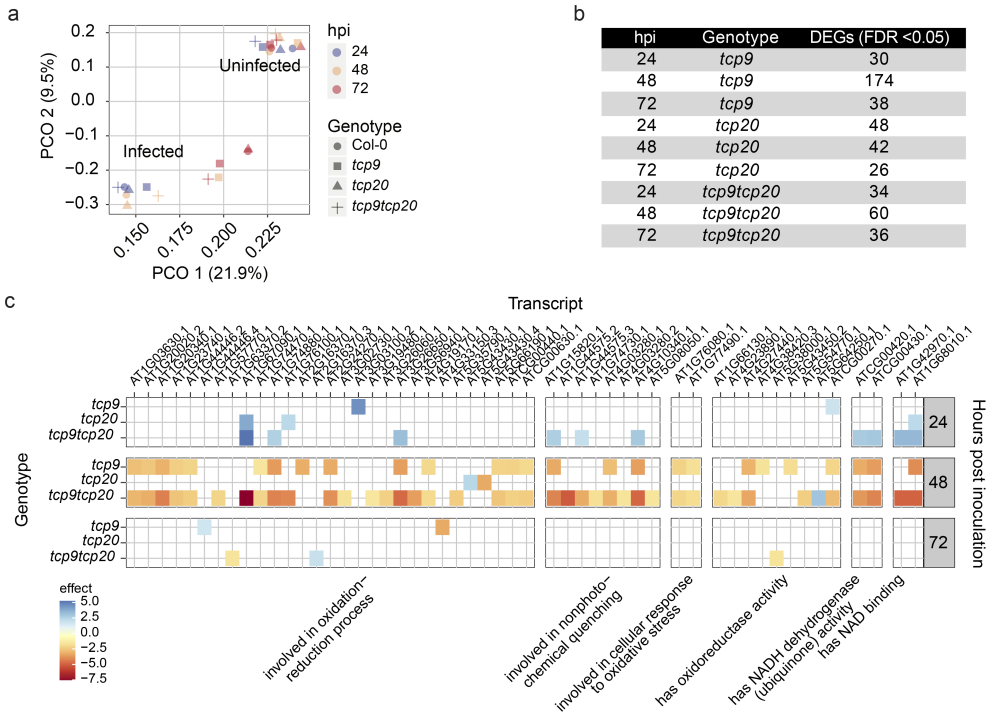

hpi	Genotype	DEGs (FDR <0.05)
24	*tcp9*	30
48	*tcp9*	174
72	*tcp9*	38
24	*tcp20*	48
48	*tcp20*	42
72	*tcp20*	26
24	*tcp9tcp20*	34
48	*tcp9tcp20*	60
72	*tcp9tcp20*	36

Figure 5: TCP9 regulates gene expression in nematode-infected roots of Arabidopsis. Four-day old Arabidopsis seedlings were inoculated with 80 juveniles of *H. schachtii* or a mock solution. At 24-, 48-, and 72-hours post inoculation (hpi) whole root samples were collected and subjected to RNA sequencing. **a)** Principal component analysis of overall variation in gene expression in wildtype Arabidopsis Col-0, and *tcp9*, *tcp20* and *tcp9tcp20* mutants at different hpi with *H. schachtii* (infected) or mock inoculation (uninfected). **b)** Number of genes that were differentially expressed (DEG) in *tcp9, tcp20,* and *tcp9tcp20* at the different hpi when compared to nematode-infected roots of wildtype Arabidopsis Col-0 (false discovery rate, FDR, correction, *q* <0.01). c**)** Subset of DEGs (from **c**) that are classified as being reactive oxygen species (ROS)-related in GO term enrichment analysis (FDR, *q* < 0.01). Colours indicate direction and size of effect of the mutations on gene expression as compared to nematode-infected wildtype Arabidopsis Col-0.

days after spraying the plants, we recorded the effect of H_2O_2 on the size of the green canopy area. This showed that the green canopy area of *tcp9* and *tcp9tcp20* mutant plants was less affected by H_2O_2 than the *tcp20* mutant and wildtype Col-0 (Fig. 6c and d). Based on these findings, we concluded that TCP9 modulates sensitivity to ROS in Arabidopsis both below and aboveground.

TCP9 affects ROS-related processes in nematode infection sites

The *tcp9* mutants might be less sensitive to hydrogen peroxide, because of enhanced ROS scavenging in this mutant. If this would hold true, we expected to find less ROS accumulation in nematode infection sites. To test this hypothesis, we inoculated *tcp9*, *tcp20*, and *tcp9tcp20* mutants and wildtype Arabidopsis seedlings with *H. schachtii* and visualized ROS accumulation in the proximity of the nematode with 3,3'-diaminobenzidine (DAB) in roots at 72 hpi (Siddique et al., 2014). In wildtype Arabidopsis plants and the *tcp20* and *tcp9tcp20* mutants, we could observe clear DAB staining in more than 80% of the infection sites (Fig. 7a and b). By contrast,

in the *tcp9* mutant, only 50% of the nematode infection sites showed DAB staining. These observations indicate that TCP9 modulates ROS homeostasis in response to nematode-infections.

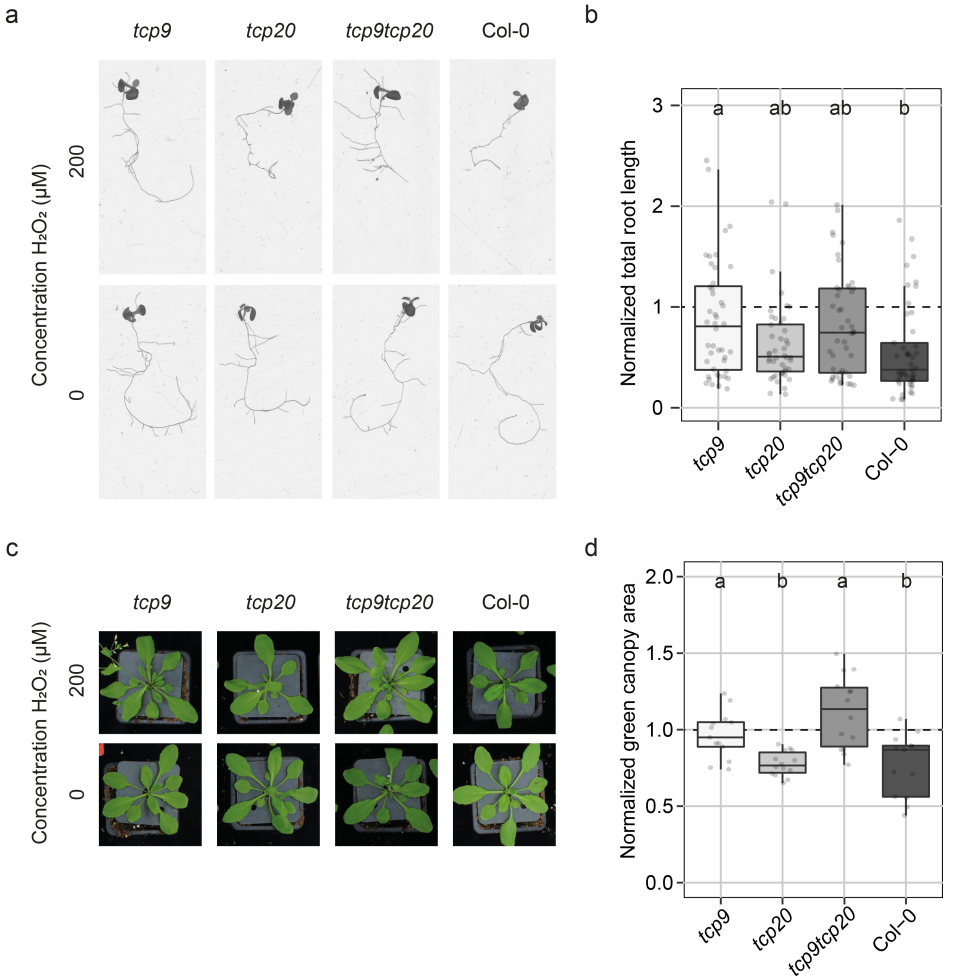

Figure 6: Root and shoot growth of *tcp9* mutant responds less to H_2O_2. a-b) Six-day old Arabidopsis (*tcp9*, *tcp20*, *tcp9tcp20* and wild-type Col-0) seedlings were transferred to liquid KNOP media containing 200 or 0 (Mock) µM H_2O_2. At eight-days post transfer the total root length was measured. **a)** Representative pictures of *tcp9, tcp20, tcp9tcp20* and wildtype Col-0 roots exposed to 0 and 200µM H_2O_2. **b)** Before analysis, the total root length of every seedling treated 200 µM H_2O_2 was normalized to the median of mock inoculated seedlings of the corresponding plant genotypes. This experiment was performed three times with similar outcomes (n=35). **c-d)** Nine-day old Arabidopsis seedlings (*tcp9, tcp20, tcp9tcp20* and wild-type Col-0) growth in pots with soil were sprayed with 200 or 0 (Mock) µM H_2O_2. At 21 days-post treatment, pictures were made of the green canopy area and the green colour was isolated from the pictures by using photoshop. **c)** Representative pictures of green canopies of plants sprayed with 200 or 0 (Mock) µM H_2O_2. **d)** Impact of 200 µM H_2O_2 on green canopy area was calculated as the green canopy area (cm^2) of H_2O_2-sprayed plants divided by the median value of mock-sprayed plants of the same genotype. This experiment was performed two times with similar outcomes (n=14-15). For both experiments, data was pooled and analysed with a one-way ANOVA with a post hoc Tukey HSD test. Letters indicate different levels of significance ($p < 0.05$).

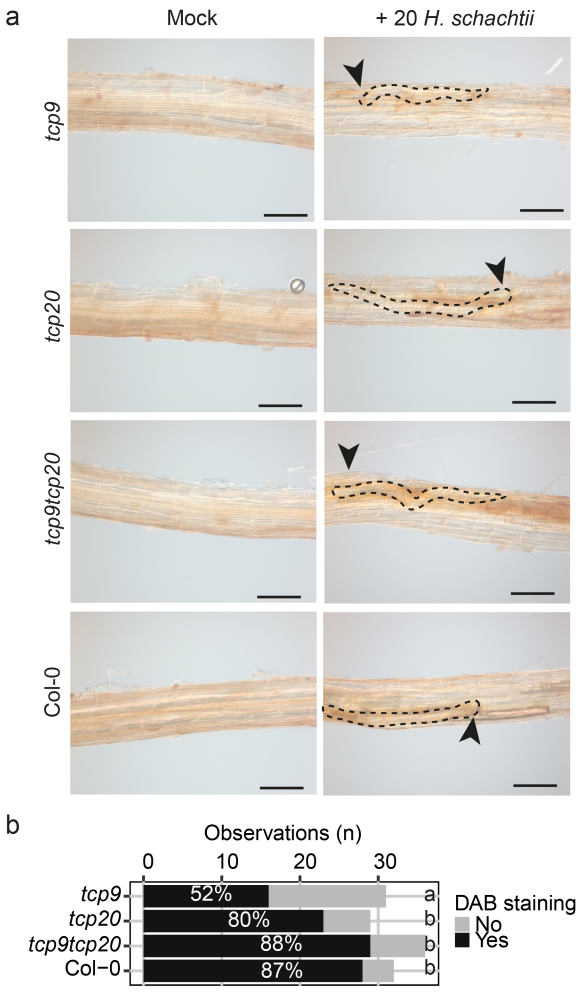

Figure 7: Significant fewer nematode infections showed DAB staining in *tcp9*. Four-day old Arabidopsis seedlings (*tcp9, tcp20, tcp9tcp20* and wild-type Col-0) were inoculated with 20 or 0 (Mock) juveniles of *H. schachtii*. At 3 days-post inoculation, the accumulation of reactive oxygen species was detected using 3,3'-diaminobenzidine (DAB). **a)** Representative pictures of root segments infected with *H. schachtii* and non-infected (Mock). Black arrowhead points at location of nematode head. Red arrowhead points at oxidized DAB staining. Scale bar = 100 µm. **b)** Absolute numbers of individual infections with or without DAB staining. This experiment was done three-times with similar outcomes. Data is pooled for statistical analysis in Fischer's exact test. Letters indicate different levels of significance ($p < 0.05$) (n=29-33).

Discussion:

Plants utilize root system architectural plasticity to cope with adverse environmental conditions in the soil. However, the molecular and genetic underpinnings of adaptive growth responses to belowground biotic stresses are not well understood. As members of the TCP transcription factor family in Arabidopsis are known to regulate root growth responses to abiotic stresses, we reasoned that they might

also play a role in root system architecture plasticity under biotic stress by root-feeding nematodes. In this study we show that the class I TCP9 transcription factor in Arabidopsis modulates adaptations in the root system architecture in response to endoparasitism by the beet cyst nematode *H. schachtii*. Our data further suggest that TCP9-modulated root plasticity in response to *H. schachtii* involves ROS-mediated processes, which remarkably do not affect the susceptibility of Arabidopsis seedlings to nematode infections. This contrasts with earlier studies showing that NAPDH oxidase-generated ROS enhances syncytium growth and nematode development in Arabidopsis infected with *H. schachtii* (Siddique et al., 2014). Our findings therefore point at a novel tolerance mechanism mitigating the impact of biotic stress rather than targeting the causal agent of this biotic stress in nematode-infected roots.

Members of the TCP family of transcription factors have been shown to regulate primary root growth and emergence of secondary roots in response to abiotic stress conditions such as high salt levels, drought, and nitrate poor substrates (Mukhopadhyay and Tyagi, 2015; Li et al., 2020; Ling et al., 2020; Liu et al., 2020). We observed that primary root growth in young Arabidopsis seedlings is significantly less inhibited by *H. schachtii* infections in the *tcp9* mutant than in wildtype Arabidopsis. In older plants and later in the infection cycle, *tcp9* reduces the impact of nematode infections on the emergence of secondary roots. It is possible that primary root growth and the emergence of secondary roots are two different outputs of the same stress mitigating process modulated by TCP9. However, these two phenomena could also be independent adaptations driven by different causes of stress on the root system. Here, it should be noted that migratory infective juveniles of *H. schachtii* induce stress by extensively damaging root tissue during host invasion at the early stages of infection, whereas later in the infection process the loss of assimilates during feeding by sedentary life stages on host cells might be the dominant cause of stress (Wyss and Grundler, 1992). It has been shown that the level and the duration of stress can determine if a condition inhibits or promotes root growth (Julkowska et al., 2014; Zhang et al., 2017). The stress levels during the brute force host invasion by cyst nematodes are probably high but last only a few hours and may induce rapid cessation of primary root growth. Here, TCP9 could modulate damage-induced stress responses during early stages of the nematode infections, which would also agree with TCP9 being up-regulated early in response to mechanical wounding (Fig. S5) (Kilian et al., 2007). By contrast, stress by nematode feeding on host cells may be milder but persist for several weeks and could induce the formation of additional secondary roots. In the latter case, TCP9 could modulate these feeding-induced stress adaptations in root system architecture to mitigate the impact of persistent biotic stress on the root system upon nematode infections.

Previously, it has been reported that TCP9 in conjunction with TCP8 is involved in host defence responses to *Pseudomonas syringae* pv. *maculicola* infections by regulating the expression of *ICS1* (Wang et al., 2015). We found that TCP9 does not affect host susceptibility to invasions by *H. schachtii,* which could otherwise alter the level of biotic stress on the root system. A weaker primary root growth inhibition could be caused by a smaller number of nematodes in the *tcp9* mutant, but we did not find fewer infections in this mutant. We therefore have no reason to assume that a lower level of biotic stress (i.e., less direct damage by invading infective juveniles) is underlying weaker primary root growth inhibition response in the *tcp9* mutant. One could also argue that TCP9 indirectly affects the root growth responses to nematode infections by modulating the re-allocation of resources from growth to defence. However, we found evidence that TCP9 is not

involved in the activation of host defences, as we observed no difference in the development and growth of nematodes and associated feeding sites between *tcp*9 mutant and wildtype Arabidopsis plants. Based on these findings, we believe to have identified a novel mechanism which mitigates the impact of biotic stress independent of susceptibility of Arabidopsis to cyst nematodes infections.

Our study provides several lines of evidence that TCP9-modulated root plasticity under biotic stress by root-feeding nematodes involves ROS-mediated regulation of plant growth. We show that TCP9 is required for transcriptional activation of enzymes involved in ROS-related processes in nematode-infected roots. We also demonstrate that the lack of TCP9 in the *tcp9* mutant makes the root and shoot system of Arabidopsis seedlings less sensitive to exogenous ROS (i.e., hydrogen peroxide). And, last, we found that TCP9 modulates the local accumulation of ROS in response to nematode infections without affecting plant susceptibility (Hewezi et al., 2010; Jin et al., 2011). Several studies have demonstrated that perturbations in local ROS-homeostasis contribute to stress-induced root growth adaptations (reviewed by (Considine and Foyer, 2021)). For instance, local ROS homeostasis plays a key role in balancing cell differentiation and elongation in root apical meristems thereby determining the rate at which roots grow (Tsukagoshi et al., 2010). ROS accumulation is shown to be required for the emergence and development of secondary roots in Arabidopsis (Orman-Ligeza et al., 2016; Huang et al., 2020). Our finding that TCP9-modulated root plasticity involves ROS-mediated processes also agrees with earlier observations on mechanisms underlying stress-induced adaptive plant growth responses by other TCPs. For instance, *PeTCP10* of *Phyllostachys edulis* is thought to increase drought tolerance in transgenic Arabidopsis via ROS-regulated root growth (Liu et al., 2020; Xu et al., 2021). McTCP1 is shown to control ROS-regulated vegetative growth of the liverwort *Marchantia polymorpha* (Busch et al., 2019). Salt stress responses mediated by *OsTCP19* in rice results in less ROS accumulation in detached leaf explants (Mukhopadhyay and Tyagi, 2015). Nevertheless, further research is needed to causally link the transcriptional regulation of ROS-related processes, ROS sensitivity, and ROS accumulation to the stress-induced growth response modulated by TCP9 in nematode-infected roots.

Our study also illustrates the complex interplay between different members of the TCP transcription factor family. Although in earlier work, TCP20 has been shown to transcriptionally regulate TCP9 during leaf development (Danisman et al., 2012), we have found no evidence that such an interaction is underlying the different phenotypes observed in our assays. We found that the *tcp20* single mutant does not phenocopy the *tcp9* mutant, and instead it behaved like wildtype Arabidopsis in our experiments. TCP20 is therefore not required for the ROS-related processes mediated by TCP9 in nematode-infected Arabidopsis roots. Nonetheless, at the transcriptome level we identified multiple genes being uniquely regulated in the *tcp9tcp20* double mutant that were not regulated in either of the single mutants. Moreover, the impact of *tcp9* on some of the ROS-related phenotypes seems to be partially mitigated in the *tcp9tcp20* double mutant (e.g., Fig. 6b), which suggests that at least some degree of interplay occurs between the networks activated by TCP9 and TCP20.

The TCP9-regulated plasticity of root system architecture points at a novel mechanism underlying tolerance to root-feeding nematodes. Infections by cyst nematodes induce alterations in root system architecture, which correlate with the level of tolerance to root-feeding nematodes (Miltner et al., 1991). However, the molecular and genetic mechanisms underlying tolerance to cyst nematode infections based on

root system architecture plasticity are not clear. An important conceptual difficulty here is the discrimination of resistance and tolerance phenotypes of nematode-infected plants. While resistance is aimed at reducing the cause of biotic stress (or stressor), tolerance concerns the mitigation of the impact of biotic stress. Our data shows that TCP9 does not affect susceptibility (and resistance) of Arabidopsis to cyst nematode infections, and therefore does not regulate the level of stress by reducing the parasite load in the plant. Instead, we show that TCP9 mitigates the impact of cyst nematode infections on primary root growth and formation of novel secondary roots. This is reminiscent to earlier observations with other TCP transcription factors contributing to tolerance to abiotic stress by regulating compensatory adaptations in root system architecture (Mukhopadhyay and Tyagi, 2015). In this context, tolerance to biotic stresses such as root-feeding nematode could be mechanistically related to tolerance to abiotic stress. The involvement of ROS-related processes in the TCP-mediated mitigation of both biotic and abiotic stresses points to this as well. Further parallels could be tested by investigating if intraspecific variation in tolerance to root-feeding nematodes correlates with variation in tolerance to abiotic stresses, such as salt and drought.

To conclude, tolerance to biotic stress, such as root-feeding by cyst nematodes, based on root system architectural plasticity is an important agronomic trait of crops as it ultimately determines damage thresholds for soilborne diseases. It has been shown that some resistant crop varieties do not tolerate low levels of nematode infections well, resulting in significantly lower damage thresholds. In contrast, more susceptible but tolerant varieties display a higher damage threshold for cyst nematodes, leading to lower yield losses despite high infection rates. Our work on the root growth responses meditated by TCP9 provides novel insights into the genetic underpinnings of tolerance to root feeding nematodes, which can provide an additional layer of protection for securing global food production besides disease resistance.

Supporting information:

Additional Supporting Information and supplementary file with code may be found in the online version of this article.

Figure S1. Effect of increasing concentrations of H2O2 on the root growth of Col-0.
Figure S2. Primary roots of *tcp20* and *tcp9tcp20* are significantly longer compared to wildtype Col-0
Figure S3. *TCP9* mutation in *tcp9* single and *tcp9tcp20* double mutant.
Figure S4. *TCP20* mutation in *tcp20* single and *tcp9tcp20* double mutant.
Figure S5. *TCP9* is up-regulated in response to wounding, oxidate stress, drought and genotoxic stress.
Table S1. Number of genes that are differentially regulated in *tcp9, tcp20* and *tcp9tcp20* compared to Col-0.
Table S2. Differentially expressed genes.
Table S3. Enrichment analysis of differentially expressed genes.
Table S4. Reactive oxygen species-related genes that are differentially expressed.

Data availability:

All relevant data can be found within the manuscript, its supporting materials and E-MTAB-11649 (https://www.ebi.ac.uk/arrayexpress/experiments/E-MTAB-11649/).

Acknowledgements:

We thank Richard Immink for sharing the *tcp9*, *tcp20* and *tcp9tcp20* Arabidopsis mutants. We thank Stefan van de Ruitenbeek for helping with depositing the RNAseq data. This work was supported by the Graduate School Experimental Plant Sciences (EPS). JJW is funded by Dutch Top Sector Horticulture & Starting Materials (TU18152). MGS was supported by NWO domain Applied and Engineering Sciences VENI grant (17282). JLLT was supported by NWO domain Applied and Engineering Sciences VENI (14250) and VIDI (18389) grants. No conflict of interest declared.

Author contributions:

GS, JJW and JB, conceived the project. JJW, JJLT, WJ, and JC designed the experiments and performed data collection. Data was analyzed and interpreted by JJW and MGS. JJW and GS wrote the article with inputs from all co-authors.

Conflict of interest:

The authors declare no conflict of interest.

References:

Baulies JL, Bresso EG, Goldy C, Palatnik JF, Schommer C (2022) Potent inhibition of TCP transcription factors by miR319 ensures proper root growth in Arabidopsis. Plant Mol Biol **108**: 93–103

Baum TJ, Wubben MJ, Hardyy KA, Su H, Rodermel SR (2000) A Screen for Arabidopsis thaliana Mutants with Altered Susceptibility to Heterodera schachtii. J Nematol **32**: 166–73

Benjamini Y, Hochberg Y (1995) Controlling the False Discovery Rate: A Practical and Powerful Approach to Multiple Testing. Journal of the Royal Statistical Society: Series B (Methodological) **57**: 289–300

Berardini TZ, Reiser L, Li D, Mezheritsky Y, Muller R, Strait E, Huala E (2015) The arabidopsis information resource: Making and mining the "gold standard" annotated reference plant genome. genesis **53**: 474–485

Buels R, Yao E, Diesh CM, Hayes RD, Munoz-Torres M, Helt G, Goodstein DM, Elsik CG, Lewis SE, Stein L, et al (2016) JBrowse: A dynamic web platform for genome visualization and analysis. Genome Biol **17**: 1–12

Busch A, Deckena M, Almeida-Trapp M, Kopischke S, Kock C, Schüssler E, Tsiantis M, Mithöfer A, Zachgo S (2019) Mp TCP 1 controls cell proliferation and redox processes in Marchantia polymorpha. New Phytologist **224**: 1627–1641

Considine MJ, Foyer CH (2021) Stress effects on the reactive oxygen species-dependent regulation of plant growth and development. J Exp Bot **72**: 5795–5806

Cubas P, Lauter N, Doebley J, Coen E (1999) The TCP domain: a motif found in proteins regulating plant growth and development. The Plant Journal **18**: 215–

222
Danisman S (2016) TCP Transcription Factors at the Interface between Environmental Challenges and the Plant's Growth Responses. Front Plant Sci **7**: 1–13
Danisman S, van der Wal F, Dhondt S, Waites R, de Folter S, Bimbo A, van Dijk AD, Muino JM, Cutri L, Dornelas MC, et al (2012) Arabidopsis Class I and Class II TCP Transcription Factors Regulate Jasmonic Acid Metabolism and Leaf Development Antagonistically. Plant Physiol **159**: 1511–1523
Diaz-Granados A, Sterken MG, Persoon J, Overmars H, Pokhare SS, Mazur MJ, Martin-Ramirez S, Holterman M, Martin EC, Pomp R, et al (2019) SlZ1 is a nuclear host target of the nematode effector GpRbp1 from Globodera pallida that acts as a negative regulator of basal plant defense to cyst nematodes. bioRxiv 725697
Fang Y, Zheng Y, Lu W, Li J, Duan Y, Zhang S, Wang Y (2021) Roles of miR319-regulated TCPs in plant development and response to abiotic stress. Crop Journal **9**: 17–28
Goverse A, Overmars H, Engelbertink J, Schots A, Bakker J, Helder J (2000) Both Induction and Morphogenesis of Cyst Nematode Feeding Cells Are Mediated by Auxin. Molecular Plant-Microbe Interactions® **13**: 1121–1129
Guan P, Wang R, Nacry P, Breton G, Kay SA, Pruneda-Paz JL, Davani A, Crawford NM (2014) Nitrate foraging by Arabidopsis roots is mediated by the transcription factor TCP20 through the systemic signaling pathway. Proceedings of the National Academy of Sciences **111**: 15267–15272
Hadley Wickham (2009) ggplot2: Elegant Graphics for Data Analysis. Springer US, New York
Hewezi T, Howe PJ, Maier TR, Hussey RS, Mitchum MG, Davis EL, Baum TJ (2010) Arabidopsis spermidine synthase is targeted by an effector protein of the cyst nematode Heterodera schachtii. Plant Physiol **152**: 968–984
Huang A, Wang Y, Liu Y, Wang G, She X (2020) Reactive oxygen species regulate auxin levels to mediate adventitious root induction in Arabidopsis hypocotyl cuttings. J Integr Plant Biol **62**: 912–926
Hur YS, Kim J, Kim S, Son O, Kim WY, Kim GT, Ohme-Takagi M, Cheon CI (2019) Identification of TCP13 as an upstream regulator of ATHB12 during leaf development. Genes (Basel). doi: 10.3390/genes10090644
Jin J, Hewezi T, Baum TJ (2011) Arabidopsis peroxidase AtPRX53 influences cell elongation and susceptibility to heterodera schachtii. Plant Signal Behav **6**: 1778–1786
Jones JT, Haegeman A, Danchin EGJ, Gaur HS, Helder J, Jones MGK, Kikuchi T, Manzanilla-López R, Palomares-Rius JE, Wesemael WML, et al (2013) Top 10 plant-parasitic nematodes in molecular plant pathology. Mol Plant Pathol **14**: 946–961
Julkowska MM, Hoefsloot HCJ, Mol S, Feron R, de Boer G-J, Haring MA, Testerink C (2014) Capturing Arabidopsis Root Architecture Dynamics with ROOT-FIT Reveals Diversity in Responses to Salinity. Plant Physiol **166**: 1387–1402
Karlova R, Boer D, Hayes S, Testerink C (2021) Root plasticity under abiotic stress. Plant Physiol **187**: 1057–1070
Kilian J, Whitehead D, Horak J, Wanke D, Weinl S, Batistic O, D'Angelo C, Bornberg-Bauer E, Kudla J, Harter K (2007) The AtGenExpress global stress expression data set: protocols, evaluation and model data analysis of UV-B light, drought and cold stress responses. The Plant Journal **50**: 347–363
Kim D, Langmead B, Salzberg SL (2015) HISAT: a fast spliced aligner with low memory requirements. Nat Methods **12**: 357–360
Koevoets IT, Venema JH, Elzenga JTM, Testerink C (2016) Roots withstanding their environment: Exploiting root system architecture responses to abiotic stress to improve crop tolerance. Front Plant Sci **7**: 1–19

Kosugi S, Ohashi Y (2002) DNA binding and dimerization specificity and potential targets for the TCP protein family. The Plant Journal **30**: 337–348

Kubota A, Ito S, Shim JS, Johnson RS, Song YH, Breton G, Goralogia GS, Kwon MS, Laboy Cintrón D, Koyama T, et al (2017) TCP4-dependent induction of CONSTANS transcription requires GIGANTEA in photoperiodic flowering in Arabidopsis. PLoS Genet **13**: e1006856

Labudda M, Różańska E, Czarnocka W, Sobczak M, Dzik JM (2018) Systemic changes in photosynthesis and reactive oxygen species homeostasis in shoots of Arabidopsis thaliana infected with the beet cyst nematode Heterodera schachtii. Mol Plant Pathol **19**: 1690–1704

Lee C, Chronis D, Kenning C, Peret B, Hewezi T, Davis EL, Baum TJ, Hussey R, Bennett M, Mitchum MG (2011) The Novel Cyst Nematode Effector Protein 19C07 Interacts with the Arabidopsis Auxin Influx Transporter LAX3 to Control Feeding Site Development. Plant Physiol **155**: 866–880

Li H, Yuan H, Liu F, Luan J, Yang Y, Ren L, An L, Jiang J (2020) BpTCP7 gene from Betula platyphylla regulates tolerance to salt and drought stress through multiple hormone pathways. Plant Cell, Tissue and Organ Culture (PCTOC) **141**: 17–30

Li S (2015) The Arabidopsis thaliana TCP transcription factors: A broadening horizon beyond development. Plant Signal Behav **10**: e1044192

Ling L, Zhang W, An Y, Du B, Wang D, Guo C (2020) Genome-wide analysis of the TCP transcription factor genes in five legume genomes and their response to salt and drought stresses. Funct Integr Genomics **20**: 537–550

Liu H, Gao Y, Wu M, Shi Y, Wang H, Wu L, Xiang Y (2020) TCP10, a TCP transcription factor in moso bamboo (Phyllostachys edulis), confers drought tolerance to transgenic plants. Environ Exp Bot 104002

Lucero LE, Manavella PA, Gras DE, Ariel FD, Gonzalez DH (2017) Class I and Class II TCP Transcription Factors Modulate SOC1-Dependent Flowering at Multiple Levels. Mol Plant **10**: 1571–1574

Miltner ED, Karnok KJ, Hussey RS (1991) Root Response of Tolerant and Intolerant Soybean Cultivars to Soybean Cyst Nematode. Agron J **83**: 571–576

Mukhopadhyay P, Tyagi AK (2015) OsTCP19 influences developmental and abiotic stress signaling by modulatingABI4-mediated pathways. Sci Rep **5**: 9998

Orman-Ligeza B, Parizot B, de Rycke R, Fernandez A, Himschoot E, Van Breusegem F, Bennett MJ, Périlleux C, Beeckman T, Draye X (2016) RBOH-mediated ROS production facilitates lateral root emergence in Arabidopsis. Development **143**: 3328–3339

Pertea M, Kim D, Pertea GM, Leek JT, Salzberg SL (2016) Transcript-level expression analysis of RNA-seq experiments with HISAT, StringTie and Ballgown. Nat Protoc **11**: 1650–1667

R Core Team (2019) R: A language and environment for statistical computing. R Foundation for Statistical Computing, Vienna, Austria

Rehman S, Butterbach P, Popeijus H, Overmars H, Davis EL, Jones JT, Goverse A, Bakker J, Smant G (2009) Identification and Characterization of the Most Abundant Cellulases in Stylet Secretions from Globodera rostochiensis. Phytopathology **99**: 194–202

Sewelam N, Kazan K, Thomas-Hall SR, Kidd BN, Manners JM, Schenk PM (2013) Ethylene Response Factor 6 Is a Regulator of Reactive Oxygen Species Signaling in Arabidopsis. PLoS One. doi: 10.1371/journal.pone.0070289

Siddique S, Matera C, Radakovic ZS, Shamim Hasan M, Gutbrod P, Rozanska E, Sobczak M, Torres MA, Grundler FMW (2014) Parasitic Worms Stimulate Host NADPH Oxidases to Produce Reactive Oxygen Species That Limit Plant Cell Death and Promote Infection. Sci Signal **7**: 1–11

Sijmons PC, Grundler FMW, Mende N, Burrows PR, Wyss U (1991) Arabidopsis thaliana as a new model host for plant-parasitic nematodes. The Plant Journal

1: 245–254

Trudgill DL, Cotes LM (1983) Tolerance of potato to potato cyst nematodes (Globodera rostochiensis and G. pallida) in relation to the growth and efficiency of the root system. Annals of Applied Biology **102**: 385–397

Tsukagoshi H, Busch W, Benfey PN (2010) Transcriptional Regulation of ROS Controls Transition from Proliferation to Differentiation in the Root. Cell **143**: 606–616

Urano K, Maruyama K, Koyama T, Gonzalez N, Inzé D, Yamaguchi-Shinozaki K, Shinozaki K (2022) CIN-like TCP13 is essential for plant growth regulation under dehydration stress. Plant Mol Biol **108**: 257–275

Viola IL, Uberti Manassero NG, Ripoll R, Gonzalez DH (2011) The Arabidopsis class I TCP transcription factor AtTCP11 is a developmental regulator with distinct DNA-binding properties due to the presence of a threonine residue at position 15 of the TCP domain. Biochemical Journal **435**: 143–155

Waese J, Fan J, Pasha A, Yu H, Fucile G, Shi R, Cumming M, Kelley LA, Sternberg MJ, Krishnakumar V, et al (2017) ePlant: Visualizing and Exploring Multiple Levels of Data for Hypothesis Generation in Plant Biology. Plant Cell **29**: 1806–1821

Wang X, Gao J, Zhu Z, Dong X, Wang X, Ren G, Zhou X, Kuai B (2015) TCP transcription factors are critical for the coordinated regulation of ISOCHORISMATE SYNTHASE 1 expression in Arabidopsis thaliana. The Plant Journal **82**: 151–162

Wang Y, Yu Y, Wang J, Chen Q, Ni Z (2020) Heterologous overexpression of the GbTCP5 gene increased root hair length, root hair and stem trichome density, and lignin content in transgenic Arabidopsis. Gene **758**: 144954

Wickham, H. F., R.; Henry, L; Müller K (2018a) tidyr: Easily Tidy Data with 'spread()' and 'gather()' Functions, pp.

Wickham, H. F., R.; Henry, L; Müller K (2018b) dplyr: A Grammar of Data Manipulation.

Wyss U, Grundler FMW (1992) Feeding behavior of sedentary plant parasitic nematodes. Netherlands Journal of Plant Pathology **98**: 165–173

Xu Y, Liu H, Gao Y, Xiong R, Wu M, Zhang K, Xiang Y (2021) The TCP transcription factor PeTCP10 modulates salt tolerance in transgenic Arabidopsis. Plant Cell Rep **40**: 1971–1987

Zhang Q, Huber H, Beljaars SJM, Birnbaum D, de Best S, de Kroon H, Visser EJW (2017) Benefits of flooding-induced aquatic adventitious roots depend on the duration of submergence: linking plant performance to root functioning. Ann Bot **120**: 171–180

Zhou M, Li D, Li Z, Hu Q, Yang C, Zhu L, Luo H (2013) Constitutive Expression of a miR319 Gene Alters Plant Development and Enhances Salt and Drought Tolerance in Transgenic Creeping Bentgrass. Plant Physiol **161**: 1375–1391

Supporting information:

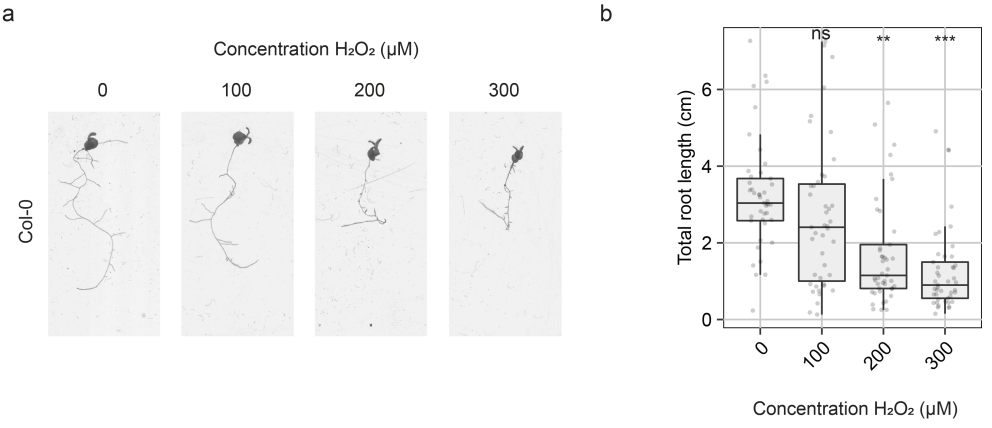

Figure S1: Effect of increasing concentrations of H_2O_2 on the root growth of Col-0. Six-day old Arabidopsis (*tcp9*, *tcp20*, *tcp9tcp20* and wild-type Col-0) seedlings were transferred to liquid KNOP media containing 0-300µM H_2O_2. At eight-days post transfer the total root length was measured. **a)** Representative pictures of wildtype Col-0 roots exposed to 0-300µM H_2O_2. **b)** The root architecture of wildtype Col-0 seedlings was quantified by total root length (cm). Data was analysed with a one-way ANOVA with a post hoc Tukey HSD test. ns= not significant, *p< 0.05, **p< 0.01, ***p<0.001 (n=35). Letters indicate different levels of significance (p< 0.05).

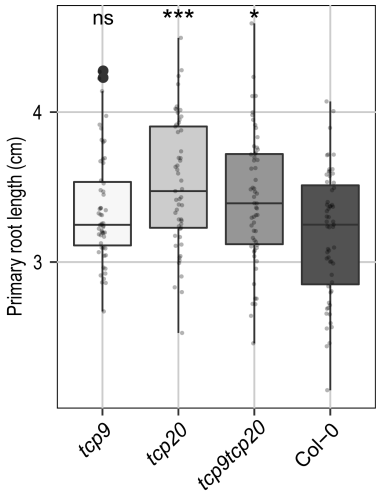

Figure S2: Primary roots of *tcp20* and *tcp9tcp20* are significantly longer compared to wildtype Col-0. Primary root length (cm) of wildtype and mutant Arabidopsis seedlings at eight days post germination. Data was analysed with a one-way ANOVA with a post hoc Tukey HSD test (n=60). ns= not significant, *p< 0.05, **p< 0.01, ***p<0.001. This experiment was performed three times with similar outcomes and pooled for data analysis.

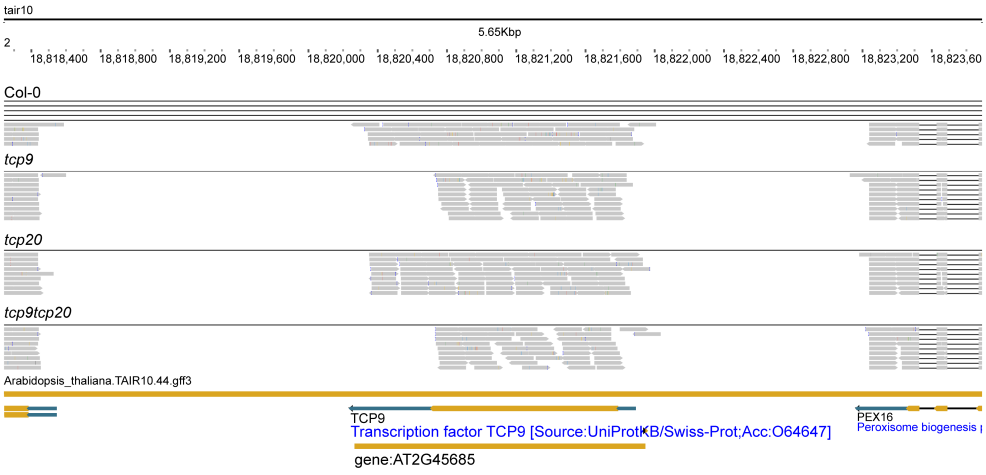

Figure S3: *TCP9* mutation in *tcp9* single and *tcp9tcp20* double mutant. RNAseq reads were mapped to the TAIR10 Arabidopsis genome. Normal length of *TCP9* transcript indicated in yellow.

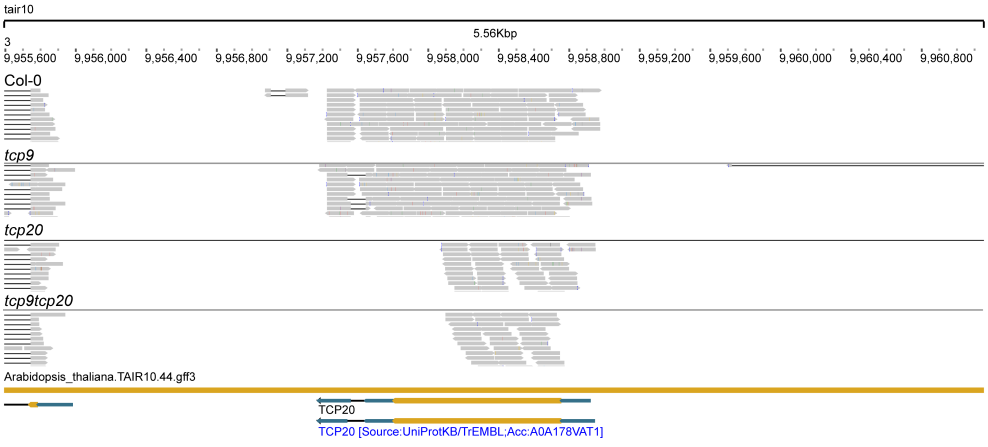

Figure S4: *TCP20* mutation in *tcp20* single and *tcp9tcp20* double mutant. RNAseq reads were mapped to the TAIR10 Arabidopsis genome. Normal length of *TCP20* transcript indicated in yellow and blue.

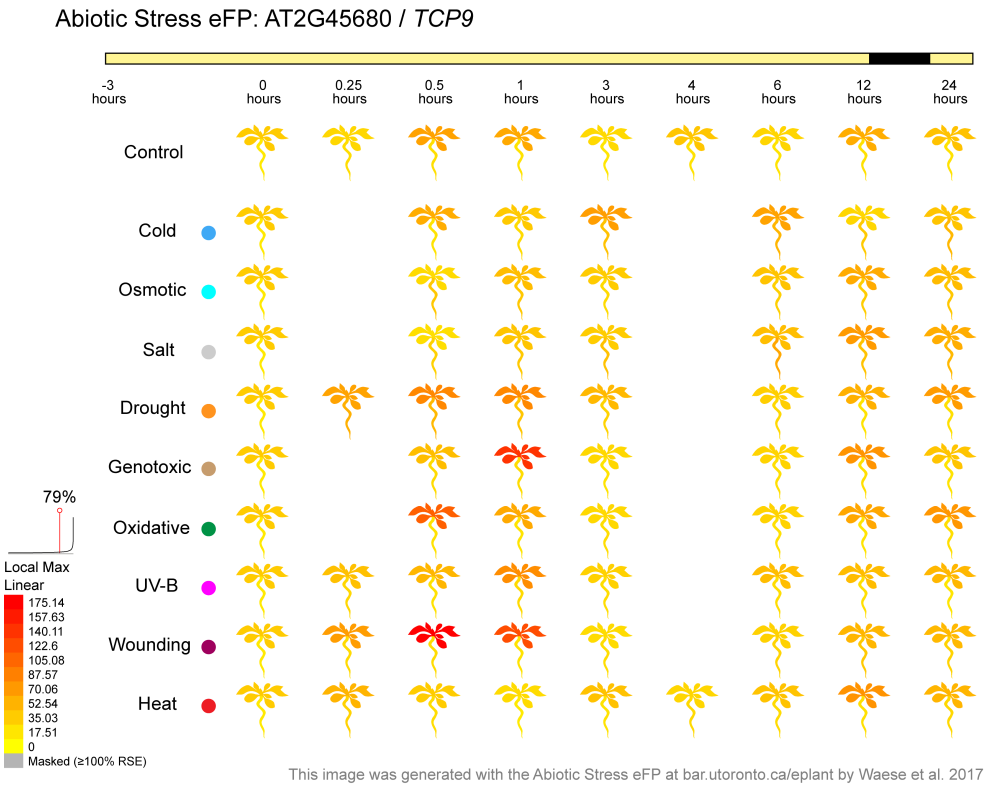

Figure S5: *TCP9* is up-regulated in response to wounding, oxidate stress, drought and genotoxic stress. Figure and data was retrieved from http://bar.utoronto.ca/eplant/ and (Kilian et al., 2007) respectively. Image was generated by (Waese et al., 2017).

Table S1: Number of genes that are differentially regulated in *tcp9, tcp20* and *tcp9tcp20* compared to Col-0.

Timepoint (hpi)	Genotype	Infected	FDR (Infected)	Uninfected	FDR (Uninfected)
24	*tcp9*	30	0.1022	103	0.0346
48	*tcp9*	174	0.0282	21	0.1560
72	*tcp9*	38	0.0519	61	0.0509
24	*tcp20*	48	0.0643	32	0.0821
48	*tcp20*	42	0.0601	27	0.0986
72	*tcp20*	26	0.0696	35	0.0882
24	*tcp9tcp20*	97	0.0410	34	0.0977
48	*tcp9tcp20*	244	0.0218	60	0.0640
72	*tcp9tcp20*	31	0.0875	36	0.0676

Chapter 7

General discussion

The revival of tolerance

Plant-parasitic nematodes inflict substantial damage on the roots of host plants, leading to reduced plant growth and more than 10% yield losses every year (Jones et al., 2013; Bebber et al., 2014; Savary et al., 2019; Sikora et al., 2023). Plants displaying less symptoms of disease than others when growing under similar infection pressure of nematodes are categorized as being more tolerant to nematode damage (Miltner et al., 1991; Potter and Dale, 1994). Studying tolerance to cyst nematode infections was in vogue in the 1970s and 1980s (Evans and Haydock, 1990). At that time, tolerance was recognized as an agronomically important trait complementing other nematode management strategies (e.g., chemical control). However, with the market release of crop cultivars harbouring highly effective nematode resistances in the 1990s, the attention of plant scientists and breeders to tolerance began to fade and as a research topic it gradually receded to the background ((Williamson and Hussey, 1996; Fuller et al., 2008); Fig. 1). Moreover, this change in research focus was also driven by challenges associated with experimentally quantifying tolerance. Robustly phenotyping tolerance to nematodes is a difficult but necessary task to resolve its complex genetic architecture. As a result, the genetic and molecular mechanisms underlying tolerance to nematodes largely remained elusive for the past thirty years. However, tolerance may undergo a revival as a desirable feature in resilient plant production systems for two reasons. First, the wide use of only few major nematode resistance genes resulted in genetic selection of virulence in nematode populations (Tzortzakakis et al., 2016), rendering these resistances less reliable at an increasing number of places. Second, new pesticide legislations banning most major nematicides further limit the options for control of nematode infestations, because chemical control becomes less as a fallback strategy (Fuller et al., 2007; Molendijk and de Jongh, 2018).

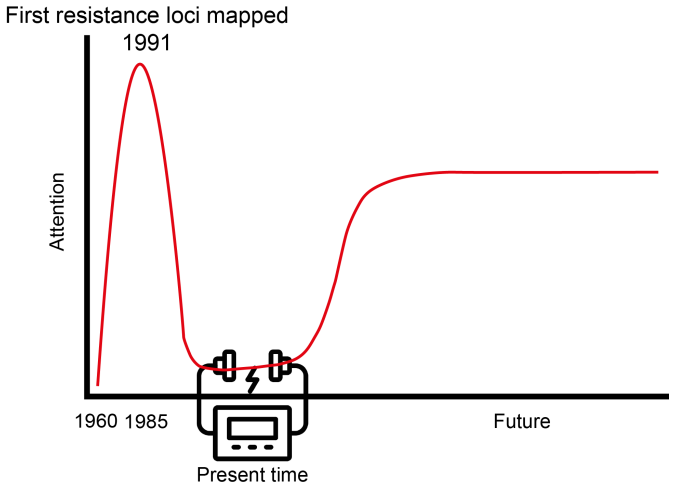

Figure 1: Societal interest for plant tolerance to nematodes described using the Gartner hype cycle. The Gartner hype cycle illustrates the amount of attention, maturity, adoption, and social application of technologies. The amount of attention is defined by the number of publications in which nematode tolerance is studied. The defibrillator illustrates the revival of tolerance (Adopted from Dedehayir & Steinert, 2016 and Evans & Haydock, 1990).

This thesis addresses several important knowledge gaps associated with plant tolerance to belowground biotic stress. More specifically, it aims to unravel the genetic and molecular mechanisms underlying tolerance to plant-parasitic nematodes in plants. The overarching hypothesis giving direction to my research entails that phenotypic plasticity in root system architecture modulates plant tolerance to biotic stress by root-feeding nematodes. Here, tolerance is defined as the ability to mitigate the impact of biotic stress on the whole plant. Thus, belowground biotic stress impacts aboveground plant development and growth, and vice versa. Tolerance levels can, therefore, be derived from local and systemic plant responses to stress. At the start of the research described in this thesis, a method to robustly monitor the impact of belowground biotic stress over time in a non-invasive manner was not available. In **Chapter 2**, we describe the development of a high-throughput phenotyping platform to quantify aboveground growth responses of *Arabidopsis thaliana* to cyst nematode infections. Developing such a platform was important to determine if Arabidopsis harbours significant quantitative variation in responses to biotic stress independent of susceptibility to cyst nematodes. In other words, we asked if the genetic architectures underlying disease tolerance and susceptibility to cyst nematodes in Arabidopsis are at least partly distinct. In **Chapter 3**, we addressed this question by genome-wide association mapping of quantitative variation in green canopy area of more than 150 ecotypes of Arabidopsis inoculated with different densities of the beet cyst nematode *Heterodera schachtii*. In addition to this explorative genome-wide approach, we also formulated specific research hypotheses based on recent literature on plant transcription factors modulating the plasticity of root system architecture in response to tissue damage and other types of abiotic stresses. In **Chapters 4** and **5**, we focused on damage-induced activation of the plant transcription factors ERF109 and WOX11 and how this contributes to tolerance of Arabidopsis to cyst nematode infections. Finally, in **Chapter 6**, we zoomed in on the TCP transcription factor family, the members of which are known to modulate root growth adaptations in response to abiotic stress (e.g., drought, salinity, and nutrient depletion). In this chapter, I will synthesize and further discuss the primary findings of my thesis to offer a groundwork for guiding future research and advancing our comprehension of tolerance to root-parasitic nematodes.

Shifting perspectives: from nematode to plant fitness

Much of the current research on nematode-plant interactions is focussing on plant factors contributing to nematode reproduction and fitness (i.e., number of penetrations, number of galls, cysts, nematode fecundity) (Lozano-Torres et al., 2014; Siddique et al., 2014; Shah et al., 2017; Anwer et al., 2018; Warmerdam et al., 2018). Indeed, for farmers, it is important to manage nematode infestations in arable crops to limit yield losses. The most cost-effective means of nematode control involves the usage of nematode-resistant cultivars, with nematode resistance measured as the relative reproduction of an inoculum on a resistant cultivar compared to a fully susceptible cultivar. However, nematode resistance is only available in a few crops and for a limited number of nematode species, or even pathotypes within a species (van der Voort et al., 1998; Rouppe van der Voort et al., 2000; Paal et al., 2004; Castagnone-Sereno et al., 2007). Furthermore, the use of resistant cultivars does not guarantee high yields, as lowly infected but intolerant plant varieties may still display a significant yield loss (Trudgill and Cotes, 1983).

For decades, nematode infestations were also chemically controlled with periodic applications of non-selective nematicides (e.g., fumigants). While these applications were specifically aimed at a few dominant nematode species in a certain area, the non-selective nature of the nematicidal compounds affected all soil-inhabiting nematodes. This meant that chemical control kept populations of many plant-parasitic nematode species below the radar (i.e., below damage thresholds). In 2005, non-selective nematicides were banned in the EU for their environmental toxicity (The European Commission, 2023). Since then, arable crops are increasingly exposed to a much wider diversity of plant-parasitic nematodes. This diversity in plant-parasitic nematodes is too large to be addressed by resistance breeding alone and may lead to more yield loss for farmers. Arable farming may thus benefit from a stronger focus on preserving yield in the presence of diverse plant-parasitic nematodes. In the end, getting a profitable yield on nematode-infested fields is more important for farmers than eradicating plant-parasitic nematode populations. However, preserving yield demands a shift of perspectives in research on nematode-plant interactions from primarily focusing on nematode fitness (i.e., resistance) toward plant fitness (i.e., tolerance).

Taking up the challenge: robustly phenotyping tolerance to belowground biotic stress

Robustly phenotyping stress tolerance in plants is difficult, because it is a complex trait involving multiple interacting physiological and developmental processes (e.g., root architecture plasticity, resource allocation, tissue regeneration, and delayed senescence). Quantifying the impact of belowground biotic stress in plants is even more difficult because it is unclear how aboveground plant features reflect belowground plant adaptations. In other words, which morphological or physiological plant parameters can be monitored over time as a valid and reliable proxy for the impact of biotic stress on roots remains challenging. At the start of this thesis research, little was known about the correlations between above- and belowground plant responses to nematode infections. In **Chapter 2**, we addressed this knowledge gap by monitoring morphological adaptations in shoots and roots at different inoculation densities of the beet cyst nematode *Heterodera schachtii* on Arabidopsis *in vitro* and in soil (**Chapter 2**, **Fig. 1**). We found that primary root length, number of flowers and basal stems, and green canopy area of Arabidopsis responded in a density-dependent manner to *H. schachtii* infections. As quantifying the number of flowers is more difficult to automate and as assessing root architecture components would require a more artificial experimental setup, we choose the green canopy area as a proxy to monitor the impact of biotic stress by nematodes in the roots. Importantly, adaptations in green canopy area under nematode-induced stress correlated well with several root architecture components (i.e., primary root length, total secondary root length, and number of secondary roots). Moreover, the green canopy area (i.e., delayed closure of crop canopy) is also used by farmers as an indicator of tolerance to nematode infections in the field.

Next, we constructed a high-throughput phenotyping platform to monitor green canopy area growth under the biotic stress induced by nematode infection over time. Previous studies mostly focused on single endpoint measurements (e.g., yield) to genetically map tolerance traits (Ravelombola et al., 2019; Ravelombola et al., 2020). While endpoint measurements reflect the outcome of interacting plant

processes underlying tolerance, we aimed to understand how different physiological processes contribute to tolerance by operating at different timepoints post inoculation. Hereto, we use a highly controlled climate room mounted with RGB cameras to simultaneously capture growth responses of 960 Arabidopsis plants challenged with *H. schachtii* at different inoculation densities for three weeks (**Chapter 2**, **Figure 2**). We chose RGB cameras over more advanced camera systems (i.e., hyperspectral camera) due to their cost-effectiveness, and simplicity and ease of use. Taking photographs at one-hour intervals for 21 days in each experiment resulted in 302,400 pictures of individual Arabidopsis plants. This allowed us to compare both the responses of different plant genotypes to nematode infections by time point, and also - after differentiating the measurements by time - changes in response rates.

The reason for building our phenotyping platform inside a climate room was that environmental conditions can strongly influence disease tolerance (Wilhelm et al., 1985; Fatemy and Evans, 1986). Even minor changes in growth conditions between experiments might result in large batch effects and thus loss of resolution when genetically mapping tolerance traits. We considered greenhouse conditions to be too variable (e.g., temperature, humidity, excessive radiation). Likewise, nematode bioassays on plants are also very sensitive to variations in soil moisture levels within and between experiments. To minimize this source of variation in the data, we placed the Arabidopsis plants on a flooding table to achieve uniform soil moisture levels.

Finally, our overarching hypothesis was that phenotypic plasticity in root system architecture forms the key to tolerance to biotic stress by root-feeding nematodes. However, the composition of the root system of Arabidopsis also varies by growth substrate. For instance, *in vitro* cultured plants form different roots than plants in soil (i.e., number of secondary roots, and root shape) (Kerstens et al., 2021). Initially, we tested soils with different compositions (i.e., organic matter, texture, and particle size). Silversand was most compatible with the flooding system and with the extraction of cysts after experimental completion. Furthermore, most plant parasitic nematodes thrive in 'light soils', such as silversand, making the phenotyping platform also suitable for experiments with other nematode species.

A modelling problem

The Seinhorst Yield Loss Model (SYLM) describes the yield of a crop as a function of the initial population density of a plant parasitic nematode species (Seinhorst, 1986). The SYLM assumes that crop yield declines by increasing initial population density following an inverse sigmoid curve. It is used to determine the tolerance limit of crops for plant-parasitic nematode infections (Seinhorst, 1986; Norshie et al., 2011; Sasanelli et al., 2013; Been et al., 2015; Moosavi, 2015). It can also be used to model minimum yield at the highest possible population density as a measure of plant tolerance. However, we experienced significant limitations of the SYLM in our data analyses. First, it is designed to handle endpoint data (i.e., predict yield) at the end of a growth season. We monitored plant performance for 21 days after inoculation, generating a far richer dataset than can be handled by the SYLM. Second, the SYLM underestimates the tolerance limit of Arabidopsis for *H. schachtii* and *Meloidogyne incognita* infections. The decline in the green canopy area of Arabidopsis by increasing initial densities of nematodes fitted the SYLM overall quite well (R^2 = 0.83 and 0.78 for *H. schachtii* and *M. incognita*, respectively). However, at low inoculation densities

of *H. schachtii* and *M. incognita*, seedlings of Arabidopsis may perform better than mock-inoculated plants at 21 days after inoculation (**Chapter 2**, **Fig. 2** and **S7**). This phenomenon is described in the literature as overcompensation (reviewed in Agathokleous et al., 2019). The SYLM cannot handle overcompensation and places the tolerance limit in any case at the first observable difference compared to mock-inoculated plants (Fig. 2).

To overcome these limitations, we developed an alternative model that makes use of the green canopy area data collected at all time points and which incorporates overcompensation effects when they occur (**Chapter 2**, **Fig. 5**). This alternative model makes use of a logistic function to determine the maximum projected green canopy area (*K*) and the intrinsic growth (*r*) (i.e., maximum achieved growth rate). Hereto, the data was fitted to a Gaussian curve (*K*) and a hyperbolic curve (*r*). The Gaussian curve reflects the damage-response curve while the hyperbolic curve reflects the maximum growth rate of a plant, irrespective of time. Instead of determining at which initial nematode density (P_i) the first observable difference occurs (i.e., larger or smaller than on the mock-inoculated plant), our model determines the P_i at which the fitted curve descends below the mock baseline (Fig. 2). In **Chapters 3** and **5**, we used our alternative model to determine the tolerance limit of twelve Arabidopsis ecotypes and the transcriptional repressor mutant *35S:WOX11-SRDX* for *H. schachtii* infections. However, like for the SYLM, in our alternative model a nematode density high enough for a plant to reach its minimal yield is needed to get an appropriate goodness of fit. Although, we exposed *35S:WOX11-SRDX* mutant plants to P_i of 0 to 10 juveniles per gram soil, which is significantly less compared to other experiments in which we exposed plants to P_i 0 to 50 or 100 juveniles per gram soil, we were still able to model the tolerance limit.

Disentangling complexities: the genetic architectures of tolerance and susceptibility to *H. schachtii* in Arabidopsis

The purpose of robustly phenotyping aboveground plant growth responses to nematode infections and using different data models to derive quantitative parameters reflecting tolerance traits was to resolve the underlying genetic architecture of tolerance. In **Chapter 3**, we described the genetic mapping of different tolerance traits of Arabidopsis infected with *H. schachtii* using a genome wide association (GWA) approach. Before starting the multiyear experiment, we investigated the presence of quantitative variation in tolerance limits of a small panel of twelve ecotypes of Arabidopsis, in which we identified tolerance limits from 0.43 to 9.73 using our alternative model (**Chapter 3, Table 1**). Based on these results, we designed our experiment to unravel the genetic architecture of tolerance. First, we exposed 154 ecotypes of Arabidopsis challenged with different inoculation densities of *H. schachtii* for a period of 21 days to assess if there is quantitative variation in growth responses. Our phenotyping platform can accommodate 960 plants, therefore we optimized the number ecotypes (i.e., 50), inoculation densities (i.e., 6; P_i 0 – 7.5), and biological replicates per density (i.e., max 3). In total, we performed five independent experiments over a period of almost three years using our phenotyping platform. As mentioned above, without nematode densities high enough for a plant to reach their minimal yield it is a challenge to get an appropriate goodness of fit. Therefore, instead, we calculated the regression coefficients of the plant response by increasing density ranges (i.e., P_i 0 - 2.5, 0 - 5.0, and 0 - 7.5) to identify which ecotypes are more

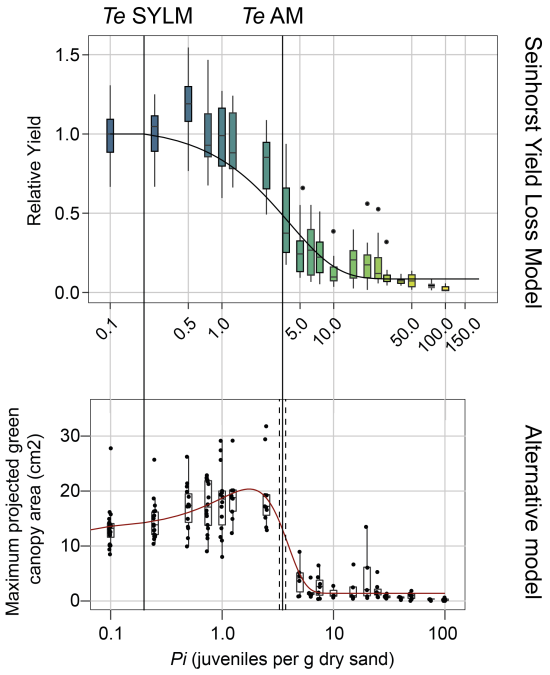

Figure 2: Illustration of different model outputs. Top graph is the output of the Seinhorst yield loss model where the tolerance limit (*Te* SYLM) is estimated around *Pi* 0.2. Bottom graph is the output of the alternative model where the tolerance limit (*Te* AM) is estimated around *Pi* 3.3).

tolerant than others. We only mapped the aboveground plant response to the lowest inoculation densities (i.e., P_i 0 – 2.5 juveniles per gram of soil) to provide a proof of concept. The data collected over this period revealed significant variation in green canopy area of Arabidopsis ecotypes challenged with *H. schachtii* (broad sense heritability R2 = 40%; **Chapter 3, Fig. 4**). Next, using a GWA mapping approach we identified two QTLs which are significantly associated with tolerance (threshold for significance $-\log_{10}(P) > 5$; **Chapter 3, Table 2**). In total, assuming that the linkage disequilibrium (LD) decays within 10 kb (Kim et al., 2007), we identified 20 candidate tolerance genes within these QTLs. In line with our overarching hypothesis, which entails that phenotypic plasticity of root system architecture is key to plant tolerance to belowground biotic stresses, we found PIN5 as a candidate tolerance gene. PIN5 is an auxin transporter that modulates intracellular auxin homeostasis and thereby plant development (Mravec et al., 2009). Also, it was found that PIN5 modulates root meristem size and root growth (Di Mambro et al., 2019). Nonetheless, more information lies in our data that still needs to be analyzed to identify more candidate tolerance genes.

Our panel of Arabidopsis ecotypes used to map the tolerance parameters does not harbour major resistance to *H. schachtii*. However, the ecotypes nonetheless vary in susceptibility independent of resistance because *H. schachtii* engages in a prolonged biotrophy with Arabidopsis. This means that the number of nematodes per plant, and thus the level of biotic stress, at a given inoculation density may also vary by ecotype. Consequently, the green canopy area measurements are a function of the level of biotic stress (i.e., susceptibility), as well as the ability to mitigate the impact of this stress (i.e., tolerance). To further pinpoint genetic variation uniquely

associated with tolerance, we also counted the number of matured cyst of each plant at 35 days-post inoculation as a measure of susceptibility. We found significant variation in the number of successful infections among the Arabidopsis ecotypes ranging from 0 to 13 cysts per plant, of which 31% can be explained by genetic variation in our panel of Arabidopsis ecotypes (**Chapter 3, Fig. 5**). This data was also mapped on the genome of Arabidopsis using association mapping, resulting in 40 QTLs significantly associating with susceptibility to *H. schachtii* (threshold for significance $-\log_{10}(P) > 5$). In total, these QTLs harbor 209 candidate susceptibility genes, many of which have been identified previously as modulators of plant susceptibility to cyst nematode infection (**Chapter 3, Table S1**).

Next, we asked to what extent nematode tolerance and susceptibility are genetically distinct traits in Arabidopsis. We addressed this question by performing Spearman correlation coefficient tests and a PERMANOVA analyses between aboveground growth responses of Arabidopsis and the number of matured cysts per plant at different inoculation densities by ecotype. We found a wide variation in correlation coefficients between green canopy areas and cysts per ecotype (**Chapter 3, Fig. 6**), indicating that there is variation in ecotype responses to successful infections. For instance, some ecotypes performed better during infection compared to others. Or, conversely, some ecotypes with low number of successful infections displayed strong disease symptoms. PERMANOVA analysis revealed that only 0.2% of the variance in aboveground plant responses in our Arabidopsis panel can be explained by the number of matured cysts. This confirms our initial hypothesis that tolerance and susceptibility are indeed two distinct plant traits.

Getting grips with a plastic root system

This thesis also focused on the phenotypic plasticity in root systems of plants as a novel tolerance mechanism to cope with belowground biotic stress. Phenotypic plasticity refers to the ability of one genotype to produce different phenotypes under different circumstances. Phenotypic plasticity enables plants to adapt to rapidly changing environmental conditions. A typical belowground symptom of nematode infections in plants is a bushy root system with shortened primary roots and extensive outgrowth of secondary roots. The function of this remarkable root phenotype is not well understood, but we hypothesized that extensive root branching is an adaptive plant response to mitigate the impact of stress by root-feeding nematodes. Post-embryonic *de novo* root organogenesis from differentiated root cells may thus contribute to plant tolerance to nematode infections. By extension, plasticity in *de novo* root organogenesis may define the level of tolerance of plants to nematode infections. Indeed, there is evidence that plants with a more plastic root system are more tolerant to nematode infections (Miltner et al., 1991). In **Chapters 4**, **5**, and **6,** we investigated whether three known modulators of stress-induced *de novo* root organogenesis contribute to tolerance of Arabidopsis to nematode infections.

Notably, the causes of stress in host plants by cyst nematode infections vary by stage of parasitism. During host invasion, cyst nematodes cause extensive tissue damage along their migratory track. In **Chapter 4**, we tested whether *de novo* root organogenesis in proximity of nematode infection sites depends on damage-signalling. We showed that nematode damage transiently induces local biosynthesis and accumulation of jasmonic acid, which activates the transcription factor Ethylene Response Factor (ERF)109. We further showed that ERF109 is required for the local

biosynthesis of auxin and subsequent formation of secondary roots at nematode infection sites, which provides a link between damage signalling and plant root architecture plasticity.

In **Chapter 5**, we demonstrated that the plant transcription factor *WUSCHEL-RELATED HOMEOBOX 11* (WOX11) modulates this formation of secondary roots close to nematode infection sites downstream of ERF109. Here, damage-induced auxin-maxima activates WOX11 expression, which marks the first steps of tissue regeneration from detached leaves and wounded roots. The involvement of WOX11, but not ARF7/ARF19, characterizes the nematode-induced secondary roots as adventitious lateral roots. We showed that nematode-induced adventitious lateral roots compensate for the inhibition of the primary root growth by nematodes, which points at a novel tolerance mechanism to nematodes based on root system plasticity. This role of WOX11-mediated formation of adventitious lateral roots as a tolerance factor in nematode-infected Arabidopsis is further substantiated by its stabilizing effect on aboveground plant growth (i.e., green canopy area). Altogether, our findings revealed how tissue damage by invading cyst nematodes triggers the local accumulation of jasmonic acid, which induces local auxin maxima initiating the formation of adventitious lateral roots and compensating for the inhibition of primary root growth.

A question that remains to be studied is if causes of stress other than tissue damage by invading nematodes contribute to the outgrowth of adventitious lateral roots. We found that damage-induced jasmonic acid-mediated signalling is transiently and locally activated in the early stages of parasitism by cyst nematodes. In fact, the WOX11-mediated formation of adventitious lateral roots in nematode-infection sites may continue after jasmonic acid biosynthesis and accumulation subside, because even in the absence of ERF109 (i.e., *erf109* knockout mutant) we observed some expression of WOX11-GFP in nematode infection sites. Furthermore, we also found indications that besides damage-induced local biosynthesis of auxin, auxin transported from the shoots towards nematode infection sites also contributes to local stress-induced auxin maxima (**Chapter 4**, **Fig. 6 and 7** and **S1**; **Chapter 5**, **Fig. 3**). This means that systemic auxin-based stress signals may contribute to the auxin-maxima driving the formation of adventitious lateral roots at nematode infection sites. Drought stress in aboveground plant parts could for instance be a trigger of systemic auxin-based stress signaling in nematode-infected plants (Balestrini et al., 2019). Shortly after host invasion, cyst nematodes modify host vascular cells into a permanent feeding structure. This permanent feeding structure takes up a large part of the vascular cylinder, interrupting the flow of water and minerals from the roots to the shoots. The interrupted connectivity of xylem vessel surrounding the permanent feeding structure may cause drought stress in shoots and trigger auxin-mediated stress signals towards nematode infection sites.

The fact that plant responses to root-feeding nematodes may have an abiotic component inspired us to focus further on TCP transcription factors as stress-induced modulators of root system architecture. We selected the TCP transcription factor family because some of its members are known to convert environmental stressors (e.g., drought, salinity, rocky soil environments) into adaptive growth responses (Danisman, 2016). For instance, TCP13 regulates leaf and root growth in Arabidopsis in response to conditions simulating drought (Urano et al., 2022). Similarly, ectopic expression of a *TCP9*-like gene in soybean increases plant tolerance to high saline conditions (Zhang et al., 2023). In **Chapter 6**, we first checked which *TCPs* are differentially regulated during the first days of *H. schachtii* infection.

TCP9 and *TCP13* were differentially expressed over all timepoints. We decided to continue with TCP9 due to its role in root growth and senescence (Danisman et al., 2012) and its, at that time, unknown role in (a)biotic stress tolerance. Subsequently, we demonstrated that the transcription factor TCP9 contributes to tolerance of Arabidopsis to cyst nematode infection by modulating root architecture plasticity. TCP9 mitigates the impact of cyst nematode infections on primary root growth and secondary root growth, probably through transcriptional regulation of ROS-related processes (i.e., sensitivity and accumulation). Our findings suggest that tolerance to biotic stress caused by root feeding nematodes to some extent reflects tolerance to abiotic stress, which agrees with observations in the field where the performance of nematode tolerant cultivars seems to depend on long-term weather conditions (Wilhelm et al., 1985; Fatemy and Evans, 1986),

Nematodes: a biological cause of abiotic stresses?

The question if nematodes induce a unique type of stress in plants, as was first posed by Wallace in 1987, still remains unanswered. One way to address this question is to dissect the underlying causes of nematode-induced stresses. Notably, these stresses may not all strictly qualify as biotic stresses. For instance, the accumulation of assimilates in nematode-feeding structures may cause osmotic stress. Nematode-induced interruptions in vascular connectivity may lead to drought stress and nutrient deficiencies. Furthermore, the initiation of adventitious lateral roots following nematode damage, parallels plant responses to coarse particles in soils (Sheng et al., 2017). So, instead of viewing biotic stress by nematodes as a unique phenomenon, it might be more productive to think of root-feeding nematodes as a biological cause of abiotic stresses. Our understanding of tolerance to biotic stress by root-feeding nematodes may therefore benefit from breaking down what is perceived as biotic stress into abiotic stress components.

However, nematode-induced stress sets itself apart from common abiotic stresses (e.g., drought and high salinity) by its spatial heterogeneity. While abiotic stress conditions are often more uniformly distributed at the scale of the whole root system, stress by microscopically small root-feeding nematodes initially occurs at the cellular level. This means that even within a single nematode-infected root system stress can be spatially highly heterogenous. This particularly holds true for sedentary plant parasitic nematodes which form permanent feeding structures within the vascular cylinder shortly after host invasion. Consequently, plant adaptations to these nematodes are also often spatially confined to nematode infection sites. For instance, in **Chapters 4** and **5** we show that tissue damage by cyst nematode triggers a transient and local jasmonic acid-dependent and auxin-mediated formation of adventitious lateral roots close to nematode infection sites. An interesting question for further research would be to investigate if plants utilize this spatial heterogeneity by inducing adaptations in distant non-infected parts of root systems to compensate for loss in nematode-infected parts of the root system. In other words, it is worth investigating whether plants reallocate resources to parts of the root system that are not challenged by nematodes.

Another, perhaps, unique cause of local stress indirectly induced by sedentary plant parasitic nematodes occurs in plants harbouring major nematode resistances. Although it may seem counterintuitive, immune responses around nematode-feeding structures initiated by the plant resistance can be the cause of

stress. These plant immune responses often involve a programmed cell death inside nematode-feeding structures or in peripheral plant cells (Balint-Kurti, 2019). Local cell death prevents nematode development (Paulson and Webster, 1972), feeding site development (Rice et al., 1985), or isolates the feeding structure from the surrounding tissue to prevent food up-take (Koropacka, 2010; Kandoth et al., 2011). This results in a resistant plant phenotype. However, elaborate cell death responses inside the vascular cylinder of resistant plants heavily challenged by sedentary nematodes may also interrupt the connectivity of surrounding xylem and phloem vessels, leading to aboveground decline. This might be the reason why, for instance, some root-knot nematode-resistant rice cultivars harbouring MG1 resistance still display symptoms of disease (Wang et al., 2023).

Both biotic and abiotically-induced stress in plants involve systemic regulation by reactive oxygen species (ROS) and calcium fluxes (Labudda et al., 2018). However, the outcome of these two processes might be different. For instance, each type of stress induces a different systemic metabolic and transcriptomic response (Suzuki et al., 2013; Zandalinas et al., 2019). One explanation could be that the cell type determines the specificity of the systemic signal that is elicited in response to a stressor (Gilroy et al., 2016; Fichman et al., 2019). Conversely, it might be that signals specific to stress, such as hormones, are transduced or generated along the trajectory of the systemic signal (Choudhury et al., 2018). Finally, a different oscillation pattern in ROS or calcium signals may convey specificity for nematode-associated stress(ors) (Keinath et al., 2015; Choi et al., 2017; Marcec et al., 2019). For instance, cyst nematode infection induces different surface potential changes, a mechanism that is associated with cytosolic Ca^{2+} transient currents, compared to artificial cell death by laser ablation (Marhavý et al., 2019). One can imagine that the production of high levels of ROS or induction of stress signaling does not promote plant growth and development. In **Chapter 6**, we show that TCP9 modulates transcriptional activation of enzymes involved in ROS-related processes in nematode-infected roots to mitigate stress responses. Additionally, we show that TCP9 modulates sensitivity to ROS in roots and shoots. We show that mitigation of (systemic) stress signaling is an interesting tolerance mechanism to study.

Biotic stress tolerance in resilient plant production systems

Tolerance to biotic stress is an underappreciated but valuable trait to reduce yield losses in plant production systems. Often plant diseases are forgotten in the context of climate change. Climate change is thought to have the largest implications for agricultural production systems worldwide. However, as a consequence of climate change, the chance and number of incidences of pathogen infection can increase (Singh et al., 2023). Additionally, with changing climates new tropical species can be introduced (Bebber et al., 2014). For instance, the tropical root-knot nematodes *Meloidogyne incognita*, *Meloidogyne javanica* and *Meloidogyne arenaria* are amongst the most rapidly spreading pests driven by climate change. In this context, nematode-induced stresses can aggravate climate-induced abiotic stress, and vice versa, leading to higher yield losses in a changing climate (Wilhelm et al., 1985; Fatemy and Evans, 1986).

Strategies, such as crop rotation, cultivar choice, soil management, targeted control, and monitoring infestations, to manage nematode outbreaks have already been applied to improve plant production systems (Sikora et al., 2023). For instance,

soil management can positively influence ecosystem services to improve efficient nutrient cycling as well as increasing disease suppressiveness for nematodes. However, as aforementioned, the majority of these strategies still focus on eradicating nematode outbreaks. Using traits, such as biotic stress tolerance, can minimize yield losses (**Chapter 5** and **6**) with increased disease pressure. At the moment, for many crops, plant breeders coincidently discover tolerance in cultivars. With adjustments in their phenotyping methods, for instance by quantifying proximate tolerance traits above ground (**Chapter 2**), tolerance and resistances can be identified in one experiment (**Chapter 3**). Introgression of biotic stress tolerance into breeding material and ultimately into crops will help reduce the damage done by pests, and because of its strong interactions with abiotic stress tolerance, may result in more resilient plants in a changing climate.

Conclusions

This thesis provides valuable leads for further research into how plant growth can be retained during nematode infections. We improved and developed methods, such as a high-throughput phenotyping system, to quantify growth responses to damage inflicted by root-parasitic nematodes (**Chapter 2**). We utilized this system to uncover the rich genetic diversity in tolerance to root-parasitic cyst nematodes in Arabidopsis (**Chapter 3**). We found multiple candidate genes related to root architectural plasticity. Also, we demonstrated that root architecture plasticity is an important trait to mitigate stress inflicted by nematodes and maintain aboveground growth (**Chapter 4**, **5**, and **6**). However, it might be challenging to use this knowledge directly in breeding programs. For instance, translating findings from Arabidopsis (i.e., candidate genes identified with GWAS) to crops is not evident. Nonetheless, to close the gap between the model plant Arabidopsis and various crops, similar studies can be performed on model crop plants like tomato. Upgrading our phenotyping platform is pivotal to monitor changes in the more complex shoot architectures of crops. An alternative system that creates 3D images of aboveground plant parts might be a solution for this. Also, more sensitive image-capturing systems than RGB cameras might be better suited to monitor physiological changes (i.e., temperature or photosynthesis capacity). For instance, to record the earliest changes not yet visible to the naked eye, one can use such a system to pinpoint the first physiological responses to nematode infections in plants. Finally, we based our analyses on correlations between in soil grown green canopies and *in vitro* grown root systems, making it difficult to estimate how much root architecture plasticity contributes to tolerance. Addressing this question, demands a different phenotyping system, which can simultaneously monitor both above- and below-ground parts of single plants in a non-destructive manner. Such a system will help to identify novel tolerance mechanisms and further resolve the underlying genetic architecture of this trait.

Acknowledgements

I thank Nina Guarneri, José L. Lozano-Torres, Mark G. Sterken, and Geert Smant for providing helpful comments on earlier version of this chapter.

References

Agathokleous E, Kitao M, Calabrese EJ (2019) Hormesis: A Compelling Platform for Sophisticated Plant Science. Trends Plant Sci **24**: 318–327

Anwer MA, Anjam MS, Shah SJ, Hasan MS, Naz AA, Grundler FMW, Siddique S (2018) Genome-wide association study uncovers a novel QTL allele of AtS40-3 that affects the sex ratio of cyst nematodes in Arabidopsis. J Exp Bot **69**: 1805–1814

Balestrini R, Rosso LC, Veronico P, Melillo MT, De Luca F, Fanelli E, Colagiero M, Di Fossalunga AS, Ciancio A, Pentimone I (2019) Transcriptomic responses to water deficit and nematode infection in mycorrhizal tomato roots. Front Microbiol. doi: 10.3389/fmicb.2019.01807

Balint-Kurti P (2019) The plant hypersensitive response: concepts, control and consequences. Mol Plant Pathol **20**: 1163–1178

Bebber DP, Holmes T, Gurr SJ (2014) The global spread of crop pests and pathogens. Global Ecology and Biogeography **23**: 1398–1407

Been TH, Teklu MG, Heve WK, Schomaker CH (2015) Damage thresholds and population dynamics of Meloidogyne chitwoodi on carrot (Daucus carota) at different seed densities. Nematology **17**: 501–514

Castagnone-Sereno P, Bongiovanni M, Wajnberg E (2007) Selection and parasite evolution: A reproductive fitness cost associated with virulence in the parthenogenetic nematode Meloidogyne incognita. Evol Ecol **21**: 259–270

Choi WG, Miller G, Wallace I, Harper J, Mittler R, Gilroy S (2017) Orchestrating rapid long-distance signaling in plants with Ca2+, ROS and electrical signals. Plant Journal **90**: 698–707

Choudhury FK, Devireddy AR, Azad RK, Shulaev V, Mittler R (2018) Local and systemic metabolic responses during light-induced rapid systemic signaling. Plant Physiol **178**: 1461–1472

Danisman S (2016) TCP Transcription Factors at the Interface between Environmental Challenges and the Plant's Growth Responses. Front Plant Sci **7**: 1–13

Danisman S, van der Wal F, Dhondt S, Waites R, de Folter S, Bimbo A, van Dijk AD, Muino JM, Cutri L, Dornelas MC, et al (2012) Arabidopsis Class I and Class II TCP Transcription Factors Regulate Jasmonic Acid Metabolism and Leaf Development Antagonistically. Plant Physiol **159**: 1511–1523

Dedehayir O, Steinert M (2016) The hype cycle model: A review and future directions. Technol Forecast Soc Change **108**: 28–41

Evans K, Haydock PPJ (1990) A review of tolerance by potato plants of cyst nematode attack, with consideration of what factors may confer tolerance and methods of assaying and improving it in crops. Annual applied Biology **117**: 703–740

Fatemy F, Evans K (1986) Effects of Globodera rostochiensis and water stress on Shoot and Root Growth and Nutrient Uptake of Potatoes. Revue Nématologie **9**: 181–184

Fichman Y, Miller G, Mittler R (2019) Whole-Plant Live Imaging of Reactive Oxygen Species. Mol Plant **12**: 1203–1210

Fuller VL, Lilley CJ, Urwin PE (2008) Nematode resistance. New Phytologist **180**: 27–44

Fuller VL, Lilley CJ, Urwin PE (2007) Nematode resistance. New Phytologist 243–255

Gilroy S, Białasek M, Suzuki N, Górecka M, Devireddy AR, Karpiński S, Mittler R (2016) ROS, Calcium, and Electric Signals: Key Mediators of Rapid Systemic Signaling in Plants. Plant Physiol **171**: 1606–1615

Jones JT, Haegeman A, Danchin EGJ, Gaur HS, Helder J, Jones MGK, Kikuchi T, Manzanilla-López R, Palomares-Rius JE, Wesemael WML, et al (2013) Top

10 plant-parasitic nematodes in molecular plant pathology. Mol Plant Pathol 14: 946–961

Kandoth PK, Ithal N, Recknor J, Maier T, Nettleton D, Baum TJ, Mitchum MG (2011) The soybean Rhg1 locus for resistance to the soybean cyst nematode Heterodera glycines regulates the expression of a large number of stress- and defense-related genes in degenerating feeding cells. Plant Physiol **155**: 1960–1975

Keinath NF, Waadt R, Brugman R, Schroeder JI, Grossmann G, Schumacher K, Krebs M (2015) Live Cell Imaging with R-GECO1 Sheds Light on flg22- and Chitin-Induced Transient [Ca2+]cyt Patterns in Arabidopsis. Mol Plant **8**: 1188–1200

Kerstens M, Hesen V, Yalamanchili K, Bimbo A, Grigg S, Opdenacker D, Beeckman T, Heidstra R, Willemsen V (2021) Nature and Nurture: Genotype-Dependent Differential Responses of Root Architecture to Agar and Soil Environments. Genes (Basel) **12**: 1028

Koropacka KB (2010) Molecular contest between potato and the potato cyst nematode Globodera pallida: modulation of Gpa2-mediated resistance. PhD Thesis. Wageningen Univ., Wageningen

Labudda M, Różańska E, Czarnocka W, Sobczak M, Dzik JM (2018) Systemic changes in photosynthesis and reactive oxygen species homeostasis in shoots of Arabidopsis thaliana infected with the beet cyst nematode Heterodera schachtii. Mol Plant Pathol **19**: 1690–1704

Lozano-Torres JL, Wilbers RHP, Warmerdam S, Finkers-Tomczak A, Diaz-Granados A, van Schaik CC, Helder J, Bakker J, Goverse A, Schots A, et al (2014) Apoplastic Venom Allergen-like Proteins of Cyst Nematodes Modulate the Activation of Basal Plant Innate Immunity by Cell Surface Receptors. PLoS Pathog. doi: 10.1371/journal.ppat.1004569

Marcec MJ, Gilroy S, Poovaiah BW, Tanaka K (2019) Mutual interplay of Ca 2+ and ROS signaling in plant immune response. Plant Science **283**: 343–354

Marhavý P, Kurenda A, Siddique S, Dénervaud Tendon V, Zhou F, Holbein J, Hasan MS, Grundler FM, Farmer EE, Geldner N (2019) Single-cell damage elicits regional, nematode-restricting ethylene responses in roots. EMBO J. doi: 10.15252/embj.2018100972

Miltner ED, Karnok KJ, Hussey RS (1991) Root Response of Tolerant and Intolerant Soybean Cultivars to Soybean Cyst Nematode. Agron J **83**: 571–576

Molendijk L, de Jongh E (2018) Beheersing van aardappelmoehied in de akkerbouw. 3–21

Moosavi MR (2015) Damage of the root-knot nematode Meloidogyne javanica to bell pepper, Capsicum annuum. Journal of Plant Diseases and Protection **122**: 244–249

Norshie PM, Been TH, Schomaker CH (2011) Estimation of partial resistance in potato genotypes against Meloidogyne chitwoodi. Nematology **13**: 477–489

Paal J, Henselewski H, Muth J, Meksem K, Menéndez CM, Salamini F, Ballvora A, Gebhardt C (2004) Molecular cloning of the potato Gro1-4 gene conferring resistance to pathotype Ro1 of the root cyst nematode Globodera rostochiensis, based on a candidate gene approach. Plant Journal **38**: 285–297

Paulson RE, Webster JM (1972) Ultrastructure of the hypersensitive reaction in roots of tomato, Lycopersicon esculentum L., to infection by the root-knot nematode, Meloidogyne incognita.

Pingali PL (2012) Green revolution: Impacts, limits, andthe path ahead. Proc Natl Acad Sci U S A **109**: 12302–12308

Potter JW, Dale A (1994) Wild and cultivated strawberries can tolerate or resist root-lesion nematode. HortScience **29**: 1074–1077

Ravelombola WS, Qin J, Shi A, Nice L, Bao Y, Lorenz A, Orf JH, Young ND, Chen S (2019) Genome-wide association study and genomic selection for soybean

chlorophyll content associated with soybean cyst nematode tolerance. BMC Genomics **20**: 1–18

Ravelombola WS, Qin J, Shi A, Nice L, Bao Y, Lorenz A, Orf JH, Young ND, Chen S (2020) Genome-wide association study and genomic selection for tolerance of soybean biomass to soybean cyst nematode infestation. PLoS One **15**: 1–20

Ray DK, Mueller ND, West PC, Foley JA (2013) Yield Trends Are Insufficient to Double Global Crop Production by 2050. PLoS One. doi: 10.1371/journal.pone.0066428

Rice SL, Leadbeater BSC, Stone AR (1985) Changes in cell structure in roots of resistant potatoes parasitized by potato cyst-nematodes. I. Potatoes with resistance gene H1 derived from Solanum tuberosum ssp. andigena. Physiol Plant Pathol **27**: 219–234

Rouppe van der Voort J, van der Vossen E, Bakker E, Overmars H, van Zandvoort P, Hutten R, Klein Lankhorst R, Bakker J (2000) Two additive QTLs conferring broad-spectrum resistance in potato to Globodera pallida are localized on resistance gene clusters. Theoretical and Applied Genetics **101**: 1122–1130

Sasanelli N, Vovlas N, Trisciuzzi N, Cantalapiedra-Navarrete C, Palomares-Rius JE, Castillo P (2013) Pathogenicity and host-parasite relationships of Heterodera cruciferae in cabbage. Plant Dis **97**: 333–338

Savary S, Willocquet L, Pethybridge SJ, Esker P, McRoberts N, Nelson A (2019) The global burden of pathogens and pests on major food crops. Nat Ecol Evol **3**: 430–439

Seinhorst JW (1986) Effects of nematode attack on the growth and yield of crop plants. *In* F Lamberti, CE Taylor, eds, Cyst Nematodes. Plenum Press, New York and London, pp 191–209

Shah SJ, Anjam MS, Mendy B, Anwer MA, Habash SS, Lozano-Torres JL, Grundler FMW, Siddique S (2017) Damage-associated responses of the host contribute to defence against cyst nematodes but not root-knot nematodes. J Exp Bot **68**: 5949–5960

Sheng L, Hu X, Du Y, Zhang G, Huang H, Scheres B, Xu L (2017) Non-canonical WOX11-mediated root branching contributes to plasticity in arabidopsis root system architecture. Development (Cambridge) **144**: 3126–3133

Siddique S, Matera C, Radakovic ZS, Shamim Hasan M, Gutbrod P, Rozanska E, Sobczak M, Torres MA, Grundler FMW (2014) Parasitic Worms Stimulate Host NADPH Oxidases to Produce Reactive Oxygen Species That Limit Plant Cell Death and Promote Infection. Sci Signal **7**: 1–11

Sikora RA, Helder J, Molendijk LPG, Desaeger J, Eves-Van Den Akker S, Mahlein A-K (2023) Integrated Nematode Management in a World in Transition: Constraints, Policy, Processes, and Technologies for the Future. Annual Reviews. doi: 10.1146/annurev-phyto-021622

Singh BK, Delgado-Baquerizo M, Egidi E, Guirado E, Leach JE, Liu H, Trivedi P (2023) Climate change impacts on plant pathogens, food security and paths forward. Nat Rev Microbiol **21**: 640–656

Suzuki N, Miller G, Salazar C, Mondal HA, Shulaev E, Cortes DF, Shuman JL, Luo X, Shah J, Schlauch K, et al (2013) Temporal-spatial interaction between reactive oxygen species and abscisic acid regulates rapid systemic acclimation in plants. Plant Cell **25**: 3553–3569

The European Commission (2023) Farm to Fork - targets - Progress. https://food.ec.europa.eu/plants/pesticides/sustainable-use-pesticides/farm-fork-targets-progress_en,

Trudgill DL, Cotes LM (1983) Tolerance of potato to potato cyst nematodes (Globodera rostochiensis and G. pallida) in relation to the growth and efficiency of the root system. Annals of Applied Biology **102**: 385–397

Tzortzakakis EA, Dos Santos MCV, Conceição I (2016) An update on the occurrence of resistance-breaking populations of root-knot nematodes (Meloidogyne spp.) on resistant tomato in Greece with six new records from Crete. Hellenic Plant Protection Journal **9**: 60–65

Urano K, Maruyama K, Koyama T, Gonzalez N, Inzé D, Yamaguchi-Shinozaki K, Shinozaki K (2022) CIN-like TCP13 is essential for plant growth regulation under dehydration stress. Plant Mol Biol **108**: 257–275

van der Voort JR, Lindeman W, Folkertsma R, Hutten R, Overmars H, van der Vossen E, Jacobsen E, Bakker J (1998) A QTL for broad-spectrum resistance to cyst nematode species (Globodera spp.) maps to a resistance gene cluster in potato. Theoretical and Applied Genetics **96**: 654–661

Wallace HR (1987) A Perception of Tolerance. Nematologica **33**: 419–432

Wang X, Cheng R, Xu D, Huang R, Li H, Jin L, Wu Y, Tang J, Sun C, Peng D, et al (2023) MG1 interacts with a protease inhibitor and confers resistance to rice root-knot nematode. Nat Commun. doi: 10.1038/s41467-023-39080-6

Warmerdam S, Sterken MG, van Schaik C, Oortwijn MEP, Sukarta OCA, Lozano-Torres JL, Dicke M, Helder J, Kammenga JE, Goverse A, et al (2018) Genome-wide association mapping of the architecture of susceptibility to the root-knot nematode Meloidogyne incognita in Arabidopsis thaliana. New Phytologist 218: 724–737

Wilhelm NS, Fisher JM, Graham RD (1985) The effect of manganese deficiency and cereal cyst nematode infection on the growth of barley. Plant Soil **85**: 23–32

Williamson VM, Hussey RS (1996) Nematode pathogenesis and resistance in plants. Plant Cell **8**: 1735–1745

Wyss U, Zunke U (1986) Observations on the behaviour of second stage juveniles of Heterodera schachtii inside host roots. Revue de nématologie **9**: 153–165

Zandalinas SI, Sengupta S, Burks D, Azad RK, Mittler R (2019) Identification and characterization of a core set of ROS wave-associated transcripts involved in the systemic acquired acclimation response of Arabidopsis to excess light. Plant Journal **98**: 126–141

Zhang Z, Zhao Y, Chen Y, Li Y, Pan L, Wang S, Wang P, Fan S (2023) Overexpression of TCP9-like gene enhances salt tolerance in transgenic soybean. PLoS One **18**: e0288985

Appendices

English summary

Plant-parasitic nematodes are microscopic organisms posing a significant threat to our food security. Symptoms of nematode infection in plants are nonspecific and can easily be confused with symptoms of abiotic stress (e.g., drought and nutrient deficiency). Key symptoms include wilting and delays in the growth and development of both above- and belowground plant parts. The damage to crops by plant-parasitic nematodes can reach up to 10% annually. Nematode outbreaks are currently controlled by using resistant crops and non-selective pesticides. However, with the phasing out of these pesticides and stricter regulations on their use, an increase in the diversity of parasitic nematode species in agricultural land is expected. Consequently, the effectiveness of resistant crops is anticipated to decrease due to their high specificity for nematode species or pathotypes. With an increase in nematode diversity and a limited number of resistant crops, future crop yield losses are also expected to increase. However, plant susceptibility to nematodes does not always correlate with yield loss due to infection, and some varieties may exhibit susceptibility without significant harvest losses—a phenomenon known as disease tolerance.

To introduce the reader to the context of this dissertation, **Chapter 1** briefly describes the three main nematode species, the stresses they cause, and presents disease tolerance as a sustainable solution to reduce crop yield loss. Chapter 1 also discusses the current status of research on tolerance, the knowledge gaps, and the role of root plasticity as a tolerance mechanism.
At the outset of this dissertation, no robust method existed to monitor the impact of belowground biotic stress caused by nematodes over time. **Chapter 2** describes new non-destructive methods to measure and quantify damage by plant-parasitic nematodes in the model plant Arabidopsis. A high-throughput phenotyping platform was built around the green leaf area of Arabidopsis to measure growth responses to nematode infection. This system led to a new analytical model that allows us to quantify the tolerance limit—the point at which tolerance breaks.

The development of this phenotyping platform was crucial to determine the genetic basis of nematode disease tolerance. In **Chapter 3**, we used it to measure growth responses of 154 ecotypes of Arabidopsis under increasing infection pressure from the sugar beet cyst nematode *Heterodera schachtii*. We also measured the susceptibility of these Arabidopsis ecotypes to *H. schachtii* to determine whether disease tolerance and susceptibility are distinct plant traits. Both traits were linked to genomic locations of our 154 Arabidopsis lines through genome-wide association (GWA), resulting in a collection of 20 genes associated with tolerance and 209 genes associated with susceptibility to cyst nematodes. Several candidate tolerance genes have been linked to root system plasticity before.

The work described in Chapters 2 and 3 took approximately four and a half years. In parallel, we also conducted hypothesis-driven research. The idea was that stress tolerance results from phenotypic plasticity in root system architecture. For example, some tolerant sugar beet varieties infected with *H. schachtii* exhibit beard growth (increase in lateral roots). Based on literature studies, we tested various candidate genes for their involvement in root plasticity. Damage responses, such as leaf cutting, induced the expression of *Ethylene Response Factor* (*ERF*)*109*, leading to lateral

root growth from these cutting sites. In **Chapter 4**, we describe that mechanical damage caused by *H. schachtii* during invasion and migration stimulates the formation of additional lateral roots. Roots of *H. schachtii*-infected knockout mutants of the damage receptor COI1 (*coi1-2*) and ERF109 (*erf109*) showed no increase in lateral roots, while the wildtype did. In wildtype plants, ERF109 induces local auxin biosynthesis around *H. schachtii* infection sites. Blocking auxin biosynthesis led to less lateral root growth during nematode infection. Finally, we showed that lateral root growth compensates for reduced main root growth during H. schachtii infection.

Similar to ERF109, the transcription factor WUSCHEL-RELATED HOMEOBOX (WOX)11 is involved in lateral root growth from cut leaves and main roots. Secondary roots can be classified either as adventitious or lateral. In **Chapter 5**, we investigated whether the secondary roots formed by *H. schachtii* infection are adventitious or lateral. By using the transcriptional repressor mutant of *WOX11* (*35S:WOX11-SRDX*), we demonstrated that *H. schachtii* induces adventitious lateral root growth. WOX11 mutants showed less lateral root growth than wildtype plants. Using confocal microscopy, we showed that *WOX11* expression depends on ERF109 and the damage receptor COI1. Lastly, we demonstrated that adventitious lateral root growth contributes to the maintenance of green leaf area and thus tolerance.

Several members of the TEOSINTE BRANCHED1/CYCLOIDEA/PROLIFERATING CELL FACTOR1 (TCP) family are known to be involved in adaptive growth responses of above- and below-ground plant parts. In **Chapter 6**, we first tested which members of the TCP family are differentially expressed in nematode infected roots and then tested whether they play a role in adaptive growth responses of the root system during *H. schachtii* infection. Transcriptome analysis showed that *TCP9* is upregulated during the first days of *H. schachtii* infection. Mutants of *tcp9* showed less severe symptoms of infection, with the root system suffering less under *H. schachtii* infection. Additionally, the mutation in *tcp9* did not affect susceptibility to *H. schachtii*. To better understand why *tcp9* displays a tolerant phenotype, we conducted transcriptome analysis during *H. schachtii* infection. This revealed that processes involved in radical oxygen group homeostasis are differently regulated. After exposing above- and below-ground plant parts to hydrogen peroxide, we found that *tcp9* mutants are less sensitive to radical oxygen groups.

In the final chapter of this thesis (**Chapter 7**), I discuss all our findings in the broader context of tolerance as an element in more resilient plant production systems.

Nederlandse samenvatting

Plant-parasitaire aaltjes zijn microscopisch kleine organismen die een grote bedreiging zijn voor onze voedselzekerheid. De symptomen van aaltjesinfectie in planten zijn niet-specifiek en kunnen gemakkelijk worden verward met symptomen van abiotische stress (bijv. droogte en nutriëntentekort). Belangrijke symptomen zijn verwelking en vertragingen in de groei en ontwikkeling van zowel bovengrondse als ondergrondse plantendelen. De jaarlijkse schade aan gewassen door plant-parasitaire aaltjes kan oplopen tot 10%. Uitbraken van aaltjes worden onderdrukt door resistente gewassen en niet-selectieve pesticiden te gebruiken. Echter, door het uitfaseren van deze pesticiden en meer beperkingen op het gebruik van de pesticiden, wordt verwacht dat er een toename in diversiteit aan parasitaire aaltjessoorten op landbouwgrond zal plaatsvinden. Een bijgevolg hiervan zal zijn dat de effectiviteit van resistente gewassen vermindert vanwege hun hoge specificiteit voor aaltjessoorten, of zelfs pathotypen. Met een toename in diversiteit van aaltjes en het beperkte aantal resistente gewassen zal in de toekomst het risico verlies in gewasopbrengst groter worden. Echter, vatbaarheid van planten voor aaltjes gaat niet altijd gepaard met verlies van opbrengst als gevolg van een infectie. Sommige rassen zijn bijvoorbeeld vatbaar voor aaltjes infectie zonder dat een hoge infectiegraad gepaard gaat met veel oogstverlies. Deze fenotypische variatie in groei onder invloed van biotische stress staat ook wel bekend als ziektetolerantie.

Om de lezer te introduceren in de context van het onderwerp van dit proefschrift, beschrijf ik in **Hoofdstuk 1** kort de drie belangrijkste aaltjes soorten en de stress die zij veroorzaken. Daarna presenteer ik ziektetolerantie als een duurzame oplossing om het verlies van gewasopbrengst te verminderen. Vervolgens bespreek ik de status van het onderzoek naar tolerantie, de kennishiaten rondom om het onderzoek naar tolerantie, evenals de rol van wortelplasticiteit als tolerantiemechanisme.

Aan het begin van mijn promotieonderzoek was nog er geen robuuste methode bekend om de impact van ondergrondse biotische stress door nematode over tijd te monitoren. **Hoofdstuk 2** beschrijft nieuwe niet-destructieve methodes om schade door plant-parasitaire aaltjes te meten en te kwantificeren in het modelplant Arabidopsis. Meerdere karakteristieken, zoals de hoofdwortel lengte, het aantal bloemetjes, en het groenbladerdek van Arabidopsis werden naarmate de infectiedruk van het bietencystenaaltje *Heterodera schachtii* toenam korter en minder. Het groenbladerdek reageerde het meest accuraat op de impact van biotische stress door *H. schachtii* en het wortelknobbelaaltje *Meloidogyne incognita*. Daarnaast was het groenbladerdek ook het makkelijkste te meten. Om deze redenen hebben wij een ‘high-throughput’ fenotypering platform gebouwd om op basis van het groenbladerdek van Arabidopsis groei responsen tijdens aaltjes infectie te meten. Hiervoor hebben we een nieuw analytisch model ontwikkeld die ons instaat stelt om de tolerantie limiet, het moment dat de tolerantie breekt, te kwantificeren.

Het ontwikkelen van dit fenotypering platform was nodig om de genetische basis van ziektetolerantie voor aaltjes te kunnen bepalen. In **Hoofdstuk 3** hebben wij ons systeem gebruikt om groei responsen van 154 ecotypen van Arabidopsis tijdens toenemende infectiedruk van *H. schachtii* te meten. Vervolgens hebben wij ook de vatbaarheid voor *H. schachtii* van deze Arabidopsis planten gemeten om uit te zoeken of ziektetolerantie en vatbaarheid te onderscheiden plant eigenschappen

zijn. Beide eigenschappen hebben we genetisch gekarteerd met behulp van 154 Arabidopsis ecotypen en genome-wide association mapping (GWA). Dit resulteerde in een verzameling van 20 genen die zijn geassocieerd met tolerantie voor en 209 genen die geassocieerd zijn met vatbaarheid van Arabidopsis voor cystenaaltjes. Meerdere kandidaat genen voor tolerantie lijken verband te houden met plasticiteit van het wortelstelsel.

Het werk wat beschreven staat in Hoofdstuk 2 en 3 heeft ongeveer vierenhalf jaar geduurd. In parallel hebben we ook hypothese-gedreven onderzoek gedaan. Het idee was dat tolerantie voor stress een afgeleide is van fenotypische plasticiteit in de architectuur van het wortelstelsel. Zo ontstaat er bijvoorbeeld bij sommige met *H. schachtii* geïnfecteerde suikerbietenrassen baardgroei (toename van zijwortels). Op basis van literatuurstudie hebben wij verschillende kandidaat genen getest voor hun betrokkenheid bij wortelplasticiteit. Schade responsen, bijvoorbeeld door het afsnijden van blaadjes, induceren de expressie van *Ethylene Response Factor* (ERF)*109*, waarna zijwortel groeien vanuit deze snijplekken. In **Hoofdstuk 4** beschrijven we dat de mechanische schade die *H. schachtii* veroorzaakt tijdens invasie en migratie het vormen van extra zijwortels stimuleert. Wortels van *H. schachtii* geïnfecteerde knock-out mutanten van de schade receptor COI1 (*coi1-2*) en ERF109 (*erf109*) lieten geen toename in zijwortels zien, terwijl het wildtype dit wel deed. In wildtype planten, induceert ERF109 lokale biosynthese van het groeihormoon auxine rondom infectie plekken van *H. schachtii*. Het blokkeren van de biosynthese van auxine leidde tot minder zijwortelgroei tijdens aaltjes infectie. Tenslotte vonden wij zien dat groei van extra zijwortels compenseert voor verminderde groei van de hoofdwortel als gevolg van *H. schachtii* infectie.

Net zoals ERF109 is de transcriptie factor WUSCHEL-RELATED HOMEOBOX (WOX)11 betrokken bij zijwortelgroei vanuit afgesneden blaadjes en hoofdwortels. Zijwortels kunnen worden geclassificeerd als adventief of lateraal. Wanneer WOX11 betrokken is bij zijwortelgroei worden de zijwortels gecategoriseerd als adventieve zijwortels. In **Hoofdstuk 5** hebben we onderzocht of de zijwortels die gevormd worden door *H. schachtii* infectie adventief zijn of lateraal zijn. Door het gebruik van de transciptionele repressor mutant van WOX11 (*35S:WOX11-SRDX*) hebben wij aangetoond dat *H. schachtii* de groei van adventieve zijwortels induceert. WOX11 mutanten lieten namelijk minder zijwortelgroei zien dan wildtype planten. Met behulp van confocale microscopie ontdekten wij dat *WOX11* expressie afhankelijk is van ERF109 en de schade receptor COI1. Als laatst laten wij zien dat adventieve zijwortelgroei bijdraagt aan het behoud van de groei van het groenbladerdek, dus tolerantie.

Meerdere leden van de TEOSINTE BRANCHED1/CYCLOIDEA/ PROLIFERATING CELL FACTOR1 (TCP) familie zijn betrokken bij adaptieve groei responsen van boven- en ondergrondse plantendelen. In **Hoofdstuk 6** hebben wij eerst getest welke leden van de TCP-familie tot expressie komen in nematode geïnfecteerde wortels, waarna we hebben getest of deze dan ook een rol spelen in adaptieve groei responsen van het wortelstelsel tijdens infectie met *H. schachtii*. Deze gen-expressie analyse liet zien dat TCP9 aanschakelt tijdens de eerste dagen van een *H. schachtii* infectie. *tcp9* mutanten van lieten minder sterke symptomen van infectie zien. Zo leed het wortelsysteem van *tcp9* minder onder *H. schachtii* infectie. Opvallende genoeg had de mutatie in *TCP9* gen geen invloed op de vatbaarheid van Arabidopsis voor

H. schachtii. Om beter te begrijpen waarom *tcp9* een tolerant fenotype heeft hebben wij transcriptoom analyse tijdens *H. schachtii* infectie uitgevoerd. Hieruit blijkt dat processen die betrokken zijn bij de homeostase van radicale zuurstofgroepen anders gereguleerd worden. Na het blootstellen van ondergrondse en bovengrondse plantdelen aan waterstofperoxide hebben wij gevonden dat *tcp9* mutanten minder sensitief zijn radicale zuurstofgroepen.

In het laatste hoofdstuk van dit proefschrift (**Hoofdstuk 7**) bespreek ik al onze bevindingen van de verschillende hoofdstukken.

Acknowledgements

This thesis represents the culmination of a long journey of hard work, during which I received invaluable help and support from many people.

First, I would like to express my gratitude to my supervisory team. My promotor and mentor, **Geert**, thank you for being such an inspiring person. Without your guidance and unique approach to supervision, this thesis would not have reached its current scientific level. Your ability to find novelty in a pile of results, identify the right angle to craft a great story, and your exceptional writing skills amaze me every time. Many thanks for all the coffees as well. I hope we will continue to create cool papers in the future.

Next, I would like to thank my co-promotors, Mark and José. **Mark**, thank you for your patience and guidance. I know I was not the easiest to teach 'R,' but because of your help, this thesis is enriched with insightful boxplots. I also appreciate our engaging conversations about academia, life, and the enjoyable bike rides. **José**, thank you for all your supervision throughout my time at Nematology. Your mentorship during my MSc thesis taught me early on how to become an independent researcher. I am grateful for your lessons on designing the best experiments and for our discussions about academia and life in general.

Jaap, you were the first person I met from the Laboratory of Nematology. Because of your excellent supervision during the Host-Parasite Interactions course and your passion for nematodes, I decided to pursue my MSc thesis at the Laboratory of Nematology. Thank you for the many enlightening meetings we had about root architecture plasticity and overcompensation. In these meetings, you always said, "everything starts with auxin." Well, after writing this thesis and my literature study from HPI, I truly believe that everything starts with ROS.

Then, I'd like to thank my academic partner, as Geert earlier called you. **Nina**, thank you for all the time we spent together working in the lab, supervising students, and collaborating on manuscripts. Our insightful discussions really made me think deeper about our research, elevating it to the next level. Your easy-going and organic interaction made my PhD journey very enjoyable.

Next, I want to thank my paranymphs, Casper and Laurens. **Casper**, thanks to you, it was always very gezellig in the SPIT- and spoel-lab. Our shared taste in music motivated everyone to work quickly, and our similar sense of humor, even if it occasionally bordered on the unacceptable, added to the fun. Because of you, I had an amazing time during my PhD. **Laurens**, you are the person I have known the longest here on campus. You taught me a lot about setting up and performing experiments during my Bachelor thesis. Since then, we have lunched together almost every week. Thank you both for being such good colleagues and, above all, friends.

I want to thank all the people from Nematology. Thank you for all the wonderful moments we have shared, including coffee breaks, lab outings, Christmas lunches, and barbecues. I could not have wished for a better lab in which to do my PhD. Thank you all for tolerating my cringy jokes.

Special thanks to the backbone of this department: the technicians **Casper**, **Joost**, **Sven**, **Hein**, **Stefan**, and **Lisa**, and the secretaries **Lisette** and **Manouk**. Because of all your efforts, this department was a very pleasant place to work at. Thank you for the administrative help and for ensuring a well-structured, efficient, and safe lab/department.

I also want to thank the other staff members **Yet**, **Ruud**, **Jessica**, **Aska**, **Jan**, **Stefan**, **Hans**, **Arjen**, and **Lisa**. Thank you for all the support and feedback you gave me throughout my PhD trajectory.

Many experiments in this thesis were performed by my students: **Devon**, **Willem**, **Ivan**, **Jingrong**, **Marie-Emma**, **Yunsong**, **Nyasha**, **Fabio**, **Sri**, **Thomas**, **Rick**, **Kai**, and **Ahmad**. Your hard work has contributed significantly to this thesis, the papers we have published and plan to publish. Thank you all for the nice and funny moments that we have shared.

Multiple people from outside the Laboratory of Nematology have contributed to this thesis. **Viola**, thank you for all your valuable feedback and input in the research we conducted. Your extensive knowledge of plant developmental biology helped elevate our studies to a higher level. **Lin**, thank you for sharing many of your mutant lines and for your help whenever I had questions. **Misghina**, thank you for the countless discussions about quantitative nematology. Your input was invaluable for multiple chapters of my thesis.

Also, I would like to thank my office mates. **Anna**, thank you for the numerous discussions we had about experiments and experimental designs. Additionally, thank you for your feedback during the PDAN meetings. **Yuhao**, thank you for all the work-related discussions and chats in the office.

Next, I want to thank all the PhDs and PostDocs from Nematology. Being part of the furniture, I have seen many PhDs come and go. Many thanks to the previous generation of PhDs: Kim, Matthijs, Sonja, Amalia, Yuqing, Qi, Paula, Koen, and PostDocs: Martijn, Erik, and Lotte for all their help, tips, and tricks for in and outside the lab.

I would also like to thank the current and new generation of PhDs. **Joris**, thank you for being such a great colleague. It was always nice and fun to have you around during coffee breaks. Together with **Dennie**, the catalyst/enhancer of making cringy jokes even more cringy, both of you helped me a lot with my struggles in R and other IT-related issues. **Marijke**, thank you for being always positive and helping me out with R (I start to see a trend here…). I could always reach out to you for helping me out making PCA plots. **Vera**, thank you for the nice and funny chats we had during the coffee breaks and on the hallway. Thanks to you I can perform pair-wise analyses and place the level of significance directly above my beautiful boxplots in ggplot2 (once again help in R). **Arno**, even though you joined Nematology much later, thank you for all the nice and funny moments we had. Your optimism is inspiring. **Robbert**, I would like to thank you for all the nice coffee moments. It is a pity we started to work together more closely while I am writing this part of my thesis. **Iqbal**, the nematode pimp of our department, I have much respect for how you managed your project. It isn't easy, forcing nematodes to mate. Thank you for all the nice moments. **Myrna**,

thank you for being such a great chair of the PhD meetings. **Alex**, thank you for all the nice coffee and drinks we had after symposia. **Daan**, I already know you for seven years. During that time, you were wearing your AVEBE hat. Now, you are also part of the PhD candidates. Thank you for the interesting discussions during our TKI meetings, and the nice moments during the coffee break. **Alejandro**, it is a pity that our 'wild' experiment in which we wanted to combine protists and nematodes did not work out as planned. Thank you for the nice moments. **Marije**, thank you for all the nice conversations we had when we were both working together in the lab. **Shunran**, **Yuxin**, **Zewen**, **Mijke**, **Geartsje**, **Sabine**, and **Jeroen**, we did not share many moments together. But, for the few moments we had, thank you.

Next I would like the PostDocs. **André**, thank you for all the nice talks about life and work. It was funny to see how you and Casper tried to talk like a Viking. I hope you can continue practicing at HLB. **Pieter**, my INHolland mate. Thank you for all the talks we had about our experiences at INHolland. **Rutger**, we did not work closely together, but it was always fun when you joined the coffee breaks. Thank you for those moments.

I also owe a great deal to the friends I made during my Master's. **Eleni**, **Daniel**, **Raul**, and **Nicolo**, who, like me, began their Master's nine years ago (we're getting old). We embarked on this journey together, and even though our paths diverged at the end of the Master's, we all ended up pursuing a PhD. I believe I started first and finished last —something I often hear from Eleni. Thank you for all the wonderful lunch and coffee moments between our classes. I frequently reminisce about how wild our conversations were and how much we laughed. Thank you for being such good friends.

Then, I would like to thank my fellow co-founders of the Young Nematologists Network (YNN): **Unnati**, **Olivera**, **Boris**, **Nina**, **Nasamu**, **Xorla**, and **Adam**. After the first Virtual Nematology Conference, Geert approached us to build this network. It was not easy, but it seems we created something durable with the new board of the YNN. Thank you for the enjoyable online events and the second conference that we organized.

Nu wil ik mijn grote liefde bedanken. Elly, bedankt voor alle onvoorwaardelijke steun die je mij hebt gegeven sinds we elkaar leerden kennen, beginnend met bijles in Organische Chemie tijdens ons eerste jaar van de Bachelor in Amsterdam. Wie had gedacht dat we, na een vraag om samen naar huis te reizen zou eindigen in 14 jaar samen zijn met, sinds 12 maanden, onze kleine Jacob. Jij haalt het beste in mij naar boven, zowel professioneel als een liefhebbende partner/vader zijn. Bedankt voor alle momenten dat ik bij jou kon ventileren, voor onze inhoudelijke discussies, en bovenal voor de liefde die je mij geeft.

Als laatst wil ik mijn zus Liselotte en mijn ouders bedanken. De reis hiernaartoe was niet makkelijk. Jullie hebben mij weleens gevraagd of ik het opnieuw zou mogen doen. Ik heb dit altijd simpel beantwoord met: 'ja natuurlijk, ik vind het leuk wat ik nu doe'. Wat ik nooit heb gezegd is dat ik dit alleen over zou doen met jullie aan mijn zijde. Jullie hebben mij altijd gestimuleerd en gemotiveerd om het beste en maximale uit mijzelf te halen. Ik denk dat dit bij deze wel gelukt is. Bedankt voor alle onvoorwaardelijke steun en liefde die jullie mij tot op de dag van vandaag geven.

List of publications

First author(s)

1. **Willig, J.**, Guarneri, N., van Steenbrugge, J.J.M., de Jong, W., Chen, J., Goverse, A., Lozano-Torres, J.L., Sterken, M.G., Bakker, J., Smant, G. (2022). The Arabidopsis transcription factor TCP9 modulates root architectural plasticity, ROS-mediated processes, and tolerance to cyst nematode infections. The Plant Journal

2. Guarneri, N., **Willig, J.**, Sterken, M.G., Zhou, W., Hasan, S., Sharon, L., Grundler, F.M.W., Willemsen, V., Goverse, A., Smant, G., Lozano-Torres, J.L. (2022). Root architecture plasticity in response to endoparasitic cyst nematodes is mediated by damage signaling**.** New Phytologist

3. **Willig, J.**, Sonneveld, D., Steenbrugge, J.J.M., Deurhof, L., van Schaik, C.C., Teklu, M.G., Goverse, A., Lozano-Torres, J.L., Smant, G., Sterken, M.G. (2023). From root to shoot; Quantifying nematode tolerance in Arabidopsis thaliana by high-throughput phenotyping of plant development.
Journal of Experimental Botany

4. **Willig, J.**, Guarneri, N., van Loon, T., Wahyuni, S., Astudillo-Estévez, I.E., Xu, L., Willemsen, V., Goverse, A., Sterken, M.G., Lozano-Torres, J.L., Bakker, J., Smant, G. (2024). Transcription factor WOX11 modulates tolerance to cyst nematodes via adventitious lateral root formation. Plant Physiology

5. Guarneri, N., **Willig, J.**, Willemsen, V., Goverse, A., Sterken, M.G., Nibbering, P., Lozano-Torres, J.L., Smant, G. (2023). WOX11 mediated cell size control in Arabidopsis attenuates fecundity of endoparasitic cyst nematodes. *bioRxiv*: 2023.10.27.564344

About the author

Jaap-Jan Willig was born on September 27, 1992, in Alkmaar and raised in Schagen. He began his education at P.C. basisschool De Wegwijzer and continued to GSG Schagen (VMBO-TL) from 2005 to 2009, and Luzac College (HAVO) in Alkmaar from 2009 to 2011.

In 2011, Jaap-Jan pursued a Bachelor's degree in Applied Life Sciences, specializing in Green Biotechnology at Hogeschool INHolland in Amsterdam. During his final year, he moved to Ede to complete his Bachelor's thesis at Wageningen University & Research in the Laboratory of Phytopathology, where he discovered his passion for phytopathology. After graduating in 2015, Jaap-Jan started a Master's program at Wageningen University & Research in Green Biotechnology, specializing in Genomics and Phytopathology. It was during his MSc and Minor thesis that he developed a keen interest in Nematology.

In 2017, Jaap-Jan commenced his PhD at the Laboratory of Nematology, focusing on the mechanisms of tolerance to root-parasitic nematodes in Arabidopsis thaliana. His collaborative efforts during his PhD resulted in four publications in high-inmpact journals. Next to his research, Jaap-Jan co-founded the Young Nematologists network, in which he contributed to the organization of online seminars, workshops and coferences to foster the professional development of early-career Nematologists.

In February 2024, Jaap-Jan began working as a Researcher at Agrosystems Research and the Laboratory of Nematology at Wageningen University & Research, continuing his studies on the interactions between crops/Arabidopsis and various species of root-parasitic nematodes.

The research described in this thesis was financially supported by the TKI project grant TU18152 of the Dutch Top Secotr Horticulture & Starting Materials.

Finanical support from Wageningen University for printing this thesis is gratefully acknowledged.

Cover design and thesis layout by Jaap-Jan Willig

Printed by ProefschriftMaken B.V. on Silk MC.